



University
of Glasgow

Dennis, Jennifer Lucy (2011) *The use of single photon emission computed tomography in the investigation of parathyroid and thyroid disorders*. PhD thesis.

<http://theses.gla.ac.uk/2354/>

Copyright and moral rights for this thesis are retained by the author

A copy can be downloaded for personal non-commercial research or study, without prior permission or charge

This thesis cannot be reproduced or quoted extensively from without first obtaining permission in writing from the Author

The content must not be changed in any way or sold commercially in any format or medium without the formal permission of the Author

When referring to this work, full bibliographic details including the author, title, awarding institution and date of the thesis must be given

**The Use of Single Photon Emission Computed
Tomography in the Investigation of Parathyroid
and Thyroid Disorders**

**Jennifer Lucy Dennis
BSc (Hons), MSc (Med Sci)**

**Submitted in fulfilment of the requirements for the
Degree of PhD**

**Department of Clinical Physics and Bioengineering
Division of Education and Administration
Faculty of Medicine
University of Glasgow**

February 2011

Abstract

Nuclear medicine is a functional imaging modality involving the administration of a radioactive material and the imaging of its distribution within the body.

Planar nuclear medicine imaging has been used for many years in the evaluation of patients with disorders of the parathyroid and thyroid glands. Single photon emission computed tomography (SPECT) can also be carried out. This is a three-dimensional nuclear medicine imaging technique that gives both increased image contrast due to the separation of overlying structures and improved information on lesion localisation.

Currently, there is no definitive procedure for parathyroid imaging, which is primarily used for localisation of adenomas or hyperplastic glands in patients with hyperparathyroidism. This information can be used to assist during surgery to remove the overactive glands. Some centres use a single-isotope, dual-phase technique with ^{99m}Tc -Sestamibi, whilst others use a dual-isotope subtraction technique with either ^{99m}Tc -pertechnetate or ^{123}I -iodide to outline the thyroid. Single-isotope SPECT is used in some institutions but there is little information on the use of dual-isotope subtraction SPECT.

Thyroid imaging with either ^{99m}Tc -pertechnetate or ^{123}I -iodide is used to characterise thyroid disorders. The thyroid uptake can also be calculated using planar images, which can assist in clinical decision making for patients with hyper- or hypothyroidism. SPECT is not commonly used in thyroid imaging at present.

This study was carried out in the Department of Nuclear Medicine, Glasgow Royal Infirmary (GRI) and was split into two distinct sections, the first being an assessment of the utility of dual-isotope subtraction SPECT for localisation of parathyroid adenomas and the second being an evaluation of the use of SPECT imaging for calculating thyroid uptake. A custom designed and built phantom was used to assess the feasibility of parathyroid and thyroid SPECT imaging and to establish suitable acquisition parameters. The results from the phantom work demonstrated that the techniques were viable and so patient SPECT data collection was commenced.

A total of 32 patients with hyperparathyroidism underwent dual-isotope SPECT imaging in addition to routine planar imaging. The SPECT images were then reconstructed and a subtraction SPECT data set was produced. An observer study was then carried out with 5 experienced observers independently reviewing the images in 4 phases. In phase 1, only the dual-isotope subtraction planar images were available for review. Phase 2 was comprised of only dual-isotope subtraction SPECT images, whilst phase 3 involved review of single-isotope ^{99m}Tc -Sestamibi planar and SPECT images in the absence of ^{123}I -iodide thyroid images. Finally, in phase 4, all of the acquired planar and SPECT images were available for review.

The patients' case notes were interrogated to obtain information on the surgical and histological reports of excised glands. A total of 17 of the 32 patients had surgery and the results were compared to the findings from the observer study to determine which type of images provided the most useful clinical information. The results of any ultrasound imaging were also obtained to compare with the surgical findings.

The total number of lesions seen by the observers was higher when dual-isotope subtraction SPECT images were part of the review than when they were not, with totals in phases 1-4 of 89, 183, 89 and 155, respectively. The calculated sensitivities relative to the surgical gold standard for phases 1-4 were 49%, 77%, 45% & 64%, respectively, with ultrasound having a sensitivity of 72% for comparison. Dual-isotope subtraction SPECT therefore has a clear advantage over planar imaging for detection and localisation of parathyroid adenomas. The specificities for phases 1-4 were calculated as 61%, 31%, 29% & 27%, with the specificity for ultrasound being 33%. These specificities are, however, unreliable due to the fact that only 2 true negatives were recorded from surgery.

This study showed a clear improvement in the sensitivity of dual-isotope subtraction SPECT imaging over planar imaging for the detection and localisation of parathyroid adenomas, as well as more detailed localisation information being available from the 3D images. As a result, clinical practice in the department has been changed and all patients now routinely undergo dual-isotope subtraction SPECT imaging.

SPECT imaging with ^{99m}Tc -pertechnetate was carried out on 57 patients with thyroid disorders. The images were reconstructed with and without the inclusion of attenuation correction and the thyroid uptake was calculated by drawing a region of interest on each slice and summing the counts within each region. A standard acquisition was also carried out to allow accurate quantification to be performed. These uptake values were compared to those from planar imaging. Similar analysis was performed on images of a phantom to determine the accuracy of the patient uptake measurements.

The various uptake values calculated from the phantom images were all similar and were slightly lower than the “true” uptake value. However, there were significant differences demonstrated between the SPECT and planar uptake values from the patient images with the SPECT uptake tending to be higher. The reasons for this are not immediately clear but are most likely related to the difference in time between injection and imaging for the planar and SPECT acquisitions at 24.5 ± 8.0 minutes (mean \pm 1SD) and 71.5 ± 17.5 minutes respectively.

Significant differences seen between the calculated uptake values from SPECT and planar images in the patient data sets were not evident in the phantom work, indicating that some physiological effect resulting in changing thyroid uptake over time was not taken into account. Further work could be undertaken to characterise this effect, but the method used to calculate the uptake from SPECT images is too cumbersome to be used routinely. Therefore, no change in clinical practice is anticipated for the calculation of thyroid uptake.

This study has therefore resulted in a change of clinical practice for parathyroid imaging at GRI, with the introduction of dual-isotope subtraction SPECT routinely. Thyroid imaging remains unchanged, however, with the thyroid uptake being calculated from planar images.

Table of Contents

Abstract	2
List of Tables	8
List of Figures	15
Acknowledgements	18
Author's Declaration	19
Chapter 1 - Introduction	20
1.1 The Thyroid and Parathyroid Glands - Anatomy and Physiology	20
1.1.1 The Thyroid Gland	20
1.1.2 The Parathyroid Glands	22
1.2 Disorders of the Thyroid and Parathyroid Glands	24
1.2.1 Disorders of the Thyroid Gland	24
1.2.2 Disorders of the Parathyroid Glands	26
1.3 Imaging of the Thyroid and Parathyroid Glands	28
1.3.1 Thyroid Imaging	28
1.3.2 Parathyroid Imaging	30
1.4 Nuclear Medicine SPECT Imaging	35
1.5 SPECT of the Thyroid and Parathyroid Glands	38
1.5.1 Thyroid SPECT	38
1.5.2 Parathyroid SPECT	38
1.6 Study Aims	39
Chapter 2 - Design, Construction and Use of a Dedicated Thyroid and Parathyroid Phantom	41
2.1 Introduction	41
2.2 Materials and Methods	42
2.2.1 Design and Construction of a Thyroid/Parathyroid Phantom	42
2.2.2 Image Acquisitions using the Phantom	46
2.3 Discussion and Conclusions	57
Chapter 3 - Parathyroid Study - Introduction	59
3.1 Parathyroid Imaging at Glasgow Royal Infirmary	59
3.1.1 Referrals	59
3.1.2 Standard Parathyroid Imaging Procedure at GRI	60
3.1.3 SPECT Imaging of the Parathyroid Glands	64
Chapter 4 - Parathyroid Study - Materials and Methods	67
4.1 Study Participants	67
4.2 Injected Activities	67
4.3 SPECT Acquisition	68
4.4 SPECT Image Reconstruction	69
4.5 SPECT Subtraction	70
4.6 Observer Image Reviews	71
4.7 Surgical and Ultrasound Results	73
Chapter 5 - Parathyroid Study - Results of Observer Study	77
5.1 Patient Demographics	77
5.2 Injected Activities	77

5.3	SPECT Reconstruction.....	79
5.4	Observer Study Results	83
5.4.1	General Comments.....	83
5.4.2	Phase 1 - Planar Images	84
5.4.3	Phase 2 - SPECT Images	85
5.4.4	Phase 3 - ^{99m} Tc-Sestamibi Planar and SPECT Images.....	87
5.4.5	Phase 4 - All Planar and SPECT Images.....	88
5.4.6	Summary of Lesions Seen	89
5.5	Comparisons of Results of Observer Study.....	91
5.5.1	Phase 2 versus Phase 1 Reviews.....	92
5.5.2	Phase 3 versus Phase 1 Reviews.....	97
5.5.3	Phase 4 versus Phase 1 Reviews.....	100
5.5.4	Phase 3 versus Phase 2 Reviews.....	104
5.5.5	Phase 4 versus Phase 2 Reviews.....	109
5.5.6	Phase 4 versus Phase 3 Reviews.....	113
5.5.7	Summary of Comparison Results	118
Chapter 6 - Parathyroid Study - Comparison of Observer Study with Surgical and US Findings		123
6.1	Surgical and Ultrasound Results	123
6.1.1	Participants Having Surgery and/or Ultrasound	123
6.2	Comparison of Observer Study with Surgical and Ultrasound Findings	127
6.2.1	Phase 1 versus Surgical and US Findings Comparison	127
6.2.2	Phase 2 versus Surgical and US Findings Comparison	136
6.2.3	Phase 3 versus Surgical and US Findings Comparison	147
6.2.4	Phase 4 versus Surgical and US Findings Comparison	157
6.2.5	Summary of Observer Study and Surgical Comparison Results	168
Chapter 7 - Parathyroid Study - Discussion, Conclusions and Suggestions for Further Work		173
7.1	Discussion	173
7.1.1	Study Participants.....	173
7.1.2	SPECT Reconstructions	173
7.1.3	General Observer Comments	175
7.1.4	Comparison of Phases of Observer Study	176
7.1.5	Comparison of Surgical and Ultrasound Findings	181
7.1.6	Comparison of Observer Study with Surgical Findings	182
7.1.7	Second Review of Phase 2 SPECT Images	187
7.1.8	Comparison of Observer Study with Ultrasound Findings.....	189
7.1.9	Comparison with Results from Other Researchers.....	193
7.1.10	Results with Equivocal Reports Taken as Positive	198
7.2	Conclusions	201
7.3	Suggestions for Further Work	203
Chapter 8 - Thyroid Uptake Calculations from SPECT Images		206
8.1	Introduction	206
8.1.1	Nuclear Medicine Thyroid Studies	206
8.1.2	The Thyroid Uptake Measurement	208
8.1.3	Glasgow Royal Infirmary Thyroid Clinic	211
8.2	Materials and Methods	212
8.2.1	Study participants.....	212
8.2.2	Planar Uptake Measurements.....	213
8.2.3	SPECT Acquisition	214

8.2.4	SPECT Image Reconstruction	215
8.2.5	Volume of Interest Definition	216
8.2.6	Thyroid Uptake Calculation.....	220
8.2.7	Uptake Calculation from Single SPECT Frame	222
8.2.8	Comparison of Planar, SPECT, Attenuation Corrected SPECT and Model Uptake Values	222
8.3	Results.....	223
8.3.1	Patient Demographics and SPECT Imaging Times.....	223
8.3.2	SPECT Reconstruction	224
8.3.3	Comparison of Calculated and Modelled Uptake Values.....	227
8.4	Discussion	239
8.5	Conclusions and Suggestions for Further Work	241
Chapter 9 - Accuracy of the Thyroid Uptake Calculation.....		243
9.1	Introduction	243
9.2	Materials and Methods	244
9.3	Results.....	249
9.3.1	Comparison with Known “Uptake” Value	249
9.3.2	Direct Comparison of Calculated Uptake Values	251
9.3.3	CT Attenuation Corrected Uptake Values	258
9.4	Discussion	260
9.5	Conclusions and Suggestions for Further Work	262
Chapter 10 - Summary of Findings		264
Appendix A - Ethics Approval Documentation		267
Appendix B - Patient Information Sheet & Consent Form		270
Appendix C - Scoring Sheets for Parathyroid Observer Study		275
Bibliography		279

List of Tables

Table 2.1 - Volume of each chamber within the two phantom inserts	45
Table 4.1 - Summary of parathyroid observer study phases	72
Table 5.1 - Administered activities of radiopharmaceutical	78
Table 5.2 - Image quality scoring for planar images in observer study phase 1..	85
Table 5.3 - Image quality scoring for SPECT images in observer study phase 2..	86
Table 5.4 - Image quality scoring for ^{99m} Tc-Sestamibi images in observer study phase 3.....	88
Table 5.5 - Image quality scoring for all planar and SPECT images in observer study phase 4	89
Table 5.6 - Comparison of number of lesions seen in phase 1 (planar only) and phase 2 (SPECT only).....	93
Table 5.7 - Results from Wilcoxon Signed Ranks test on differences in number of lesions seen (phase 2 vs phase 1)	93
Table 5.8 - Results from comparison of confidence levels expressed (phase 2 vs phase 1).....	94
Table 5.9 - Results from Wilcoxon Signed Ranks test on differences in expressed confidence level (phase 2 vs phase 1).....	95
Table 5.10 - Results of comparison in left/right location between lesions seen on SPECT and planar images.....	96
Table 5.11 - Results of comparison in upper/lower location between lesions seen on SPECT and planar images	96
Table 5.12 - Results of combined left/right and upper/lower location comparisons between lesions seen on SPECT and planar images.....	96
Table 5.13 - Comparison of number of lesions seen in phase 1 (planar only) and phase 3 (Sestamibi only)	97
Table 5.14 - Results from Wilcoxon Signed Ranks test on differences in number of lesions seen (phase 3 vs phase 1)	97
Table 5.15 - Results from comparison of confidence levels expressed (phase 3 vs phase 1).....	98
Table 5.16 - Results from Wilcoxon Signed Ranks test on differences in expressed confidence level (phase 3 vs phase 1).....	99
Table 5.17 - Results of comparison in left/right location between lesions seen on Sestamibi only and planar images.....	99
Table 5.18 - Results of comparison in upper/lower location between lesions seen on Sestamibi only and planar images.....	100
Table 5.19 - Results of combined left/right and upper/lower location comparisons between lesions seen on Sestamibi only and planar images.....	100
Table 5.20 - Comparison of number of lesions seen in phase 1 (planar only) and phase 4 (all images).....	101

Table 5.21 - Results from Wilcoxon Signed Ranks test on differences in number of lesions seen (phase 4 vs phase 1)	101
Table 5.22 - Results from comparison of confidence levels expressed (phase 4 vs phase 1).....	102
Table 5.23 - Results from Wilcoxon Signed Ranks test on differences in expressed confidence level (phase 4 vs phase 1).....	102
Table 5.24 - Results of comparison in left/right location between lesions seen on all images and planar only	103
Table 5.25 - Results of comparison in upper/lower location between lesions seen on all images and planar only	103
Table 5.26 - Results of combined left/right and upper/lower location comparisons between lesions seen on all images and planar only	104
Table 5.27 - Comparison of number of lesions seen in phase 2 (SPECT) and phase 3 (Sestamibi only)	105
Table 5.28 - Results from Wilcoxon Signed Ranks test on differences in number of lesions seen (phase 3 vs phase 2)	105
Table 5.29 - Results from comparison of confidence levels expressed (phase 3 vs phase 2).....	106
Table 5.30 - Results from Wilcoxon Signed Ranks test on differences in expressed confidence level (phase 3 vs phase 2).....	106
Table 5.31 - Results of comparison in left/right location between lesions seen on Sestamibi only and SPECT images.....	107
Table 5.32 - Results of comparison in upper/lower location between lesions seen on Sestamibi only and SPECT images	107
Table 5.33 - Results of combined left/right and upper/lower location comparisons between lesions seen on Sestamibi only and SPECT images.....	108
Table 5.34 - Results of comparison in anterior/posterior location between lesions seen on Sestamibi only and SPECT images.....	108
Table 5.35 - Results of combined left/right, upper/lower and anterior/posterior location comparisons between lesions seen on Sestamibi only and SPECT images	108
Table 5.36 - Comparison of number of lesions seen in phase 2 (SPECT) and phase 4 (all images).....	109
Table 5.37 - Results from Wilcoxon Signed Ranks test on differences in number of lesions seen (phase 4 vs phase 2)	110
Table 5.38 - Results from comparison of confidence levels expressed (phase 4 vs phase 2).....	110
Table 5.39 - Results from Wilcoxon Signed Ranks test on differences in expressed confidence level (phase 4 vs phase 2).....	111
Table 5.40 - Results of comparison in left/right location between lesions seen on all images and SPECT only	111
Table 5.41 - Results of comparison in upper/lower location between lesions seen on all images and SPECT only.....	112

Table 5.42 - Results of combined left/right and upper/lower location comparisons between lesions seen on all images and SPECT only	112
Table 5.43 - Results of comparison in anterior/posterior location between lesions seen on all images and SPECT alone.....	113
Table 5.44 - Results of combined left/right, upper/lower and anterior/posterior location comparisons between lesions seen on all images and SPECT only.....	113
Table 5.45 - Comparison of number of lesions seen in phase 3 (Sestamibi only) and phase 4 (all images).....	114
Table 5.46 - Results from Wilcoxon Signed Ranks test on differences in number of lesions seen (phase 4 vs phase 3)	114
Table 5.47 - Results from comparison of confidence levels expressed (phase 4 vs phase 3).....	115
Table 5.48 - Results from Wilcoxon Signed Ranks test on differences in expressed confidence level (phase 4 vs phase 3).....	115
Table 5.49 - Results of comparison in left/right location between lesions seen on all images and Sestamibi only	116
Table 5.50 - Results of comparison in upper/lower location between lesions seen on all images and Sestamibi only	116
Table 5.51 - Results of combined left/right and upper/lower location comparisons between lesions seen on all images and Sestamibi only	117
Table 5.52 - Results of comparison in anterior/posterior location between lesions seen on all images and Sestamibi alone.....	117
Table 5.53 - Results of combined left/right, upper/lower and anterior/posterior location comparisons between lesions seen on all images and Sestamibi only..	117
Table 6.1 - Surgical findings for patients undergoing parathyroidectomy	124
Table 6.2 - Ultrasound (US) findings for patients who had parathyroid surgery	125
Table 6.3 - Ultrasound (US) findings for patients who did not have parathyroid surgery	126
Table 6.4 - Comparison of number of samples resected at surgery and number of lesions seen in phase 1 (planar)	127
Table 6.5 - Results from Wilcoxon Signed Ranks test on differences in number of lesions seen (surgery vs phase 1).....	128
Table 6.6 - Results from comparison of positive/negative findings (surgery vs phase 1).....	129
Table 6.7 - Results from Wilcoxon Signed Ranks Test on positive/negative comparison (surgery vs phase 1)	129
Table 6.8 - Results of comparison in left/right location between lesions resected at surgery and those seen on planar images	130
Table 6.9 - Results of comparison in upper/lower location between lesions resected at surgery and those seen on planar images	130
Table 6.10 - Results of combined left/right and upper/lower location comparisons between lesions resected at surgery and those seen on planar images.....	131

Table 6.11- Calculated sensitivity and specificity values for comparison of surgical and planar imaging results	131
Table 6.12 - Comparison of number of lesions seen on ultrasound and in phase 1 (planar)	133
Table 6.13 - Results from Wilcoxon Signed Ranks test on differences in number of lesions seen (ultrasound vs phase 1).....	133
Table 6.14 - Results from comparison of positive/negative findings (ultrasound vs phase 1).....	134
Table 6.15 - Results from Wilcoxon Signed Ranks Test on positive/negative comparison (ultrasound vs phase 1)	134
Table 6.16 - Results of comparison in left/right location between lesions seen on ultrasound and those seen on planar images.....	134
Table 6.17 - Results of comparison in upper/lower location between lesions seen on ultrasound and those seen on planar images	135
Table 6.18 - Results of combined left/right and upper/lower location comparisons between lesions seen on ultrasound and those seen on planar images.....	135
Table 6.19 - Calculated sensitivity and specificity values for comparison of US and planar imaging results	136
Table 6.20 - Comparison of number of samples resected at surgery and number of lesions seen in phase 2 (SPECT).....	137
Table 6.21 - Results from Wilcoxon Signed Ranks test on differences in number of lesions seen (surgery vs phase 2).....	137
Table 6.22 - Results from comparison of positive/negative findings (surgery vs phase 2).....	138
Table 6.23 - Results from Wilcoxon Signed Ranks Test on positive/negative comparison (surgery vs phase 2)	138
Table 6.24 - Results of comparison in left/right location between lesions resected at surgery and those seen on SPECT images	139
Table 6.25 - Results of comparison in upper/lower location between lesions resected at surgery and those seen on SPECT images	139
Table 6.26 - Results of combined left/right and upper/lower location comparisons between lesions resected at surgery and those seen on SPECT images.....	140
Table 6.27 - Results of comparison in anterior/posterior location between lesions resected at surgery and those seen on SPECT images	140
Table 6.28 - Results of combined left/right, upper/lower and anterior/posterior location comparisons between lesions resected at surgery and those seen on SPECT images	141
Table 6.29 - Calculated sensitivity and specificity values for comparison of surgical and SPECT imaging results	141
Table 6.30 - Comparison of number of lesions seen on ultrasound and in phase 2 (SPECT).....	142

Table 6.31 - Results from Wilcoxon Signed Ranks test on differences in number of lesions seen (ultrasound vs phase 2).....	143
Table 6.32 - Results from comparison of positive/negative findings (ultrasound vs phase 2).....	143
Table 6.33 - Results from Wilcoxon Signed Ranks Test on positive/negative comparison (ultrasound vs phase 2)	144
Table 6.34 - Results of comparison in left/right location between lesions seen on ultrasound and those seen on SPECT images	144
Table 6.35 - Results of comparison in upper/lower location between lesions seen on ultrasound and those seen on SPECT images	145
Table 6.36 - Results of combined left/right and upper/lower location comparisons between lesions seen on ultrasound and those seen on SPECT images.....	145
Table 6.37 - Results of comparison in anterior/posterior location between lesions seen on ultrasound and those seen on SPECT images	145
Table 6.38 - Results of combined left/right, upper/lower and anterior/posterior location comparisons between lesions seen on ultrasound and those seen on SPECT images	146
Table 6.39 - Calculated sensitivity and specificity values for comparison of US and SPECT imaging results	146
Table 6.40 - Comparison of number of samples resected at surgery and number of lesions seen in phase 3 (Sestamibi only)	147
Table 6.41 - Results from Wilcoxon Signed Ranks test on differences in number of lesions seen (surgery vs phase 3).....	148
Table 6.42 - Results from comparison of positive/negative findings (surgery vs phase 3).....	148
Table 6.43 - Results from Wilcoxon Signed Ranks Test on positive/negative comparison (surgery vs phase 3)	149
Table 6.44 - Results of comparison in left/right location between lesions resected at surgery and those seen on Sestamibi only images	149
Table 6.45 - Results of comparison in upper/lower location between lesions resected at surgery and those seen on Sestamibi only images	150
Table 6.46 - Results of combined left/right and upper/lower location comparisons between lesions resected at surgery and those seen on Sestamibi only images.....	150
Table 6.47 - Results of comparison in anterior/posterior location between lesions resected at surgery and those seen on Sestamibi only images	150
Table 6.48 - Results of combined left/right, upper/lower and anterior/posterior location comparisons between lesions resected at surgery and those seen on Sestamibi only images	151
Table 6.49- Calculated sensitivity and specificity values for comparison of surgical and Sestamibi only imaging.....	151
Table 6.50 - Comparison of number of lesions seen on ultrasound and in phase 3 (Sestamibi only)	153

Table 6.51 - Results from Wilcoxon Signed Ranks test on differences in number of lesions seen (ultrasound vs phase 3).....	153
Table 6.52 - Results from comparison of positive/negative findings (ultrasound vs phase 3).....	154
Table 6.53 - Results from Wilcoxon Signed Ranks Test on positive/negative comparison (ultrasound vs phase 3)	154
Table 6.54 - Results of comparison in left/right location between lesions seen on ultrasound and those seen on Sestamibi only images	155
Table 6.55 - Results of comparison in upper/lower location between lesions seen on ultrasound and those seen on Sestamibi only images	155
Table 6.56 - Results of combined left/right and upper/lower location comparisons between lesions seen on ultrasound and those seen on Sestamibi only images.....	156
Table 6.57 - Results of comparison in anterior/posterior location between lesions seen on ultrasound and those seen on Sestamibi only images.....	156
Table 6.58 - Results of combined left/right, upper/lower and anterior/posterior location comparisons between lesions seen on ultrasound and those seen on Sestamibi only images	156
Table 6.59- Calculated sensitivity and specificity values for comparison of US and Sestamibi only imaging results	157
Table 6.60 - Comparison of number of samples resected at surgery and number of lesions seen in phase 4 (all images)	158
Table 6.61 - Results from Wilcoxon Signed Ranks test on differences in number of lesions seen (surgery vs phase 4).....	158
Table 6.62 - Results from comparison of positive/negative findings (surgery vs phase 4).....	159
Table 6.63 - Results from Wilcoxon Signed Ranks Test on positive/negative comparison (surgery vs phase 4)	159
Table 6.64 - Results of comparison in left/right location between lesions resected at surgery and those seen on review of all images.....	160
Table 6.65 - Results of comparison in upper/lower location between lesions resected at surgery and those seen on review of all images.....	160
Table 6.66 - Results of combined left/right and upper/lower location comparisons between lesions resected at surgery and those seen on review of all images.....	161
Table 6.67 - Results of comparison in anterior/posterior location between lesions resected at surgery and those seen on review of all images.....	161
Table 6.68 - Results of combined left/right, upper/lower and anterior/posterior location comparisons between lesions resected at surgery and those seen on review of all images.....	162
Table 6.69 - Calculated sensitivity and specificity values for comparison of surgical and all dual-isotope subtraction imaging	162
Table 6.70 - Comparison of number of lesions seen on ultrasound and in phase 4 (all images).....	163

Table 6.71 - Results from Wilcoxon Signed Ranks test on differences in number of lesions seen (ultrasound vs phase 4).....	164
Table 6.72 - Results from comparison of positive/negative findings (ultrasound vs phase 4).....	164
Table 6.73 - Results from Wilcoxon Signed Ranks Test on positive/negative comparison (ultrasound vs phase 4)	165
Table 6.74 - Results of comparison in left/right location between lesions seen on ultrasound and those seen on review of all images	165
Table 6.75 - Results of comparison in upper/lower location between lesions seen on ultrasound and those seen on review of all images.....	165
Table 6.76 - Results of combined left/right and upper/lower location comparisons between lesions seen on ultrasound and those seen on review of all images.....	166
Table 6.77 - Results of comparison in anterior/posterior location between lesions seen on ultrasound and those seen on review of all images	166
Table 6.78 - Results of combined left/right, upper/lower and anterior/posterior location comparisons between lesions seen on ultrasound and those seen on review of all images.....	167
Table 6.79- Calculated sensitivity and specificity values for comparison of US and all dual-isotope subtraction imaging	167
Table 7.1 - Overall sensitivity and specificity values for comparison of results of observer study and ultrasound imaging with surgical results	186
Table 7.2 - Calculated sensitivity and specificity relative to surgical findings for first and second SPECT image reviews	188
Table 7.3 - Overall sensitivity and specificity values for comparison of results of observer study with ultrasound imaging results	193
Table 7.4 - Sensitivity and specificity results for equivocal taken as negative and positive.....	200
Table 8.1 - Basic descriptive statistics for thyroid uptake results calculated with different methods	227
Table 8.2 - Summary of results from Wilcoxon Signed Ranks statistical test applied to differences in calculated uptake from each alternative imaging method.....	238
Table 9.1 - Results of Wilcoxon Signed Ranks statistical test applied to differences between known and calculated uptake values	251
Table 9.2 - Results of uptake measurements on 3 phantom acquisitions that included SPECT/CT.....	259

List of Figures

Figure 1.1 - Normal location of the thyroid gland	21
Figure 1.2 - Structure of the thyroid gland	21
Figure 1.3 - Some potential ectopic locations for thyroid tissue	22
Figure 1.4 - Typical location of the parathyroid glands	23
Figure 1.5 - Normal and ectopic locations of parathyroid glands	24
Figure 2.1 - Dimensions of thyroid for phantom inserts	43
Figure 2.2 - Specification for phantom thyroid insert	44
Figure 2.3 - Specification for phantom parathyroid insert	44
Figure 2.4 - Photographs of completed phantom	45
Figure 2.5 - Geometry of the pinhole collimator of a gamma camera	47
Figure 2.6 - Planar images of phantom with thyroid insert acquired using a pinhole collimator	48
Figure 2.7 - Planar images of phantom with thyroid insert acquired using parallel hole LEHR collimator	49
Figure 2.8 - Example planar patient thyroid studies	50
Figure 2.9 - Spectrum of dual-isotope $^{99m}\text{Tc}/^{123}\text{I}$ acquisition showing offset energy windows	51
Figure 2.10 - Planar images of phantom with parathyroid insert acquired using a pinhole collimator	52
Figure 2.11 - Planar images of phantom with parathyroid insert acquired using a parallel hole LEHR collimator	52
Figure 2.12 - Example planar patient parathyroid studies	53
Figure 2.13 - Reconstructed SPECT images of thyroid phantom insert	55
Figure 2.14 - Reconstructed SPECT images of parathyroid phantom insert	56
Figure 2.15 - Subtraction SPECT images of parathyroid phantom insert	57
Figure 3.1 - Dual-isotope $^{99m}\text{Tc}/^{123}\text{I}$ acquisition spectrum showing overlapping photopeaks and standard ^{99m}Tc energy window	63
Figure 3.2 - Spectrum of dual-isotope $^{99m}\text{Tc}/^{123}\text{I}$ acquisition showing offset energy windows	63
Figure 3.3 - Example of typical planar parathyroid images from GRI	65
Figure 4.1 - Parathyroid SPECT image data in "Multimodality" display program ..	70
Figure 4.2 - Resultant subtraction image from "Multimodality" program	71
Figure 5.1 - Distribution of administered activities	78
Figure 5.2 - Unfiltered reconstructed parathyroid SPECT images	80
Figure 5.3 - Overly smoothed parathyroid SPECT images	80
Figure 5.4 - Overly sharp parathyroid SPECT images	81
Figure 5.5 - Parathyroid images acceptably filtered	82

Figure 5.6 - Subtraction SPECT images	82
Figure 5.7 - Bar chart of number of lesions seen	90
Figure 5.8 - Bar chart of lesions seen by each observer	90
Figure 5.9 - Bar chart of comparisons in number of lesions seen	118
Figure 5.10 - Bar chart of comparisons in expressed confidence level	119
Figure 5.11 - Bar chart of comparisons in given left/right lesion location.....	120
Figure 5.12 - Bar chart of comparisons in given overall lesion location.....	121
Figure 6.1 - Bar chart of differences in number of lesions	168
Figure 6.2 - Bar chart of comparisons in positive/negative findings.....	169
Figure 6.3 - Bar chart of comparisons in left/right locations	170
Figure 6.4 - Bar chart of comparisons in overall given location	171
Figure 7.1 - Comparison of lesions seen on first and second reviews of SPECT data.....	188
Figure 7.2 - Comparison of number of positive lesions seen when equivocal taken as negative and positive.....	199
Figure 7.3 - Comparison of number of same positive/negative reports when equivocal taken as negative and then positive	200
Figure 8.1 - Threshold VOI	217
Figure 8.2 - Seed ROI	218
Figure 8.3 - Threshold ROIs	219
Figure 8.4 - Hand-drawn ROI.....	219
Figure 8.5 - Typical thyroid and background ROIs	220
Figure 8.6 - Histogram of imaging time post injection.....	224
Figure 8.7 - Overly smoothed thyroid SPECT images	225
Figure 8.9 - Overly sharp thyroid SPECT images	226
Figure 8.10 - Best compromise thyroid SPECT images	226
Figure 8.11 - Uptake from SPECT versus uptake from planar images.....	229
Figure 8.12 - Difference in calculated uptake (P - S) versus acquisition time difference	229
Figure 8.13 - Uptake from frame SPECT versus uptake from planar images.....	230
Figure 8.14 - Difference in calculated uptake (P - FS) versus acquisition time difference	231
Figure 8.15 - Uptake from SPECT images versus uptake from frame SPECT image	232
Figure 8.16 - Uptake from AC SPECT images versus uptake from planar image.	233
Figure 8.17 - Uptake from AC SPECT images versus uptake from SPECT images	234
Figure 8.18 - Uptake from AC SPECT images versus uptake from frame SPECT image.....	235

Figure 8.19 - Uptake from SPECT images versus expected SPECT uptake from ICRP model	236
Figure 8.20 - Uptake from frame SPECT image versus expected uptake from ICRP model.....	237
Figure 8.21 - Uptake from AC SPECT images versus expected uptake from ICRP model.....	238
Figure 9.1 - Energy spectrum of ^{99m}Tc acquisition showing image and scatter correction acquisition windows	248
Figure 9.2- Measured uptake versus known uptake for phantom acquisitions...	250
Figure 9.3 - Plot of uptake from frame SPECT image versus uptake from planar image.....	253
Figure 9.4 - Plot of uptake from SPECT images versus uptake from planar image	254
Figure 9.5 - Plot of uptake from SPECT images versus uptake from frame SPECT image.....	255
Figure 9.6 - Plot of uptake from attenuation corrected SPECT images versus uptake from planar image.....	256
Figure 9.7 - Plot of uptake from attenuation corrected SPECT images versus uptake from frame SPECT image.....	257
Figure 9.8 - Plot of uptake from attenuation corrected SPECT images versus uptake from SPECT images.....	258

Acknowledgements

I would like to thank all the staff in the Department of Nuclear Medicine at Glasgow Royal Infirmary for their patience and assistance throughout the duration of this project. Particular thanks to the technical staff for helping acquire patient image data sets and giving me time to carry out phantom acquisitions in the busy clinical department, especially the Chief Technologist, Mrs Ann French, who also assisted in obtaining informed consent from patients when I was unavailable to do so. Also thanks to Mrs Carol Norwood for her assistance in obtaining patient case notes for review.

Special thanks to Dr J. Brian Neilly, Dr Fat Wei Poon, Dr Sai Han, Dr Glen G. Gardner and Dr Alison A. Bolster for taking the time to review many images as part of the parathyroid observer study. Also thanks to Dr. Toby Beveridge for his assistance in obtaining the results for the second observer review of the phase 2 dual-isotope subtraction SPECT parathyroid images.

I would also like to thank my advisor and Head of Department, Professor Alex T. Elliott for his advice and encouragement during the period of research.

Special thanks also to Dr Alison A. Bolster for her supervision of this project and her support and help in the preparation of this thesis.

Finally, I would like to say a special thank you to Mr Simon D. Dennis for his patience, encouragement and support throughout the study period and his assistance in producing images for this thesis.

Author's Declaration

I declare that this thesis represents my own work except where referenced to others.

I declare that this thesis does not include work forming part of a thesis presented successfully for another degree.

Jennifer Lucy Dennis

February 2011

Chapter 1 – Introduction

1.1 The Thyroid and Parathyroid Glands – Anatomy and Physiology

The thyroid and parathyroid glands form part of the body's endocrine system and produce hormones that provide important regulatory functions. Both types of gland are subject to disorders that can lead to either an increase or decrease in hormone levels within the body, and hence an imbalance in the regulatory function. Nuclear medicine imaging can be used to visualise the function of the thyroid and parathyroid glands in an attempt to assist in diagnosis, characterisation or localisation of such disorders.

1.1.1 The Thyroid Gland

The thyroid gland is located in the anterior aspect of the neck, lying over the anterior surface of the trachea (Martini, 2001). Figure 1.1 shows the typical size, shape and position of the gland, which is composed of two lobes - left and right - which are connected via a thin central isthmus. The thyroid gland produces thyroid hormones which are active in the regulation of overall metabolic rate within the cells of the body and so are vital for growth and mental development (Berne & Levy, 1993, Martini, 2001, Longmore *et al.*, 2007). The function of the thyroid gland is itself regulated by the secretion of thyroid stimulating hormone (TSH) from the pituitary gland, which is situated in the brain (Moore & Agur, 2007).

The thyroid is composed of a large number of follicles, consisting of rings of cells enclosing a follicular cavity, as shown in Figure 1.2. Thyroid hormones are synthesised and then stored in a colloid within the follicular cavities. When stimulated by TSH, the hormones are released into the blood stream and transported around the body, where they bind with receptors within cells (Berne & Levy, 1993, Martini, 2001). This then results in a variety of different metabolic actions depending on the target tissue.

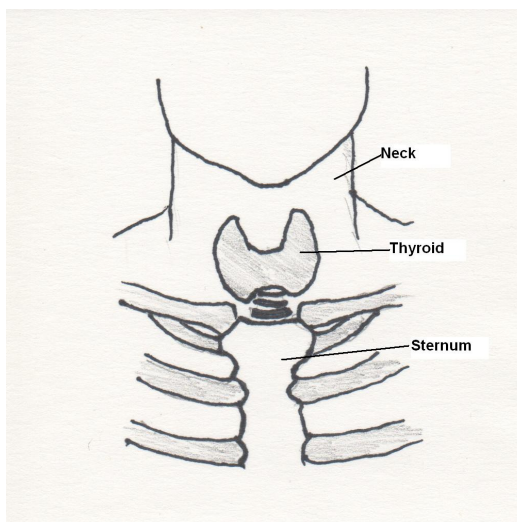


Figure 1.1 - Normal location of the thyroid gland
Diagrammatic view of the typical size, shape and position of the thyroid gland in the neck.

There are two main hormones produced and secreted by the thyroid gland - thyroxine (also known as T_4) and triiodothyronine (or T_3). T_4 accounts for approximately 90% of thyroid hormone production, with the remaining 10% being T_3 (Martini, 2001). Iodine is a key component of both T_3 and T_4 and so the thyroid actively concentrates around one-third of dietary iodine (Sharp *et al.*, 1998), although the exact proportion will vary depending on the amount of

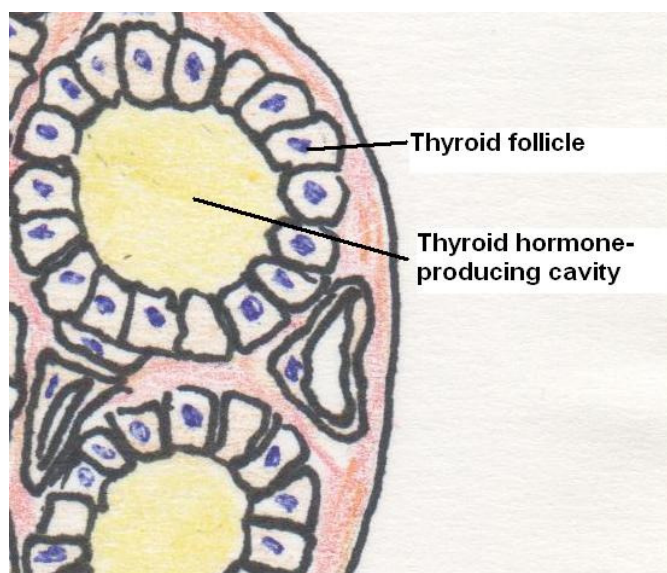


Figure 1.2 - Structure of the thyroid gland
Magnified diagrammatic view of the thyroid gland showing follicle cells surrounding the follicular cavities, within which thyroid hormones are synthesised and stored.

iodine in the diet. The thyroid will typically utilise $70\mu\text{g}$ - $80\mu\text{g}$ of iodine in the production of T_3 and T_4 on a daily basis (Berne & Levy, 1993). Production of thyroid hormones can be affected if there is a deficiency of dietary iodine,

although this is uncommon in developed countries. Excess iodine is primarily excreted in the urine via the kidneys (Martini, 2001).

Thyroid tissue may also be present in ectopic locations and can be found at any point between the anterior mediastinum and the base of the tongue (Sharp *et al.*, 1998), as shown in Figure 1.3. In most cases, normally functioning ectopic thyroid tissue causes no problems but it may on occasion be responsible for constriction of other tissues (e.g. the trachea) or difficulty in swallowing.

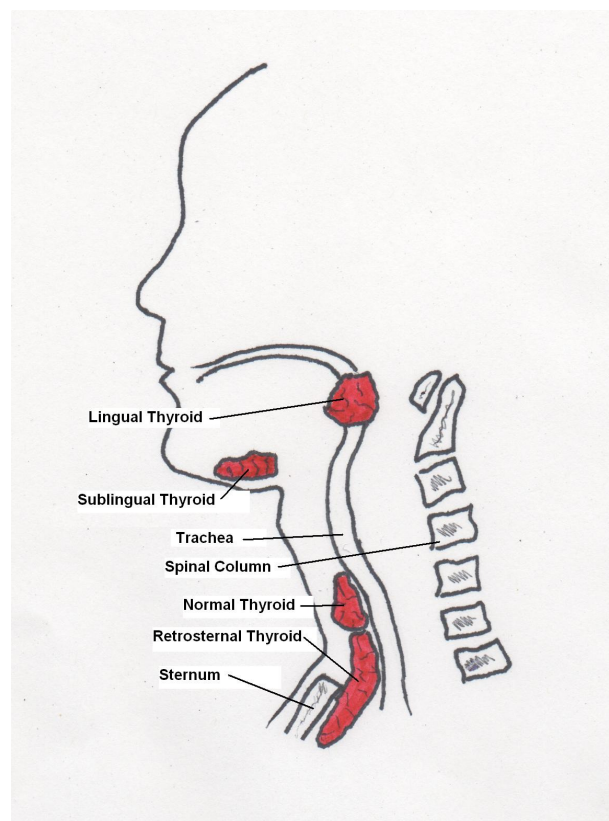


Figure 1.3 - Some potential ectopic locations for thyroid tissue
Thyroid tissue can be present throughout the neck and upper mediastinum.

Disorders of the thyroid gland related to increased or decreased production and secretion of thyroid hormones are discussed in Section 1.2.1 below.

1.1.2 The Parathyroid Glands

The parathyroid glands are very small and are usually located on the posterior surface of the thyroid, as shown in Figure 1.4. There are normally four glands in total, with two behind each thyroid lobe, one superior and one inferior (Moore & Agur, 2007) with a combined total mass of around 1.6g (Martini, 2001).

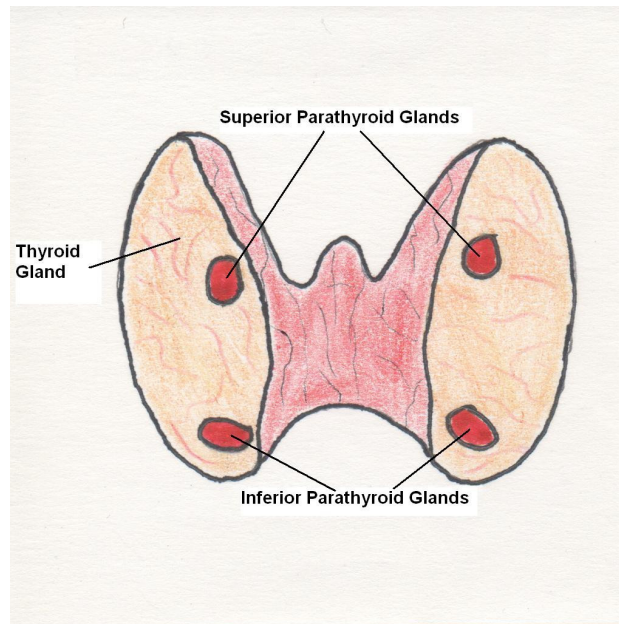


Figure 1.4 - Typical location of the parathyroid glands
Posterior view of the thyroid gland showing the normal positions of the four parathyroid glands – superior and inferior relative to each of the thyroid lobes.

However, it is relatively common for there to be any number between 2 and 6 glands (Moore & Agur, 2007) and for one or more to be located ectopically, away from the thyroid (Thomas & Wishart, 2003). Like the thyroid, parathyroid tissue can be found anywhere from the base of the tongue to the mediastinum, with the most common ectopic location being around the thymus (Sharp *et al.*, 1998). Some typical ectopic locations are shown in Figure 1.5.

The glands are composed of two types of cells: oxyphils and chief cells, the latter of which produce and secrete parathyroid hormone or parathormone (PTH). PTH is responsible for controlling the levels of calcium and phosphorus in the blood (Moore & Agur, 2007) and therefore helps to regulate serum calcium levels and maintain calcium and vitamin D homeostasis (Hindié *et al.*, 2009).

PTH is secreted by the parathyroids via a feedback mechanism in response to low serum Ca^{2+} levels. It acts by increasing osteoclast activity in the bones to increase release of Ca^{2+} and PO_4^{3-} from the bones to the bloodstream and increases reabsorption of Ca^{2+} in the kidney (Longmore *et al.*, 2007). Osteoblast activity within the bones is also inhibited, meaning that the rate of calcium deposition in bone is reduced (Martini, 2001).

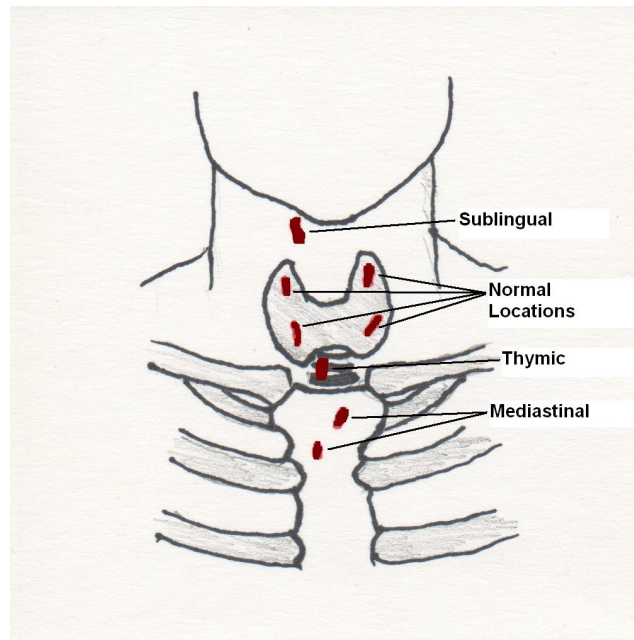


Figure 1.5 - Normal and ectopic locations of parathyroid glands
 Typical locations of ectopic parathyroid glands in the sub-lingual region, around the thymus and retrosternally in the mediastinum.

Increased or decreased production and secretion of PTH by the parathyroid glands will therefore lead to an imbalance in serum calcium levels. Such disorders and their resultant effects are discussed further in Section 1.2.2 below.

1.2 Disorders of the Thyroid and Parathyroid Glands

1.2.1 Disorders of the Thyroid Gland

There are a number of disorders that can affect the thyroid gland and the production of thyroid hormones. Such disorders are only rarely caused by the pituitary gland and its production of TSH and are almost exclusively due to problems within the thyroid gland itself (Longmore *et al.*, 2007). The result can be either underproduction (hypothyroidism) or overproduction (hyperthyroidism) of hormones.

Hypothyroidism can either be due to a developmental deficiency in the thyroid gland, which occurs in 1 in 4000-5000 live births (Robin, 1996), or acquired as the result of an autoimmune disorder (Besser *et al.*, 1994, Longmore *et al.*, 2007). The latter is common, occurring in 2-4% of the population as a whole

with an annual incidence of 2 per 1000 population (Besser *et al.*, 1994). The condition is a factor of 10 more common in middle aged women than in the rest of the population (Besser *et al.*, 1994). Other causes of hypothyroidism include a drug induced reduction in hormone levels or iodine deficiency (Berne & Levy, 1993, Longmore *et al.*, 2007). Secondary hypothyroidism as the result of other conditions also exists, although this is less common (Longmore *et al.*, 2007).

The lower than normal metabolic rate that occurs as a result of hypothyroidism results in weight gain, a lowering of body temperature, tiredness, lethargy and a dislike of cold, amongst other symptoms (Berne & Levy, 1993, Longmore *et al.*, 2007). Significant retardation in growth and rate of development occur in infants suffering from untreated hypothyroidism (Berne & Levy, 1993).

Hypothyroidism is easy to treat and is normally treated medically with thyroxine (T₄), which ensures an adequate supply of thyroid hormone within the body (Berne & Levy, 1993, Longmore *et al.*, 2007). Symptoms can quickly resolve with adequate treatment.

Hyperthyroidism has a similar incidence in the adult population as hypothyroidism at 1.8% and is again around 10 times more common in middle-aged women (Besser *et al.*, 1994). There are several possible causes of hyperthyroidism, with the most common being Graves' disease, which is hyperplasia (an increase in the total number of cells) of the entire gland as a result of an autoimmune disorder. Benign tumours or adenomas within the thyroid can also result in an oversecretion of thyroid hormones, whilst inflammation of the gland is much less common but can, on occasion, lead to hyperactivity of the gland (Berne & Levy, 1993). Toxic multinodular goitre is a condition characterised by thyroid nodules that secrete active thyroid hormones and is most commonly seen in the elderly and in people with iodine-deficient diets. Thyrotoxicosis is the clinical and biochemical effect of excess thyroid hormone due to hyperthyroidism (Longmore *et al.*, 2007).

Symptoms of hyperthyroidism include weight loss despite increased appetite, heat intolerance, sweating, irritability, frenetic activity & psychosis, amongst others. Protruding eyes and goitre (swelling of the thyroid) are also common in Graves' disease (Berne & Levy, 1993, Martini, 2001, Longmore *et al.*, 2007).

Hyperthyroidism can be treated medically with drugs to block the synthesis of thyroid hormones, but is most effectively treated by surgery (partial or total thyroidectomy) or radionuclide therapy with iodine-131 (Berne & Levy, 1993). The last option makes use of the iodine concentrating properties of the thyroid and the beta emissions from the radioactive iodine-131, resulting in cellular damage and a corresponding reduction in the total number of active thyroid cells, leading to a reduction in thyroid hormone synthesis and secretion (Sharp *et al.*, 1998). There is no evidence of increased cancer risk in patients who undergo iodine-131 therapy, although patients commonly experience post-treatment hypothyroidism, which can be treated in the same way as other forms of hypothyroidism, which is discussed above (Longmore *et al.*, 2007).

1.2.2 Disorders of the Parathyroid Glands

In the same way as for the thyroid gland, disorders of the parathyroids can lead to either under- or overproduction of PTH and hence hypo- or hyperparathyroidism. Diagnosis of a parathyroid disorder is biochemical (Coakley, 2003, Hindié *et al.*, 2009), in that levels of calcium and PTH in the blood are increased or decreased abnormally.

Hypoparathyroidism is by far the less common of the two and results in low serum calcium levels. In many cases the cause is uncertain, but the condition can be primary, in which case it is an autoimmune disorder (Longmore *et al.*, 2007), or secondary in that it develops after thyroidectomy if the parathyroid glands are removed with the thyroid or have their blood supply restricted. The main symptoms involve the muscles and the nervous system, which become more excitable in response to the low calcium levels and this can lead to dangerous spasms (Martini, 2001). Due to the lack of availability of parathyroid hormone, treatment for hypoparathyroidism tends to be via calcium supplements in conjunction with vitamin D to promote calcium absorption (Berne & Levy, 1993, Martini, 2001).

Much more prevalent is hyperparathyroidism which is characterised by high levels of PTH and calcium in the blood. There are two main and distinct forms of hyperparathyroidism. Primary hyperparathyroidism is the result of a benign or malignant tumour of one or more glands. Involvement of one gland in benign

disease is usually known as an adenoma, whilst if multiple glands are involved, the patient is said to have parathyroid hyperplasia. The rare malignant disease is termed parathyroid carcinoma (Sathe *et al.*, 2009). Secondary hyperparathyroidism occurs in patients with chronic renal failure when the amount of PTH secreted by the parathyroids is increased in response to the failure of the hormonal regulation provided by the kidneys. Another commonly acknowledged form of hyperparathyroidism is tertiary hyperparathyroidism. This occurs after prolonged secondary hyperparathyroidism, when the hormone feedback mechanism fails and the parathyroid glands begin to act autonomously (Longmore *et al.*, 2007).

The prevalence of primary hyperparathyroidism within the population is ~1 in 1000 which increases with age and the condition is 3 times more common in women than in men (Robin, 1996). Approximately 85% of patients with hyperparathyroidism have an adenoma, 12% have hyperplasia and 3% have carcinoma (Hall & Evered, 1990, Thomas & Wishart, 2003, Longmore *et al.*, 2007). Primary hyperparathyroidism is often asymptomatic, with raised serum Ca^{2+} being noted on routine blood tests for other pre-existing conditions. Symptoms can include weakness, tiredness, depression, renal stones and osteoporosis.

The only curative treatment for hyperparathyroidism is surgical excision of the adenoma or hyperplastic glands (Thomas & Wishart, 2003). However, in mild and asymptomatic cases, surgery may not be merited and patients can be medically managed (Longmore *et al.*, 2007). Parathyroidectomy surgery offers a long-term cure in more than 95% of cases (Rodgers *et al.*, 2008) but complications include hypoparathyroidism and damage to the recurrent laryngeal nerve in the neck (Longmore *et al.*, 2007). Surgery for hyperplasia often requires complete removal of the parathyroid glands from the neck followed by autotransplantation of a small amount of tissue, normally in the lower arm (Sathe *et al.*, 2009) or, as is the case in Glasgow, the thigh.

The standard surgical technique used by endocrine surgeons for many years was to perform bilateral surgery, whereby the entire thyroid area was exposed and all parathyroid glands were located. Those glands visually suggestive of adenoma or hyperplasia were then removed.

However, in recent years it has been noted that bilateral surgery may not be necessary in all cases due to the high incidence of single gland disease (Russell *et al.*, 2006). There has therefore been a trend away from bilateral exploration towards unilateral and minimally invasive techniques (Greene *et al.*, 2009). In order to successfully perform such techniques, some localisation of the parathyroid adenoma or hyperplastic glands is necessary. This can be performed using pre-operative imaging, which is discussed in detail in Section 1.3.2 below, or by radioguided surgery with a gamma probe in theatre (Cayo & Chen, 2008) after intravenous injection of a radioactive substance which localises in parathyroid tissue. Intra-operative PTH assay can then be used to confirm removal of the overactive parathyroid tissue (Longmore *et al.*, 2007) by detecting the rapid reduction in serum PTH levels. Post-surgical follow-up for patients then includes regular biochemical analysis of blood samples to ensure that PTH and calcium levels revert to being within the normal range.

1.3 Imaging of the Thyroid and Parathyroid Glands

1.3.1 Thyroid Imaging

Imaging is frequently used in the assessment of thyroid disorders in order to provide more detailed information on the type of disease and to assist the clinician in deciding the most appropriate course of treatment. The thyroid is most commonly imaged with ultrasound (US) or nuclear medicine scintigraphy (NM), although X-ray computed tomography (CT) and magnetic resonance imaging (MRI) are occasionally used for anatomical thyroid imaging (Meller & Becker, 2002). US provides anatomical imaging, showing the overall morphology of the gland and any nodules or cysts present. In contrast, NM allows the acquisition of functional images, showing the parts of the thyroid that are more or less active than others.

The main use of US is to determine the presence and type of thyroid nodules. It can distinguish between cystic and solid nodules, the former of which are usually benign and the latter of which may be malignant (Longmore *et al.*, 2007). However, US cannot be used in the assessment of retrosternal or mediastinal thyroid tissue due to its inability to image through bone. Further assessment can

then be undertaken using fine needle aspiration (FNA) of any suspicious nodules, giving a definitive diagnosis of benign or malignant disease.

Early NM studies of the thyroid took advantage of the known fact that the thyroid concentrates iodine, by utilising the radioactive isotope ^{131}I as an intravenous injection of ^{131}I -iodide. However, the high energy gamma emission of ^{131}I (364keV) is not ideal for gamma camera imaging and the coexisting beta emissions result in a high radiation dose (Sharp *et al.*, 1998, Meller & Becker, 2002). The main use of ^{131}I was in determining the uptake of the thyroid gland - that is, the percentage of injected iodine present in the thyroid after a set period of time, giving an indication of the overall activity of the thyroid - rather than for imaging. Further details of the process of calculating thyroid uptake are given in Chapter 8 of this thesis and no further discussion will be included here.

An alternative isotope of iodine, ^{123}I , has a more suitable gamma emission energy for imaging at 159keV and has no beta emission, meaning that the radiation dose is considerably reduced and image quality is markedly improved. Images using ^{123}I -iodide are of good quality with low background and an assessment of thyroid uptake can be made from the images. The main drawback of using ^{123}I is the considerable cost due to the isotope being cyclotron produced.

It has been discovered, however, that the pertechnetate ion (TcO_4^-) is also concentrated by the thyroid in much the same way as iodine - a very useful fact given that the isotope $^{99\text{m}}\text{Tc}$ is the most commonly used radionuclide for NM imaging, meaning that good quality images can be obtained at relatively low cost. Indeed, pertechnetate seems to have a very similar distribution throughout the body as iodine, although the quantitative uptake in tissue is lower (Andros *et al.*, 1965, Hays & Berman, 1977). The thyroid to background ratio is therefore lower than with isotopes of iodine (Shimmins *et al.*, 1969) but is sufficiently good to provide useful clinical information for the management of patients with thyroid disease.

Pertechnetate images can also be used for the calculation of thyroid uptake. However, since pertechnetate is not organified by the thyroid - that is, pertechnetate is not incorporated into thyroid hormones - the measurement

does not give a true indication of thyroid uptake. Nevertheless, pertechnetate uptakes can still be useful in determining the presence of hypo- or hyperthyroidism if a normal range for the population under consideration is established (Shimmins *et al.*, 1968, Esser *et al.*, 1973).

NM scanning with either ^{99m}Tc -pertechnetate or ^{123}I -iodide is useful for determining the causes of hyperthyroidism and the status of nodules as “hot” or “cold” in reference to the relative accumulation of radiopharmaceutical. Around 20% of cold nodules are malignant whereas few neutral and almost no hot nodules are malignant so the uptake status of a suspicious nodule is very important (Longmore *et al.*, 2007). Retrosternal goitre, ectopic thyroid tissue and thyroid metastases can also be detected using NM imaging, although ^{123}I -iodide imaging is often more useful than ^{99m}Tc -pertechnetate in these circumstances due to the higher thyroid to background ratio. However, most nuclear medicine departments primarily use ^{99m}Tc -pertechnetate routinely for thyroid imaging and uptake measurements as it is cheaper and more readily available than ^{123}I -iodide, which can normally only be obtained on certain days of the week whilst ^{99m}Tc -pertechnetate will be available on a daily basis.

NM functional imaging normally takes the form of planar imaging with an uptake measurement, although 3-dimensional SPECT imaging can sometimes be used, as discussed in detail in Section 1.5.1 below. Planar images can be acquired using either a pinhole collimator, which produces a magnified image of the gland but is subject to geometrical distortions due to the effects of parallax, or a parallel hole collimator with software zoom, which gives a better sensitivity in terms of counts/s/MBq. The exact technique employed is a matter of preference for the imaging centre.

1.3.2 Parathyroid Imaging

Imaging of the parathyroids is not used to diagnose disease as this is performed using biochemical analysis of blood samples. However, imaging can be used to assist the endocrine surgeon in localising the abnormal gland or glands prior to surgery (Coakley, 2003, Hindié *et al.*, 2009) in patients with hyperparathyroidism. In general, parathyroid glands of normal size are too small to be resolved on imaging and only adenomas or hyperplastic glands can be

visualised (Sandler & Patton, 1987). For this reason, imaging is not routinely carried out in cases of hypoparathyroidism, as no further useful clinical information can be gained.

As for the thyroid, various imaging modalities can be utilised for parathyroid localisation including US, NM, CT and MRI, although once again US and NM are most commonly used. CT tends to have a lower sensitivity for detection of normally located parathyroid adenomas than the other modalities (Moinuddin & Whynott, 1996, Peeler *et al.*, 1997), although it can be useful for detecting ectopic mediastinal adenomas (Sandler & Patton, 1987, Beierwaltes, 1991). MRI is particularly useful for mediastinal imaging (Sandler & Patton, 1987) and has been demonstrated to have a sensitivity similar to or slightly lower than US and NM at between 55% and 80% (Moinuddin & Whynott, 1996, Peeler *et al.*, 1997, Ishibashi *et al.*, 1998, Hänninen *et al.*, 2000, Wakamatsu *et al.*, 2001, Saeed *et al.*, 2006) but is limited by high cost and low specificity due to being unable to differentiate between parathyroid adenomas and thyroid disorders (Beierwaltes, 1991).

Enlarged parathyroid glands can be readily visualised on US as they tend to be hypoechoic with respect to the surrounding tissues (Sandler & Patton, 1987) and the technique has the advantages of being low cost and not using ionising radiation (Mariani *et al.*, 2003). However, the sensitivity of US varies due to the fact that it is very operator dependent (Rodgers *et al.*, 2008) and it is particularly ineffective at detecting ectopic glands in the mediastinum (Beierwaltes, 1991, Carlier *et al.*, 2008). Despite this, the sensitivity of US imaging by an experienced operator can be high, with values around 75% being quoted in the literature (e.g. Ishibashi *et al.*, 1998, Tublin *et al.*, 2009), although values as low as 38-45% have been found (Hewin *et al.*, 1997, Peeler *et al.*, 1997), clearly demonstrating the high operator dependence of the technique.

The main advantage of NM imaging over the other modalities is that it represents the function of the parathyroid tissue, rather than the visual anatomy, meaning that hyperactive glands can be distinguished from normally functioning tissue. However, no single radiopharmaceutical exists that is localised only to parathyroid tissue - in every case there is simultaneous uptake in the thyroid

gland so a variety of different techniques have been employed to visualise and localise parathyroid adenomas and hyperplastic glands.

Early attempts at parathyroid imaging in NM involved the use of methionine, which had been shown to concentrate in the parathyroid glands (DiGiulio & Beierwaltes, 1964). The methionine was labelled with the radioisotope ^{75}Se and the neck was scanned using a scintillation detector or gamma camera to determine any areas of increased uptake (DiGiulio & Beierwaltes, 1964, Haynie *et al.*, 1964, Ashkar *et al.*, 1971). Although the results were encouraging with several successful localisations reported, the high radiation dose due to the long half-life of ^{75}Se (119.8 days) (ICRP, 1988, Delacroix *et al.*, 2002) meant that only small activities could be administered to patients, resulting in poor image quality and the technique was soon superseded.

Attempts were then made to localise parathyroid adenomas using ^{67}Ga -citrate, with some level of success (Bekerman *et al.*, 1977, Cann & Prussin, 1980), but the first technique used widely was that of ^{201}Tl -thallous chloride/ $^{99\text{m}}\text{Tc}$ -pertechnetate subtraction imaging (Sharp *et al.*, 1998). The ^{201}Tc -thallous chloride is taken up in both the thyroid and parathyroid tissues, whilst the $^{99\text{m}}\text{Tc}$ -pertechnetate is only taken up in the thyroid, meaning that subtraction imaging can be performed to visualise only the uptake in the parathyroids. The method commonly used was to inject the ^{201}Tc -thallous chloride and acquire an image of the neck area. The $^{99\text{m}}\text{Tc}$ -pertechnetate would then be injected and a corresponding image of its distribution acquired. This second image could then be subtracted digitally from the first, removing the thyroid from the image and leaving only the activity in the parathyroid glands. In order to ensure correct image registration and prevent artefacts in the subtraction image, however, it was necessary to immobilise the patient throughout the imaging procedure (Sharp *et al.*, 1998). A slight variation on this method involved the use of ^{123}I -iodide as the thyroid imaging agent, giving a better thyroid to background ratio, although the overall procedure did not vary significantly from that described above (Pattou *et al.*, 1998, O'Doherty & Kettle, 2003).

In the early 1990s, a new cardiac imaging agent called $^{99\text{m}}\text{Tc}$ -Sestamibi (MIBI) was introduced which was soon demonstrated have a similar distribution in man to thallous chloride and therefore to concentrate in the thyroid and parathyroid

glands (Bristol-Myers Squibb, 2005). The uptake mechanisms of MIBI remain uncertain (Hung *et al.*, 2003) but the fact that it is labelled with ^{99m}Tc makes it more attractive for imaging studies than ^{201}Tl . At present, there is no definitive protocol for imaging of parathyroids using ^{99m}Tc -Sestamibi, with two main methods commonly employed (Hindié *et al.*, 2009).

The first of these methods takes advantage of the fact that MIBI has been shown to demonstrate differential washout from the parathyroids with respect to the thyroid gland (Taillefer *et al.*, 1992) and is named the dual-phase technique. Images are taken at around 15 minutes and 2 hours post-injection of MIBI, with a parathyroid adenoma or hyperplastic gland being more easily visualised on the later image due to the delayed MIBI washout. This technique has been employed successfully by a number of groups, showing increased sensitivity over imaging with ^{201}Tl (Rauth *et al.*, 1996, Peeler *et al.*, 1997, Wakamatsu *et al.*, 2001, Erbil *et al.*, 2006). However, problems have also been demonstrated in that the differential washout does not appear to be universal (Bénard *et al.*, 1995, Calendini-Viallet, 1997, Krausz *et al.*, 2001) and some thyroid adenomas can preferentially retain MIBI relative to the rest of the thyroid, giving false-positive results (Kresnik *et al.*, 1997).

The second method in widespread use utilises dual-isotope subtraction imaging in much the same way as with ^{201}Tl with either ^{99m}Tc -pertechnetate or ^{123}I -iodide used as the thyroid imaging agent. MIBI/pertechnetate subtraction requires consecutive imaging of the two agents as the same radionuclide is used in both. The ^{99m}Tc -pertechnetate is administered first, followed by imaging of the thyroid. An administration of perchlorate can be used to wash the pertechnetate out of the thyroid prior to injection of the ^{99m}Tc -Sestamibi (Gallowitsch *et al.*, 1997, Rubello *et al.*, 2000). The MIBI distribution is then imaged, with the patient requiring to be immobilised throughout the procedure to prevent misregistration artefacts in the subsequent subtraction image. In contrast, the MIBI/iodide subtraction technique uses two different radionuclides with different gamma emission energies (140keV and 159keV respectively). Dual-isotope image acquisition is therefore possible resulting in reduced imaging time (Hindié *et al.*, 1998). However, there is a significant cost implication in using ^{123}I , as has been discussed for thyroid imaging above, and so the cheaper pertechnetate subtraction remains common.

Comparisons have been carried out between the dual-phase and dual-isotope techniques, with a better sensitivity in correctly localising parathyroid lesions with dual-isotope imaging reported by several groups (Hindié *et al.*, 1998, Leslie *et al.*, 2002, Wakamatsu *et al.*, 2003). Also, one of the most common reasons for failed localisation and hence the requirement for bilateral neck exploration is the presence of concomitant thyroid disease, such as multinodular goitre (Gallowitsch *et al.*, 1997, Casara *et al.*, 2001, Gates *et al.*, 2009), meaning that an assessment of the thyroid can be very useful for the surgeon. However, the dual-phase technique remains popular with many centres finding satisfactory results with the method.

Another cardiac imaging agent that has been investigated for use in parathyroid imaging is ^{99m}Tc -Tetrofosmin. This agent has similar characteristics to ^{99m}Tc -Sestamibi but does not display differential washout and so subtraction imaging is required (Fjeld *et al.*, 1997, Gallowitsch *et al.*, 1997 & 2000, Fröberg *et al.*, 2003). Its use in parathyroid imaging is, however, not widespread and the product is not licensed for parathyroid imaging in the UK (personal communication, Dot Robinson, GE Healthcare).

As is the case for thyroid imaging (see Section 1.3.1 above), most NM parathyroid imaging is carried out using planar techniques. Also, there is the option to use either a pinhole or parallel hole collimator. Some groups have found an increased sensitivity for detecting parathyroid adenomas with a pinhole collimator (Takamiya *et al.*, 2004, Tomas *et al.*, 2008), but its use remains a matter of preference for the imaging centre. Three-dimensional SPECT imaging with ^{99m}Tc -Sestamibi has also been investigated in an attempt to increase both the sensitivity and the spatial information provided for preoperative localisation, and this is discussed in detail in Section 1.5.2 below.

One final imaging method is available for the localisation of parathyroid adenomas and hyperplastic glands. Positron emission tomography (PET) is becoming more widely available and it provides an opportunity to once again image the parathyroid glands with methionine, although for PET it is labelled with ^{11}C rather than with ^{75}Se . Several studies have been carried out to assess the clinical utility of ^{11}C -methionine, finding sensitivities of between 50% and 85% (Sundin, *et al.*, 1996, Otto *et al.*, 2004, Beggs & Hain, 2005, Rubello *et al.*,

2006, Herrmann *et al.*, 2009). However, standard NM techniques with ^{99m}Tc -Sestamibi remain in more common usage due to the wider availability of gamma cameras.

1.4 Nuclear Medicine SPECT Imaging

Traditionally, nuclear medicine imaging has been a planar technique, producing images that are a 2-dimensional projection of the 3-dimensional distribution of radiopharmaceutical within the patient. Single photon emission computed tomography (SPECT) is a technique that allows reconstruction of images in multiple planes. The gamma camera rotates around the patient, acquiring a number of frames at different projection angles. A computer is then used to reconstruct these frames to produce a full 3-dimensional image data set (Sharp *et al.*, 1998). Theoretically, an infinite number of projections are required to reconstruct the true distribution of activity within the patient, but a good estimate can still be obtained with a limited number of projections (Bruyant, 2002).

SPECT does not give improved resolution over planar imaging. However, the contrast is markedly improved due to the separation of activity in overlying and underlying structures which is not possible in planar imaging (Sharp *et al.*, 1998, Wagner *et al.*, 1999, Bruyant, 2002). Theoretically, acquisition of projection data over only 180° is required as opposing projections contain the same image information. However, due to the fact that there is an inherent loss of resolution with depth in nuclear medicine imaging and that the gamma photons may be differentially attenuated by different sides of the body, opposing projections are in reality different, which means that 360° of data is often acquired. For imaging of structures close to one surface of the body, the use of 360° of projection data in reconstructing SPECT images can simply lead to an unacceptable increase in the noise level. For example, the thyroid lies close to the anterior surface of the neck and will be poorly visualised in the posterior projections, which would add noise and little useful information to the reconstructed images. In these cases, 180° of acquired projection data is sufficient to produce an acceptable SPECT reconstruction of the activity distribution in the structure of interest (Wagner *et al.*, 1999).

There are various possible mathematical methods of reconstructing the 3-dimensional images from the projection data. For many years, the most commonly used technique was filtered back projection (FBP), the mathematics of which was first described in the 1960s (Bracewell & Riddle, 1967). This method is described in detail elsewhere (e.g. Sharp *et al.*, 1998) and so no further discussion will be given here. FBP is computationally relatively simple and hence reconstruction times are fast, but significant artefacts can be introduced to the images, particularly around areas of very high or low count densities where streaks occur. The reconstructed images also require to be filtered in order to reduce blurring artefacts and high background noise levels, but this leads to a compromise between spatial resolution and noise, as noise is represented by high spatial frequencies (Sharp *et al.*, 1998, Bruyant, 2002).

The last 10 years or so has seen a significant improvement in the processing capabilities of computers, meaning that other more computationally demanding reconstruction methods have become viable. The most commonly implemented of these are the iterative methods, such as Maximum Likelihood Expectation Maximisation (MLEM) or the related Ordered Subsets Expectation Maximisation (OSEM) (Sharp *et al.*, 1998, Bruyant, 2002, Takahashi *et al.*, 2003). These methods involve beginning with an assumed activity distribution (such as a uniform distribution with all pixels having the same value) which would give a certain estimated set of projection images. The actual acquired projection data are compared to the estimated values by taking the ratio of measured to estimated counts and the original estimate is then updated to account for these differences. The whole process is then repeated and the estimated activity distribution becomes closer to the true activity distribution with each iteration. The process converges to a solution whereby the change in the estimated activity between successive iterations is minimal (Bruyant, 2002).

Iterative techniques tend to result in fewer image artefacts and can give accurate estimates of the true activity distribution with a smaller number of projection images than are required for filtered back projection (Takahashi *et al.*, 2003). Improved spatial resolution and increased lesion detection over FBP images have also been reported (Shepp & Vardi, 1982, Tourassi *et al.*, 1991, Moka *et al.*, 2000a, Brambilla *et al.*, 2005).

Various corrections can be made to SPECT data either before, during or after reconstruction in order to increase the accuracy of the final image data set. These include scatter correction, cross-talk correction, distortion corrections and, most commonly, attenuation correction (AC). Performing AC aims to reduce the dependency of the number of counts recorded on the depth of the origin of the photons within the patient. There are several different AC methods available (Walters *et al.*, 1981, Webb *et al.*, 1983, Sharp *et al.*, 1998), which range from a linear correction method which assumes that the attenuation throughout the patient volume is entirely uniform, to the acquisition of an X-ray computed tomography (CT) image, which is used to produce a map of the actual attenuation at all points in the image. All of these corrections can be incorporated into an iterative reconstruction algorithm, whereas FBP requires the various corrections to be made either pre- or post-reconstruction (Bruyant, 2002).

SPECT studies are most often acquired using a parallel hole collimator, but it is possible to perform pinhole SPECT. The main difficulty with the use of the pinhole collimator is the introduction of geometrical distortions in the projection images due to parallax (Mavai & Caride, 1996). Standard reconstruction algorithms are not designed to deal with such cone beam data and so special algorithms must be used (Wanet *et al.*, 1996, Vanhove *et al.*, 2000). Slight changes in the relative angle of the collimator to the area of interest have been shown to result in significant distortions in the final reconstructed images (Mavai & Caride, 1996). The method is therefore not commonly used in routine practice.

Over the last few years, there has been an increase in the use of SPECT/CT systems, which allow the acquisition of fully registered SPECT and X-ray CT images. A single gantry supports both a double headed gamma camera and a CT scanner. The patient first undergoes a SPECT scan and then, without the patient moving, the imaging couch is moved into the CT scanner and an X-ray CT of the same area is taken. Registered functional and anatomical images can therefore be acquired together as well as allowing CT attenuation maps to be used in the attenuation correction of the SPECT images.

1.5 SPECT of the Thyroid and Parathyroid Glands

1.5.1 Thyroid SPECT

SPECT imaging is not commonly used in the assessment of thyroid disorders, although it has been shown to be useful on occasion (Chen *et al.*, 1988, Wanet *et al.*, 1996, Krausz *et al.*, 1997). In particular, SPECT has been shown to allow visualisation of cold nodules which are not seen on planar imaging due to high levels of surrounding activity (Chen *et al.*, 1988, Krausz *et al.*, 1997). However, ultrasound imaging offers good visualisation of thyroid nodules without the use of ionising radiation and so is often the preferred imaging tool for clinicians.

Thyroid SPECT has most often been used in the estimation of thyroid volume (e.g. Chen *et al.*, 1988, Wanet *et al.*, 1996, Zaidi, 1996, van Isselt *et al.*, 2003, Pant *et al.*, 2003), which is useful as an aid to determining a suitable therapeutic ^{131}I -iodide activity to administer to a patient with hyperthyroidism. SPECT has been shown to be considerably superior to planar imaging for volume measurements, but shows no significant improvement over ultrasound methods (Zaidi, 1996, van Isselt *et al.*, 2003, Pant *et al.*, 2003).

In summary, thyroid SPECT can be useful in certain circumstances but is not used routinely in many imaging centres.

1.5.2 Parathyroid SPECT

The use of SPECT in parathyroid imaging is becoming more widespread, although it is by no means a universally accepted technique (Pattou *et al.*, 1998, Hindié *et al.*, 2009). There is a large amount of published data relating to the use of single-isotope $^{99\text{m}}\text{Tc}$ -Sestamibi SPECT (Billotey *et al.*, 1996a & 1996b, Torres *et al.*, 1996, Chen *et al.*, 1997, Moka *et al.*, 2000b, Lorberboym *et al.*, 2003, Schachter *et al.*, 2004, Spanu *et al.*, 2004, Slater & Gleeson, 2005, Ansquer *et al.*, 2008, Carlier *et al.*, 2008, Ho Shon *et al.*, 2008, Nichols *et al.*, 2008, Thomas *et al.*, 2009) with most studies demonstrating an increase in sensitivity in the detection and localisation of parathyroid adenomas over planar imaging. MIBI SPECT has been shown to be particularly effective in localising ectopic

parathyroid adenomas (Billotey *et al.*, 1996a, Lorberboym *et al.*, 2003) as well as being more sensitive than ultrasound imaging (Quiros *et al.*, 2004).

Despite the widespread use of planar subtraction imaging, only one group, led by Donald R. Neumann and based in Cleveland, Ohio, has published data on the use of dual-isotope subtraction SPECT for localising parathyroid adenomas. The group's various papers on the topic (Neumann *et al.*, 1997b, 1998, 2000, 2008) have demonstrated that dual-isotope subtraction SPECT is superior to single-isotope ^{99m}Tc -Sestamibi SPECT and is a clinically useful imaging technique.

In the same way as for thyroid imaging, it is possible to carry out pinhole SPECT for parathyroid disorders, which has been shown to give increased sensitivity over planar imaging (Profanter *et al.*, 2003). However, the same issues with geometric distortions in the images and the requirement to use cone beam reconstruction algorithms affect parathyroid pinhole SPECT as they do for thyroid pinhole SPECT (see Section 1.5.1 above).

SPECT/CT is not yet commonly used for either thyroid or parathyroid imaging. However, the literature suggests (Even-Sapir *et al.*, 2001, Gayed, *et al.*, 2005, Krausz, *et al.*, 2006, Lavelly *et al.*, 2007, Neumann *et al.*, 2008, Papathanassiou *et al.*, 2008, Akram *et al.*, 2009) that it may be particularly useful in parathyroid imaging for patients who have had previous neck surgery or have one or more ectopically located parathyroid adenomas.

1.6 Study Aims

The aims of this study involve the assessment of the use of SPECT imaging in thyroid and parathyroid disorders using both phantom and patient data.

Firstly, it aims to assess the clinical utility of ^{99m}Tc -Sestamibi/ ^{123}I -iodide dual-isotope subtraction SPECT imaging for localisation of hyperactive parathyroid glands. This will be achieved by performing dual-isotope scans using a custom designed and built thyroid/parathyroid phantom to determine suitable imaging and SPECT reconstruction and analysis parameters followed by an observer study reviewing dual-isotope subtraction SPECT patient data sets.

Secondly, this study aims to assess the possibility of performing thyroid uptake measurements from ^{99m}Tc -pertechnetate SPECT acquisitions. As for the parathyroid study, the new thyroid/parathyroid phantom will be used to determine appropriate imaging and SPECT reconstruction parameters as well as a method for calculating the uptake from these images. These methods will then be applied to patient data and the results compared with those for the standard uptake measurement from planar images.

A detailed description of the phantom custom designed and built for this study and the work carried out using it is given in Chapter 2 of this thesis. Chapters 3 - 7 then describe the parathyroid observer study and discuss the findings in relation to work carried out by other groups. Finally, Chapters 8 & 9 describe the work on calculation of thyroid uptake from SPECT images using both patient and phantom image data.

Chapter 2 – Design, Construction and Use of a Dedicated Thyroid and Parathyroid Phantom

2.1 Introduction

Phantoms have been used in nuclear medicine imaging for many years to simulate a patient during image acquisition. A phantom is generally made of a tissue-equivalent material and can be filled with a radioactive substance repeatedly to test imaging or analysis parameters without the need to expose a person to radiation via intravenous injection, inhalation or ingestion. They also provide consistent imaging conditions in terms of their attenuation properties and the relative distances between particular points, which are difficult to obtain reproducibly with human subjects. The resultant reproducibility of acquired images means that phantoms are particularly useful in quality assurance of imaging systems.

Information on the attenuation and scatter properties of various human tissues and tissue substitutes can be found in a report by the International Commission on Radiation Units and Measurements (ICRU, 1989).

This study concentrated on the use of single photon emission computed tomography (SPECT) imaging of the thyroid and parathyroid glands, which has not been routine practice in the Nuclear Medicine department at Glasgow Royal Infirmary (GRI). In order to ensure that suitable acquisition parameters for the SPECT data were in place prior to any participants undergoing imaging, it was decided that a new thyroid/parathyroid phantom would be created so that different parameters could be tested and a suitable protocol established. The phantom would simulate the neck area and would be capable of providing imaging conditions similar to those of patient thyroid and parathyroid studies.

2.2 Materials and Methods

2.2.1 Design and Construction of a Thyroid/Parathyroid Phantom

In 1975, the International Commission on Radiological Protection (ICRP) published a report giving information on “Reference Man” (ICRP, 1975). This report brought together large quantities of published data on the typical anatomy, physiology and metabolism of humans. It then defined the various characteristics of a “Reference Man” that can be used for calculations of radiation dose to a reference individual such that comparisons of results from different types of exposure can easily be made. The information in this report was used as the basis for the design of the thyroid/parathyroid phantom for this study such that the phantom would give a good representation of a standard patient.

The phantom was designed so that it could be manufactured from Perspex (polymethylmethacrylate) and filled with water, both of which have attenuation properties similar to soft tissue for the 140keV gamma photons of ^{99m}Tc and the 159keV gamma photons of ^{123}I (ICRU, 1989), which were the isotopes to be used for this study. At 140keV, the linear attenuation coefficient (μ) of soft tissue is 0.159cm^{-1} (ICRU, 1989), whilst for water $\mu=0.155\text{cm}^{-1}$, and for Perspex $\mu=0.178\text{cm}^{-1}$ (Hubbell & Seltzer, 1996). At the 159keV photon energy of ^{123}I , the linear attenuation coefficients of soft tissue, water and Perspex are $\mu=0.153\text{cm}^{-1}$, $\mu=0.148\text{cm}^{-1}$ and $\mu=0.171\text{cm}^{-1}$, respectively. It was also important that the phantom could easily be opened and closed with a watertight seal so that radioactive liquids could be introduced to the water chambers repeatedly without significant risk of a spillage of radioactive material.

The main body of the phantom was designed to be a hollow cylinder of diameter 15cm to simulate the neck. It was necessary that the chamber could be filled with water, which may or may not contain a small amount of radioactive liquid to act as a background activity, and sealed. Two interchangeable inserts were then designed to be used for simulating thyroid and parathyroid imaging respectively. Each insert was to consist of a hollow thyroid-shaped chamber of the same internal dimensions, which are shown in Figure 2.1. The dimensions

were taken as the approximate mean value of the range given in the ICRP report (ICRP, 1975) for the thyroid gland. Each insert was to be mounted at a maximum depth of 2cm from the face of the outer cylinder, as this is the maximum thickness of tissue overlying the thyroid specified in the ICRP report (ICRP, 1975).

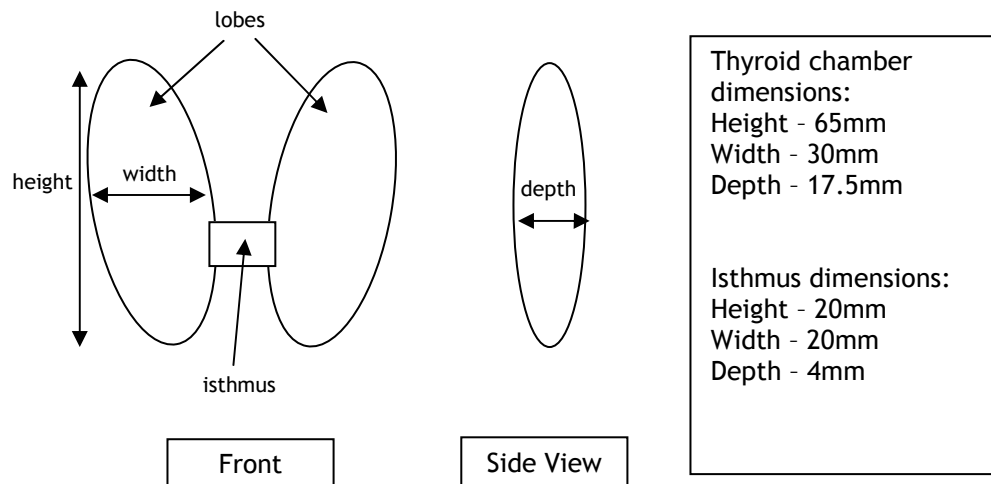


Figure 2.1 - Dimensions of thyroid for phantom inserts

The thyroid insert was also to include features within the thyroid that could be used to simulate hot and cold nodules of various sizes. Visualisation of the different sized “nodules” could help give an indication of the contrast and resolution of the images acquired with the phantom. Three pairs of nodules were to be included, with diameters of 15mm, 10mm and 5mm respectively. The cold nodules were to be simulated by solid rods running through the depth of the thyroid insert (anterior-posterior) where no radioactivity could be present. The hot nodules were designed as chambers also running through the depth of the thyroid insert but which could be filled and sealed separately from the main chamber. This would allow liquid to be added to these chambers which had a higher concentration of radioactivity (MBq/ml) than the liquid in the main chamber. These chambers would then appear hotter than the main body of the thyroid on the final acquired image. The specification for these “nodules” is shown in Figure 2.2.

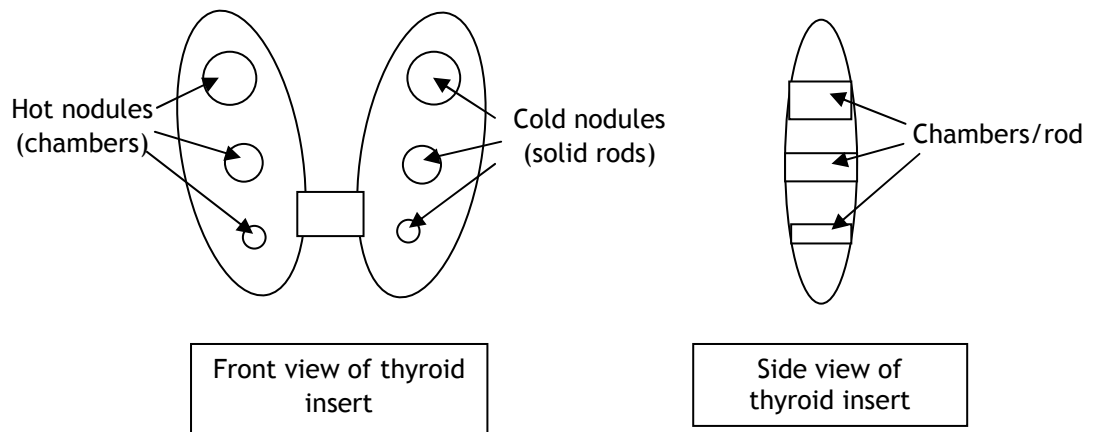


Figure 2.2 - Specification for phantom thyroid insert

The parathyroid insert was to have four small chambers of varying volume on its posterior surface which could be independently filled and sealed to represent the parathyroid glands. Parathyroid glands are very small and are typically spherical or ovoid with a combined weight for all four glands of around 1.3g (ICRP, 1975). The ICRP report gives suggested dimensions for each gland, but these are very small (1-15mm) and would be difficult to manufacture. It was instead decided that the size of each chamber would be defined by its individual volume. Small volumes of <math><1\text{ml}</math> were used because of the small dimensions of true parathyroid glands. The resulting specification for the insert is shown in Figure 2.3. A typical parathyroid adenoma is around 100mg - 1500mg in weight, corresponding to a volume of 0.1ml - 1.5ml. The chambers in the phantom ranged in volume from 0.11ml - 0.46ml to simulate a variety of adenoma sizes.

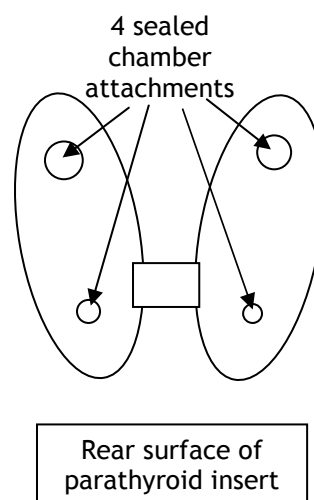


Figure 2.3 - Specification for phantom parathyroid insert

The final specification for the phantom was passed to the Department of Clinical Physics and Bio-engineering Mechanical Workshop at the Western Infirmary, Glasgow for manufacture. The workshop mounted each insert on its own lid so that the position of the insert relative to the sides of the cylinder could be maintained. The main cylinder and lids were constructed of 6mm thick Perspex, whilst the inserts were made from 3mm thick Perspex. The exception to this was the cold nodules, which were made of solid rods of Perspex. All the chambers were sealed with Perspex screws, a washer and an “o”-ring. Photographs of the completed phantom are shown in Figure 2.4.



Figure 2.4 - Photographs of completed phantom
Photographs showing the phantom with the thyroid insert in place and the parathyroid insert alongside.

Once the manufacture and leak testing was completed by the workshop, the phantom was filled with water and the exact volume of each chamber in both inserts was ascertained. These measured volumes are shown in Table 2.1. Knowing the relative volumes of the different chambers made it possible to test different relative activity concentrations (MBq/ml) accurately.

Thyroid Insert		Parathyroid Insert	
Chamber	Volume (ml)	Chamber	Volume (ml)
Thyroid	41.5	Thyroid	55.0
Hot nodule 1	3.30	Parathyroid 1	0.46
Hot nodule 2	1.75	Parathyroid 2	0.28
Hot nodule 3	0.35	Parathyroid 3	0.18
		Parathyroid 4	0.11
Total Nodules	5.40	Total Parathyroids	1.03

Table 2.1 - Volume of each chamber within the two phantom inserts

Each time the phantom was filled for imaging, a small volume of water was removed from each chamber using a syringe and needle in order to create an air bubble. The required activity of radioisotope was then injected into the chamber and mixed thoroughly to ensure uniform activity throughout the chamber. The remaining air bubble was then removed by injecting more water into the chamber before sealing it. Once each chamber was filled, the phantom was ready to be imaged as described in Section 2.2.2 below.

The thyroid insert was filled only with ^{99m}Tc as thyroid imaging at GRI is a single isotope procedure. The activity was introduced into the thyroid chamber, the 3 hot nodule chambers and the main phantom cylinder to simulate physiological uptake of ^{99m}Tc -pertechnetate in the neck region. In contrast, both ^{99m}Tc and ^{123}I were used for the parathyroid insert as the imaging procedure for this type of investigation at GRI is dual-isotope. The thyroid had both ^{99m}Tc and ^{123}I introduced into it whilst the parathyroid chambers and main cylinder only contained ^{99m}Tc , again in order to best simulate physiological uptake.

2.2.2 Image Acquisitions using the Phantom

The first images acquired of the new phantom were planar views in an anterior orientation, as is the case for standard thyroid and parathyroid imaging at GRI. The images of the phantom could therefore be directly compared with patient images acquired using the standard protocol to determine how well it simulated the physiological distribution of radiopharmaceutical. A variety of SPECT image data acquisitions were then obtained in order to assess the potential usefulness of the phantom for determining suitable SPECT acquisition parameters for both thyroid and parathyroid imaging and the feasibility of performing dual-isotope subtraction SPECT on parathyroid images.

2.2.2.1 Thyroid Insert Planar Acquisitions

The thyroid insert was filled to give a simulated total thyroid uptake of around 2%, which lies within the normal range for a patient study. It was then imaged using both a pinhole collimator and a parallel hole low energy, high resolution (LEHR) collimator. The geometry of the pinhole gives an inherently zoomed image, meaning that a small organ such as the thyroid can be imaged in greater

detail. The use of a pinhole collimator does, however, introduce geometric distortions to the images, as shown in Figure 2.5. Modern gamma cameras now have the facility to produce a software zoom when using a standard parallel hole collimator. Software zoom involves selecting the central area of the image acquisition matrix and rebinning the acquired counts into a larger matrix, resulting in the image of the area of interest filling a larger area of the final image matrix. This gives a distortion-free image whilst still giving good resolution detail of a small area. However, the use of software zoom results in a reduction in resolution due to the fact that the area of interest comprises a larger part of the final image matrix without any increase in acquisition resolution.

When this study began, the department at GRI was moving from pinhole to parallel hole imaging due to the replacement of the gamma camera that had a pinhole collimator. For all planar imaging, an energy window of $\pm 10\%$ centred on 140keV was used along with a 128^2 image matrix, which are the standard acquisition parameters used at GRI.

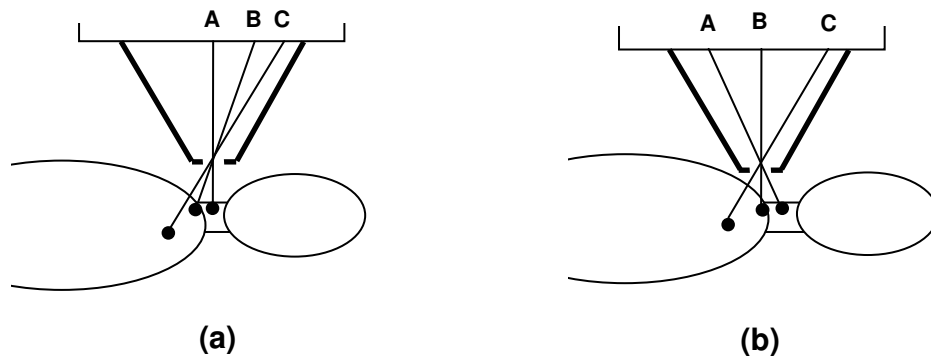


Figure 2.5 - Geometry of the pinhole collimator of a gamma camera

Diagram showing the position on the gamma camera detector of counts originating from three identical points with the pinhole collimator (a) centred over the thyroid and (b) centred over the sternal notch. In the projected images, distance AB is approximately equal but the distance BC is shorter in the first image, demonstrating the significant effect of acquisition geometry on the final image when using a pinhole collimator.

Example images of the thyroid insert obtained using a pinhole collimator are shown in Figure 2.6. The image on the left shows a 60 second (s) acquisition with a total of 54,000 counts whilst that on the right shows an acquisition with a total number of counts in the image of 200,000. The two lobes of the thyroid insert are clearly seen, as are all three “hot” nodules and 2 of the 3 cold

nodules. The smallest cold nodule (5mm diameter) is not visible on this image due to the limiting low contrast resolution of the gamma camera. The length of time to acquire the 200,000 count image (around 4 minutes) was similar to that required for acquisition of a 200,000 count patient image.

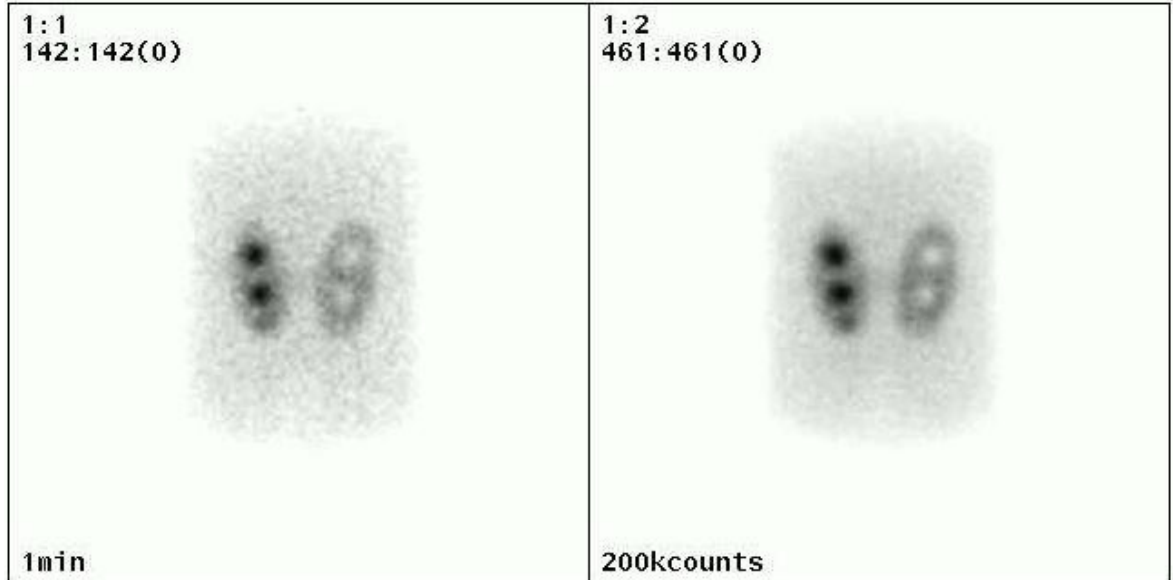


Figure 2.6 - Planar images of phantom with thyroid insert acquired using a pinhole collimator

Image on left was acquired for 60s and image on right was acquired to a total of 200,000 counts.

Figure 2.7 shows images of the thyroid insert in the phantom acquired using a parallel hole low energy high resolution (LEHR) collimator. The images were acquired on the same day as those in Figure 2.6 and so the relative activity concentrations in the different chambers were identical. The first two images were acquired with the same stopping conditions as those in Figure 2.6 with no software zoom applied. The 60s image had a total of 117,000 counts and the time taken to acquire the 200,000 count image was around 2 minutes, demonstrating the improved sensitivity of the parallel hole collimator relative to the pinhole. The final image, on the right, shows a 200,000 count acquisition with an applied software zoom of 1.33, which was found to result in the thyroid insert being approximately the same size on the final image as was seen on the pinhole images. Again, the time taken to acquire the 200,000 count image (approximately 2 minutes) was similar to that for a patient study using this collimator.

A visual comparison of the images in Figure 2.6 and Figure 2.7 clearly demonstrates the geometric distortions in the images acquired using the pinhole collimator. The upper and lower edges of the main phantom cylinder are very flat in the LEHR images, but are rounded in the pinhole views. The images acquired with the LEHR collimator also show all three “hot” nodules and two of the “cold” nodules, suggesting that the resolution is not significantly degraded.

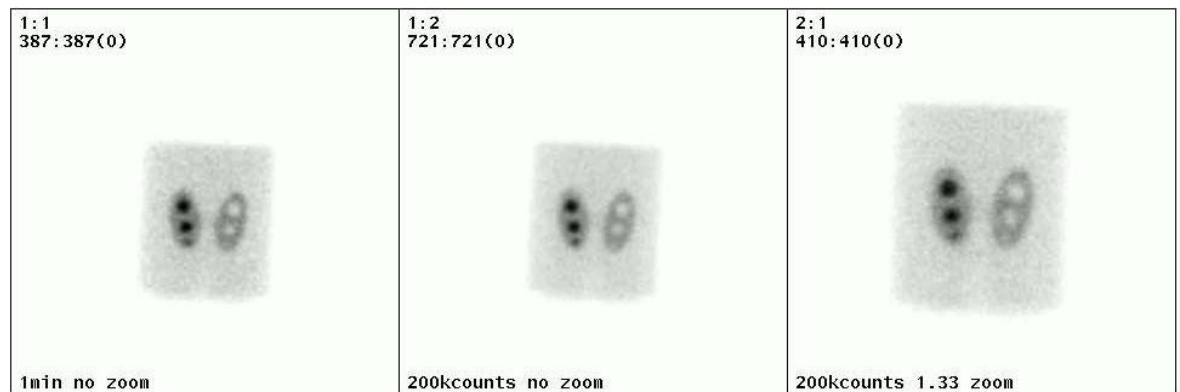


Figure 2.7 - Planar images of phantom with thyroid insert acquired using parallel hole LEHR collimator

Image on left was acquired for 60s, image in centre was acquired to a total of 200,000 counts and the image on the right was acquired to a total of 200,000 counts with an applied software zoom factor of 1.33.

The images from the phantom acquisitions were then compared to patient data sets to assess their usefulness in simulating true physiological uptake in the thyroid. Example patient images demonstrating a normal thyroid gland and a multinodular gland are shown in Figure 2.8. The upper images were acquired using the pinhole collimator and the lower images with a parallel hole LEHR collimator. The difference in zoom factor is due to the different positioning geometries that were used in the image acquisition. It was felt that the phantom, whilst not totally physiologically accurate, was suitable for use in assessing SPECT acquisition parameters.

2.2.2.2 Parathyroid Insert Planar Acquisitions

Planar images were also acquired of the parathyroid phantom insert using both available collimators. A dual-isotope acquisition lasting 10 minutes was performed, according to the standard departmental protocol. The images were then processed to produce a subtraction image in an attempt to show only the parathyroid chambers. As with the thyroid insert, physiological activities

simulating thyroid and parathyroid uptake were added to the phantom. In this case, a thyroid uptake of ^{123}I -iodide of 5-10% was assumed, along with an uptake of $^{99\text{m}}\text{Tc}$ in the thyroid of around 0.1%. The activity concentration in the parathyroid chambers was then varied such that it was between 2 and 6 times greater than that in the thyroid chamber for each separate acquisition,

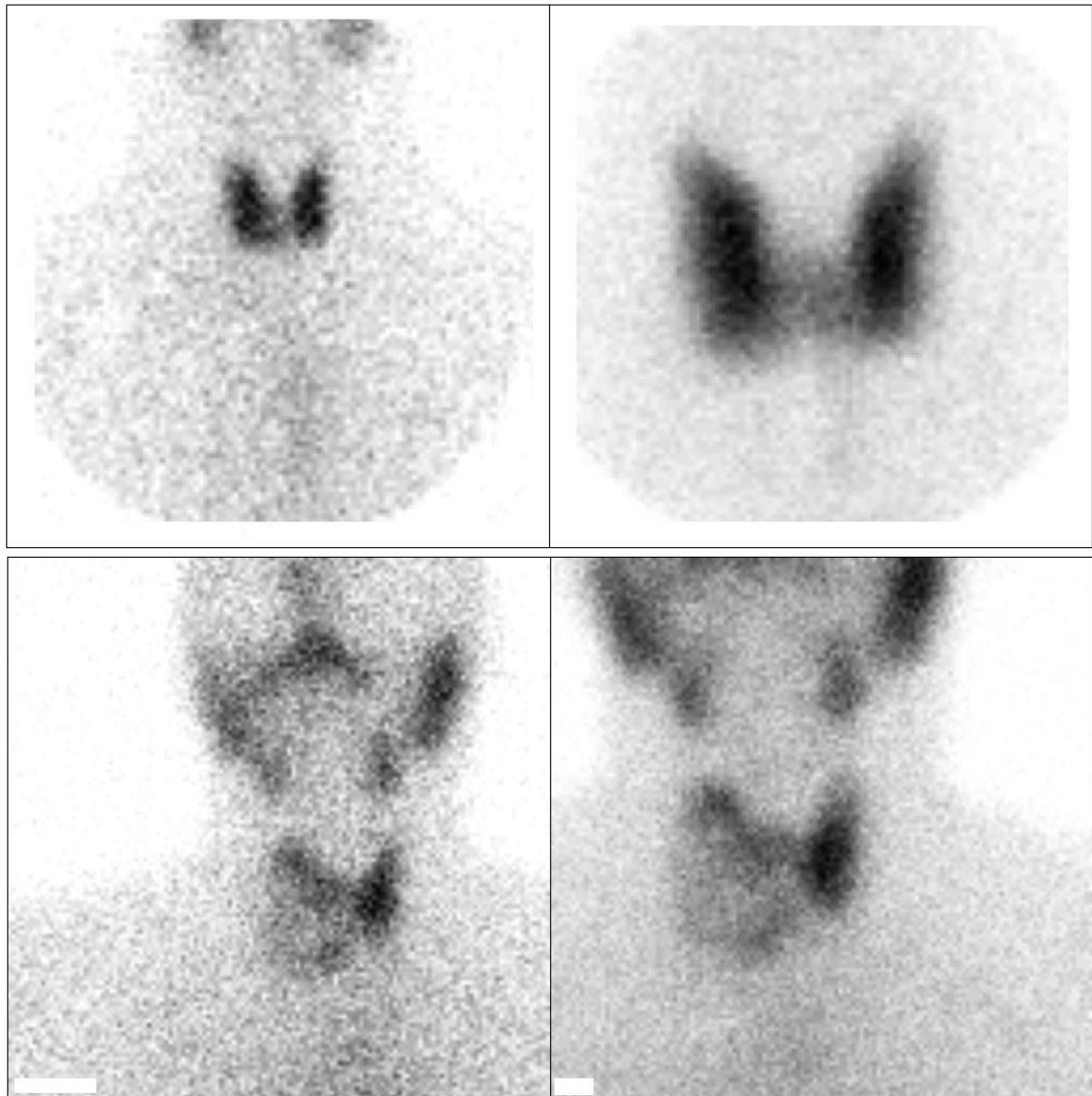


Figure 2.8 - Example planar patient thyroid studies
 Images of two patients with a normal thyroid acquired with a pinhole collimator (top) and multinodular gland acquired with a parallel hole LEHR collimator (bottom). Left hand images are 60s acquisitions and right hand views are to 200,000 total counts.

simulating different levels of uptake in a parathyroid adenoma. The dual-isotope acquisitions were performed using a 128^2 image matrix and energy windows of $135\text{keV} \pm 10\%$ for $^{99\text{m}}\text{Tc}$ and $165\text{keV} \pm 10\%$ for ^{123}I respectively, which are the standard parameters used for parathyroid acquisitions at GRI. An example energy spectrum from the gamma camera for a dual-isotope $^{99\text{m}}\text{Tc}/^{123}\text{I}$

acquisition showing both the acquisition energy windows and the photopeaks from the two isotopes is shown in Figure 2.9.

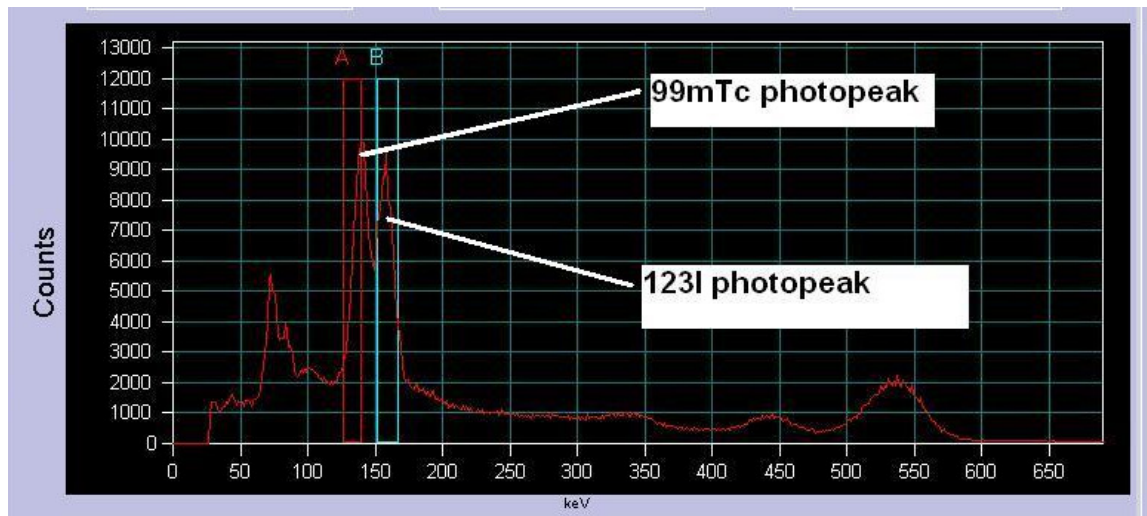


Figure 2.9 - Spectrum of dual-isotope $^{99m}\text{Tc}/^{123}\text{I}$ acquisition showing offset energy windows Spectrum captured from a gamma camera showing the overlapping photopeaks of the ^{99m}Tc (left) and ^{123}I (right). The acquisition energy windows are shown as red box A (^{99m}Tc) and blue box B (^{123}I), respectively.

Example images of a planar acquisition using the pinhole collimator are shown in Figure 2.10. The left hand image shows ^{99m}Tc distribution, the centre image is of ^{123}I distribution and the view on the right is the subtraction image, created using the scaling method described in Section 4.5. As with the thyroid insert, the geometric distortion produced by the use of the pinhole collimator is clearly visible. This particular acquisition was taken with a ^{99m}Tc activity concentration in the parathyroids of around 4x that in the thyroid. It is clear that none of the parathyroid chambers are visible on the subtraction image and indeed this was the case up to 6x relative concentration.

A similar acquisition was performed on the same day using the LEHR collimator and the resultant images, with an applied software zoom of 1.33, are shown in Figure 2.11. Again, there is poor visualisation of the parathyroid chambers on the subtraction image, although the largest is just visible at the upper left pole of the thyroid chamber. The visualisation of the parathyroid chambers was therefore slightly better with the parallel hole collimator than with the pinhole. This is principally due to the fact that the sensitivity of the LEHR collimator is significantly higher than the pinhole - at around 2.5:1 for ^{99m}Tc - and so more

counts were registered over the 10 minute acquisition period and the image statistics were considerably improved.

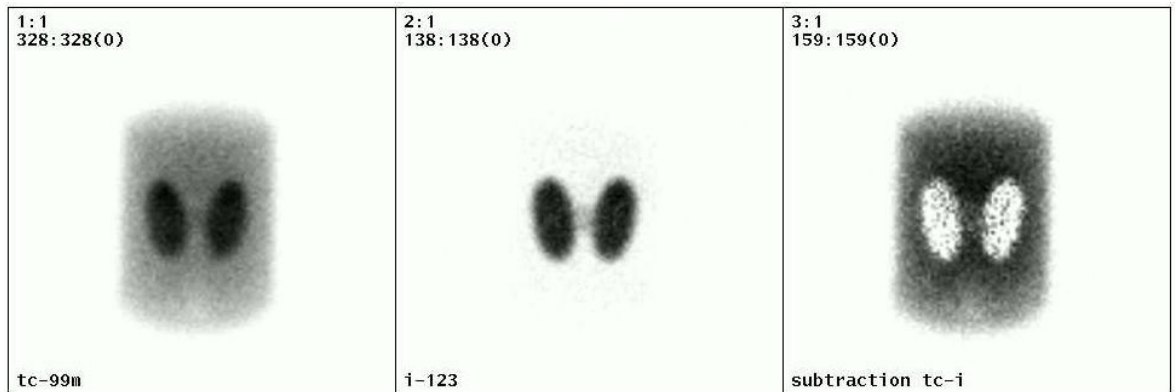


Figure 2.10 - Planar images of phantom with parathyroid insert acquired using a pinhole collimator
Image on left is of ^{99m}Tc distribution, image in centre is ^{123}I distribution and image on right is subtraction.

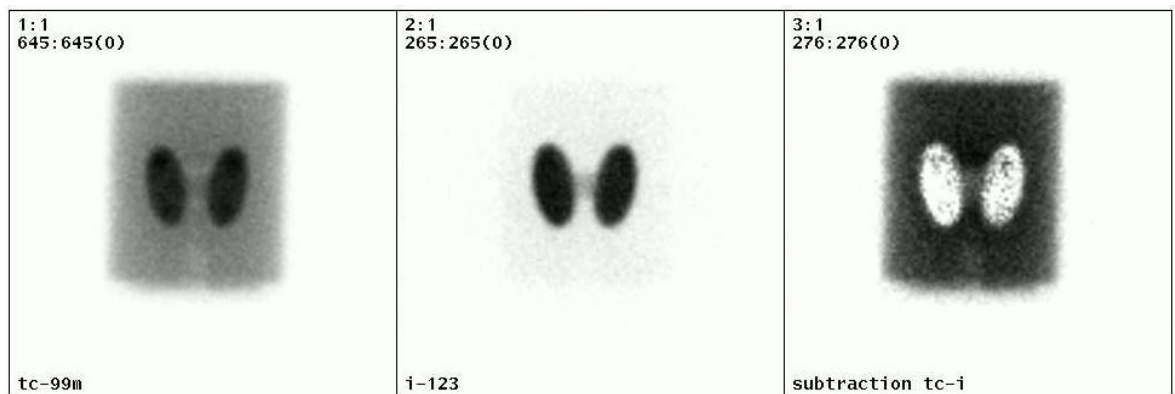


Figure 2.11 - Planar images of phantom with parathyroid insert acquired using a parallel hole LEHR collimator
Image on left is of ^{99m}Tc distribution, image in centre is ^{123}I distribution and image on right is subtraction.

As with the images of the thyroid insert, a comparison with patient images was carried out to assess how accurately the phantom simulated the patient situation. Example patient images are shown in Figure 2.12.

The phantom was felt to simulate patient acquisitions reasonably well, although there was some concern over the inability to clearly see the parathyroid chambers on subtraction images. It was felt that the two most likely reasons for this were that the parathyroid chambers were too small and therefore could contain an activity too small to be perceived on subtraction, or that the anterior orientation of the planar images was masking the presence of the chambers on

the posterior surface of the phantom thyroid. In order to determine which of these was the reason for the poor parathyroid visibility, SPECT images of the phantom were acquired to remove the possibility of anterior masking before a re-design of the phantom was considered.

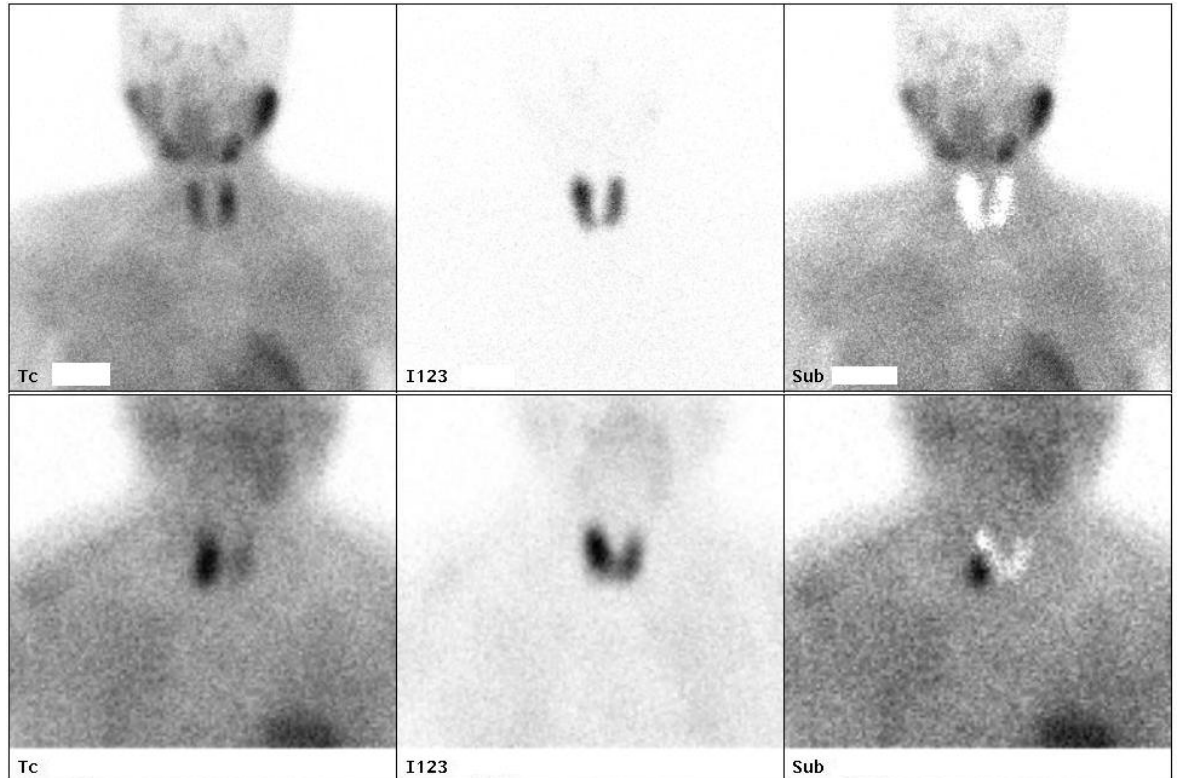


Figure 2.12 - Example planar patient parathyroid studies
 Top row shows negative study, bottom row shows study positive for parathyroid adenoma at right lower pole. Left hand images are ^{99m}Tc -Sestamibi distribution, centre images are ^{123}I -iodide distribution and right hand views are subtraction images.

2.2.2.3 Thyroid Insert SPECT Acquisitions

The parameters for the SPECT acquisitions were chosen in order to give good image quality in terms of the number of counts acquired in each SPECT frame whilst keeping the overall imaging time low enough to be tolerated by a patient. The parameters that had been chosen by a number of other groups performing similar acquisitions were taken into account (Chen *et al.*, 1988, Neumann, 1992, Torres *et al.*, 1996, Wanet *et al.*, 1996, Chen *et al.*, 1997, Moka *et al.*, 2000b, van Isselt *et al.*, 2003, Pant *et al.*, 2003, Lorberboym *et al.*, 2003, Schachter *et al.*, 2004, Spanu *et al.*, 2004), as were the standard SPECT acquisition parameters used at GRI for other types of imaging investigation.

The final chosen parameters were as follows: LEHR collimators on the double-headed Philips Forte gamma camera with the heads in the 90° orientation, 180° anterior circular acquisition, 60x40s frames with a 3° rotation between frames, giving a total acquisition time of 20 minutes and a 30cm square roving zoom applied. The 180° anterior acquisition was chosen due to the fact that the areas of interest (thyroid and parathyroid glands) lie anterior in the neck and so the posterior image information would be of poorer quality and would not contribute an increase in the final image quality. For acquisitions using the thyroid insert, a 10% energy window centred on 140keV was used whilst for those with the parathyroid insert, a dual-isotope acquisition was performed with energy windows of 135keV \pm 10% for ^{99m}Tc and 165keV \pm 10% for ^{123}I . These are the same energy windows as were used for the planar acquisitions.

The SPECT data was reconstructed on the department's HERMES imaging computer system (Nuclear Diagnostics Ltd.) using the Ordered Subsets Expectation Maximisation (OSEM) iterative method. The reconstructions were carried out with 15 subsets and 4 iterations, upon the recommendation of Nuclear Diagnostics staff. A post-reconstruction filter was then applied to smooth the images to maximise image quality. The chosen filter for the reconstruction of phantom images was not necessarily the same as that used later for the reconstruction of patient image data (see Sections 5.3 & 8.3.2).

Figure 2.13 shows an example of the reconstructed images produced after a SPECT acquisition of the thyroid insert. The images represent a simulated total thyroid uptake of around 2% (which lies in the normal range at GRI) with 3 hot and 3 cold nodules present. The two lobes of thyroid can clearly be seen, as can the hot and cold nodules. However, as was the case for the planar images of the phantom, the smallest hot nodule cannot be resolved on these images. In these images, the hot nodules contain an activity concentration (MBq/ml) of approximately 4x that in the thyroid chamber. Other acquisitions carried out with different relative concentrations up to 7x confirmed that the smallest hot nodule is not visible on the SPECT images. Higher relative concentrations were not tested as they were felt to be physiologically unlikely.

The findings from the SPECT acquisitions of the phantom demonstrated that the overall resolution of the SPECT images was not significantly different from that

of the planar images. However, the low contrast resolution was slightly improved in that the smallest cold chamber was visible on the reconstructed SPECT images. They also showed that the chosen parameters for the SPECT acquisition were reasonable in order to obtain reconstructed SPECT images of acceptable quality clinically in terms of the target: background ratio and resolution.

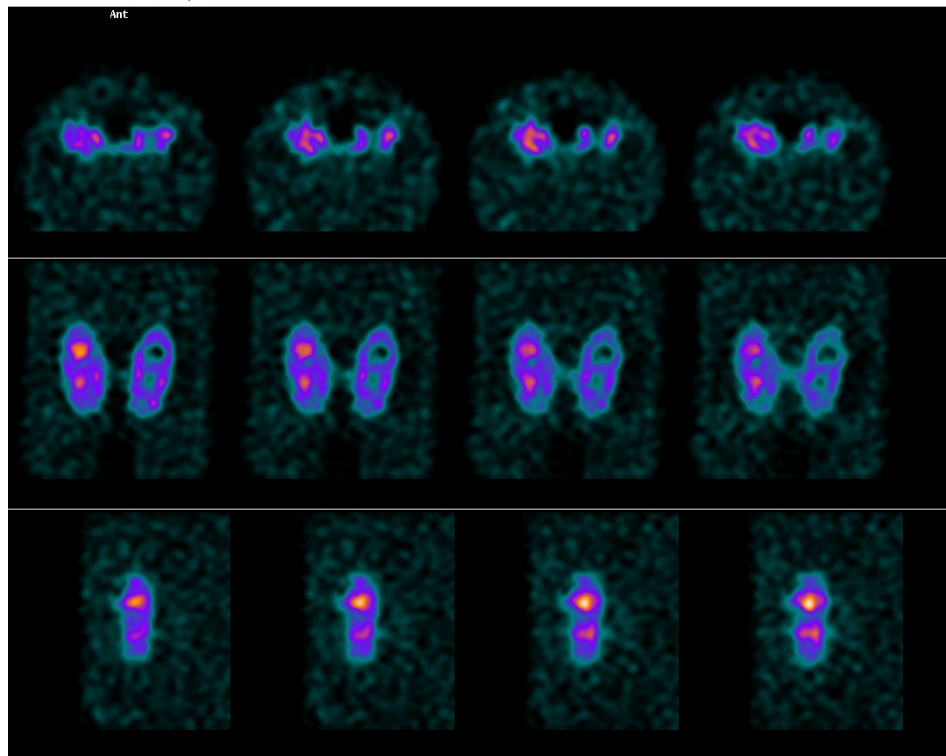


Figure 2.13 - Reconstructed SPECT images of thyroid phantom insert
Top line shows transverse slices, middle line is coronal slices and bottom line is sagittal slices through the phantom.

2.2.2.4 Parathyroid Insert SPECT Acquisitions

The process of SPECT acquisition was then repeated using the parathyroid insert filled with physiologically appropriate activities of ^{99m}Tc and ^{123}I and a dual-isotope SPECT acquisition. Once again, uptakes in the thyroid of 0.1% for ^{99m}Tc -Sestamibi and 10% ^{123}I -iodide were assumed. Various ratios of ^{99m}Tc activity concentration between the parathyroid chambers and the main thyroid chamber were imaged, in the same way as for planar imaging. An example of the reconstructed dual-isotope SPECT images is shown in Figure 2.14 with the ^{99m}Tc images on the left and the registered ^{123}I images on the right. On this occasion,

the activity concentration in the parathyroids was approximately 4x that in the thyroid.

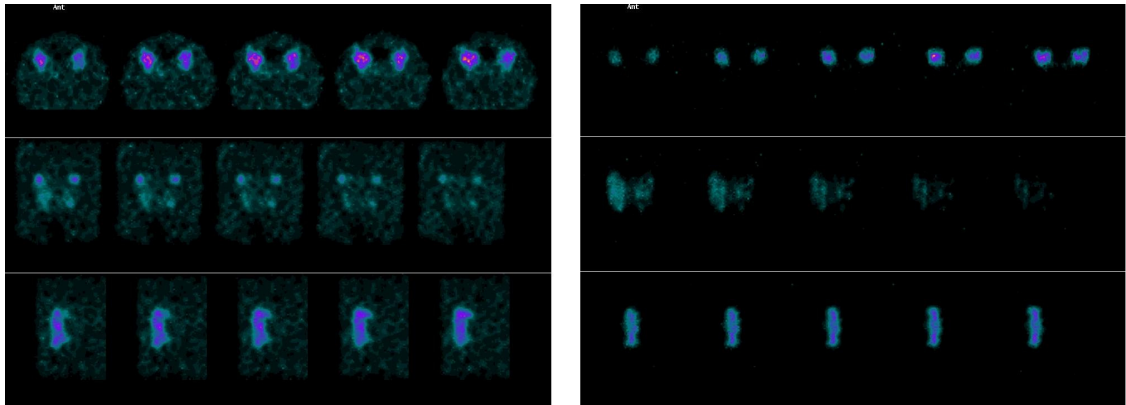


Figure 2.14 - Reconstructed SPECT images of parathyroid phantom insert
 Left hand images are ^{99m}Tc distribution and right are co-registered ^{123}I images. Within each image set, top row is transverse, middle row is coronal and bottom row is sagittal slices.

The images show that the acquisition parameters are reasonable in order to acquire enough counts in each SPECT frame to produce reconstructed images of sufficiently good quality to be used clinically. The two lobes of thyroid are also clearly defined on both sets of images.

The HERMES computer system was then used to produce subtraction SPECT images in order to remove the image of the thyroid so that only the signal from the parathyroids remains. The exact method used to achieve this is described in depth in Chapter 4 and will not be discussed further here. However, an example of a subtraction SPECT data set produced from the ^{99m}Tc and ^{123}I images in Figure 2.14 is shown in Figure 2.15.

In these images, the signal from the thyroid chamber has been almost completely removed, leaving a void in the image. The images also clearly show residual activity in all 4 of the parathyroid chambers, demonstrating that the subtraction technique used is sound. At lower ratios of activity concentration in the parathyroids to that in the thyroid, the smallest chamber (volume 0.11ml) was not visible, but the other 3 were always visible on the subtraction images. This is in contrast to the situation with planar imaging, where visualisation of the parathyroid chambers on subtraction was always poor.

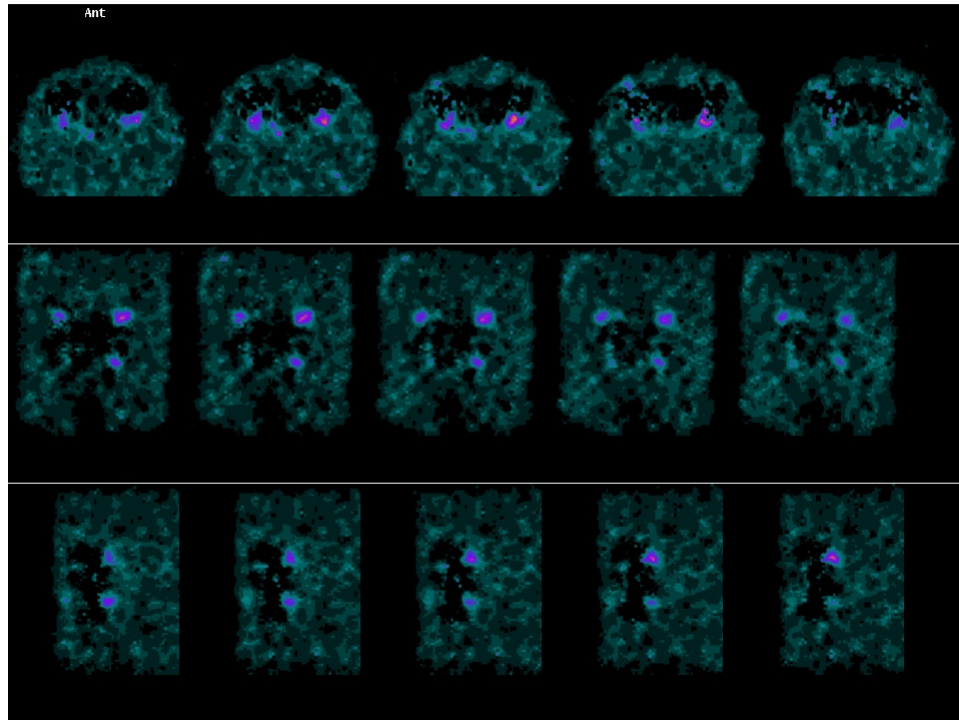


Figure 2.15 - Subtraction SPECT images of parathyroid phantom insert
Subtracted images of same data set shown in Figure 2.14, showing residual activity in areas of parathyroid chambers. Top row is transverse, middle row is coronal and bottom row is sagittal slices.

2.3 Discussion and Conclusions

The phantom designed and built for the purposes of this study was imaged under a variety of conditions in order to test its ease of use, physiological accuracy and usefulness in determining SPECT imaging parameters for thyroid and parathyroid SPECT. The planar images acquired using both the thyroid and parathyroid inserts were of good quality and replicated patient studies sufficiently well to be used to assist in determining appropriate acquisition parameters for SPECT. The known geometrical distortions present when using a pinhole collimator were clearly demonstrated, as was the good imaging resolution.

The activities of radioisotopes used in the phantom were chosen to be similar to those found in the clinical setting in order to simulate the true physiological uptake of the relevant radiopharmaceuticals in the neck. The count rates obtained on planar imaging were similar to those found in patient studies, demonstrating that the physiological accuracy of the phantom was sufficiently good for the purposes of determining suitable SPECT acquisition parameters for patient studies.

The relative resolution of the planar and SPECT images was similar, with the smallest nodules on the thyroid phantom being difficult to visualise on both types of image. The use of SPECT imaging for patient studies would therefore not significantly degrade image resolution.

The lack of visualisation of the parathyroid chambers on planar subtraction imaging which were then visible on SPECT imaging with a similar activity distribution demonstrates the problems with an anterior-only planar acquisition for parathyroid imaging. Since the parathyroid glands tend to sit on the posterior surface of the thyroid, there is a risk that an anterior image will result in masking of the signal from the parathyroids and images in which a parathyroid adenoma is present could be reported as normal. These results were encouraging in that they demonstrated the possible increased accuracy that may be obtained with dual-isotope subtraction SPECT parathyroid imaging for patients. This is discussed in more detail in Chapters 3 - 7 of this thesis.

The phantom with its two interchangeable inserts was felt to represent a good simulation of patient studies. The phantom was therefore used to good effect in determining suitable SPECT acquisition parameters for patient parathyroid and thyroid studies as well as for work on thyroid uptake measurements, which is discussed in Chapters 8 & 9.

Chapter 3 – Parathyroid Study – Introduction

3.1 Parathyroid Imaging at Glasgow Royal Infirmary

3.1.1 Referrals

Patients are referred to the Nuclear Medicine department at Glasgow Royal Infirmary (GRI) from a number of different hospitals in the Greater Glasgow & Clyde and Lanarkshire Health Board areas. Referrals normally come from physicians in endocrine clinics which patients have been attending after high levels of calcium (Ca^{2+}) and parathyroid hormone (PTH) have been found in blood samples. The physician will request imaging to confirm the presence of a parathyroid adenoma and to give its location with respect to the thyroid gland. The information from the nuclear medicine study is then often combined with the complementary anatomical information from an ultrasound (US) scan to give a full account of the patient's condition.

The patient may then be referred to an endocrine surgeon for the adenoma to be removed. The surgeon will use the information from the imaging studies to allow a minimally invasive unilateral neck exploration to be carried out, which results in a shorter operating time and carries a lower morbidity rate than the more traditional bilateral neck exploration, whilst providing equivalent curative results (Bergenfelz *et al.*, 2002, Russell *et al.*, 2006, Westerdahl & Bergenfelz, 2007, Adler *et al.*, 2008 & 2009). In some cases, a patient may not undergo surgery for a number of possible reasons, which include no adenoma being visualised on imaging, another condition being present that could account for the high Ca^{2+} and PTH levels, the patient being asymptomatic or the patient simply refusing surgery.

It should be noted that the standard patient pathway and referral process used at GRI is different from that used at other institutions. The literature suggests that most other centres refer patients for localisation imaging only after the decision is made to perform surgery (e.g. Billotey *et al.*, 1996a, Hindié *et al.*, 1998, Sidhu *et al.*, 2003). The information required from the imaging study by the referring clinician will therefore differ depending on the type of referral.

If surgery is definitely to take place, the imaging study is used simply to guide the surgeon to the most likely site of the parathyroid adenoma so that minimally invasive surgery can be performed. Should the surgeon fail to find a suspicious lesion at the suggested position, further investigation can be carried out to locate the parathyroid adenoma or hyperplastic glands responsible for the patient's hyperparathyroidism. The sensitivity of the imaging technique is therefore important in order to best locate lesions, but the specificity is less so as the patient will undergo surgery regardless of whether or not a lesion is identified on imaging.

In contrast, the requirements from a parathyroid imaging study at GRI are very different. The patient will only undergo surgery if a suspicious lesion is identified on imaging and the patient's symptoms suggest a significant improvement in quality of life will result from the removal of the overactive gland(s). It is therefore important that the clinicians reviewing the nuclear medicine studies are certain of the presence of a suspicious lesion before reporting its presence so that a patient will not undergo unnecessary surgery. In this case, high specificity of the imaging technique is important to ensure that false positive reports are kept to a minimum.

The standard patient pathway at GRI is therefore likely to lead to a tendency for the nuclear medicine clinicians to under-report suspicious lesions to prevent false positive results. A larger number of negative and equivocal reports would therefore be expected in comparison to an institution that uses the other referral pattern.

3.1.2 Standard Parathyroid Imaging Procedure at GRI

There are a number of different methods available for the detection of parathyroid adenomas using functional nuclear medicine imaging, as has been described in detail in Section 1.3.2 of this thesis. The standard procedure used in the Nuclear Medicine department at GRI is a combination of two of these options, washout and subtraction imaging.

3.1.2.1 Injection and Imaging Procedure

When the patient attends the department, the test is first described in detail to ensure the patient is comfortable with the procedure before receiving any radiopharmaceuticals. An intravenous injection of 20MBq of ^{123}I -sodium iodide, which represents the ARSAC limit for this type of imaging, is then given to the patient. The iodine is taken up by the thyroid gland only. After a period of at least 20 minutes, a further intravenous injection of $^{99\text{m}}\text{Tc}$ -Sestamibi is given. At the beginning of the study period, the standard activity ordered for use was 750MBq - although the ARSAC limit is 900MBq - which was felt to give sufficient image quality for diagnosis whilst keeping radiation dose to the patient to a minimum. The $^{99\text{m}}\text{Tc}$ -Sestamibi will be taken up by both the thyroid and parathyroid glands. The activity in the syringe prior to each injection is measured using a Capintec isotope calibrator and is printed on the patient request card so that a full record of the administrations is kept.

After a further wait of 15 minutes to allow uptake of the $^{99\text{m}}\text{Tc}$ -Sestamibi in the thyroid and parathyroid glands, the patient is seated in front of a gamma camera fitted with a low energy high resolution (LEHR) collimator, and a series of planar anterior images is acquired. The first acquisition is a view of the neck area and consists of 10x60s frames, which are then summed to give a single planar image of 10 minutes duration. The dynamic acquisition allows motion correction to be carried out prior to the images being summed in the event of the patient changing position during the 10 minutes of the acquisition. A further short acquisition lasting 1-2 minutes is then performed with a marker placed over the sternal notch to give positional information for the reporting clinician. Finally, a 3 minute acquisition of the chest area is performed to allow visualisation of any ectopic parathyroid glands lying inferior to the thyroid gland.

The patient is then asked to wait within the department and a second set of images, consisting of the same three acquisitions as described above, is acquired at 2 hours post-injection of Sestamibi. A comparison of the relative washout of Sestamibi between the early (15 minutes post-injection of Sestamibi) and late (2 hours post-Sestamibi) acquisitions can then be used to demonstrate the presence of a parathyroid adenoma (see Section 1.3.2).

3.1.2.2 Energy Windows and Image Processing

Since the gamma emissions of the ^{123}I and $^{99\text{m}}\text{Tc}$ have different energies (159keV and 140keV, respectively), it is possible to acquire dual-isotope images, giving fully registered images showing the distribution of the different radiopharmaceuticals. Since the iodine is taken up only by the thyroid gland and the Sestamibi is taken up by both thyroid and parathyroids, subtracting the iodine image from the Sestamibi image should remove the thyroid from the resultant image and allow direct visualisation of a parathyroid adenoma, if one is present. Subtraction is therefore performed on the summed 10-minute neck acquisitions from both the early and late sets of images.

When imaging the distribution of a single radioisotope within the body, the energy window of the gamma camera is usually set up to include the whole of the photopeak of the spectrum of gamma photon energies incident upon the crystal. A gamma camera is unable to precisely quantify the energy of each incident photon and so a slight spread is seen in the spectrum from a radioisotope producing mono-energetic gamma radiation (e.g. $^{99\text{m}}\text{Tc}$ at 140keV). The energy resolution of a gamma camera system is defined as the full width half maximum (FWHM) of the photopeak of $^{99\text{m}}\text{Tc}$ expressed as a percentage of the 140keV gamma emission photon energy (Bolster & Waddington, 1996). Values for energy resolution of <10% are typical (Dr G Gardner, personal communication).

The energies of the principal gamma ray emissions from ^{123}I and $^{99\text{m}}\text{Tc}$ are, however, very close together, meaning that the photopeaks overlap somewhat, and the photopeak of ^{123}I lies partially within the standard $^{99\text{m}}\text{Tc}$ 10% window centred on 140keV, as shown in Figure 3.1. The dual energy acquisition parameters are therefore set such that the window for each isotope is narrower than normal and is centred slightly away from the maximum of the peak, as shown in Figure 3.2. This results in poorer sensitivity (counts/s/MBq) in each window but provides sufficient discrimination between the photopeaks to allow accurate images of the relative distributions of the two radioisotopes to be obtained with minimal cross-talk between the acquired energy windows (Hindié *et al.*, 1998). The energy windows used at GRI are 148.5keV - 181.5keV for ^{123}I

($\pm 10\%$ window centred on 165keV) and 121.5keV - 148.5keV for ^{99m}Tc ($\pm 10\%$ window centred on 135keV), as shown in Figure 3.2.

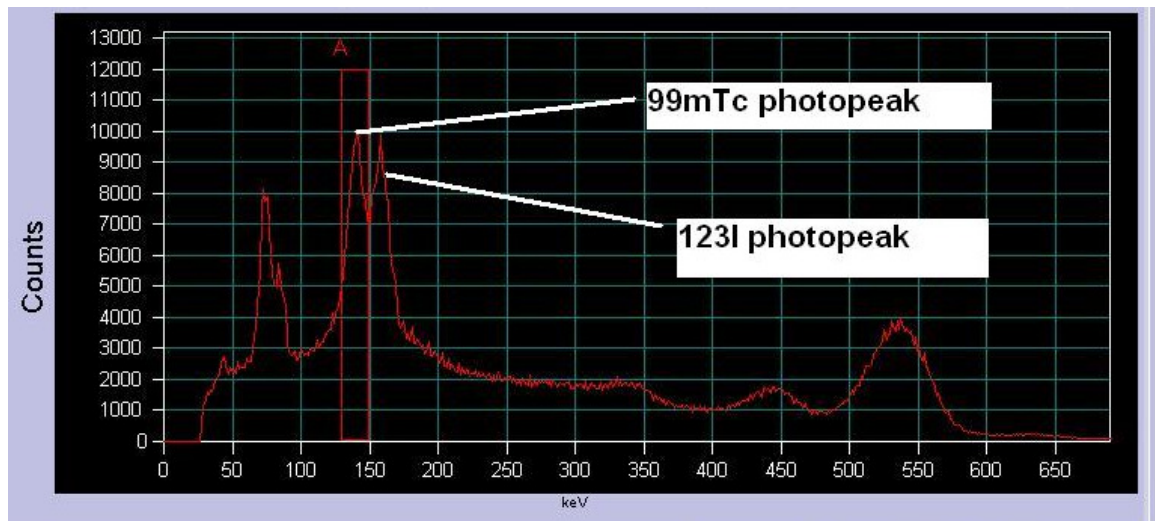


Figure 3.1 - Dual-isotope $^{99m}\text{Tc}/^{123}\text{I}$ acquisition spectrum showing overlapping photopeaks and standard ^{99m}Tc energy window
Energy spectrum acquired using a gamma camera showing the overlapping ^{99m}Tc (left) and ^{123}I (right) photopeaks. The standard acquisition energy window for ^{99m}Tc , centred on 140keV, is shown as the red box A, which contains some of the ^{123}I photopeak.

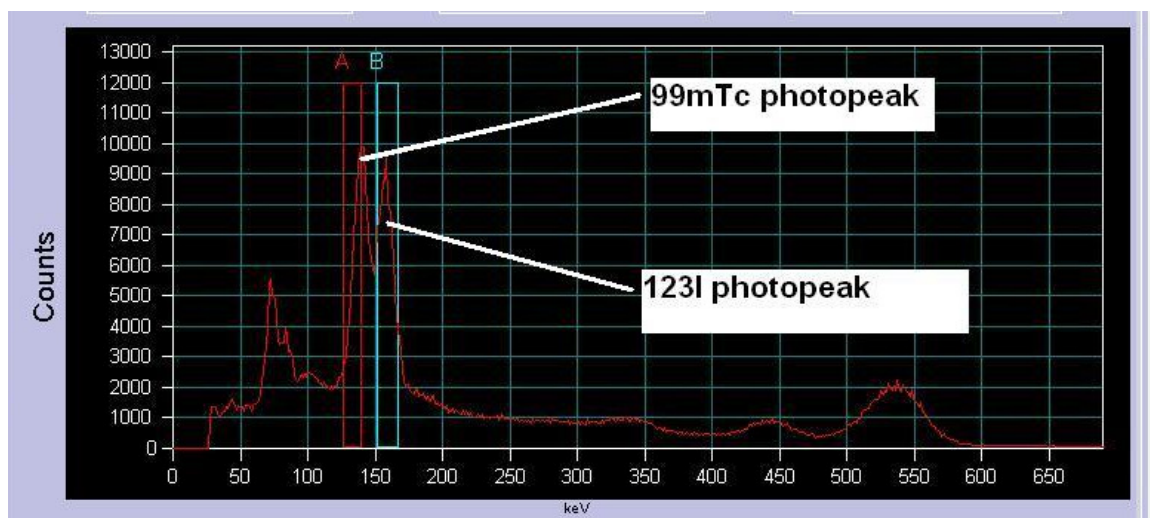


Figure 3.2 - Spectrum of dual-isotope $^{99m}\text{Tc}/^{123}\text{I}$ acquisition showing offset energy windows
Spectrum captured from a gamma camera showing the overlapping photopeaks of the ^{99m}Tc (left) and ^{123}I (right). The acquisition energy windows are shown as red box A (^{99m}Tc) and blue box B (^{123}I), respectively.

As the images for the two isotopes are acquired simultaneously using the different energy windows, they are inherently registered. This means that there is no need to use anatomical markers or any other method to allow registration to be performed after acquisition, making the subtraction processing

considerably easier than it would be if the two sets of data were acquired consecutively.

Direct subtraction of the iodine image would not give an acceptable result since the relative counts in the two images will be different. A scaling factor must therefore be applied to the iodine image before performing the subtraction. To obtain an appropriate scaling factor, a region of interest (ROI) is drawn around the thyroid gland on the iodine image. The ROI is then also applied to the registered Sestamibi image and the total number of counts within the ROI on each image is noted. The counts in the Sestamibi ROI are divided by those in the iodine ROI to give the scaling factor. The counts in every pixel of the iodine image are then multiplied by this scaling factor and the iodine image is subtracted, pixel by pixel, from the Sestamibi image.

An example of typical summed 10-minute anterior planar parathyroid images is shown in Figure 3.3. The early and late ^{99m}Tc and ^{123}I neck images are demonstrated, along with the resultant subtraction images. On the subtraction, a residual area of activity is seen at the lower pole of the right lobe of thyroid, which strongly suggests the presence of a parathyroid adenoma at this site. The washout study involving only the early and late ^{99m}Tc images is less clear, but also suggests an area of relatively increased activity in the late image, which is further evidence of the presence of a parathyroid adenoma.

3.1.3 SPECT Imaging of the Parathyroid Glands

Prior to the commencement of this study, the department at GRI had no experience of performing SPECT parathyroid studies. However, it was recognised by both the medical and scientific staff in the department that the standard anterior planar imaging procedure may not allow sufficient visualisation of parathyroid adenomas lying posterior to the thyroid. One alternative procedure could have been to acquire lateral or anterior oblique planar images to give a more direct line-of-sight to the posterior of the thyroid gland, as has been performed by other groups (Krausz *et al.*, 1995, Billotey *et al.*, 1996a, Hindié *et al.*, 2000 & 2009, Arveschoug *et al.*, 2007). It was agreed, however, that a study on SPECT acquisition would provide an interesting assessment of the

extra information available to the reporting clinician from the three-dimensional images.

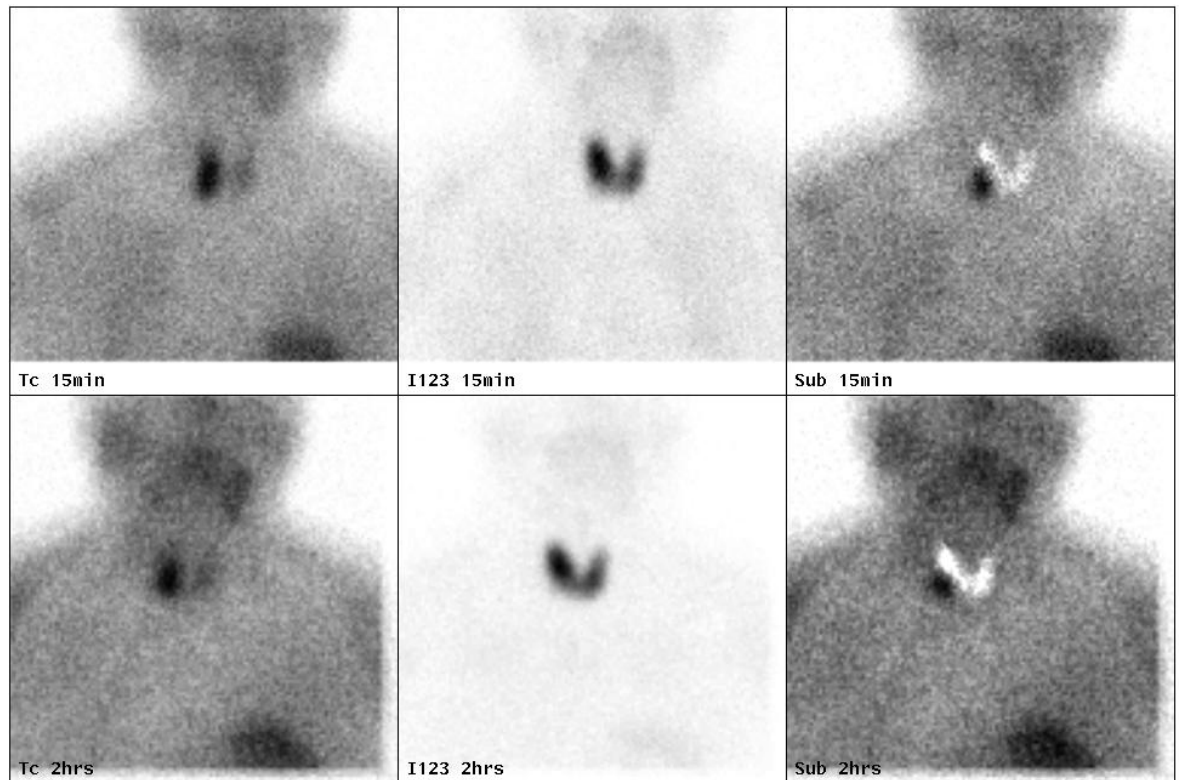


Figure 3.3 - Example of typical planar parathyroid images from GRI

The top row shows the early neck area images (15 minutes post-injection of Sestamibi) and the bottom row shows the late images (2 hours post-Sestamibi). The left-hand images are of ^{99m}Tc -Sestamibi distribution, in the middle are the ^{123}I -iodide images and the subtraction is shown on the right.

Many groups have published data on single-isotope parathyroid SPECT using ^{99m}Tc -Sestamibi alone (Bilotey *et al.*, 1996a & 1996b, Torres *et al.*, 1996, Chen *et al.*, 1997, Neumann *et al.*, 1997a, Moka *et al.*, 2000b, Lorberboym *et al.*, 2003, Schachter *et al.*, 2004, Spanu *et al.*, 2004, Slater & Gleeson, 2005, Ansquer *et al.*, 2008, Carlier *et al.*, 2008, Ho Shon *et al.*, 2008, Nichols *et al.*, 2008, Thomas *et al.*, 2009) but at the time of the study being set up (2004), only one group had published results in the literature relating to the use of dual-isotope subtraction SPECT for parathyroid localisation (Neumann *et al.*, 1997b, 1998 & 2000). Since the standard procedure at GRI involves subtraction imaging, it was decided that the study should look into the use of dual-isotope subtraction SPECT parathyroid imaging. In the event that the method proved useful in providing extra relevant clinical information to the reporting clinician, one of the sets of planar images in the standard GRI procedure could be replaced

by a SPECT acquisition with little or no increase in the total imaging time. This study commenced in early 2006 and the following chapters describe the study and results in detail.

3.1.3.1 Ethics Approval

Approval for the study was sought from the local research ethics committee (LREC) at GRI. An application was submitted on the basis of patients receiving an extra scan but no other intervention, with particular emphasis placed on the fact that no administration of a radiopharmaceutical was required beyond that necessary for the scan for which the patient had been referred to the department. A copy of the approval notice from the LREC is included in Appendix A.

In order to gain ethics approval, it was necessary to create a patient information sheet and consent form that could be given to potential participants in advance of their attendance at the department. The information sheet had to explain the aims of the research as well as any potential benefits and/or risks to participants. The consent form had to be completed by each participant and a member of departmental staff (usually the lead researcher) prior to any additional imaging taking place. A copy of the information sheet and consent form is included in Appendix B.

Chapter 4 – Parathyroid Study – Materials and Methods

4.1 Study Participants

All patients referred to the Nuclear Medicine department at Glasgow Royal Infirmary (GRI) for a parathyroid study between February 2006 and October 2008 were sent a copy of the patient information sheet and consent form for this study (see Appendix B) with their appointment letter. These letters are usually sent to patients around 2 weeks prior to the appointment date. Patients who expressed an interest in participating were given the opportunity to speak privately to either the principal researcher or another member of staff familiar with the aims and requirements of the study. Those willing to take part were then asked to sign the consent form, which was also signed by the staff member seeking the consent. There were no particular exclusion criteria, although claustrophobic patients tended to decline the opportunity to take part. Patients on anti-thyroid medications may have presented a problem in that the uptake of ^{123}I -iodide in the thyroid gland would have been considerably reduced, leading to potential difficulties in the subtraction process, but none referred for parathyroid imaging during the study period were taking such medications. On occasion, time constraints on the clinical service in the department meant that it was not possible to carry out the SPECT acquisition for this study, in which case the patient was informed of the situation and did not complete the consent form. A total of 32 participants were recruited over the 33-month period of the study.

4.2 Injected Activities

The pre-injection activity of each radiopharmaceutical ($^{99\text{m}}\text{Tc}$ -Sestamibi and ^{123}I -iodide) in the syringe was measured using the departmental Capintec and was recorded on the request card, as per standard departmental procedure. The residual activity in each syringe was also measured and recorded post-injection to allow an accurate assessment of the total injected activity to be made for each patient.

4.3 SPECT Acquisition

The SPECT acquisition was carried out between the two sets of planar images that are acquired according to the department's standard protocol (see Section 3.1.2 for details). This meant that the participants were not required to remain in the department beyond the normal requirements for parathyroid imaging. The timing of the SPECT acquisition post-injection was not fixed but varied due to the requirements of the clinical service. However, in most cases the SPECT images were acquired immediately after the first set of planar images and so commenced at around 35 minutes post-injection of ^{99m}Tc -Sestamibi.

The parameters for the SPECT acquisition were determined using the parathyroid phantom designed and constructed especially for this study (see Chapter 2 for further details). All acquisitions were performed on a double headed Philips ADAC Forte gamma camera with the patient lying supine and using a head rest to ensure the head and neck remained still throughout the acquisition. For a SPECT acquisition, acquisition data covering 180° is sufficient to accurately reconstruct the distribution of radiopharmaceutical within a patient (Wagner *et al.*, 1999). Since the area of interest for this study - the thyroid and parathyroid glands - lies close to the anterior surface of the neck, it was felt that there was no need to collect posterior image frames. The parathyroid phantom described in Chapter 2 was used to acquire image data sets with both 180° and 360° rotations and these confirmed that a 180° acquisition arc produced satisfactory reconstructed images. The acquisition was therefore carried out over a 180° anterior arc with the gamma camera heads at a relative angle of 90° .

The remaining acquisition parameters were as follows: 128^2 acquisition matrix, energy windows of $135\text{keV} \pm 10\%$ for ^{99m}Tc and $165\text{keV} \pm 10\%$ for ^{123}I , parallel hole high resolution (VXHR) collimators, 180° anterior circular rotation, 60 frames, 30s acquisition time per frame. A roving zoom of a 30cm square centred on the thyroid gland was also applied to the acquired frames. The patient was positioned as close as possible to each of the gamma camera heads consistent with their comfort and the need for the circular rotation of the gantry. The simultaneous dual-isotope acquisition ensured that the two sets of reconstructed SPECT images from the two energy windows would be inherently registered with

no need for anatomical markers or other means of registering the images after acquisition.

The total imaging time for this protocol was therefore 15 minutes. This was felt to be short enough to prevent significant discomfort for the patient resulting in movement but long enough that an acceptable number of counts would be collected in each acquisition frame in order to produce reconstructed SPECT images of diagnostic quality.

4.4 SPECT Image Reconstruction

For each patient, the two sets of SPECT images - from the dual-isotope acquisition - were reconstructed using the iterative Ordered Subsets Expectation Maximisation (OSEM) algorithm on the department's HERMES imaging computer system (Nuclear Diagnostics Ltd.). In accordance with recommendations from the software writers at Nuclear Diagnostics, the reconstruction for both isotopes was performed using 15 subsets and 4 iterations in order to obtain good quality images that accurately represented the isotope distribution in the body whilst keeping reconstruction time acceptably short. The reconstruction for each data set took around 1 minute. The reconstruction included no correction for attenuation, since the area of interest lies so close to the anterior surface of the neck, or for scatter.

A post-reconstruction filter was then applied to smooth the SPECT images. The final choice of filter was reached after a process of trial-and-error using both patient and phantom data. The chosen filter had to provide the best compromise between sharpness and excessive image noise. It was hoped that a single filter could be used for both the ^{99m}Tc and ^{123}I data sets to simplify the image processing procedure, but it was realised that this would be unlikely due to the differences in the levels of background tissue activity and uptake in the thyroid gland for the different isotopes.

4.5 SPECT Subtraction

As with the SPECT image reconstruction, the SPECT subtraction was performed on the HERMES computer system. The two sets of inherently registered transverse image slices were loaded side-by-side into the “Multimodality” display program, as shown in Figure 4.1. An image slice giving a clear view of the thyroid gland was selected. The “ROI Analysis” option was then chosen in order to draw a free-hand region of interest (ROI) around the thyroid gland on the ^{123}I image and the Multimodality program automatically applied the same ROI to the $^{99\text{m}}\text{Tc}$. The counts within the ROI on each image were noted and the ratio of $^{99\text{m}}\text{Tc}$ counts to ^{123}I counts was calculated to produce a scaling factor, k .

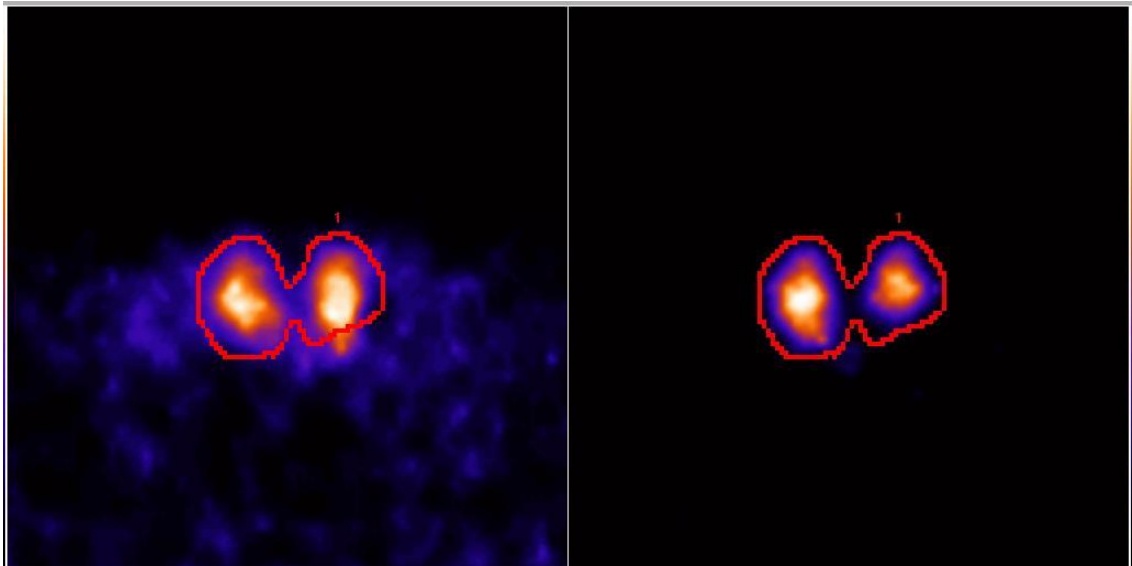


Figure 4.1 - Parathyroid SPECT image data in “Multimodality” display program
 Example of patient image data showing a single transverse SPECT slice with $^{99\text{m}}\text{Tc}$ -Sestamibi image on the left, the ^{123}I -iodide on the right and the hand-drawn thyroid ROI in red. The ROI was defined using the ^{123}I image. The images are inherently co-registered due to the dual-isotope acquisition.

The “Volume Math” option within Multimodality was then used to multiply the counts in each pixel in the ^{123}I image by the scaling factor and then subtract the full ^{123}I SPECT data set from the $^{99\text{m}}\text{Tc}$ data set. The formula used in the subtraction was therefore:

$$I_{sub} = I_{Tc} - (k \times I_I)$$

Equation 4.1

where I_{sub} is the resultant subtracted image data set, I_{Tc} is the reconstructed $^{99\text{m}}\text{Tc}$ SPECT data set, k is the scaling factor described above and I_{I} is the ^{123}I SPECT image data set.

An example of the resultant Multimodality display is shown in Figure 4.2. The display shows the original $^{99\text{m}}\text{Tc}$ SPECT on the left and the subtraction SPECT data set on the right. The area from which the thyroid gland has been subtracted out of the image is clearly visible as an area of little or zero counts, whilst a residual area of activity is seen posterior to the left lobe of thyroid, strongly suggesting the presence of a parathyroid adenoma in this case.

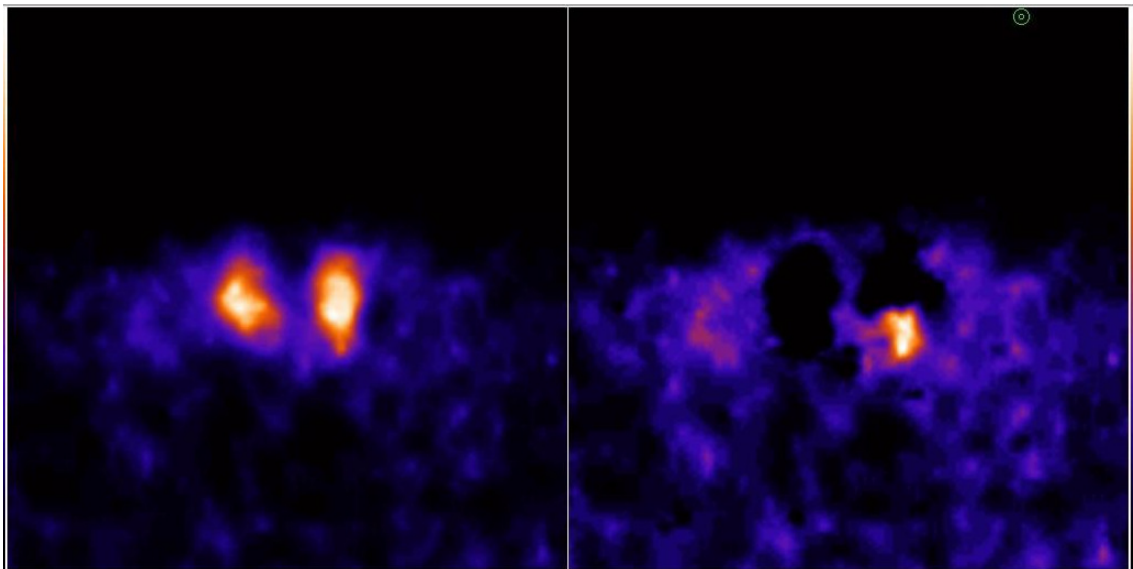


Figure 4.2 - Resultant subtraction image from "Multimodality" program
Images show the original $^{99\text{m}}\text{Tc}$ -Sestamibi SPECT data on the left and the co-registered subtraction image on the right. An area of residual activity posterior to the left lobe of thyroid can be seen on the subtraction image.

4.6 Observer Image Reviews

In order to assess the relative clinical utility of the various different sets of planar and SPECT images acquired for this study, a number of observer reviews were carried out. The results from the various reviews could then be compared with each other and with the surgical results to assess the relative clinical utility of different sets of image data.

A total of 5 observers took part in the study. Two of the observers were consultant nuclear medicine physicians, one was a consultant radiologist and the

final two were experienced nuclear medicine clinical scientists. Each observer was asked to review the images independently of the other observers. There was also a time gap of a minimum of several weeks between different phases of the study for each observer. This was to ensure that the risk of the observer remembering particular patient images and giving answers based upon a previous review was minimised.

Prior to the reviews commencing, all the image data was anonymised to prevent both issues of confidentiality and also to prevent observers recalling specific individuals at any time. Each image set was given the generic patient name "Patient X", where X was a number between 1 and 32. The order of the individual patients was based on the image acquisition date for some reviews and on the alphabetical listing of the participant surname for others to ensure that the observers could not recall the order of the data sets between reviews.

The observers were asked to review images in 4 phases, with each phase involving different sets of images from all 32 study participants. The first review included only the planar image data, consisting of ^{99m}Tc -Sestamibi, ^{123}I -iodide and subtraction images acquired at 15 minutes and 2 hours post-injection of Sestamibi. The second review involved only the reconstructed SPECT image data at a single time point, but again showing ^{99m}Tc , ^{123}I and subtraction images. The third review was of the planar and SPECT image data acquired in the ^{99m}Tc energy window only, which simulated the conditions under which many departments perform single-isotope parathyroid studies. The fourth and final review included all the available planar and SPECT images. A summary of the 4 phases and the images included for review in each is given in Table 4.1.

Phase	Images included for review
1	Planar only - both ^{99m}Tc -Sestamibi & ^{123}I -iodide
2	SPECT only - both ^{99m}Tc -Sestamibi & ^{123}I -iodide
3	^{99m}Tc -Sestamibi only - both planar & SPECT
4	All images - both planar & SPECT and both ^{99m}Tc -Sestamibi & ^{123}I -iodide

Table 4.1 - Summary of parathyroid observer study phases

For each patient in each phase of the reviews, the observers were asked to give information on any lesions they could see in the displayed images. Scoring sheets were used to record their answers, and these were completed by the

principal investigator who attended every review session. The number of lesions seen, their location(s) and the observer's confidence that each lesion represented a true parathyroid adenoma (as opposed to image artefact or some other pathology) were recorded. The location was specified in relation to the thyroid gland and classed as left or right, upper or lower, anterior or posterior and medial or lateral or as ectopic. The confidence of the observer was classed on a 4-point scale as definite, suggestive, equivocal or negative, with the first two being taken as a positive report for parathyroid adenoma and the latter two as a negative report. A score from 1-5 was also given for the quality of each set of image data, where 1 equates to poor and 5 to excellent.

The scoring sheets varied slightly between the phases due to the different information available in the images - for example, the position of a lesion in the antero-posterior direction cannot be obtained from an anterior planar image - and the sheets are shown in Appendix C.

The results from each phase of the review were then entered into a Microsoft Excel spreadsheet for analysis. As there were 5 observers and 32 patients, there were a total of 160 reviews in each phase. Therefore, there were a total of 640 reviews over the 4 phases of the observer study. Comparisons were made between the results for the same observer and same patient for the different study phases. A total of 6 comparisons for each of the 5 observers for each of the 32 patients were therefore carried out. The difference in number of lesions seen was calculated along with the difference in confidence level. Also, the given location of any lesions seen was compared to determine if the same lesion was being observed on different sets of images for the same patient. The comparison data was then transferred into the Minitab software package so that statistical analyses could be performed on the results and any statistically significant trends could be identified.

4.7 Surgical and Ultrasound Results

The gold standard and only definitive method for determining the presence or otherwise of a parathyroid adenoma or hyperplasia of the parathyroid glands is pathology analysis via a frozen section of the gland(s) resected at surgery. The

results of the observer image reviews therefore needed to be correlated to surgical findings to determine the true clinical utility of the various types of available planar and SPECT images.

In order to carry out a comparison of the image reviews and surgical findings, the case notes for each patient were examined to establish both the clinical diagnosis given prior to imaging and/or surgery and also the pathology results post-surgery. The endocrine surgeon records the location of any resected samples relative to the thyroid gland or other anatomical structures on the surgical notes, which are then included in the case notes. The pathology analysis results are also included in the case notes. All locations of resected parathyroid glands and the results of the pathology analysis were noted for each patient.

It was soon discovered, however, that not all of the patients had undergone parathyroidectomy surgery after nuclear medicine imaging. This could be for a number of reasons, such as the lack of a visualised lesion on imaging, the presence of another condition which could lead to the symptoms and blood analysis results seen in the patient, the patient being asymptomatic or the patient refusing to undergo surgery.

Unfortunately, when the individual participants agreed to take part in the study, there was no possible way of knowing which would or would not have surgery. In the case of those patients who did not have surgery, another standard for comparison was required to evaluate the relative clinical utility of the different nuclear medicine images available from this study. After discussion with various clinicians, the decision was made to use the findings of anatomical ultrasound (US) imaging as the standard. All the patient case notes were therefore re-examined and the results of any US imaging were noted. The location of any lesions observed during US was noted, along with the certainty expressed by the US reporter that the any lesion represented a true parathyroid adenoma. It was recognised, however, that ultrasound imaging is not a true gold standard in that it cannot absolutely confirm or deny the presence of a parathyroid adenoma and must be subject to a comparison with surgical findings in the same way as nuclear medicine imaging. Nevertheless, in the absence of gold standard surgical information, a comparison of the findings of the observer study with

ultrasound findings should give an indication of the relative merits of the different types of nuclear medicine image being evaluated.

The results from each of the 4 phases of observer image reviews were then compared to the surgical or US findings using a spreadsheet, in a similar fashion to the comparisons from the different image reviews discussed in Section 4.6. The Minitab package was also used again to carry out statistical analyses on the findings. The clinical utility of the various sets of available images could therefore be assessed in the presence of the gold standard information.

The percentage sensitivity and specificity of adenoma detection relative to the surgical results for each observer were then calculated separately for each phase of the study. Only the positive/negative result and the given left/right location were considered in the calculations, since these are the most important pieces of information for the endocrine surgeon prior to carrying out minimally invasive surgery (Anderson *et al.*, 2008). The sensitivity was taken to be:

$$\text{Sensitivity} = \frac{TP}{TP + FN} \times 100\%$$

Equation 4.2

where TP is the number of true positive results and FN is the number of false negative results. The specificity was calculated as:

$$\text{Specificity} = \frac{TN}{TN + FP} \times 100\%$$

Equation 4.3

where TN is the number of true negative results and FP is the number of false positive results. The results for all 5 observers were then combined to give an overall measure of sensitivity and specificity for each study phase. The sensitivity and specificity of the ultrasound results relative to the surgical results was also calculated.

Since a significant number of the study participants did not undergo surgery, the sensitivity and specificity of the observers reviewing the images was also calculated relative to the results of ultrasound scanning to provide an alternative measure of accuracy of the nuclear medicine imaging. In this case, the ultrasound result was taken to be the gold standard and the sensitivity and specificity of the nuclear medicine imaging were calculated using Equation 4.2 and Equation 4.3.

Chapter 5 – Parathyroid Study – Results of Observer Study

5.1 Patient Demographics

A total of 32 patients took part in the study, with 13 males (41%) and 19 females (59%). The average age of the participants was 56.7 ± 12.9 years (mean \pm 1SD) with a range of 28 to 83 years. All patients were referred with high blood serum levels of parathyroid hormone (PTH) and calcium and all referrals asked for confirmation of the presence of a parathyroid adenoma to explain these results and any other symptoms the patient may have been experiencing. Primary hyperparathyroidism had been diagnosed in 29 of the participants, whilst the remaining 3 had secondary hyperparathyroidism as a result of chronic renal failure. In general, hyperplastic glands in secondary hyperparathyroidism are smaller than the parathyroid adenomas seen in primary disease and so are likely to be less easily visualised on imaging.

5.2 Injected Activities

The recorded activities in the syringes pre- and post-injection were used to calculate the mean, maximum and minimum administered activities of ^{99m}Tc -Sestamibi and ^{123}I -iodide for the 32 patients. The distribution of administered activities is shown in Figure 5.1 and shows that the activity of ^{99m}Tc -Sestamibi administered to the patients was relatively variable and often well below the intended activity of 700MBq. The main reason for this is that Sestamibi has a tendency to stick to the walls of the glass vial and plastic syringe, meaning that not all of the available activity is administered to the patient. Also, the administered activity of ^{99m}Tc -Sestamibi for patients 29-32 can be seen to be generally higher than for the preceding patients. This is due to the fact that standard departmental procedure was modified at the time these patients attended the department and the activity ordered for administration was increased to the ARSAC limit of 900MBq in order to provide better image quality for diagnostic purposes.

Table 5.1 shows the mean, maximum and minimum administered activities of ^{99m}Tc -Sestamibi and ^{123}I -iodide for the 32 patients. It is immediately clear from the table that the maximum and minimum values for administered activity of ^{123}I -iodide are considerably different to the intended 20MBq activity. The maximum occurred due to an error by the operator in drawing up the

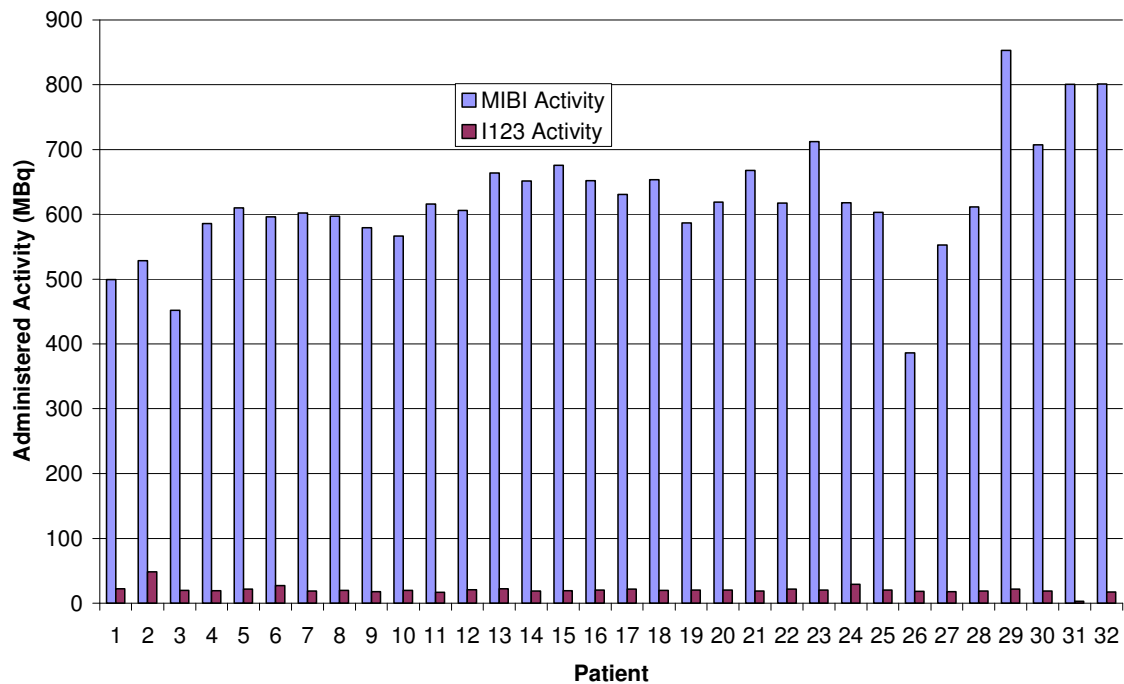


Figure 5.1 - Distribution of administered activities
Column chart showing the administered activity in MBq of ^{99m}Tc -Sestamibi (blue) and ^{123}I -iodide (brown) for each of the 32 study participants

radiopharmaceutical from the syringe. The minimum occurred when there was a shortage of available ^{123}I -iodide. The ARSAC certificate holder felt, however, that in this instance, the test should continue as valuable clinical information could still be gained even with a low administered activity.

	Administered Activity (MBq)			
	Intended	Mean	Maximum	Minimum
^{99m}Tc -Sestamibi	700	621.9	852.8	386.5
^{123}I -iodide	20	20.8	48.8	3.4

Table 5.1 - Administered activities of radiopharmaceutical
Intended, mean, maximum and minimum administered activities of ^{99m}Tc -Sestamibi and ^{123}I -iodide for the 32 study participants

5.3 SPECT Reconstruction

The primary aim in reconstructing the SPECT image data was to produce clinically acceptable images. It was therefore important to achieve a good balance between excessive smoothing, which can lead to blurring and a loss of resolution, and excessive sharpness, when the noise level in the image becomes unacceptably high. Due to the different count density in the two acquisition energy windows (^{99m}Tc and ^{123}I), the same reconstruction parameters applied to both data sets may not provide suitable image quality in both cases. Some trial and error was therefore required to find the parameters giving acceptable image quality for the two sets of images.

The superior-inferior extent of the reconstruction for all the SPECT data sets was selected to ensure that both the salivary glands and heart were visible in the ^{99m}Tc -Sestamibi images. This was in order to provide some useful anatomical location information for the observers reviewing the images. The ^{123}I -iodide images were then reconstructed with the same superior-inferior extent so that the inherent registration of the two sets of image data was maintained.

As discussed in the previous chapter (Section 4.4), the number of subsets and iterations used in the Ordered Subsets Expectation Maximisation (OSEM) reconstruction on the department's HERMES computer system (Nuclear Diagnostics Ltd.) were set to 15 and 4 respectively for both the ^{99m}Tc and ^{123}I image data, which gave rapid convergence to the physiological distribution of activity. The resultant images from this reconstruction were felt to be too sharp and contained too much noise. An example of unfiltered ^{99m}Tc and ^{123}I reconstructed images for a single patient is shown in Figure 5.2, clearly demonstrating the need for some post-reconstruction smoothing.

The following filters, with the option to vary certain parameters (given in brackets for each), are available from the HERMES system: Butterworth (cutoff frequency in cycles/cm and order), Hanning (cutoff frequency in cycles/cm), Low Pass (cutoff frequency in cycles/cm), Metz (Metz factor and MTF resolution from very low to very high) and 3x3x3 smoothing (no variable parameters). All the filters were tested on a number of patient data sets using the data acquired

in both the ^{99m}Tc and ^{123}I energy windows. For each type of filter, a number of different image data sets were produced after varying the optional parameters. The goal was to produce images with the best compromise between sharpness and excessive image noise.

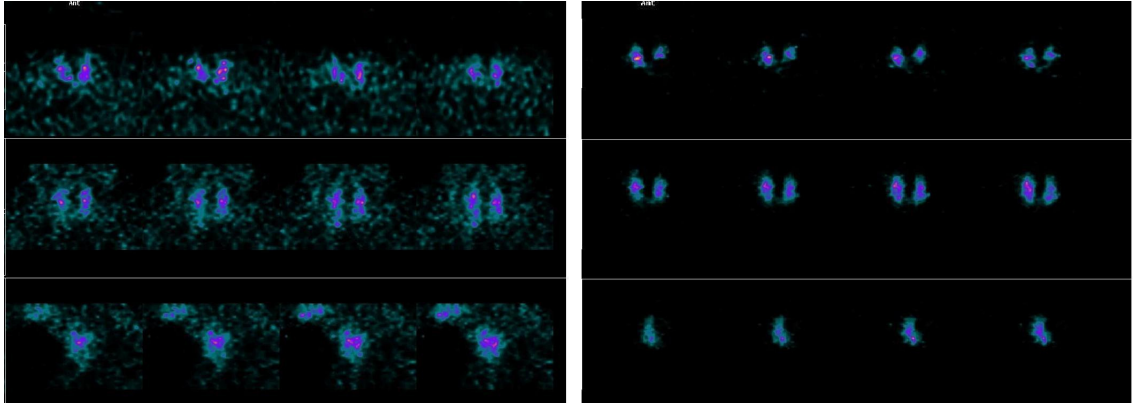


Figure 5.2 - Unfiltered reconstructed parathyroid SPECT images

Example of reconstructed patient parathyroid images without post-reconstruction filter applied. On the left are the ^{99m}Tc -Sestamibi images and on the right are the co-registered ^{123}I -iodide images. On each, the top row is transverse slices, the middle row is coronal slices and the bottom row is sagittal slices.

An example of a reconstructed dual-isotope SPECT data set is shown in Figure 5.3. In this case, the filter applied post-reconstruction has resulted in excessive image smoothing, meaning that the structure of the thyroid gland cannot be discerned.

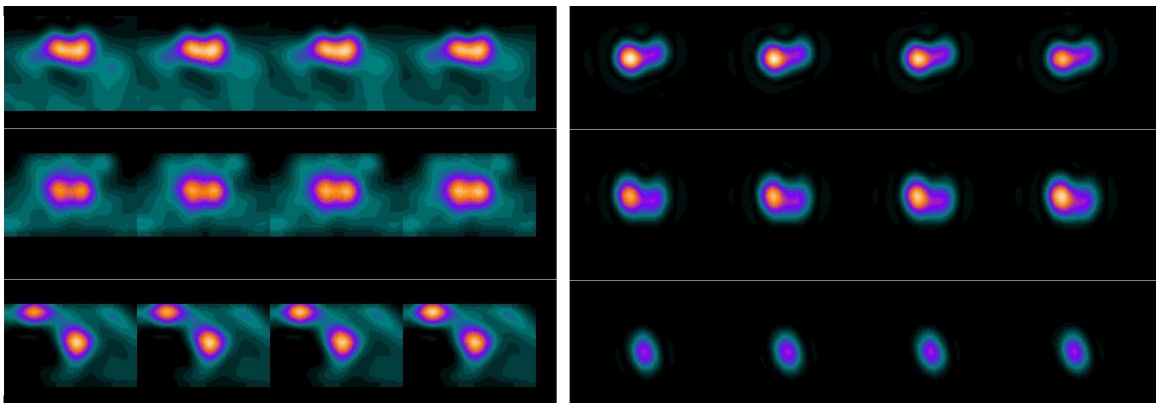


Figure 5.3 - Overly smoothed parathyroid SPECT images

Example of patient parathyroid SPECT data that has been excessively smoothed by the post reconstruction filter. Figure shows the same slices in the same layout as in Figure 5.2.

In contrast, the images shown in Figure 5.4 have been insufficiently filtered and so are too sharp and noisy. The images in Figure 5.4 represent the same slices from the same patient data set as shown in Figure 5.2 and Figure 5.3.

The images shown in Figure 5.5 are the same slices from the same patient data set as shown in Figure 5.2, Figure 5.3 & Figure 5.4, but in this case, the post-reconstruction filter applied gives a much better compromise between smoothing and noise. These images represent an example of the final choice of post-reconstruction filter, which was decided upon by asking experienced physicians and clinical scientists to view a number of SPECT image data sets, to which different post-reconstruction filters had been applied, for several different patient acquisitions. Each reviewer was asked to nominate the images they felt produced the best compromise between smoothing and noise and the consensus view was taken as the most appropriate filter to use for this study. Although objective measures - such as resolution, contrast or signal-to-noise ratio (SNR) - can be used to compare images to which different post-reconstruction filters have been applied, the subjective method used here is the most commonly applied. This is due to the fact that human observers will report from the final images and so they must be subjectively acceptable to the observer.

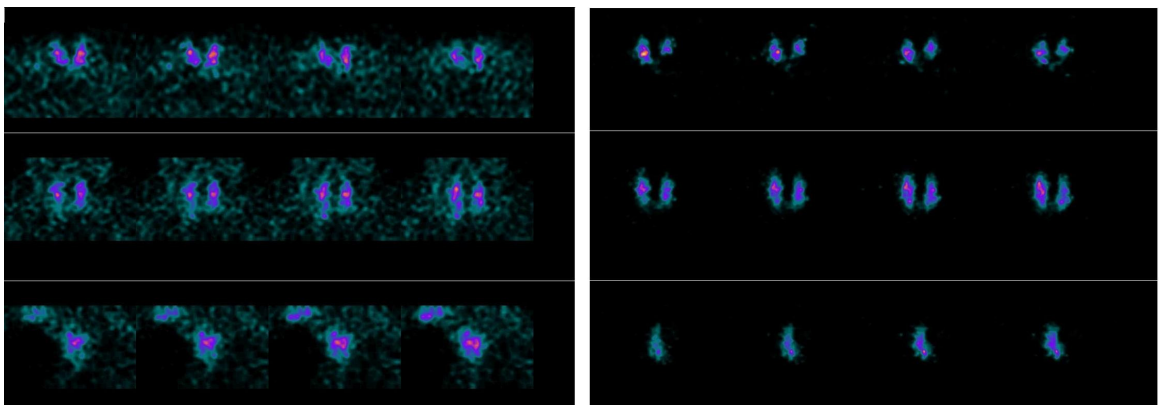


Figure 5.4 - Overly sharp parathyroid SPECT images

Example of patient parathyroid SPECT data that remains too sharp after the application of the post-reconstruction filter. Figure shows the same slices in the same layout as in Figure 5.2.

Unexpectedly, the same Hanning filter with a cutoff frequency of 3 cycles/cm gave acceptable image quality for both the reconstructed ^{99m}Tc and ^{123}I image

data for a number of different patient data sets. This filter was therefore applied to all the reconstructed data prior to performing image subtraction.

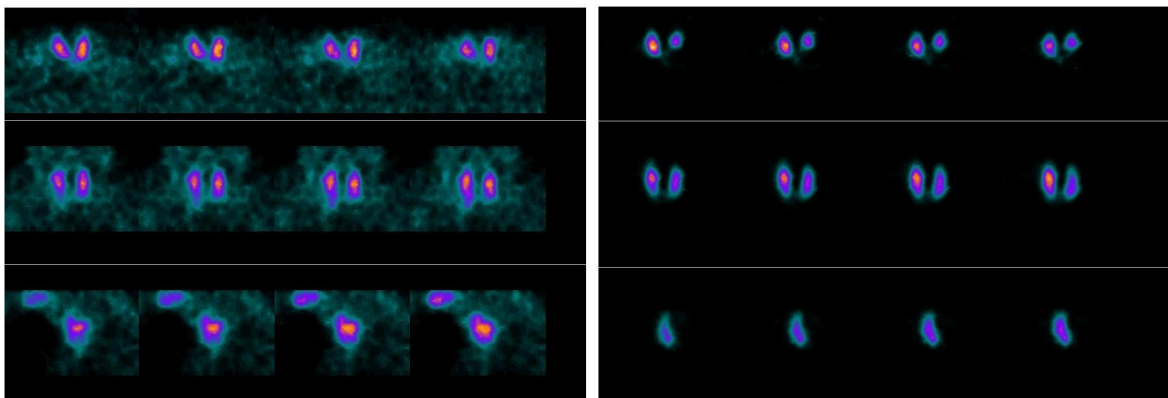


Figure 5.5 - Parathyroid images acceptably filtered
Example of patient parathyroid SPECT data that has been filtered to give the best compromise between smoothing and excessive image noise. Figure shows the same slices in the same layout as in Figure 5.2.

Subtraction SPECT images were then created for each patient data set and all images were anonymised before being shown to the observers. An example of a subtraction SPECT data set demonstrating an area of residual activity consistent with a parathyroid adenoma is shown in Figure 5.6.

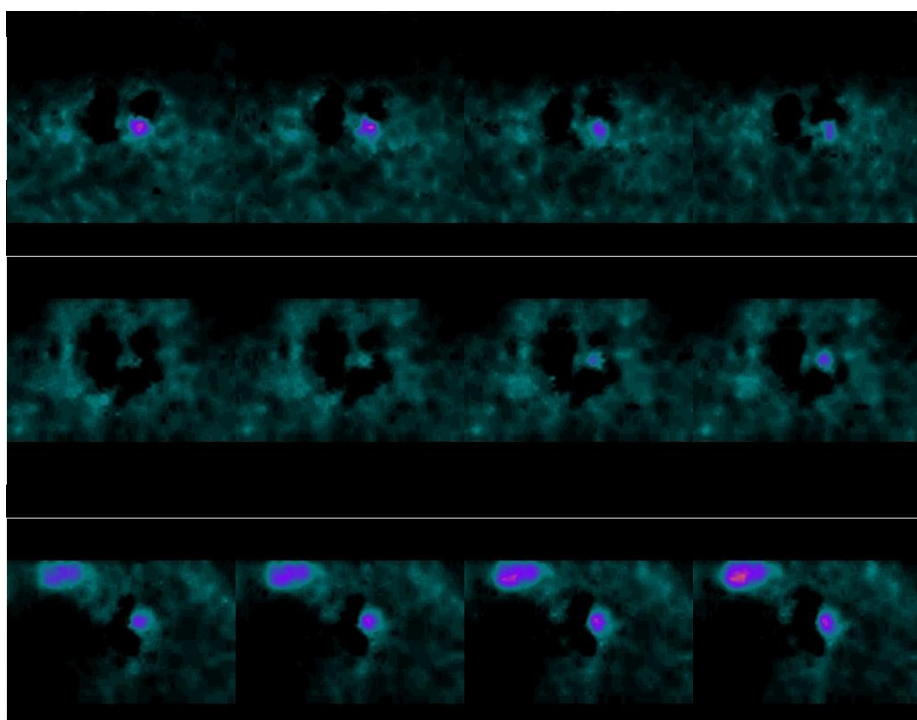


Figure 5.6 - Subtraction SPECT images
Example of patient parathyroid subtraction SPECT images with area of residual activity seen posterior to the left lobe of thyroid, indicating the presence of a parathyroid adenoma. The same slices are shown in the same layout as in Figure 5.2.

5.4 Observer Study Results

5.4.1 General Comments

All five observers took part in all 4 phases of the observer study (see Table 4.1 for list of phases), each reviewing the 32 patient image data sets in each phase. Detailed feedback was provided for each image data set reviewed, but the observers were also asked for general comments during the process. An overview of these comments will now be given.

All the observers were comfortable reviewing the images shown during the first phase of the study, which were the planar images acquired according to the department's standard protocol. The second phase gave the observers the opportunity to review the SPECT images (including the subtraction images) in the absence of the planar images. This brought a mixture of feedback with general agreement that the anterior-posterior information available from the SPECT images was useful but that the amount of available data meant that the process of review was sometimes more complicated than with the planar images. Most of the observers also commented that by the time they were reviewing the last few sets of patient data, they were more comfortable with the SPECT data than they had been at the start of this phase, when viewing parathyroid SPECT data was entirely new to them. This may have affected the image quality scores given for this phase of the study.

All the observers felt that not enough clinical information was available to them during the third phase of reviewing the ^{99m}Tc -Sestamibi images only, even though both planar and SPECT images were shown. The lack of specific image information delineating the thyroid gland meant that the observers were often unsure if a possible lesion was thyroid tissue or was indeed a parathyroid adenoma. Although this feedback was essentially negative, the fact that all the observers are used to seeing the ^{123}I thyroid images in their normal practice may have been a significant factor.

The final phase of the review process involved the observers reviewing all the planar and SPECT images together. The comments received for this phase were

almost all positive with the observers feeling that the SPECT images often helped to confirm or deny a possible lesion seen on the planar images. They also commented that there were a number of lesions seen only on the SPECT images that were not visualised on the planar images. One of the observers also consistently commented that SPECT/CT data would be even more useful than just SPECT as it would give more anatomical detail to aid in the localisation of any lesions. The other observers did not share this feeling, however, and felt that only in the case of an obviously ectopic parathyroid adenoma would CT data provide any significant localisation information.

In all the results presented in the remainder of this chapter and in Chapter 6, the observers are numbered 1-5 in the same order each time. Observers 1 & 3 were consultant nuclear medicine physicians, observer 2 was a consultant radiologist (all ARSAC certificate holders), and observers 4 & 5 were experienced clinical scientists in nuclear medicine physics.

5.4.2 Phase 1 – Planar Images

5.4.2.1 Lesions Seen

When reviewing the planar images only, the 5 observers noted a total of 89 lesions. Of these, 42 (47%) were deemed to definitely represent a parathyroid adenoma, 19 (21%) were suggestive for parathyroid adenoma and the remaining 28 (32%) were classed as equivocal lesions. The observers therefore saw a total of 61 lesions that they felt positively demonstrated the presence of a parathyroid adenoma as equivocal reports were taken as negative in this study. Of the 160 reviews in this phase (32 patients each reviewed by 5 observers), 80 (50%) were classed as negative for the presence of any lesions.

5.4.2.2 Image Quality and Usefulness Scores

Scores were also given for the quality of the ^{99m}Tc -Sestamibi images, the ^{123}I -iodide images and the subtraction images for each patient. The scoring scale was from 1 to 5 with 1 representing poor and 5 excellent image quality. The observers were also asked to give a score on the same scale for the relative usefulness of the subtraction images. Average values of these scores were taken

for each patient and then the average of these results taken over the 32 patients to assess the relative quality of the different images. Average scores were also calculated for each observer and compared.

The variation in the given scores was wide between patients but less so between different observers. The average scores for each of the individual observers and overall are shown in Table 5.2. The results show that all observers gave higher scores for image quality to the ^{123}I -iodide images than to the $^{99\text{m}}\text{Tc}$ -Sestamibi images. Indeed, the observers commented that the lack of background activity on the ^{123}I -iodide images tends to automatically lead to better image quality than is seen for the $^{99\text{m}}\text{Tc}$ -Sestamibi or subtraction images. The usefulness of subtraction results show that, in general, the observers found these images more useful than not, in that the mean scores are above 3 (the median of the scoring scale) for each observer.

Observer	$^{99\text{m}}\text{Tc}$ -Sestamibi	^{123}I -Iodide	Subtraction	Usefulness of Subtraction
1	3.0	3.3	3.2	3.1
2	3.4	3.6	3.7	3.8
3	3.3	3.7	3.5	3.5
4	3.4	3.7	3.4	3.3
5	2.6	3.8	3.4	3.7
Overall	3.2	3.6	3.4	3.5

Table 5.2 - Image quality scoring for planar images in observer study phase 1
Average image quality scores given by each observer and for all observers together on a scale of 1 (poor) to 5 (excellent).

The information on the location of any lesions seen by the observers will not be discussed in detail here. Instead, the findings will be compared with those from the other phases of the observer study in Section 5.5.

5.4.3 Phase 2 – SPECT Images

5.4.3.1 Lesions Seen

The observers commented on the presence of a total of 183 lesions whilst reviewing the SPECT image data in isolation from the planar views. In 89 (49%) cases, the observers were confident that the lesion definitely represented a parathyroid adenoma, in 45 (24%) instances they felt the lesion was suggestive

for a parathyroid adenoma, whilst in the remaining 49 (27%) cases they classed the lesion as equivocal. A total of 24 (15%) of the 160 reviews in this phase were reported as negative by the observers. There were therefore a total of 134 lesions reported as positive for parathyroid adenoma, which is a significant increase on the 61 positive lesions seen on the planar image in phase 1 of the review.

5.4.3.2 Image Quality and Usefulness Scores

As for phase 1 of this review, the observers were asked to give scores for the quality and usefulness of the images shown for each patient data set. The same scale was used and, once again, scores were given for the quality of the ^{99m}Tc -Sestamibi, ^{123}I -iodide and subtraction SPECT images. A score was also given for the overall usefulness of the subtraction SPECT data set for assisting the observer in determining the presence or otherwise of a parathyroid adenoma.

The average scores for each individual observer and for all the observers together were again calculated and these are shown in Table 5.3. As for the planar image reviews, the scores given to the ^{123}I -iodide images were consistently higher than those given for the ^{99m}Tc -Sestamibi images. Most of the scores given in this phase were lower than those in phase 1, which may in part be attributed to the fact that the observers had not seen parathyroid SPECT image data prior to this phase of the study and so were not used to reviewing the images. However, the observers still generally found the subtraction images useful, with only observer 4 giving an average score of less than 3.

Observer	^{99m}Tc -Sestamibi	^{123}I -Iodide	Subtraction	Usefulness of Subtraction
1	2.7	3.3	3.3	3.4
2	3.2	3.5	3.6	3.4
3	2.6	3.0	2.7	3.3
4	3.1	3.5	3.0	2.9
5	2.7	3.3	2.9	3.4
Overall	2.8	3.3	3.1	3.3

Table 5.3 - Image quality scoring for SPECT images in observer study phase 2
Average image quality scores given by each observer and for all observers together on a scale of 1 (poor) to 5 (excellent).

Once again, the detail of the location of the lesions seen will not be discussed here but comparisons with the results from other phases of the observer study are discussed in Section 5.5.

5.4.4 Phase 3 – ^{99m}Tc-Sestamibi Planar and SPECT Images

5.4.4.1 Lesions Seen

For the third phase of the observer study, the observers were asked to review the image data collected in the ^{99m}Tc energy window only - that is, the images demonstrating the distribution of ^{99m}Tc-Sestamibi within the patient. Both planar and SPECT images acquired in the ^{99m}Tc energy window were shown but no ¹²³I-iodide or subtraction images were included in this phase. The observers reported seeing a total of 116 lesions, which is more than were on the planar dual-isotope and subtraction planar scans shown in phase 1 but fewer than when the observers reviewed the SPECT images in phase 2. Of these 116 lesions, 25 (22%) were classed by the observers as definitely parathyroid adenoma, 37 (32%) were judged to be suggestive for parathyroid adenoma and the final 54 (46%) were said to be equivocal. In total 57 (36%) of the reviews in this phase were reported as negative by the observers. Therefore, there were a total of 62 lesions deemed positive for the presence of parathyroid adenoma seen in this phase of the study, which is similar to the number given as positive in phase 1.

5.4.4.2 Image Quality and Usefulness Scores

On this occasion, scores were given for the quality of the planar and SPECT images and for the usefulness of the SPECT image in determining the presence or absence of a parathyroid adenoma and the results are shown in Table 5.4. Interestingly, the scores given for planar image quality are generally lower than those given for the ^{99m}Tc-Sestamibi planar images in phase 1, even though the images shown were exactly the same. Similarly, the scores given for the SPECT images in phase 3 were generally lower than those given for the ^{99m}Tc-Sestamibi SPECT images in phase 2. These findings indicate that the presence of the ¹²³I-iodide images showing uptake only in the thyroid gland has a bearing on the perceived quality of the much noisier ^{99m}Tc-Sestamibi images. The observers gave a mixed response to the usefulness of the SPECT images for the review,

with three (observers 1, 3 and 5) giving average scores of greater than 3, whilst the others (observers 2 and 4) gave average scores of less than 3.

Observer	Planar	SPECT	Usefulness of SPECT
1	2.9	3.1	3.8
2	3.2	2.9	2.5
3	3.4	2.8	3.2
4	3.3	3.2	2.9
5	2.4	3.0	3.3
Overall	3.0	3.0	3.1

Table 5.4 – Image quality scoring for ^{99m}Tc -Sestamibi images in observer study phase 3
Average image quality scores given by each observer and for all observers together on a scale of 1 (poor) to 5 (excellent).

The comparisons between the results from this phase of the study with those from the other phases are discussed in Section 5.5 and so no further details will be given here.

5.4.5 Phase 4 – All Planar and SPECT Images

5.4.5.1 Lesions Seen

The fourth and final phase of the observer study involved asking the observers to review all the available image data for each patient together. That is, the observers were shown the planar and SPECT images from both the ^{99m}Tc and ^{123}I acquisition energy windows as well as the planar and SPECT subtraction images. The observers reported a total of 155 lesions in this phase of the study, which is lower than the total number seen in phase 2 but higher than in either phase 1 or phase 3. In 70 (45%) cases the observers felt that the lesion seen was definitely a parathyroid adenoma, whilst in 33 (21%) they felt that the lesion was suggestive for the presence of a parathyroid adenoma and in the remaining 52 (34%) the lesion was classed as equivocal. Negative results were reported in 33 (21%) of the 160 reviews. There were therefore 103 lesions positively identified as parathyroid adenoma in this phase of the study, which is a higher number than seen in phases 1 and 3 but considerably fewer than seen in phase 2.

5.4.5.2 Image Quality and Usefulness Scores

As was the case in phase 3, the observers were asked to give scores for the quality of the planar and SPECT images as well as giving a score for the usefulness of the SPECT images in reaching a final conclusion. The results are shown in Table 5.5 and indicate that the observers generally found the quality of the SPECT and planar images to be similar. The scores given for the usefulness of the SPECT images indicate that all the observers generally found the SPECT data helpful in reaching a conclusion as to the presence or otherwise of a parathyroid adenoma. Observer 5, in particular, gave high scores for the usefulness of SPECT resulting in an average score of greater than 4.

As was the case for the previous phases, the detail of the lesions seen will not be discussed here but instead will be commented upon in Section 5.5 where the results from this phase of the study are compared with those from the preceding three phases.

Observer	Planar	SPECT	Usefulness of SPECT
1	3.2	3.0	3.6
2	3.7	3.3	3.3
3	3.3	3.0	3.2
4	3.1	3.4	3.7
5	3.1	3.2	4.3
Overall	3.3	3.2	3.6

Table 5.5 - Image quality scoring for all planar and SPECT images in observer study phase 4
Average image quality scores given by each observer and for all observers together on a scale of 1 (poor) to 5 (excellent).

5.4.6 Summary of Lesions Seen

Figure 5.7 shows the total number of lesions seen by the 5 observers on each phase of the observer study. It also shows the number of lesions on each phase that the observers felt were “definite”, “suggestive”, “equivocal” or “negative” for parathyroid adenoma. It is immediately clear that the highest number of lesions were seen in phases 2 & 4 of the study, which are those phases that included the review of the dual-isotope subtraction SPECT images. The phase with the fewest lesions seen in total, as well as the highest number of negative reports, was phase 1, in which only planar images were available for review. The numbers of equivocal and negative reports for phase 3 were also high,

confirming that the observers were not confident reviewing images in the absence of the ^{123}I -iodide thyroid images.

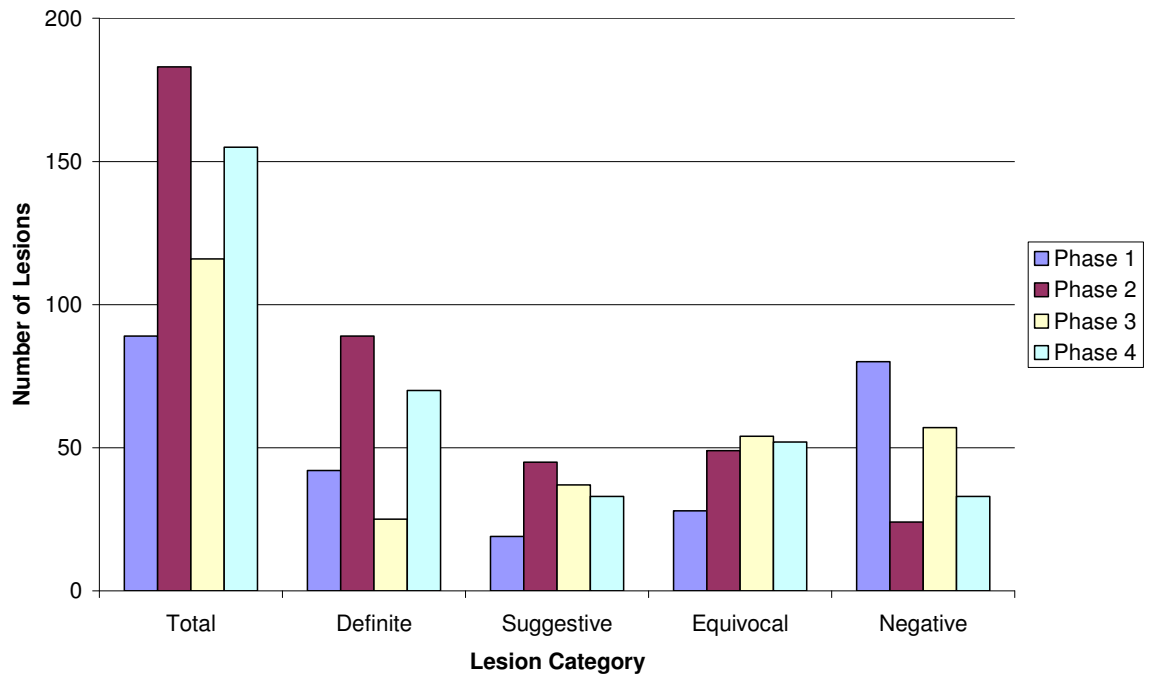


Figure 5.7 - Bar chart of number of lesions seen

Bar chart showing the total number of lesions seen by the 5 observers on each phase of the observer study as well as the numbers given in each category of confidence.

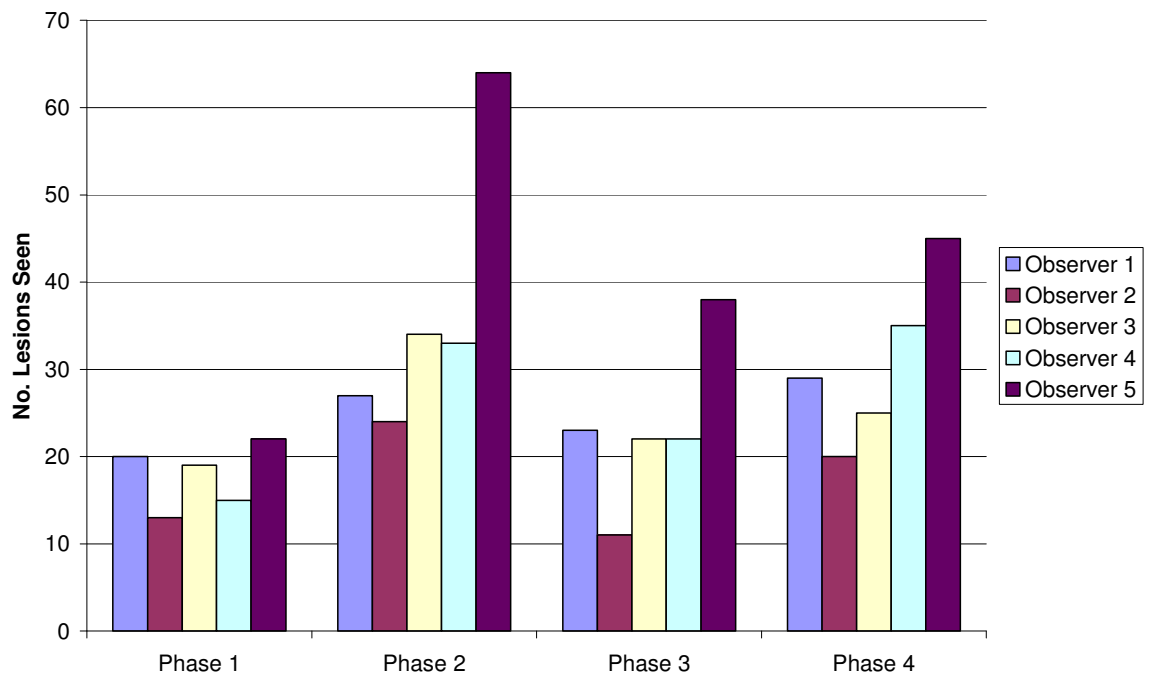


Figure 5.8 - Bar chart of lesions seen by each observer

Bar chart showing the number of lesions seen by each of the 5 observers individually on each of the 4 phases of the observer study

A bar chart showing the number of lesions that was seen by each individual observer on each of the 4 study phases is shown in Figure 5.8. Observer 5 has a clear tendency to see more lesions on the images than any of the other observers. In contrast, observer 2 saw fewer lesions than all other observers on all 4 phases of the study. The chart also confirms the fact that more lesions were seen on phases 2 & 4 of the study, when the dual-isotope subtraction SPECT images were available for review, than on the other phases.

5.5 Comparisons of Results of Observer Study

The information provided by the observers from each phase of the study was compared to that from each of the other phases to assess the differences between the number of lesions seen, the certainty that the lesions seen represented true parathyroid adenomas and the locations of the lesions. The reported information from each individual observer for each patient was compared directly to determine any differences. In cases where multiple lesions were seen in one or other of the phases being compared, comparisons were made between each individual lesion seen in one phase with each individual lesion seen in the other phase. That is, if an observer saw 2 lesions in one phase of the study and 3 in another, a total of 6 comparisons were carried out.

The difference in the number of lesions seen in the different phases was calculated and then the Wilcoxon Signed Ranks test was applied using the Minitab software (Minitab Inc.) to establish if any statistical differences existed. The number of instances for each observer of the number of lesions seen in one phase being higher, lower and the same as seen in the other phase was also determined. The comparison of the observers' certainty that a given lesion represented a true parathyroid adenoma yielded a result of "more", "same" or "less" certain. Reviews classed as negative were placed at the bottom of the certainty scale. For each patient, an overall certainty comparison was made by summing the number of "more", "same" and "less" results and determining the class with the highest total. The Wilcoxon Signed Ranks test was also applied to the results from each observer and to the combined results for all observers by giving each "more" result a value of 1, "same" a value of 0 and "less" a value of -1.

Finally, the location of lesions reported in the different phases was compared. The given location was classed as “same” or “different” for left versus right, upper versus lower, anterior versus posterior and medial versus lateral. The left versus right and upper versus lower results were then combined using the logical “AND” function to give a “same” or “different” result for establishing if the same lesion was seen in the different phases. For comparisons involving only phases 2, 3 and 4, the anterior versus posterior information was also added. In comparisons involving phase 1, no anterior/posterior data was included as it is not possible to determine the position of a lesion in this plane from anterior planar images only. The given medial/lateral information was not included in the comparison because the observers often felt that it was not appropriate to report on this aspect of the location of an observed lesion. Statistical testing was not applied to the location information due to the fact that the comparisons of different phases were not necessarily of the same lesion. This means that the data are not truly paired and applying the Wilcoxon Signed Ranks test could give misleading and inaccurate results.

In the following sections, the differences between the number of lesions seen are always quoted as the later phase minus the earlier phase. Also, a letter has been used to designate the number of lesions seen in each phase of the study as follows: P for phase 1 (dual-isotope planar images), S for phase 2 (dual-isotope SPECT images), M for phase 3 (Sestamibi SPECT and planar images) and A for phase 4 (all planar and SPECT images). A category described as “M>S”, for example, therefore means that the number of lesions seen on phase 3 was greater than the number seen on phase 2 of the study.

5.5.1 Phase 2 versus Phase 1 Reviews

5.5.1.1 Number of Lesions Seen

The number of lesions seen in phase 1 (planar only) was subtracted from the number seen in phase 2 (SPECT only). Table 5.6 summarises the number of times each observer saw more, the same or fewer lesions on the SPECT images. It shows that in most cases, the number of lesions seen on reviewing the SPECT images is the same as the number seen on the planar images. However, there are more cases of the number of lesions seen being greater on the SPECT than on

the planar images. Observer 5 has the highest number in the “S>P” category whilst observer 1 has the fewest.

Observer	S > P	S < P	S = P	Total
1	9	3	20	32
2	11	1	20	32
3	14	2	16	32
4	15	0	17	32
5	21	0	11	32
Total	70	6	84	160

Table 5.6 - Comparison of number of lesions seen in phase 1 (planar only) and phase 2 (SPECT only)

S>P = number of times more lesions were seen on SPECT than planar, S<P = number of times fewer lesions were seen on SPECT than on planar, S=P = number of times same number of lesions were seen on SPECT as on planar.

The Wilcoxon Signed Ranks non-parametric statistical test was applied to the differences in the number of lesions seen for each observer individually as well as for all the reviews in total. Each application of the test gave a p-value of statistical significance, an estimated median and a 95% confidence interval (CI). A p-value of less than 0.05 was taken to indicate a statistically significant result. The results are shown in Table 5.7. It should be noted that the lowest p-value the software will define is 0.001 so any value lower than this is stated as <0.001.

Observer	p-value	Estimated median	95% CI
1	0.108	0.0	(0.0, 0.5)
2	0.011	0.5	(0.0, 0.5)
3	0.006	0.5	(0.0, 0.5)
4	0.001	0.5	(0.5, 1.0)
5	<0.001	1.0	(1.0, 1.5)
Overall	<0.001	0.5	(0.5, 0.5)

Table 5.7 - Results from Wilcoxon Signed Ranks test on differences in number of lesions seen (phase 2 vs phase 1)

Output from Minitab software applied to the differences in the number of lesions seen between the SPECT and planar images.

These results clearly show that for 4 of the 5 observers and for the data from all the observers combined, there is a statistically significant difference in the number of lesions seen with $p < 0.05$. However, for the other observer (observer 1), the result of $p = 0.108$ indicates that no such statistically significant difference exists. This is in keeping with the results in Table 5.6 where this observer had the lowest number in the “S>P” category. In contrast, observer 5 has both the lowest p-value and highest estimated median of all the observers, which again supports the results shown in Table 5.6. The estimated median values from the

test are all ≥ 0 , indicating that, in general, more lesions are seen on the SPECT than on the planar images.

5.5.1.2 Confidence of Lesions Representing True Adenoma

A total of 224 comparisons were carried out between the confidence level expressed by the observer from the review of the SPECT images and the confidence scores from the planar images. The number of comparisons falling into each of the “more”, “same” and “less” categories from each observer and the combined numbers overall are shown in Table 5.8. It can be seen that observers 1-4 all have more than 50% of the comparisons in the “more” category, with observer 3 having the highest proportion at 60%, meaning that the observers are all more confident that they are seeing true lesions on SPECT images more than half of the time. Although observer 5 had slightly less than 50% in this category, it still represented the highest proportion for this observer. Observer 5 also had the highest number of comparisons carried out in total, meaning that this observer tended to see more lesions than the others.

Observer	No. More (%)	No. Same (%)	No. Less (%)	Total
1	18 (53%)	13 (38%)	3 (9%)	34
2	18 (51%)	14 (40%)	3 (9%)	35
3	25 (60%)	14 (33%)	3 (7%)	42
4	23 (57%)	13 (32%)	4 (10%)	40
5	36 (49%)	27 (36%)	11 (15%)	74
Overall	119 (53%)	81 (36%)	24 (11%)	224

Table 5.8 - Results from comparison of confidence levels expressed (phase 2 vs phase 1) Number of comparisons between expressed confidence levels that showed observers as more, same or less confident looking at the SPECT images as compared to the planar. Percentages of the total in each category for each observer and overall are given in brackets.

For 19 (59%) of the 32 patients, the observers were generally more confident that the lesions they saw in the SPECT were true lesions when compared to their confidence reviewing the planar images, whilst for 12 (38%) patients they expressed the same level of confidence. Therefore, they were generally less confident for only 1 (3%) patient, indicating that the SPECT images give a significant increase in the confidence level. The results of the Wilcoxon Signed Ranks test applied to the comparisons for each observer and for the results for all the observers combined are shown in Table 5.9. Again, a p-value of <0.05 was taken to be statistically significant.

The results clearly show that a statistically significant difference exists for all the observers with $p < 0.05$ in all cases. The fact that the estimated median values are all > 0 and the 95% CIs are all positive is as expected, given that the observers are more confident when reporting from the SPECT images than from the planar.

Observer	p-value	Estimated median	95% CI
1	0.004	0.5	(0.0, 0.5)
2	0.004	0.5	(0.0, 0.5)
3	< 0.001	0.5	(0.5, 1.0)
4	0.001	0.5	(0.5, 1.0)
5	0.002	0.5	(0.0, 0.5)
Overall	< 0.001	0.5	(0.5, 0.5)

Table 5.9 - Results from Wilcoxon Signed Ranks test on differences in expressed confidence level (phase 2 vs phase 1)
Output from Minitab software applied to the comparison of confidence level expressed by the observers between the SPECT and planar images.

5.5.1.3 Location of Observed Lesions

The given locations of any lesions reported by the observers were compared between the two phases of the review. The left/right locations were compared separately from the upper/lower results, all locations being relative to the thyroid gland. The findings were then combined using the logical AND function to determine how many lesions were seen at the same location on both sets of images. As discussed in Section 5.5, no comparison of the anterior/posterior locations was possible due to the lack of information in this plane on the planar images.

Table 5.10 gives the results of the left/right comparison, showing the number (and percentage) of lesions seen in the same and different locations for each observer. The results show that there are roughly equal proportions in each category for each of the observers individually and for all observers combined. Observer 1 has the highest proportion of lesion to which the same left/right location was given at 57% whilst observer 5 has the lowest fraction at 43%.

The findings from the comparison of the given upper/lower locations are summarised in Table 5.11. Again, the proportions in the two categories are similar, but there is a tendency for the number of lesions given different

locations to be slightly higher. Once again, observer 5 had the lowest proportion of lesions reported at the same location on the two sets of images.

Observer	No. Same (%)	No. Different (%)	Total
1	20 (57%)	15 (43%)	35
2	19 (56%)	15 (44%)	34
3	21 (50%)	21 (50%)	42
4	19 (48%)	21 (52%)	40
5	32 (43%)	42 (57%)	74
Overall	111 (49%)	114 (51%)	225

Table 5.10 - Results of comparison in left/right location between lesions seen on SPECT and planar images

Number and percentage of lesions seen in the same and different left/right location for each observer and for the combined for all observers.

Observer	No. Same (%)	No. Different (%)	Total
1	18 (51%)	17 (49%)	35
2	16 (47%)	18 (53%)	34
3	19 (45%)	23 (55%)	42
4	18 (45%)	22 (55%)	40
5	29 (39%)	45 (61%)	74
Overall	100 (44%)	125 (56%)	225

Table 5.11 - Results of comparison in upper/lower location between lesions seen on SPECT and planar images

Number and percentage of lesions seen in the same and different upper/lower location for each observer and for the combined for all observers.

A summary of the results from combining the data on differences in location is given in Table 5.12. The data shows that for each observer, the number of lesions seen at different overall locations was greater than the number seen at the same location. This will be partly explained by the fact that more lesions were seen on the SPECT images than the planar but it is interesting to note that it was not necessarily the same lesion that was seen on both planar and SPECT images for an individual patient.

Observer	No. Same (%)	No. Different (%)	Total
1	16 (46%)	19 (54%)	35
2	16 (47%)	18 (53%)	34
3	18 (43%)	24 (57%)	42
4	18 (45%)	22 (55%)	40
5	24 (32%)	50 (68%)	74
Overall	91 (41%)	133 (59%)	225

Table 5.12 - Results of combined left/right and upper/lower location comparisons between lesions seen on SPECT and planar images

Number and percentage of lesions seen in the same and different overall location for each observer and for the combined for all observers.

5.5.2 Phase 3 versus Phase 1 Reviews

5.5.2.1 Number of Lesions Seen

The number of lesions seen in phase 1 (planar only) was subtracted from the number seen in phase 3 (Sestamibi only, planar + SPECT). A summary of these results is shown in Table 5.13. As was the case for the phase 1 vs phase 2 comparison, an identical number of lesions were seen on the two sets of images more often than not. Observer 2 has the lowest number in the “M>P” category whilst observer 5 has the highest.

Observer	M > P	M < P	M = P	Total
1	10	6	16	32
2	5	7	20	32
3	9	4	19	32
4	11	5	16	32
5	15	4	13	32
Total	50	26	84	160

Table 5.13 - Comparison of number of lesions seen in phase 1 (planar only) and phase 3 (Sestamibi only)

M>P = number of times more lesions were seen on Sestamibi (MIBI) than planar, M<P = number of times fewer lesions were seen on Sestamibi than on planar, M=P = number of times same number of lesions were seen on Sestamibi as on planar.

The Wilcoxon Signed Ranks test was applied to the data from this comparison in the same way as discussed in Section 5.5.1.1. The results are shown in Table 5.14.

Observer	p-value	Estimated median	95% CI
1	0.394	0.0	(0.0, 0.5)
2	0.638	0.0	(-0.5, 0.0)
3	0.382	0.0	(0.0, 0.5)
4	0.155	0.0	(0.0, 0.5)
5	0.009	0.5	(0.0, 1.0)
Overall	0.008	0.0	(0.0, 0.5)

Table 5.14 - Results from Wilcoxon Signed Ranks test on differences in number of lesions seen (phase 3 vs phase 1)

Output from Minitab software applied to the differences in the number of lesions seen between the Sestamibi only and planar images.

In this instance, for 4 of the 5 observers (observers 1-4), no statistically significant difference existed between the number of lesions seen in the two phases of the study. Only the results for observer 5 and the combined data from all the observers shows statistical significance with $p < 0.05$. The estimated

median of 0.5 for observer 5 indicates that this observer tended to see more lesions on the Sestamibi only images than on the planar, which supports the results shown in Table 5.13.

5.5.2.2 Confidence of Lesions Representing True Adenoma

There were a total of 185 comparisons carried out on the confidence level differences expressed by the observers in the two phases. The results are shown in Table 5.15. On this occasion, the spread of results is much more even, with the highest number falling into the “same” category. Once again, however, observer 5 had the highest total number of comparisons, meaning that this observer tends to see more lesions in the images than do the other observers.

Observer	No. More (%)	No. Same (%)	No. Less (%)	Total
1	10 (30%)	12 (35%)	12 (35%)	34
2	6 (19%)	17 (53%)	9 (28%)	32
3	11 (32%)	12 (35%)	11 (32%)	34
4	13 (37%)	13 (37%)	9 (26%)	35
5	19 (38%)	14 (28%)	17 (34%)	50
Overall	59 (32%)	68 (37%)	58 (31%)	285

Table 5.15 - Results from comparison of confidence levels expressed (phase 3 vs phase 1) Number of comparisons between expressed confidence levels that showed observers as more, same or less confident looking at the Sestamibi only images as compared to the planar. Percentages of the total in each category for each observer and overall are given in brackets.

The observers were generally more confident that they were seeing true lesions on the Sestamibi planar + SPECT images in 10 (31%) of the 32 patients, less confident in 9 (28%) and they expressed similar levels of confidence in 13 (41%) patients. This suggests that there is no significant difference in the level of confidence derived by the observers from reviewing planar images alone or the Sestamibi planar + SPECT images. The results of the comparison were subjected to a Wilcoxon Signed Ranks test, the results of which are given in Table 5.16.

There are clearly no statistically significant differences demonstrated by the Wilcoxon Signed Ranks test, supporting the conclusions from the data in Table 5.15. There is therefore no evidence to support the possibility of increased confidence being gained from reviewing Sestamibi planar + SPECT images in comparison to planar ^{99m}Tc -Sestamibi + ^{123}I -iodide images.

Observer	p-value	Estimated median	95% CI
1	0.721	0.0	(-0.5, 0.0)
2	0.514	0.0	(-0.5, 0.0)
3	1.000	0.0	(-0.5, 0.5)
4	0.465	0.0	(0.0, 0.5)
5	0.777	0.0	(0.0, 0.5)
Overall	0.873	0.0	(0.0, 0.0)

Table 5.16 - Results from Wilcoxon Signed Ranks test on differences in expressed confidence level (phase 3 vs phase 1)

Output from Minitab software applied to the comparison of confidence level expressed by the observers between the Sestamibi and planar images.

5.5.2.3 Location of Observed Lesions

Once again, the left/right and upper/lower location results were compared separately first and then combined. As in Section 5.5.1.3, no anterior/posterior information was included in the comparison due to the lack of information in this plane on the planar images.

The results of the left/right comparison are given in Table 5.17. Once again, the proportions in each category are similar, but with the number of lesions given in the same left/right comparison being slightly higher than those given in different positions. Observer 2 has the highest proportion of lesions given the same left/right location at 66%, whilst observer 1 has the lowest at 50%.

Observer	No. Same (%)	No. Different (%)	Total
1	17 (50%)	17 (50%)	34
2	21 (66%)	11 (34%)	32
3	19 (56%)	15 (44%)	34
4	19 (54%)	16 (46%)	35
5	26 (52%)	24 (48%)	50
Overall	102 (55%)	83 (45%)	185

Table 5.17 - Results of comparison in left/right location between lesions seen on Sestamibi only and planar images

Number and percentage of lesions seen in the same and different left/right location for each observer and for the combined for all observers.

Table 5.18 gives the results of the comparison of the upper/lower locations reported by the observers. Once more, the proportions in the two categories overall are similar but there are significant differences between the individual observers with observer 2 having the highest number of lesions reported at the same location at 63% whilst observer 1 had the lowest at 41%.

Observer	No. Same (%)	No. Different (%)	Total
1	14 (41%)	20 (59%)	34
2	20 (63%)	12 (37%)	32
3	17 (50%)	17 (50%)	34
4	16 (46%)	19 (54%)	35
5	21 (42%)	29 (58%)	50
Overall	88 (48%)	97 (52%)	185

Table 5.18 - Results of comparison in upper/lower location between lesions seen on Sestamibi only and planar images
Number and percentage of lesions seen in the same and different upper/lower location for each observer and for the combined for all observers.

The results of the left/right and upper/lower given location comparisons were then combined and the results are given in Table 5.19. The data confirms the differences between observers with observer 2 seeing 63% of lesions in the same overall location whilst observer 1 only reported 35% of lesions at the same location. The overall results show similar proportions in the “same” and “different” categories, once again suggesting that it may not always be the same lesion seen on both planar and Sestamibi only (planar + SPECT) images for an individual patient.

Observer	No. Same (%)	No. Different (%)	Total
1	12 (35%)	22 (65%)	34
2	20 (63%)	12 (37%)	32
3	17 (50%)	17 (50%)	34
4	16 (46%)	19 (54%)	35
5	20 (40%)	30 (60%)	50
Overall	85 (46%)	100 (54%)	185

Table 5.19 - Results of combined left/right and upper/lower location comparisons between lesions seen on Sestamibi only and planar images
Number and percentage of lesions seen in the same and different overall location for each observer and for the combined for all observers.

5.5.3 Phase 4 versus Phase 1 Reviews

5.5.3.1 Number of Lesions Seen

The difference between the number of lesions seen in phase 4 (all planar and SPECT images) and phase 1 (planar only) was obtained for each observer for each of the 32 patients. Table 5.20 summarises the results. It is immediately clear that the number of times fewer lesions were seen on review of all available images than on the planar only views is very small. Three of the observers and

the combined results have most entries in the “A=P” category, suggesting that in general there is no difference in the number of lesions seen.

As discussed in Section 5.5.1.1, a Wilcoxon Signed Ranks test was applied to the difference data and the results are shown in Table 5.21.

Observer	A > P	A < P	A = P	Total
1	10	1	21	32
2	8	1	23	32
3	7	2	23	32
4	18	1	13	32
5	16	1	15	32
Total	59	6	95	160

Table 5.20 - Comparison of number of lesions seen in phase 1 (planar only) and phase 4 (all images)

A>P = number of times more lesions were seen on review of all images than planar, A<P = number of times fewer lesions were seen on all images than on planar, A=P = number of times same number of lesions were seen on all images as on planar.

The statistical test shows that 4 of the 5 observers saw a statistically different ($p \leq 0.05$) number of lesions on reviewing all the images together than on reviewing only the planar images. Only the reports of observer 3 showed no statistically significant difference. The estimated medians of ≥ 0 for all observers individually as well as the combined results indicates that there is a tendency for more lesions to be seen when all images are reviewed together as compared to review of only the planar images.

Observer	p-value	Estimated median	95% CI
1	0.050	0.5	(0.0, 0.5)
2	0.044	0.0	(0.0, 0.5)
3	0.124	0.0	(0.0, 0.5)
4	<0.001	0.5	(0.5, 1.0)
5	0.001	0.5	(0.5, 1.0)
Overall	<0.001	0.5	(0.0, 0.5)

Table 5.21 - Results from Wilcoxon Signed Ranks test on differences in number of lesions seen (phase 4 vs phase 1)

Output from Minitab software applied to the differences in the number of lesions seen between all images and planar views.

5.5.3.2 Confidence of Lesions Representing True Adenoma

A total of 204 comparisons were made between the confidence level expressed by the observers when reviewing all the available images together and that given when looking at the planar images only. Table 5.22 shows the results of the

comparison, which demonstrate that there are similar proportions in the “more” and “same” categories and significantly fewer in the “less” category. As was the case for the previous 2 comparisons, observer 5 had the highest total number of comparisons, meaning that this observer tends to see more lesions in the images than do the other observers.

Observer	No. More (%)	No. Same (%)	No. Less (%)	Total
1	17 (43%)	19 (49%)	3 (8%)	39
2	13 (41%)	17 (53%)	2 (6%)	32
3	19 (50%)	18 (47%)	1 (3%)	38
4	25 (62%)	12 (30%)	3 (8%)	40
5	24 (44%)	22 (40%)	9 (16%)	55
Overall	98 (48%)	88 (43%)	18 (9%)	204

Table 5.22 - Results from comparison of confidence levels expressed (phase 4 vs phase 1) Number of comparisons between expressed confidence levels that showed observers as more, same or less confident looking at all the images as compared to the planar. Percentages of the total in each category for each observer and overall are given in brackets.

For 15 (47%) of the 32 patients, the observers were generally more confident when reviewing all the images as compared to the planar views. They expressed similar levels of confidence in 17 (53%) patients and lower confidence in none (0%). This indicates that reviewing all the images together is either more helpful or similarly helpful to reviewing the planar images alone but it is not less helpful. The results of applying the Wilcoxon Signed Ranks test to the confidence data are shown in Table 5.23.

Observer	p-value	Estimated median	95% CI
1	0.006	0.5	(0.0, 0.5)
2	0.013	0.5	(0.0, 0.5)
3	0.001	0.5	(0.5, 0.5)
4	<0.001	0.5	(0.5, 1.0)
5	0.023	0.5	(0.0, 0.5)
Overall	<0.001	0.5	(0.5, 0.5)

Table 5.23 - Results from Wilcoxon Signed Ranks test on differences in expressed confidence level (phase 4 vs phase 1) Output from Minitab software applied to the comparison of confidence level expressed by the observers between all images and planar images.

Statistically significant differences ($p < 0.05$) are demonstrated for all the observers and the estimated median and 95% CI values indicate that the observers are more confident that they are seeing a true lesion when all the images are viewed together than when they are reviewing the planar images only.

5.5.3.3 Location of Observed Lesions

As previously, the left/right and upper/lower location results were compared separately first and then combined and no anterior/posterior information was included in the comparison.

The results of the comparison of the given left/right location are shown in Table 5.24. For observers 1-3, there were a significantly higher proportion of lesions given in the same left/right location as in a different location. Observers 4-5 had similar proportions in each category. Observers 2 & 3 reported the highest fraction in the same location at 66%, whilst observer 4 gave the lowest at 48%.

Observer	No. Same (%)	No. Different (%)	Total
1	24 (61%)	15 (39%)	39
2	21 (66%)	11 (34%)	32
3	25 (66%)	13 (34%)	38
4	19 (48%)	21 (52%)	40
5	27 (49%)	28 (51%)	55
Overall	116 (57%)	88 (43%)	204

Table 5.24 - Results of comparison in left/right location between lesions seen on all images and planar only
Number and percentage of lesions seen in the same and different left/right location for each observer and for the combined for all observers.

A summary of the results of the upper/lower locations is given in Table 5.25. The overall numbers in the two categories are similar but the different observers have significantly different results. Observer 2 has the highest proportion of lesions given at the same upper/lower location at 62%, whereas observer 4 gave the lowest fraction at 43%.

Observer	No. Same (%)	No. Different (%)	Total
1	20 (51%)	19 (49%)	39
2	20 (62%)	12 (38%)	32
3	23 (60%)	15 (40%)	38
4	17 (43%)	23 (57%)	40
5	25 (46%)	30 (54%)	55
Overall	105 (51%)	99 (49%)	204

Table 5.25 - Results of comparison in upper/lower location between lesions seen on all images and planar only
Number and percentage of lesions seen in the same and different upper/lower location for each observer and for the combined for all observers.

The combined results from the left/right and upper/lower comparisons are shown in Table 5.26. Once again, the overall results show no difference with a 50%:50% split between the two categories, but there are differences demonstrated between the observers. Observer 2 gave more lesions at the same overall location than any of the others at 62%, whilst observer 4 gave the lowest proportion at the same location with just 40%.

Observer	No. Same (%)	No. Different (%)	Total
1	20 (51%)	19 (49%)	39
2	20 (62%)	12 (38%)	32
3	23 (60%)	15 (40%)	38
4	16 (40%)	24 (60%)	40
5	23 (42%)	32 (58%)	55
Overall	102 (50%)	102 (50%)	204

Table 5.26 - Results of combined left/right and upper/lower location comparisons between lesions seen on all images and planar only
Number and percentage of lesions seen in the same and different overall location for each observer and for the combined for all observers.

5.5.4 Phase 3 versus Phase 2 Reviews

5.5.4.1 Number of Lesions Seen

Table 5.27 gives a summary of the difference in the number of lesions seen by each observer in phase 3 (Sestamibi only, planar + SPECT) as compared to those seen in phase 2 (SPECT, ^{99m}Tc-Sestamibi + ¹²³I-iodide + subtraction). The results clearly show that there are significantly fewer occasions on which more lesions were seen on the Sestamibi only images than on the SPECT when compared to the number of times fewer lesions were seen. For observers 1-4 and the combined results, the highest number was in the “M=S” category, whereas observer 5 had the highest number in “M<S”. There were no instances of “M>S” being the largest category, indicating that there are generally the same number or fewer lesions seen on the Sestamibi only images than on the planar.

The results of the Wilcoxon Signed Ranks test applied to this data are shown in Table 5.28. Of the 5 observers, only 1 - observer 1 - failed to demonstrate a statistically significant difference (i.e. $p < 0.05$) between the number of lesions seen in these two phases of the study. Of the others, all had an estimated

median of <1, indicating that they were seeing fewer lesions on the Sestamibi only than on the SPECT images.

Observer	M > S	M < S	M = S	Total
1	3	7	22	32
2	1	13	18	32
3	2	11	19	32
4	3	12	17	32
5	2	21	9	32
Total	11	64	85	160

Table 5.27 - Comparison of number of lesions seen in phase 2 (SPECT) and phase 3 (Sestamibi only)

M>S = number of times more lesions were seen on Sestamibi only images than on SPECT, M<S = number of times fewer lesions were seen on Sestamibi only than on SPECT, M=S = number of times same number of lesions were seen on Sestamibi only images as on SPECT.

Observer	p-value	Estimated median	95% CI
1	0.285	0.0	(-0.5, 0.0)
2	0.005	-0.5	(-0.5, 0.0)
3	0.017	-0.5	(-0.5, 0.0)
4	0.036	-0.5	(-0.5, 0.0)
5	<0.001	-1.0	(-1.0, -0.5)
Overall	<0.001	-0.5	(-0.5, -0.5)

Table 5.28 - Results from Wilcoxon Signed Ranks test on differences in number of lesions seen (phase 3 vs phase 2)

Output from Minitab software applied to the differences in the number of lesions seen between Sestamibi only and SPECT images.

5.5.4.2 Confidence of Lesions Representing True Adenoma

There were 236 comparisons of the confidence level indicated by the observers during the different phases of the review. A summary of the results is shown in Table 5.29. For each observer and for the combined results, over half of the results fall into the “less” category, meaning that the observers are less confident when reviewing the Sestamibi only images than when they are reporting from the SPECT image data. The lowest number for each observer was in the “more” category. As before, observer 5 had the highest total number of comparisons, meaning that this observer tends to see more lesions in the images than do the other observers.

The observers were generally more confident on reviewing the Sestamibi images as compared to the SPECT data for 2 (6%) of the 32 patients and had similar confidence levels for 9 (28%) patients. They were therefore less confident for 21

(66%) of the patients, indicating that they generally preferred reporting from the SPECT images that included the ^{123}I -iodide images than from the Sestamibi only images, even though both planar and SPECT images were available. The Wilcoxon Signed Ranks test was then applied to the data, and the results are shown in Table 5.30.

Observer	No. More (%)	No. Same (%)	No. Less (%)	Total
1	3 (9%)	10 (30%)	20 (61%)	33
2	5 (13%)	11 (32%)	18 (53%)	34
3	5 (13%)	9 (24%)	24 (63%)	38
4	5 (12%)	13 (32%)	23 (56%)	41
5	18 (20%)	26 (29%)	46 (51%)	90
Overall	36 (15%)	69 (29%)	131 (56%)	236

Table 5.29 - Results from comparison of confidence levels expressed (phase 3 vs phase 2) Number of comparisons between expressed confidence levels that showed observers as more, same or less confident reviewing the Sestamibi only images as compared to the SPECT. Percentages of the total in each category for each observer and overall are given in brackets.

Observer	p-value	Estimated median	95% CI
1	0.002	-0.5	(-1.0, -0.5)
2	0.018	-0.5	(-0.5, 0.0)
3	0.002	-0.5	(-1.0, -0.5)
4	0.003	-0.5	(-0.5, 0.0)
5	0.002	-0.5	(-0.5, 0.0)
Overall	<0.001	-0.5	(-0.5, -0.5)

Table 5.30 - Results from Wilcoxon Signed Ranks test on differences in expressed confidence level (phase 3 vs phase 2) Output from Minitab software applied to the comparison of confidence level expressed by the observers between Sestamibi only and SPECT images.

The results clearly show that statistically significant differences ($p < 0.05$) exist between the confidence levels expressed by every observer between the two phases of the study. The negative estimated median and 95% CI values show that the observers are less confident on reviewing the Sestamibi images than the SPECT.

5.5.4.3 Location of Observed Lesions

As previously, the left/right and upper/lower location results were compared separately first and then combined. However, because SPECT images were included in both phases of this comparison, anterior/posterior information was also analysed, at first separately and then in combination with both the left/right and upper/lower results.

Table 5.31 gives a summary of the results of comparing the left/right location given by each observer for each lesion. All the observers reported more lesions at the same site than at a different site. The lowest proportion at the same site was given by observer 5 at 52%.

Observer	No. Same (%)	No. Different (%)	Total
1	19 (58%)	14 (42%)	33
2	18 (53%)	16 (47%)	34
3	22 (58%)	16 (42%)	38
4	24 (58%)	17 (42%)	41
5	47 (52%)	43 (48%)	90
Overall	130 (55%)	106 (45%)	236

Table 5.31 - Results of comparison in left/right location between lesions seen on Sestamibi only and SPECT images
Number and percentage of lesions seen in the same and different left/right location for each observer and for the combined for all observers.

The results of the comparison in the given upper/lower locations are shown in Table 5.32. There are generally more lesions reported at a different location than at the same, although observer 2 gave 56% of lesions at the same location.

Observer	No. Same (%)	No. Different (%)	Total
1	17 (51%)	16 (49%)	33
2	19 (56%)	15 (44%)	34
3	18 (47%)	20 (53%)	38
4	16 (39%)	25 (61%)	41
5	32 (36%)	58 (64%)	90
Overall	102 (43%)	134 (57%)	236

Table 5.32 - Results of comparison in upper/lower location between lesions seen on Sestamibi only and SPECT images
Number and percentage of lesions seen in the same and different upper/lower location for each observer and for the combined for all observers.

Table 5.33 shows the combined results of the comparison of the left/right and upper/lower locations. The overall tendency is for a different location to be given for a lesion seen on each of the two study phases, with observer 5 seeing only 23% of lesions at the same site. Observer 2 saw 50% each at the same and different sites. Once again, this indicates that it is not always the same lesion that is being seen on the two phases of the study or that there is some difficulty in giving accurate location information from one or other set of images.

Observer	No. Same (%)	No. Different (%)	Total
1	14 (42%)	19 (58%)	33
2	17 (50%)	17 (50%)	34
3	17 (45%)	21 (55%)	38
4	16 (39%)	25 (61%)	41
5	21 (23%)	69 (77%)	90
Overall	85 (36%)	151 (64%)	236

Table 5.33 - Results of combined left/right and upper/lower location comparisons between lesions seen on Sestamibi only and SPECT images
Number and percentage of lesions seen in the same and different overall location for each observer and for the combined for all observers.

The anterior/posterior comparison results are shown in Table 5.34. There is a wide variation between the observers with observer 1 giving 64% of lesions at the same site but observer 4 giving a similar fraction of 66% at different sites.

Observer	No. Same (%)	No. Different (%)	Total
1	21 (64%)	12 (36%)	33
2	15 (44%)	19 (56%)	34
3	20 (53%)	18 (47%)	38
4	14 (34%)	27 (66%)	41
5	35 (39%)	55 (61%)	90
Overall	105 (45%)	131 (55%)	236

Table 5.34 - Results of comparison in anterior/posterior location between lesions seen on Sestamibi only and SPECT images
Number and percentage of lesions seen in the same and different anterior/posterior location for each observer and for the combined for all observers.

Table 5.35 shows the results of combining all the comparisons in location to determine if the same or a different overall location was given for each lesion seen on the Sestamibi only and SPECT images. None of the observers have a greater proportion of lesions given at the same location than at a different location. Indeed, observers 4 and 5 have very small proportion in the “same”

Observer	No. Same (%)	No. Different (%)	Total
1	12 (36%)	21 (64%)	33
2	13 (38%)	21 (62%)	34
3	16 (42%)	22 (58%)	38
4	8 (20%)	33 (80%)	41
5	12 (13%)	78 (87%)	90
Overall	61 (26%)	175 (74%)	236

Table 5.35 - Results of combined left/right, upper/lower and anterior/posterior location comparisons between lesions seen on Sestamibi only and SPECT images
Number and percentage of lesions seen in the same and different overall location for each observer and for the combined for all observers.

category at 20% and 13% respectively. Again, this suggests that either different lesions were observed on the two phases or that the different image data available to the observers in some way affected the reported location of the lesions.

5.5.5 Phase 4 versus Phase 2 Reviews

5.5.5.1 Number of Lesions Seen

The difference between the number of lesions seen by each observer for each of the 32 patients in phase 4 (all images together) and the number seen in phase 2 (SPECT) was calculated. A summary of the results is shown in Table 5.36. It is clear that on most occasions, the same number of lesions were seen in the two phases of the study. However, observer 5 has a higher number in the “A<S” category than in “A=S”, indicating that this observer tended to see fewer lesions when reviewing all images together than when looking at the SPECT images in isolation from the planar.

Observer	A > S	A < S	A = S	Total
1	6	5	21	32
2	2	6	24	32
3	2	8	22	32
4	8	6	18	32
5	3	18	11	32
Total	21	43	96	160

Table 5.36 - Comparison of number of lesions seen in phase 2 (SPECT) and phase 4 (all images)

A>S = number of times more lesions were seen on all images than on SPECT, A<S = number of times fewer lesions were seen on all images than on SPECT, A=S = number of times same number of lesions were seen on all images as on SPECT.

The Wilcoxon Signed Ranks test was then applied to the difference values and the results are shown in Table 5.37. Only observer 5 and the overall combined results show a statistically significant difference ($p<0.05$). The estimated median and 95% CI for observer 5 are negative, indicating that this observer did indeed tend to see fewer lesions in phase 4 than phase 2, as was suggested from the data in Table 5.36.

5.5.5.2 Confidence of Lesions Representing True Adenoma

Table 5.38 summarises the results of the comparison of the confidence level expressed by the observers as they reviewed the images. There were a total of 255 comparisons and it can be seen from the results that there is a wide variation between the observers. Overall, the highest number of comparisons fell into the “same” category with the fewest in “more”, indicating that the

Observer	p-value	Estimated median	95% CI
1	0.657	0.0	(0.0, 0.0)
2	0.234	0.0	(-0.5, 0.0)
3	0.053	0.0	(-0.5, 0.0)
4	0.530	0.0	(0.0, 0.5)
5	0.012	-0.5	(-1.0, -0.5)
Overall	0.017	0.0	(0.0, 0.0)

Table 5.37 - Results from Wilcoxon Signed Ranks test on differences in number of lesions seen (phase 4 vs phase 2)
Output from Minitab software applied to the differences in the number of lesions seen between all images and SPECT only.

observers generally expressed a similar or lower level of confidence when reviewing all the images together than when looking at the SPECT alone. Once again, observer 5 had the highest total number of comparisons, meaning that this observer saw more lesions on reviewing the images than did the others.

Observer	No. More (%)	No. Same (%)	No. Less (%)	Total
1	6 (16%)	22 (60%)	9 (24%)	37
2	5 (15%)	21 (62%)	8 (23%)	34
3	7 (17%)	15 (37%)	19 (46%)	41
4	12 (26%)	24 (51%)	11 (23%)	47
5	18 (18%)	39 (41%)	39 (41%)	96
Overall	48 (19%)	121 (47%)	86 (34%)	255

Table 5.38 - Results from comparison of confidence levels expressed (phase 4 vs phase 2)
Number of comparisons between expressed confidence levels that showed observers as more, same or less confident reviewing all images together as compared to the SPECT. Percentages of the total in each category for each observer and overall are given in brackets.

In general, the observers were more confident on reviewing all the images together than looking at the SPECT alone for 1 (3%) of the 32 patients. They were equally confident for 20 (63%) of the patients and less confident in 11 (34%). This indicates that there is a tendency for the observers to be more confident that they are seeing true lesions when looking at the SPECT data alone

than when looking at the SPECT and planar images together. The results of the Wilcoxon Signed Ranks test applied to the data are shown in Table 5.39.

Statistically significant differences ($p < 0.05$) are seen for observers 3 and 5 as well as the combined results. Although the data for the other observers was not statistically significant, the estimate median and 95% CI values show that there is a tendency for the observers to be less confident when looking at all the images together than they are when reviewing the SPECT data in isolation.

Observer	p-value	Estimated median	95% CI
1	0.514	0.0	(-0.5, 0.0)
2	0.363	0.0	(-0.5, 0.0)
3	0.041	-0.5	(-0.5, 0.0)
4	0.867	0.0	(0.0, 0.0)
5	0.016	0.0	(-0.5, 0.0)
Overall	0.004	0.0	(-0.5, 0.0)

Table 5.39 - Results from Wilcoxon Signed Ranks test on differences in expressed confidence level (phase 4 vs phase 2)

Output from Minitab software applied to the comparison of confidence level expressed by the observers between all images and SPECT alone.

5.5.5.3 Location of Observed Lesions

The given left/right, upper/lower and anterior/posterior locations were then compared and combined in the same way as in Section 5.5.4.3.

The results of the left/right location comparison are given in Table 5.40. For 4 of the 5 observers and for the combined results, there were more lesions given at the same site than at a different location with observer 2 having the highest proportion at the same left/right location at 76%. Observer 5 gave similar numbers at the same and different sites.

Observer	No. Same (%)	No. Different (%)	Total
1	25 (68%)	12 (32%)	37
2	26 (76%)	8 (24%)	34
3	25 (61%)	16 (39%)	41
4	30 (64%)	17 (36%)	47
5	47 (49%)	49 (51%)	96
Overall	153 (60%)	102 (40%)	255

Table 5.40 - Results of comparison in left/right location between lesions seen on all images and SPECT only

Number and percentage of lesions seen in the same and different left/right location for each observer and for the combined for all observers.

The upper/lower locations were also compared and the results are shown in Table 5.41. It can clearly be seen that all observers saw more lesions at the same location than at a different site, with observers 1 and 2 having the highest proportion at 65%.

Observer	No. Same (%)	No. Different (%)	Total
1	24 (65%)	13 (35%)	37
2	22 (65%)	12 (35%)	34
3	22 (54%)	19 (46%)	41
4	24 (51%)	23 (49%)	47
5	50 (52%)	46 (48%)	96
Overall	142 (56%)	113 (44%)	255

Table 5.41 - Results of comparison in upper/lower location between lesions seen on all images and SPECT only
Number and percentage of lesions seen in the same and different upper/lower location for each observer and for the combined for all observers.

The comparisons of the left/right and upper/lower locations were then combined and the results are shown in Table 5.42. There are significant differences between the results for the different observers with observers 1 and 2 having the highest fraction (62%) of lesions at the same overall location, while observer 5 gave only 34% at the same site. The combined totals for all the observers can be seen to be similar.

Observer	No. Same (%)	No. Different (%)	Total
1	23 (62%)	14 (38%)	37
2	21 (62%)	13 (38%)	34
3	21 (51%)	20 (49%)	41
4	22 (47%)	25 (53%)	47
5	33 (34%)	63 (66%)	96
Overall	120 (47%)	135 (53%)	255

Table 5.42 - Results of combined left/right and upper/lower location comparisons between lesions seen on all images and SPECT only
Number and percentage of lesions seen in the same and different overall location for each observer and for the combined for all observers.

Table 5.43 gives the results of the anterior/posterior location comparison. Again, there is a wide variation between the results for the different observers with observer 2 seeing 65% of lesions at the same site but observer 5 seeing only 47% at the same location.

Observer	No. Same (%)	No. Different (%)	Total
1	23 (62%)	14 (38%)	37
2	22 (65%)	12 (35%)	34
3	23 (56%)	18 (44%)	41
4	23 (49%)	24 (51%)	47
5	45 (47%)	51 (53%)	96
Overall	136 (53%)	119 (47%)	255

Table 5.43 - Results of comparison in anterior/posterior location between lesions seen on all images and SPECT alone

Number and percentage of lesions seen in the same and different anterior/posterior location for each observer and for the combined for all observers.

All the comparisons in the given location of lesions between phase 2 and phase 4 of the study were then combined and the results are shown in Table 5.44.

Observers 1, 2 and 3 gave similar numbers at the same overall location as at a different location, whilst observers 4 and 5 saw only a small proportion - 38% and 26% respectively - at the same site. Once more, these results suggest that either different lesions were observed on the two phases or that the different image data available to the observers in some way affected the reported location of the lesions.

Observer	No. Same (%)	No. Different (%)	Total
1	20 (54%)	17 (46%)	37
2	17 (50%)	17 (50%)	34
3	20 (49%)	21 (51%)	41
4	18 (38%)	29 (62%)	47
5	25 (26%)	71 (74%)	96
Overall	100 (39%)	155 (61%)	255

Table 5.44 - Results of combined left/right, upper/lower and anterior/posterior location comparisons between lesions seen on all images and SPECT only

Number and percentage of lesions seen in the same and different overall location for each observer and for the combined for all observers.

5.5.6 Phase 4 versus Phase 3 Reviews

5.5.6.1 Number of Lesions Seen

The final comparison between the results of different phases of the observer study was between phase 3 (Sestamibi only) and phase 4 (all images). A summary of the difference between the number of lesions seen in the two phases is shown in Table 5.45.

The data show that there is a tendency to see the same number or more lesions when reviewing all the available images than when reporting from the Sestamibi images only. The category with the highest number for each observer is that for the same number of lesions seen in the two phases whilst that with the lowest number for all observers is when there were fewer lesions seen on phase 4 than on phase 3.

Observer	A > M	A < M	A = M	Total
1	11	7	14	32
2	10	2	20	32
3	6	4	22	32
4	13	2	17	32
5	8	6	18	32
Total	48	21	91	160

Table 5.45 - Comparison of number of lesions seen in phase 3 (Sestamibi only) and phase 4 (all images)

A>M = number of times more lesions were seen on all images than on Sestamibi only, A<M = number of times fewer lesions were seen on all images than on Sestamibi only, A=M = number of times same number of lesions were seen on all images as on Sestamibi only.

Table 5.46 shows the results of the Wilcoxon Signed Ranks test being applied to the differences in the number of lesions seen on the two phases. The results for observers 2 and 4 as well as the all the data combined are statistically significant ($p < 0.05$) whilst for the other observers, no statistically significant difference is demonstrated. The 95% CI results do, however, suggest that there is a tendency to see more lesions on review of all the images than when viewing the Sestamibi images only as they are weighted above 0.

Observer	p-value	Estimated median	95% CI
1	0.338	0.0	(0.0, 0.5)
2	0.045	0.0	(0.0, 0.5)
3	0.610	0.0	(0.0, 0.0)
4	0.008	0.5	(0.0, 0.5)
5	0.414	0.0	(0.0, 0.5)
Overall	0.001	0.0	(0.0, 0.5)

Table 5.46 - Results from Wilcoxon Signed Ranks test on differences in number of lesions seen (phase 4 vs phase 3)

Output from Minitab software applied to the differences in the number of lesions seen between all images and Sestamibi only.

5.5.6.2 Confidence of Lesions Representing True Adenoma

The comparisons between the confidence level expressed by the observer during the two phases of the study numbered 209 in total and a summary of the results

is shown in Table 5.47. The observers were altogether more confident when reviewing all the available images than when reporting from the Sestamibi images alone. Observer 4 had the highest proportion in this category at 55%, whereas observer 3 had the lowest at 38% and did, in fact, have a higher proportion at the same confidence level (44%). As was the case for all other comparisons, observer 5 had the highest total number of comparisons, once more indicating that this observer tended to see more lesions than the others.

Observer	No. More (%)	No. Same (%)	No. Less (%)	Total
1	19 (53%)	9 (25%)	8 (22%)	36
2	15 (47%)	13 (41%)	4 (12%)	32
3	13 (38%)	15 (44%)	6 (18%)	34
4	23 (55%)	13 (31%)	6 (14%)	42
5	29 (45%)	19 (29%)	17 (26%)	65
Overall	99 (47%)	69 (33%)	41 (20%)	209

Table 5.47 - Results from comparison of confidence levels expressed (phase 4 vs phase 3) Number of comparisons between expressed confidence levels that showed observers as more, same or less confident reviewing all images together as compared to the Sestamibi only. Percentages of the total in each category for each observer and overall are given in brackets.

In 17 (53%) of the 32 patients, the observers were generally more confident when reviewing all the images as compared to the Sestamibi only views and expressed similar levels of confidence in 11 (34%). Therefore, they were less confident for only 4 (13%) of the 32 patients. The results of Wilcoxon Signed Ranks test being applied to this data are shown in Table 5.48.

Observer	p-value	Estimated median	95% CI
1	0.066	0.5	(0.0, 0.5)
2	0.028	0.5	(0.0, 0.5)
3	0.165	0.0	(0.0, 0.5)
4	0.006	0.5	(0.0, 0.5)
5	0.125	0.0	(0.0, 0.5)
Overall	<0.001	0.5	(0.0, 0.5)

Table 5.48 - Results from Wilcoxon Signed Ranks test on differences in expressed confidence level (phase 4 vs phase 3) Output from Minitab software applied to the comparison of confidence level expressed by the observers between all images and Sestamibi only.

Statistically significant differences ($p < 0.05$) exist between the levels of confidence expressed in the two phases of the study by observers 2 and 4 and for the overall combined results from all the observers. The estimated median and 95% CI values are all ≥ 0 , indicating that the observers are generally more

confident when reporting from all the images together than from the Sestamibi only images, as was suggested in Table 5.47.

5.5.6.3 Location of Observed Lesions

The same comparisons of given location were carried out as in Sections 5.5.4.3 and 5.5.5.3 and the results of the left/right comparison are shown in Table 5.49. The numbers of lesions given at the same and different locations are similar overall, although there was a tendency for more to be seen at the same location. However, observer 1 saw less than half of the lesions (47%) at the same site.

Observer	No. Same (%)	No. Different (%)	Total
1	17 (47%)	19 (53%)	36
2	19 (59%)	13 (41%)	32
3	20 (59%)	14 (41%)	34
4	24 (57%)	18 (43%)	42
5	38 (58%)	27 (42%)	65
Overall	118 (56%)	91 (44%)	209

Table 5.49 - Results of comparison in left/right location between lesions seen on all images and Sestamibi only
Number and percentage of lesions seen in the same and different left/right location for each observer and for the combined for all observers.

A summary of the upper/lower comparison is given in Table 5.50. There were generally more occasions when a lesion was given at a different location, although observers 2 & 3 gave 59% and 56% of lesions at the same site, respectively.

Observer	No. Same (%)	No. Different (%)	Total
1	16 (44%)	20 (56%)	36
2	19 (59%)	13 (41%)	32
3	19 (56%)	15 (44%)	34
4	17 (41%)	25 (59%)	42
5	27 (42%)	38 (58%)	65
Overall	98 (47%)	111 (53%)	209

Table 5.50 - Results of comparison in upper/lower location between lesions seen on all images and Sestamibi only
Number and percentage of lesions seen in the same and different upper/lower location for each observer and for the combined for all observers.

The combined results from comparing the left/right and upper/lower locations are shown in Table 5.51. There are significant differences between the results

for the different observers with observer 2 seeing as many as 56% at the same overall location whilst observer 4 saw only 36% of lesions at the same site.

Observer	No. Same (%)	No. Different (%)	Total
1	14 (39%)	22 (61%)	36
2	18 (56%)	14 (44%)	32
3	18 (53%)	16 (47%)	34
4	15 (36%)	27 (64%)	42
5	25 (39%)	40 (61%)	65
Overall	90 (43%)	119 (57%)	209

Table 5.51 - Results of combined left/right and upper/lower location comparisons between lesions seen on all images and Sestamibi only
Number and percentage of lesions seen in the same and different overall location for each observer and for the combined for all observers.

Table 5.52 shows the results of the anterior/posterior comparison. Once again, the results for the different observers are varied with observer 3 giving 56% of lesions at the same site and observer 4 seeing only 36% of lesions at the same location.

Observer	No. Same (%)	No. Different (%)	Total
1	19 (53%)	17 (47%)	36
2	17 (53%)	15 (47%)	32
3	19 (56%)	15 (44%)	34
4	15 (36%)	27 (64%)	42
5	30 (46%)	35 (56%)	65
Overall	100 (48%)	109 (52%)	209

Table 5.52 - Results of comparison in anterior/posterior location between lesions seen on all images and Sestamibi alone
Number and percentage of lesions seen in the same and different anterior/posterior location for each observer and for the combined for all observers.

All the location comparisons were then combined and the results are shown in Table 5.53. It can clearly be seen that for each observer, fewer lesions were seen at the same overall location as were seen in a different place. Observer 4

Observer	No. Same (%)	No. Different (%)	Total
1	13 (36%)	23 (64%)	36
2	15 (47%)	17 (53%)	32
3	16 (47%)	18 (53%)	34
4	8 (19%)	34 (81%)	42
5	16 (25%)	49 (75%)	65
Overall	68 (33%)	141 (67%)	209

Table 5.53 - Results of combined left/right, upper/lower and anterior/posterior location comparisons between lesions seen on all images and Sestamibi only
Number and percentage of lesions seen in the same and different overall location for each observer and for the combined for all observers.

gave only 19% of lesions at the same overall location, which is a very small proportion. Once more, this suggests that either different lesions were observed on the two phases or that the different image data available to the observers in some way affected the reported location of the lesions.

5.5.7 Summary of Comparison Results

This section gives graphical summaries of the above results, allowing more direct assessments of the comparisons between the different phases of the observer study. As above, when comparisons between phases are being described, the differences are always taken as the later phase minus the earlier phase.

Figure 5.9 shows the frequency of “more”, “same” or “less” findings for the number of lesions seen when each of the phases of the observer study was compared against each of the others.

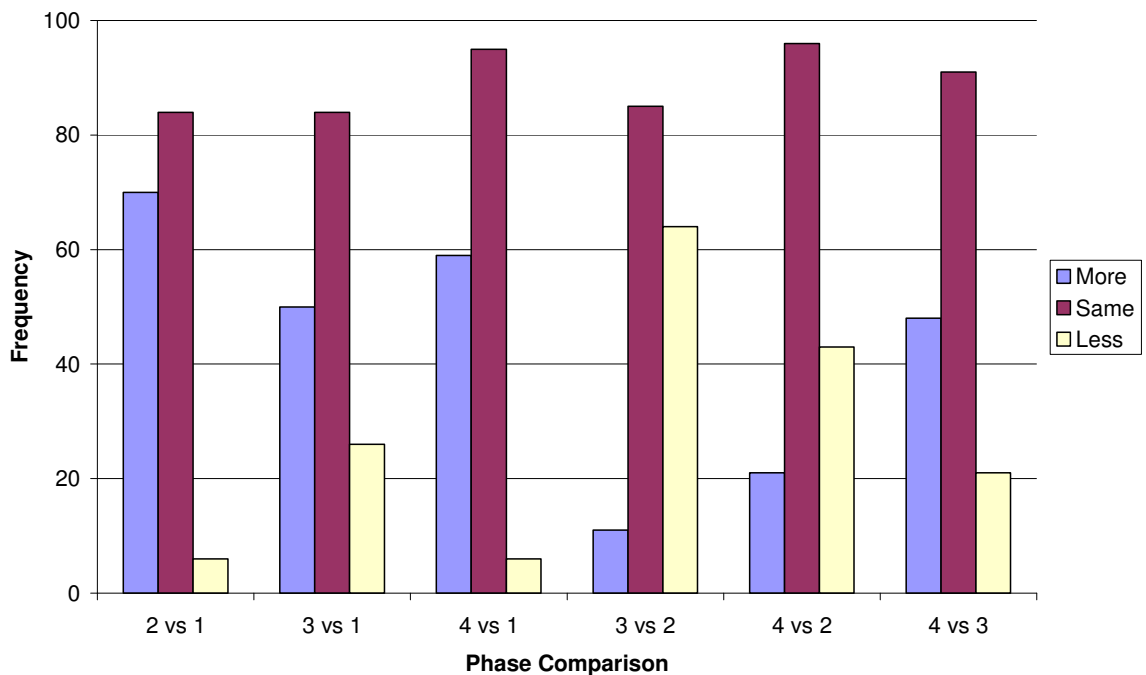


Figure 5.9 - Bar chart of comparisons in number of lesions seen
 Frequency of “more”, “same” and “less” findings for comparison of number of lesions seen in each phase of the study. 2vs1 = lesions seen on phase 2 minus lesions seen on phase 1 (similar for comparisons of other phases)

It is immediately clear that the “same” category is the highest for all of the phase comparisons, indicating that the observers reported the same number of

lesions on two phases of the study more frequently than giving a different number.

The “more” category is higher than “less” for all of the comparisons involving phase 1 (planar images only), indicating that generally fewer lesions were seen on phase 1 than on the other phases. In contrast, the “less” category is higher than “more” for the 3vs2 and 4vs2 comparisons. All of these findings indicate that the observers were seeing more lesions on the dual-isotope subtraction SPECT images of phase 2 than on the other phases, which is most pronounced in the 2vs1 and 3vs2 comparisons.

A similar plot showing the differences in the confidence level expressed by the observers when reviewing the images in each phase is shown in Figure 5.10. In this case, the “same” category is often not the highest, meaning that there was often a significant difference in the level of confidence that a true parathyroid adenoma was visible in the image between different phases of the observer study.

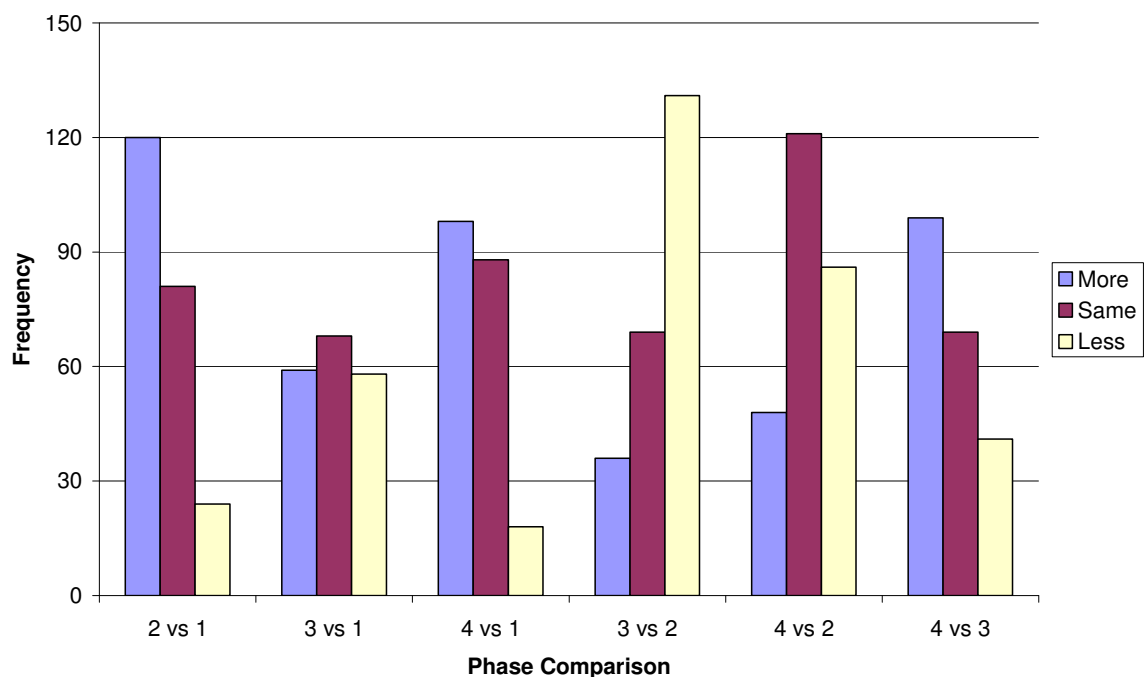


Figure 5.10 - Bar chart of comparisons in expressed confidence level
 Frequency of “more”, “same” and “less” findings for comparison of confidence level expressed in each phase of the study. 2vs1 = confidence expressed on phase 2 versus confidence expressed on phase 1 (similar for comparisons of other phases)

The most striking differences are seen in the 2vs1 and 3vs2 comparisons. In both instances, the level of confidence expressed by the observers from the review of the SPECT-only images (phase 2) is considerably higher than on the other phase being compared (phases 1 & 3 respectively). In contrast, the highest category in the 4vs2 comparison is “same”, indicating that there are fewer differences in confidence level between the two phases in which the dual-isotope subtraction SPECT images were available than between the others. This suggests that the inclusion of dual-isotope subtraction SPECT images increases the confidence of the reporting observer but the combination of planar and SPECT subtraction images does not lead to a further increase in confidence.

A plot of the number of times the same or different left/right location was given for lesions in each of the phases of the observer study if shown in Figure 5.11. It can clearly be seen that in all but one case (2vs1), the number of times the same left/right location was given in the two different phases exceeded the number of times a different site was reported. This demonstrates that, more often than not, potential parathyroid lesions are being seen on the same side of the neck (relative to the thyroid gland) than on the contra-lateral side regardless of the type of images being reviewed.

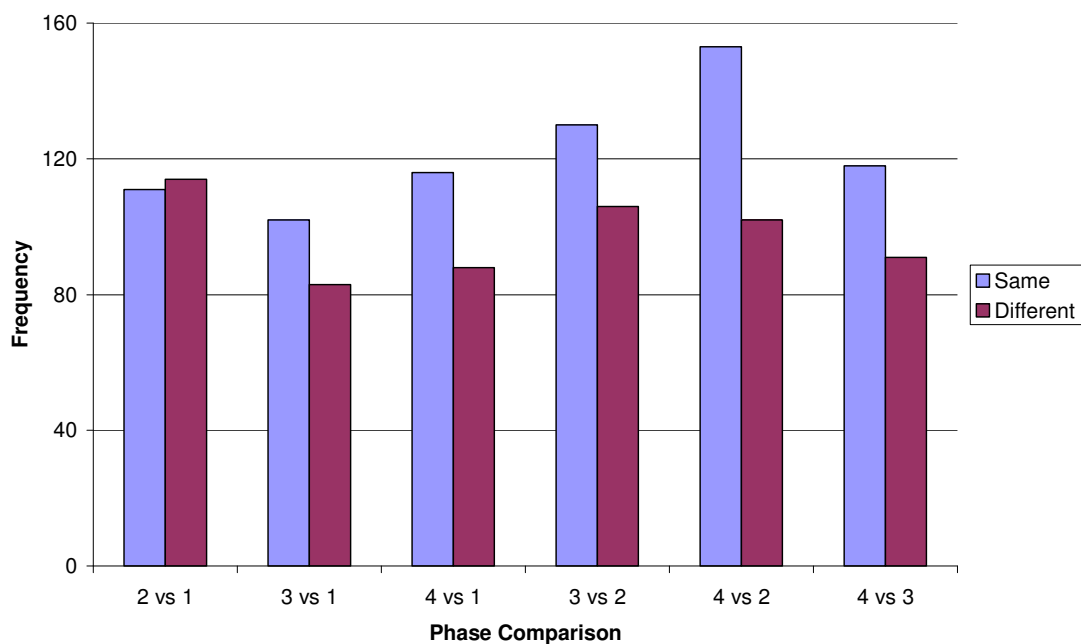


Figure 5.11 - Bar chart of comparisons in given left/right lesion location
Frequency of “same” and “different” findings for comparison of given left/right location of each lesion in each phase of the study. 2vs1 = lesions seen on phase 2 versus lesions seen on phase 1 (similar for comparisons of other phases)

The most likely reason for the difference demonstrated in the 2vs1 comparison is the fact that far more lesions in total were seen on phase 2 than on phase 1 (see Figure 5.7 above). This means that several lesions seen on the dual-isotope subtraction SPECT images (phase 2) were being compared to each single lesion seen on the planar images (phase 1), resulting in many comparisons that were not like-for-like and hence a significant number of lesions were at a different left/right site on the comparison.

Figure 5.12 is similar to Figure 5.11, but in this case the comparisons shown are of the overall given location of the lesions seen, taking into account the left/right, upper/lower and anterior/posterior position specified by the observer. It should be noted that, as in the discussions in Sections 5.5.1 - 5.5.3 above, no anterior/posterior information was included for any comparisons involving phase 1 as it is not possible to determine the anterior/posterior location of a lesion from an anterior planar image. These comparisons therefore only take into account the combination of the given left/right and upper/lower locations.

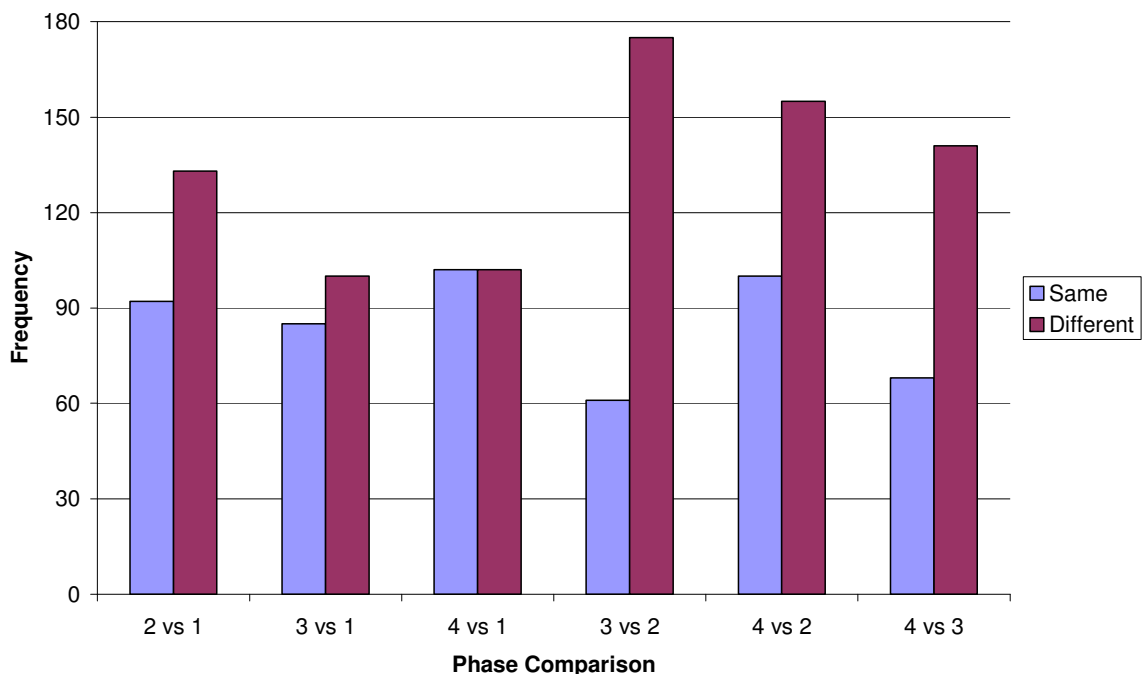


Figure 5.12 - Bar chart of comparisons in given overall lesion location
Frequency of “same” and “different” findings for comparison of given overall location of each lesion in each phase of the study. 2vs1 = lesions seen on phase 2 versus lesions seen on phase 1 (similar for comparisons of other phases)

It can clearly be seen from the chart that in all cases, the number of comparisons given a “different” overall location is greater than the number given at the “same” overall locations, with the exception of the comparison of phases 1 & 4, where the relative numbers in the two categories are equal. All of the comparisons involving phase 2 (SPECT only) have a high proportion in the “different” category. This is most likely due to the fact that more lesions were seen on phase 2 than any other, meaning that each lesion seen on the other three phases was being compared to several lesions seen on phase 2, resulting in a significant number of “different” location findings.

Chapter 6 – Parathyroid Study – Comparison of Observer Study with Surgical and US Findings

6.1 Surgical and Ultrasound Results

6.1.1 Participants Having Surgery and/or Ultrasound

The results of any parathyroid surgery and/or ultrasound scanning of the neck performed on each patient were obtained from the patient case notes. Of the 32 patients who took part in this study, 17 (53%) have since undergone parathyroidectomy surgery and 13 of these patients also had an ultrasound scan. Of the remaining 15 (47%) patients, 12 (38%) have had further imaging using ultrasound. There were therefore 25 (78%) patients who had ultrasound scanning. The remaining 3 (9%) patients have had follow-up that has included neither surgery nor ultrasound and their symptoms are currently being managed clinically. A full list of the surgical findings for the patients who underwent parathyroidectomy is given in Table 6.1.

The histological results were examined for each patient who underwent parathyroidectomy to determine the presence or otherwise of a parathyroid adenoma or hyperplastic parathyroid glands in each case. A total of 20 samples suspected of being parathyroid adenomas were resected, 18 of which were positive for either parathyroid adenoma or hyperplasia. Of the 17 patients who had surgery, 16 (94%) results were positive for parathyroid adenoma or hyperplasia, with 14 cases of single adenoma and 2 of hyperplasia. The parathyroid sample from the remaining patient was found to be histologically normal. Three of the patients who had surgery had an ectopic parathyroid adenoma removed, with 2 being in the thymic tract and one in a retrosternal location.

The surgical results show only 2 normal glands were resected, which means that there are only 2 true negative results in total. The specificity depends heavily upon the true negative rate (see Equation 4.3) and so the small rate may strongly affect the calculated specificity for the observer study. It is also an

indication of the role the experience of the endocrine surgeon plays in selecting lesions for resection that are most likely to be hyperplastic glands or adenomas.

Patient No.	No. Lesions Resected	Position	Histological Findings
1	1	Left posterior lower lateral	Adenoma
2	1	Left posterior lower lateral	Normal
3	1	Ectopic - right thymic tract	Adenoma
4	1	Right upper	Adenoma
5	1	Left posterior lower	Adenoma
7	1	Ectopic - intrathyroidic	Adenoma
8	1	Left posterior lower	Adenoma
9	1	Right posterior lower lateral	Adenoma
11	1	Right posterior upper lateral	Adenoma
12	1	Left posterior lower	Adenoma
17	1	Right posterior upper	Adenoma
20	2	Right posterior upper Right posterior lower	Hyperplasia
21	2	Left posterior upper Left posterior lower	Hyperplasia (mild)
22	2	Ectopic - retrosternal Right posterior lower	Adenoma Normal
23	1	Right posterior lower lateral	Adenoma
26	1	Right posterior lower lateral	Adenoma
31	1	Left posterior upper	Adenoma

Table 6.1 - Surgical findings for patients undergoing parathyroidectomy
Full list of results from surgery for all 17 patients who had surgery after nuclear medicine parathyroid imaging. Position is given as either relative to the thyroid gland or ectopic.

Of the 25 patients who had a neck ultrasound scan, 14 (56%) had a positive report for parathyroid adenoma, with the remaining 11 having a negative ultrasound result. And of the 13 patients who had both surgery and ultrasound, there were a total of 10 (77%) cases where the same result was given. In all these cases, a positive report was given from both surgery and ultrasound. The remaining 3 (23%) patients all had positive surgical results following a negative ultrasound scan. There were no cases of negative surgery after a positive report from ultrasound. The ultrasound report results for the 13 patients who had both ultrasound and surgery are given in Table 6.2, whilst Table 6.3 shows the ultrasound results for the 12 patients who had ultrasound imaging but did not have surgery.

When the results in Table 6.2 are compared to those for the same patients in Table 6.1, it can clearly be seen that 7 of the surgical and ultrasound reports (patients 5, 8, 11, 12, 17, 23 & 26) give the same left/right location for a

positively identified adenoma or hyperplastic parathyroid gland. The three negative ultrasound reports (patients 9, 20 & 21) were all given for patients who had positive samples resected at surgery. Two of the three remaining patients (patients 4 & 31) had suspicious lesions noted on ultrasound imaging that were at a different left/right location to the histologically positive parathyroid adenomas at surgery. The remaining one patient (patient 22) had an ectopic retrosternal adenoma removed at surgery which was not identified on ultrasound imaging. However, another sample was removed at surgery from a location corresponding to that reported as suspicious on the ultrasound scan but which was proven to be normal parathyroid tissue on histological examination.

Patient No.	No. Lesions Seen on US	Position	Positive/Negative
4	1	Left posterior upper	Positive
5	1	Left posterior lower	Positive
8	1	Left posterior lower	Positive
9	0	N/A	Negative
11	1	Right posterior	Positive
12	1	Left posterior lower	Positive
17	1	Right posterior lower	Positive
20	0	N/A	Negative
21	0	N/A	Negative
22	1	Right posterior lower	Positive
23	1	Right posterior lower lateral	Positive
26	1	Right posterior lower	Positive
31	1	Right posterior lower lateral	Positive

Table 6.2 - Ultrasound (US) findings for patients who had parathyroid surgery
Full list of ultrasound results for the patients who had both ultrasound imaging and parathyroidectomy after nuclear medicine parathyroid imaging. Position is given relative to the thyroid gland.

The information contained in Table 6.1 and Table 6.2 was then used to calculate the sensitivity and specificity of ultrasound scanning relative to the gold standard of surgery in the study participants using Equation 4.2 and Equation 4.3. The sensitivity and specificity were calculated based on the given positive/negative and left/right findings only (see Section 4.7) and were found to be 72% and 33%, respectively. These calculated values could then be compared to those from the 4 phases of the observer study, detailed in Chapter 5, to determine the relative sensitivity and specificity from review of different types of images.

The relatively low sensitivity and specificity for ultrasound in comparison to surgery demonstrates that ultrasound imaging cannot be used as a true gold standard for comparison of the findings of the nuclear medicine observer study. However, it was felt that a comparison could still provide valuable information on the comparative merits of the planar and SPECT images in order to determine if routine SPECT imaging would be preferable to the current use of planar scans for parathyroid adenoma detection and localisation.

Patient No.	No. Lesions Seen on US	Position	Positive/Negative
6	1	Right posterior lower	Positive
10	1	Right posterior upper lateral	Positive
14	0	N/A	Negative
15	1	Left posterior upper	Positive
18	0	N/A	Negative
19	0	N/A	Negative
24	0	N/A	Negative
25	0	N/A	Negative
27	0	N/A	Negative
28	0	N/A	Negative
30	1	Right posterior upper medial	Positive
32	0	N/A	Negative

Table 6.3 - Ultrasound (US) findings for patients who did not have parathyroid surgery
Full list of ultrasound results for the patients who had only ultrasound imaging but not parathyroidectomy after nuclear medicine parathyroid imaging. Position is given relative to the thyroid gland.

The data in Table 6.3 show that the majority of patients (8 of 12) who had ultrasound imaging but did not undergo parathyroid surgery had a negative report from the ultrasound scan. This highlights the way that referrals for surgery are carried out at Glasgow Royal Infirmary (GRI) - normally only after positive localisation imaging will a patient be referred to the endocrine surgeons. Negative imaging results are often followed by medical management rather than surgery. Of the 4 patients with positive ultrasound findings, 2 were deemed to be asymptomatic and therefore not in need of surgery and the other two were both keen to avoid surgery and to be managed medically if possible. The possibility of these patients having surgery in future exists, but none have elected to do so to date.

There were different reasons for a lack of follow-up in each of the 3 patients who had neither surgery nor ultrasound imaging. All 3 had negative reports from

planar nuclear medicine imaging. One of the patients had known sarcoidosis and it was felt that the high blood calcium level was most likely due to disease activity rather than a parathyroid adenoma. This patient's PTH level was only borderline elevated and the blood calcium level was easily controlled by diet and so it was felt that no further investigations were required. The second of the three patients had known Paget's disease with only mildly elevated calcium and PTH levels. These were attributed to the active Paget's by the endocrine physicians and so, again, no further investigation was deemed necessary. The final patient in this group was asymptomatic, with no renal stones or other symptoms of high calcium levels. The decision was made to continue monitoring of blood calcium and PTH levels and to manage the patient clinically with no surgery planned.

6.2 Comparison of Observer Study with Surgical and Ultrasound Findings

6.2.1 Phase 1 versus Surgical and US Findings Comparison

6.2.1.1 Surgical Results Comparison

The difference in the number of suspected parathyroid adenoma samples resected at surgery and the number of lesions seen on the planar images in phase 1 of the observer study was calculated for each of the 17 patients for the 5 observers separately. The results were then categorised as in Section 5.5 and the results are shown in Table 6.4.

Observer	Sur > P	Sur < P	Sur = P	Total
1	4	1	12	17
2	8	0	9	17
3	6	1	10	17
4	7	1	9	17
5	6	2	9	17
Total	31	5	49	85

Table 6.4 - Comparison of number of samples resected at surgery and number of lesions seen in phase 1 (planar)

Sur>P = number of times more lesions were resected than were seen on planar images,
 Sur<P = number of times fewer lesions were resected than were seen on planar images,
 Sur=P = number of times same number of lesions were resected as were seen on planar images.

It can clearly be seen that there are very few occasions when fewer lesions were resected than were seen on the planar images and that the situation which occurred most frequently was that when the same number of samples were resected as were seen on the planar images. However, in more than one third of cases (36%), more lesions were resected than had been seen on the planar images. This indicates that there are a significant number of cases in which positive lesions are not seen on planar imaging alone.

The non-parametric Wilcoxon Signed Ranks statistical test was then applied to the data and the results of this are shown in Table 6.5. As previously, a result was taken to be statistically significant if $p < 0.05$.

Observer	p-value	Estimated Median	95% CI
1	0.225	0.0	(0.0, 0.5)
2	0.014	0.5	(0.0, 1.0)
3	0.205	0.5	(0.0, 1.0)
4	0.050	0.5	(0.0, 1.0)
5	0.294	0.5	(0.0, 1.0)
Overall	<0.001	0.5	(0.0, 0.5)

Table 6.5 - Results from Wilcoxon Signed Ranks test on differences in number of lesions seen (surgery vs phase 1)
Output from Minitab software applied to the differences in the number of lesions resected at surgery and the number seen on planar imaging.

The results indicate that for only one observer (observer 2) and for the combined overall values, there was a statistically significant difference between the number of lesions they saw on the planar images and the number resected at surgery. All other results showed no statistical significance. The Wilcoxon Signed Ranks test applied to the combined data will be considerably more powerful than when applied to the data for individual observers due to the larger sample size and so a statistically significant result is more likely. For all the observers individually and combined, the estimated median and 95% CI were ≥ 0 , indicating that there is a tendency for more lesions to have been resected at surgery than were seen on the planar images, which is as expected, given the results in Table 6.4.

A comparison was then made between the reported positive/negative result for each lesion resected and each lesion seen on phase 1 of the observer study. The results for each observer as well as the overall combined values are shown in

Table 6.6. These results indicate that around half of the lesions are being given a different positive/negative report by the observers individually and overall when compared to the surgical results. Observer 5 has the highest number in the “same” category at 61%. Since 18 of the 20 lesions resected at surgery were found to be positive for adenoma or hyperplasia, these results suggest that the observers are either not seeing some lesions on planar imaging that are in fact true adenomas or are not confident that a lesion they see is a true adenoma and so are giving an equivocal report.

Observer	No. Same +/- (%)	No. Different +/- (%)	Total
1	11 (48%)	12 (52%)	23
2	10 (50%)	10 (50%)	20
3	10 (46%)	12 (54%)	22
4	10 (48%)	11 (52%)	21
5	14 (61%)	9 (39%)	23
Overall	55 (51%)	54 (49%)	109

Table 6.6 - Results from comparison of positive/negative findings (surgery vs phase 1)
Number of comparisons between the overall given positive/negative report for a lesion that were the same and different between the surgically resected lesions and those seen on the planar images. Percentages of the total in each category for each observer and overall are given in brackets.

The Wilcoxon Signed Ranks test was then applied to the results of the positive/negative comparisons by giving each “same” result a value of 1 and each “different” result a value of -1. Table 6.7 gives the results of the statistical test and there are no statistically significant differences demonstrated which is as expected from the results in Table 6.6.

Observer	p-value	Estimated Median	95% CI
1	0.867	0.0	(-1.0, 0.0)
2	1.000	0.0	(-1.0, 1.0)
3	0.721	0.0	(-1.0, 0.0)
4	0.862	0.0	(-1.0, 0.0)
5	0.370	0.0	(0.0, 1.0)
Overall	0.935	0.0	(0.0, 0.0)

Table 6.7 - Results from Wilcoxon Signed Ranks Test on positive/negative comparison (surgery vs phase 1)
Output from statistical test applied to comparison between the positive/negative report findings for surgical results and those given from review of the planar images.

A comparison was then made of the given location of each lesion, with the surgical report compared to the positions given by the observers on review of the planar images. The comparison was carried out in the same way as in Section 5.5 and no anterior/posterior information was included since this cannot

be gained from anterior planar imaging. The results of the left/right location comparison are shown in Table 6.8 and it should be noted that lesions reported as being in an ectopic location were not included in this analysis.

Observer	No. Same (%)	No. Different (%)	Total
1	13 (68%)	6 (32%)	19
2	7 (41%)	10 (59%)	17
3	10 (59%)	7 (41%)	17
4	9 (53%)	8 (47%)	17
5	11 (61%)	7 (39%)	18
Overall	50 (57%)	38 (43%)	88

Table 6.8 - Results of comparison in left/right location between lesions resected at surgery and those seen on planar images
Number and percentage of lesions seen in the same and different left/right location for each observer and combined for all observers.

The results show that, in general, more of the lesions were seen by the observers at the same left/right location as those that were resected at surgery. However, observer 2 saw fewer than half (41%) of the lesions at the same left/right location.

The results of a similar comparison carried out on the upper/lower location information are shown in Table 6.9. On this occasion, it is immediately clear that for each observer individually as well as for the combined results, fewer than half of the lesions are being seen at the same upper/lower location on planar images as those that are being resected during surgery. Again, observer 2 has the fewest number in the “same” category at just 35%.

Observer	No. Same (%)	No. Different (%)	Total
1	9 (47%)	10 (53%)	19
2	6 (35%)	11 (65%)	17
3	7 (41%)	10 (59%)	17
4	7 (41%)	10 (59%)	17
5	7 (39%)	11 (61%)	18
Overall	36 (41%)	52 (59%)	88

Table 6.9 - Results of comparison in upper/lower location between lesions resected at surgery and those seen on planar images
Number and percentage of lesions seen in the same and different upper/lower location for each observer and combined for all observers.

The results of the left/right and upper/lower location comparisons were then combined to give a comparison of the overall location of each lesion. The results of this analysis are shown in Table 6.10.

Observer	No. Same (%)	No. Different (%)	Total
1	9 (47%)	10 (53%)	19
2	6 (35%)	11 (65%)	17
3	7 (41%)	10 (59%)	17
4	7 (41%)	10 (59%)	17
5	7 (39%)	11 (61%)	18
Overall	36 (41%)	52 (59%)	88

Table 6.10 - Results of combined left/right and upper/lower location comparisons between lesions resected at surgery and those seen on planar images
Number and percentage of lesions seen in the same and different overall location for each observer and for the combined for all observers.

A comparison of the results in Table 6.9 and Table 6.10 shows that the values given in each category are identical. This indicates that on every occasion when the correct upper/lower location was given by the observer reviewing the planar images, the correct left/right location was also given. There were therefore also other occasions on which the correct left/right position was reported by the observer but the upper/lower result was incorrect. It should be noted, however, that the given left/right and upper/lower locations from the nuclear medicine images are always with respect to the location of the thyroid gland, whereas the locations given by the surgeon may be with respect to a variety of other anatomical landmarks. It is therefore the case that the location definitions may be different and the same lesion may appear to be given at a different location.

The sensitivity and specificity taking into account the given positive/negative result and left/right location were then calculated for each observer and for all the observers combined. The results are shown in Table 6.11.

Observer	Sensitivity (%)	Specificity (%)
1	50	67
2	46	67
3	47	75
4	47	67
5	60	40
Overall	49	61
US	72	33

Table 6.11- Calculated sensitivity and specificity values for comparison of surgical and planar imaging results
Percentage sensitivity and specificity values are given for each observer and for the combined results of all observers as well as for US imaging to provide a comparison

The results in Table 6.11 show clearly that the planar dual-isotope subtraction nuclear medicine imaging technique is considerably less sensitive than

ultrasound imaging for detecting parathyroid adenomas. However, the specificity is generally higher, indicating that the observers are reporting fewer false positive results than were indicated by US imaging. A combination of planar nuclear medicine and US imaging could therefore provide more accurate localisation overall than each independently. For example, performing an US study first would take advantage of the higher sensitivity of that modality. In instances where an equivocal or uncertain result is reported, carrying out planar nuclear medicine imaging with its higher specificity could help to confirm or deny the presence of an adenoma or hyperplastic gland. This would have the advantage of using a non-ionising imaging technique first, therefore potentially removing the need for patients to receive a radiation dose. However, the two imaging studies would not be truly independent and the results of the planar nuclear medicine imaging could be heavily influenced by the report from US. Also, US is not a functional imaging technique and can therefore not determine for certain the presence of a functionally overactive gland. The high sensitivity demonstrated here may be partly attributed to the fact that at GRI, US normally takes place after nuclear medicine imaging, and so the operator could be influenced by the pre-existing nuclear medicine report.

From the results in Table 6.11, it can be seen that observer 5 has both the highest sensitivity and lowest specificity values at 60% and 40%, respectively. This suggests that this observer tends to report more positive lesions from the images than the others, leading to the correct identification of more true positive lesions but also more false positive results. Throughout the observer study, observer 5 was seen to report more lesions than the other observers and so this is not a surprising result.

6.2.1.2 Ultrasound Results Comparison

The results of the comparison between ultrasound imaging and phase 1 of the observer study were subjected to the same analysis as in Section 6.2.1.1. The results of the comparison in the number of lesions seen on ultrasound imaging and planar nuclear medicine imaging for each of the 25 patients who had ultrasound are shown in Table 6.12 and the results from applying the Wilcoxon Signed Ranks test to this data are shown in Table 6.13.

Observer	US > P	US < P	US = P	Total
1	3	4	18	25
2	7	3	15	25
3	4	4	17	25
4	6	3	16	25
5	3	5	17	25
Total	23	19	83	125

Table 6.12 - Comparison of number of lesions seen on ultrasound and in phase 1 (planar)
US>P = number of times more lesions were seen on ultrasound than on planar images,
US<P = number of times fewer lesions were seen on ultrasound than on planar images,
US=P = number of times same number of lesions were seen on ultrasound than on planar images.

Observer	p-value	Estimated Median	95% CI
1	0.225	0.0	(0.0, 0.5)
2	0.014	0.5	(0.0, 1.0)
3	0.205	0.5	(0.0, 1.0)
4	0.050	0.5	(0.0, 1.0)
5	0.294	0.5	(0.0, 1.0)
Overall	<0.001	0.5	(0.0, 0.5)

Table 6.13 - Results from Wilcoxon Signed Ranks test on differences in number of lesions seen (ultrasound vs phase 1)

Output from Minitab software applied to the differences in the number of lesions seen on ultrasound and those seen on planar imaging.

On this occasion, it is clear that there are more instances where the same number of lesions was seen on the ultrasound and nuclear medicine planar images than in either of the other two categories. The Wilcoxon Signed Ranks test supported this finding for 4 of the 5 observers, with $p > 0.05$. However, observer 2 had a statistically significant difference demonstrated between the number of lesions seen on each time of imaging. The estimated median and 95% CI values being > 0 indicates that there is a tendency for more lesions to be reported from ultrasound imaging than from the planar images.

The results of the comparison of positive/negative reports between the ultrasound and planar imaging are shown in Table 6.14. When these results are compared with those in Table 6.6, it can be seen that the comparison of positive/negative reports between the ultrasound and planar images gives more results that are the same than when the comparison is between resected lesions at surgery and planar imaging.

The results of applying the Wilcoxon Signed Ranks test to these data are shown in Table 6.15, with the level of statistical significance once again taken to be $p < 0.05$. The only result demonstrating statistical significance is the combined

overall data from all 5 observers, which is most likely to be because of the increased power of the test calculation due to the larger sample involved. The 95% CI values for each observer are, however, ≥ 0 which indicates that the observers tend to give more reports with the same positive/negative result than they do different.

Observer	No. Same +/- (%)	No. Different +/- (%)	Total
1	17 (68%)	8 (32%)	25
2	14 (56%)	11 (44%)	25
3	15 (60%)	10 (40%)	25
4	15 (60%)	10 (40%)	25
5	17 (65%)	9 (35%)	26
Overall	78 (62%)	48 (38%)	126

Table 6.14 - Results from comparison of positive/negative findings (ultrasound vs phase 1) Number of comparisons between the overall given positive/negative report for a lesion that were the same and different between those seen on ultrasound imaging and those seen on the planar images. Percentages of the total in each category for each observer and overall are given in brackets.

Observer	p-value	Estimated Median	95% CI
1	0.119	0.0	(0.0, 1.0)
2	0.609	0.0	(0.0, 1.0)
3	0.389	0.0	(0.0, 1.0)
4	0.389	0.0	(0.0, 1.0)
5	0.174	0.0	(0.0, 1.0)
Overall	0.020	0.0	(0.0, 0.0)

Table 6.15 - Results from Wilcoxon Signed Ranks Test on positive/negative comparison (ultrasound vs phase 1)

Output from statistical test applied to comparison between the positive/negative report findings from ultrasound and those given from review of the planar images.

The results of the comparison between the given left/right locations relative to the thyroid gland are given in Table 6.16. As was seen in Table 6.8, observer 2 tends to see the lowest proportion of lesions at the same left/right location as

Observer	No. Same (%)	No. Different (%)	Total
1	10 (71%)	4 (29%)	14
2	5 (36%)	9 (64%)	14
3	9 (64%)	5 (36%)	14
4	7 (50%)	7 (50%)	14
5	10 (67%)	5 (33%)	15
Overall	41 (58%)	30 (42%)	71

Table 6.16 - Results of comparison in left/right location between lesions seen on ultrasound and those seen on planar images

Number and percentage of lesions seen in the same and different left/right location for each observer and combined for all observers.

they are seen on ultrasound whilst the others all see the same or more lesions on the same side.

Table 6.17 shows the results of the comparison of the given upper/lower location. It should be noted that for one of the lesions seen on ultrasound, no upper/lower location information was reported, meaning that this lesion has not been included in this analysis. There is a wide variation between the results for

Observer	No. Same (%)	No. Different (%)	Total
1	6 (46%)	7 (54%)	13
2	4 (31%)	9 (69%)	13
3	7 (54%)	6 (46%)	13
4	6 (46%)	7 (54%)	13
5	8 (57%)	6 (43%)	14
Overall	31 (47%)	35 (53%)	66

Table 6.17 - Results of comparison in upper/lower location between lesions seen on ultrasound and those seen on planar images
Number and percentage of lesions seen in the same and different upper/lower location for each observer and combined for all observers.

different observers, with observer 4 seeing only 31% of the lesions in the same upper/lower location as was reported from ultrasound, whilst observer 5 sees 57% in the same place. The combined results for all the observers show similar proportions given as being at the same and different sites.

A comparison of the overall location given for each lesion was then obtained by combining the results of the left/right and upper/lower analyses and the results are given in Table 6.18.

Observer	No. Same (%)	No. Different (%)	Total
1	7 (50%)	7 (50%)	14
2	5 (36%)	9 (64%)	14
3	8 (57%)	6 (43%)	14
4	7 (50%)	7 (50%)	14
5	8 (53%)	7 (47%)	15
Overall	35 (49%)	36 (51%)	71

Table 6.18 - Results of combined left/right and upper/lower location comparisons between lesions seen on ultrasound and those seen on planar images
Number and percentage of lesions seen in the same and different overall location for each observer and for the combined for all observers.

Each of the observers reported a similar proportion of lesions at the same and different overall location from the planar images as were seen on the ultrasound

scan. The exception is observer 2, who gave only 36% of lesions at the same overall location.

Taking the result from the ultrasound scan as the comparison standard, the sensitivity and specificity were calculated for each observer and for all the observers combined and the results are shown in Table 6.19.

Observer	Sensitivity (%)	Specificity (%)
1	54	77
2	27	71
3	38	69
4	45	75
5	62	69
Overall	46	72

Table 6.19 - Calculated sensitivity and specificity values for comparison of US and planar imaging results

Percentage sensitivity and specificity values are given for each observer and for the combined results of all observers

The results indicate that the specificity is relatively good for all the observers as well as the combined value. However, the sensitivity is less so, with three of the observers and the overall result having values of <50%. This demonstrates that there are a significant number of occasions when a lesion observed on ultrasound imaging is not observed on planar dual-isotope subtraction imaging but that a negative ultrasound result is often accompanied by a negative nuclear medicine result.

6.2.2 Phase 2 versus Surgical and US Findings Comparison

6.2.2.1 Surgical Results Comparison

The number of suspected parathyroid adenomas seen in phase 2 (SPECT images) of the observer study was then compared to the number of samples resected at surgery. The difference in the number of lesions was calculated for the 5 observers independently for each of the 17 patients. The results were categorised as before and are shown in Table 6.20.

In this case, the largest category is that where the number of lesions resected at surgery was equal to the number seen on SPECT imaging. For 4 of the 5 observers, this was the largest category. However, observer 5 tended to see

more lesions on the SPECT images than were sampled by the surgeon. In only 14 (16%) of the comparisons were more lesions resected than had been observed from the SPECT images, indicating that fewer lesions are missed when reviewing SPECT images than planar (compare with results in Section 6.2.1.1).

Observer	Sur > S	Sur < S	Sur = S	Total
1	3	0	14	17
2	5	1	11	17
3	3	4	10	17
4	3	4	10	17
5	0	10	7	17
Total	14	19	52	85

Table 6.20 - Comparison of number of samples resected at surgery and number of lesions seen in phase 2 (SPECT)

Sur>S = number of times more lesions were resected than were seen on SPECT images,
 Sur<S = number of times fewer lesions were resected than were seen on SPECT images,
 Sur=S = number of times same number of lesions were resected as were seen on SPECT images.

The data were then subjected to the Wilcoxon Signed Ranks test, for which a result of $p < 0.05$ was again taken to be significant. The results are shown in Table 6.21.

Observer	p-value	Estimated Median	95% CI
1	0.181	0.0	(0.0, 0.5)
2	0.142	0.0	(0.0, 0.5)
3	0.800	0.0	(-0.5, 0.5)
4	0.866	0.0	(-0.5, 0.5)
5	0.006	-1.0	(-1.5, -0.5)
Overall	0.292	0.0	(0.0, 0.0)

Table 6.21 - Results from Wilcoxon Signed Ranks test on differences in number of lesions seen (surgery vs phase 2)

Output from Minitab software applied to the differences in the number of lesions resected at surgery and the number seen on SPECT imaging.

It can be seen from the table that only the data from observer 5 demonstrated a statistically significant difference ($p < 0.05$) between the number of lesions resected and those reported from the SPECT images. The fact that the estimated median and 95% CI are < 0 shows that this observer tended to see more lesions on the SPECT images than the surgeon sampled, which is as expected, given the results in Table 6.20.

Table 6.22 gives the results of the comparison between the positive/negative result reported for each lesion sampled and each lesion reported by the observers from the SPECT images.

Observer	No. Same +/- (%)	No. Different +/- (%)	Total
1	14 (70%)	6 (30%)	20
2	12 (57%)	9 (43%)	21
3	18 (75%)	6 (25%)	24
4	19 (76%)	6 (24%)	25
5	31 (72%)	12 (28%)	43
Overall	94 (71%)	39 (29%)	133

Table 6.22 - Results from comparison of positive/negative findings (surgery vs phase 2)
Number of comparisons between the overall given positive/negative report for a lesion that were the same and different between the surgically resected lesions and those seen on the SPECT images. Percentages of the total in each category for each observer and overall are given in brackets.

For all observers, the number reported with the same result is higher than that given a different result, with observer 4 having the highest proportion as the same at 76% and observer 2 having the lowest fraction the same at 57%. These results are considerably better than those from Table 6.6 when the lesions observed on planar images were considered. This indicates that the SPECT images do provide some improvement in reporting of possible adenomas.

The results of the application of the Wilcoxon Signed Ranks test to this data are shown in Table 6.23. Three of the 5 observers and the overall combined data show statistically significant differences with $p < 0.05$. Only observers 1 & 2 do not have $p < 0.05$, which is to be expected if the results in Table 6.22 are considered since these were the two observers with the lowest proportion in the “same” category.

Observer	p-value	Estimated Median	95% CI
1	0.121	0.5	(0.0, 1.0)
2	0.578	0.0	(0.0, 1.0)
3	0.033	1.0	(0.0, 1.0)
4	0.024	1.0	(0.0, 1.0)
5	0.012	1.0	(0.0, 1.0)
Overall	<0.001	1.0	(0.0, 1.0)

Table 6.23 - Results from Wilcoxon Signed Ranks Test on positive/negative comparison (surgery vs phase 2)
Output from statistical test applied to comparison between the positive/negative report findings for surgical results and those given from review of the SPECT images.

The location of each resected sample and lesion seen on the SPECT images was then compared. Since an indication of the anterior/posterior position of a lesion can be gained from SPECT images, this information was included in the overall comparison.

Table 6.24 gives the results of the left/right location comparison. Once again, lesions reported by the observers as being in an ectopic location were not included in this analysis.

Observer	No. Same (%)	No. Different (%)	Total
1	14 (82%)	3 (18%)	17
2	11 (65%)	6 (35%)	17
3	16 (80%)	4 (20%)	20
4	15 (79%)	4 (21%)	19
5	21 (62%)	13 (38%)	34
Overall	77 (72%)	30 (28%)	107

Table 6.24 - Results of comparison in left/right location between lesions resected at surgery and those seen on SPECT images
Number and percentage of lesions seen in the same and different left/right location for each observer and combined for all observers.

For each observer, well over 50% of the lesions were seen on the same side (left/right) as those samples taken at surgery, with observer 5 demonstrating the lowest proportion at 62%. It should also be noted that observer 5 has the highest total number of comparisons, meaning that this observer tended to see more lesions than the others, as has already been remarked upon in Section 5.4.6.

The given upper/lower locations were then compared and the results are shown in Table 6.25. It can be seen that the results for each observer vary considerably with observer 1 seeing as many as 76% of lesions in the same

Observer	No. Same (%)	No. Different (%)	Total
1	13 (76%)	4 (24%)	17
2	7 (41%)	10 (59%)	17
3	10 (50%)	10 (50%)	20
4	10 (53%)	9 (47%)	19
5	16 (47%)	18 (53%)	34
Overall	56 (52%)	51 (48%)	107

Table 6.25 - Results of comparison in upper/lower location between lesions resected at surgery and those seen on SPECT images
Number and percentage of lesions seen in the same and different upper/lower location for each observer and combined for all observers.

upper/lower position as the lesions resected at surgery whilst observer 2 saw only 41% at the same site.

The results of the combined analysis of the left/right and upper/lower comparisons to give an assessment of any differences in the overall given location for each lesion are shown in Table 6.26.

Observer	No. Same (%)	No. Different (%)	Total
1	11 (65%)	6 (35%)	17
2	6 (35%)	11 (65%)	17
3	8 (40%)	12 (60%)	20
4	9 (47%)	10 (53%)	19
5	11 (32%)	23 (68%)	34
Overall	45 (42%)	62 (58%)	107

Table 6.26 - Results of combined left/right and upper/lower location comparisons between lesions resected at surgery and those seen on SPECT images
Number and percentage of lesions seen in the same and different overall location for each observer and for the combined for all observers.

It is immediately clear that only observer 1 has >50% of the lesions given at the same overall site, whilst all of the other observers as well as the combined results are <50%. Observer 5 had the smallest proportion at the same overall site with 32%.

Comparisons were then made of the given anterior/posterior location for each lesion and the results are shown in Table 6.27. One of the samples resected at surgery had no anterior/posterior information given and so is excluded from the results in the table.

Observer	No. Same (%)	No. Different (%)	Total
1	15 (94%)	1 (6%)	16
2	9 (56%)	7 (44%)	16
3	14 (78%)	4 (22%)	18
4	10 (56%)	8 (44%)	18
5	18 (56%)	14 (44%)	32
Overall	66 (66%)	34 (34%)	100

Table 6.27 - Results of comparison in anterior/posterior location between lesions resected at surgery and those seen on SPECT images
Number and percentage of lesions seen in the same and different anterior/posterior location for each observer and combined for all observers.

As for the left/right location, all the observers gave >50% of lesions at the same anterior/posterior location as they were found by the surgeon. Observer 1 had

the highest proportion at 94% whilst the overall combined result for all the observers showed that almost 2/3 of the lesions were given at the same site.

An overall comparison was then made of the location of each given lesion by combining all the results for the left/right, upper/lower and anterior/posterior comparisons. The results are shown in Table 6.28.

Observer	No. Same (%)	No. Different (%)	Total
1	10 (59%)	7 (41%)	17
2	4 (24%)	13 (76%)	17
3	7 (35%)	13 (65%)	20
4	6 (32%)	13 (68%)	19
5	6 (18%)	28 (82%)	34
Overall	33 (31%)	74 (69%)	107

Table 6.28 - Results of combined left/right, upper/lower and anterior/posterior location comparisons between lesions resected at surgery and those seen on SPECT images
Number and percentage of lesions seen in the same and different overall location for each observer and for the combined for all observers.

Again, only observer 1 saw more than half of the lesions at the same place as the surgeon resected sampled whilst observer 5 saw only 18% at the same overall location.

The sensitivity and specificity of true lesion detection were again calculated for each individual observer as well as for the overall combined results. Table 6.29 shows these calculated values along with the sensitivity and specificity for ultrasound imaging, to act as a comparison.

Observer	Sensitivity (%)	Specificity (%)
1	80	33
2	57	25
3	75	60
4	85	0
5	84	40
Overall	77	31
US	72	33

Table 6.29 - Calculated sensitivity and specificity values for comparison of surgical and SPECT imaging results
Percentage sensitivity and specificity values are given for each observer and for the combined results of all observers as well as for US imaging to provide a comparison

The observers' sensitivity and specificity values can be seen to be comparable to or better than those from ultrasound imaging, with the exception of observer 2 having a sensitivity of just 57% and observer 4 having a 0% specificity value.

When these results are compared with those in Table 6.11, it can clearly be seen that the sensitivity is considerably improved when the observers are reviewing the SPECT images, meaning that more true lesions are seen. However, the specificity is poorer, indicating that there are more false positive findings from the SPECT images and that the observers believe that image artefacts are in fact true lesions. This is in keeping with the results of the direct comparison between Phases 1 and 2 of the observer study (see Section 5.5.1), where more lesions were seen on the SPECT images than on the planar.

6.2.2.2 Ultrasound Results Comparison

Table 6.30 shows the results of the comparison of the number of lesions seen on ultrasound imaging and the number seen on the SPECT images by each of the observers for each of the 25 patients. It can be seen that there were very few occasions in which more lesions were seen on the ultrasound images than were reported by the observers from the SPECT imaging. As for the comparison with the surgical results (Section 6.2.2.1), the largest category is that where the number of lesions seen was equal. However, there were a significant number (42%) of cases in which fewer lesions were seen on ultrasound than were reported from the SPECT observer study.

Observer	US > S	US < S	US = S	Total
1	0	7	18	25
2	2	7	16	25
3	0	12	13	25
4	0	8	17	25
5	0	19	6	25
Total	2	53	70	125

Table 6.30 - Comparison of number of lesions seen on ultrasound and in phase 2 (SPECT)
US>S = number of times more lesions were seen on ultrasound than on SPECT images,
US<S = number of times fewer lesions were seen on ultrasound than on SPECT images,
US=S = number of times same number of lesions were seen on ultrasound as on SPECT images.

The results of applying the Wilcoxon Signed Ranks test to this data are shown in Table 6.31. For 4 of the 5 observers as well as the combined data, $p < 0.05$ and therefore a statistically significant difference in the number of lesions seen is demonstrated. Observer 2 is the only observer for whom there is no statistically significant difference. However, all estimated median and 95% CI values are ≤ 0 ,

meaning that there is a tendency to see more lesions on the SPECT images than are reported on ultrasound.

Observer	p-value	Estimated Median	95% CI
1	0.022	0.0	(-0.5, 0.0)
2	0.155	0.0	(-0.5, 0.0)
3	0.003	-0.5	(-1.0, 0.0)
4	0.014	-0.5	(-0.5, 0.0)
5	<0.001	-1.5	(-2.0, -1.0)
Overall	<0.001	-0.5	(-0.5, -0.5)

Table 6.31 - Results from Wilcoxon Signed Ranks test on differences in number of lesions seen (ultrasound vs phase 2)

Output from Minitab software applied to the differences in the number of lesions seen on ultrasound and those seen on SPECT imaging.

The reported positive/negative status of each lesion was then compared and the results are given in Table 6.32. As was the case in Table 6.22 when the surgical and SPECT reports were compared, there are >50% of the results in the “same” category for each of the observers. On this occasion, observer 3 has the lowest proportion in this category with 59%, whilst observer 4 has the highest with 85%.

Observer	No. Same +/- (%)	No. Different +/- (%)	Total
1	20 (77%)	6 (23%)	26
2	18 (69%)	8 (31%)	26
3	17 (59%)	12 (41%)	29
4	23 (85%)	4 (15%)	27
5	35 (71%)	14 (29%)	49
Overall	113 (72%)	44 (28%)	157

Table 6.32 - Results from comparison of positive/negative findings (ultrasound vs phase 2)
Number of comparisons between the overall given positive/negative report for a lesion that were the same and different between those seen on ultrasound imaging and those seen on the SPECT images. Percentages of the total in each category for each observer and overall are given in brackets.

The Wilcoxon Signed Ranks test was then applied to the data and the results are given in Table 6.33. As before, $p < 0.05$ was taken to be the level of statistical significance. On this occasion, only the results for observers 2 & 3 do not demonstrate statistical significance. The estimated median and 95% CI values for all the observers are, however ≥ 0 , suggesting that there are more reports given with the same positive/negative result than are given a different result.

The left/right location comparison was then carried out and the results are shown in Table 6.34.

Observer	p-value	Estimated Median	95% CI
1	0.017	1.0	(0.0, 1.0)
2	0.089	0.0	(0.0, 1.0)
3	0.424	0.0	(0.0, 1.0)
4	0.001	1.0	(1.0, 1.0)
5	0.009	1.0	(0.0, 1.0)
Overall	<0.001	1.0	(0.0, 1.0)

Table 6.33 - Results from Wilcoxon Signed Ranks Test on positive/negative comparison (ultrasound vs phase 2)

Output from statistical test applied to comparison between the positive/negative report findings from ultrasound imaging and those given from review of the SPECT images.

Observer	No. Same (%)	No. Different (%)	Total
1	10 (71%)	4 (29%)	14
2	10 (67%)	5 (33%)	15
3	13 (76%)	4 (24%)	17
4	11 (69%)	5 (31%)	16
5	16 (64%)	9 (36%)	25
Overall	60 (69%)	27 (31%)	87

Table 6.34 - Results of comparison in left/right location between lesions seen on ultrasound and those seen on SPECT images

Number and percentage of lesions seen in the same and different left/right location for each observer and combined for all observers.

It can clearly be seen that in the majority of cases for each observer, the same left/right location was given for a lesion when compared to that reported from the ultrasound. The lowest proportion given at the same location was 64% from observer 5, who once again also had the highest total number of comparisons and therefore reported more lesions than the other observers.

Table 6.35 gives the results of the upper/lower location comparison. Only observer 4 gave fewer lesions at the same location (47%) than at a different site when compared to the ultrasound report. Observer 1 saw as many as 69% at the same location, meaning that there was once again a large variation between the results for the different observers.

The combined results for the left/right and upper/lower comparisons are shown in Table 6.36. Once again, observer 1 had the highest proportion of lesions given at the same overall location at 64% whilst observers 2 & 5 reported only 40% at the same site as the ultrasound.

Observer	No. Same (%)	No. Different (%)	Total
1	9 (69%)	4 (31%)	13
2	7 (50%)	7 (50%)	14
3	9 (56%)	7 (44%)	16
4	7 (47%)	8 (53%)	15
5	12 (50%)	12 (50%)	24
Overall	44 (54%)	38 (46%)	82

Table 6.35 - Results of comparison in upper/lower location between lesions seen on ultrasound and those seen on SPECT images
Number and percentage of lesions seen in the same and different upper/lower location for each observer and combined for all observers.

Observer	No. Same (%)	No. Different (%)	Total
1	9 (64%)	5 (36%)	14
2	6 (40%)	9 (60%)	15
3	9 (53%)	8 (47%)	17
4	8 (50%)	8 (50%)	16
5	10 (40%)	15 (60%)	25
Overall	42 (48%)	45 (52%)	87

Table 6.36 - Results of combined left/right and upper/lower location comparisons between lesions seen on ultrasound and those seen on SPECT images
Number and percentage of lesions seen in the same and different overall location for each observer and for the combined for all observers.

The given anterior/posterior locations were then compared and the results are shown in Table 6.37. All the observers reported >50% of lesions at the same anterior/posterior location as was given by the ultrasound report. However, there was again a wide variation between the observers with observer 1 giving as many as 93% at the same site whilst observer 4 had only 56% in this category.

Observer	No. Same (%)	No. Different (%)	Total
1	13 (93%)	1 (7%)	14
2	11 (73%)	4 (27%)	15
3	14 (82%)	3 (18%)	17
4	9 (56%)	7 (44%)	16
5	16 (64%)	9 (36%)	25
Overall	63 (72%)	24 (28%)	87

Table 6.37 - Results of comparison in anterior/posterior location between lesions seen on ultrasound and those seen on SPECT images
Number and percentage of lesions seen in the same and different anterior/posterior location for each observer and combined for all observers.

The anterior/posterior comparison findings were then combined with those for the left/right and upper/lower comparisons and a comparison of the overall location in 3 dimensions was produced. The results are given in Table 6.38.

Observer	No. Same (%)	No. Different (%)	Total
1	9 (64%)	5 (36%)	14
2	5 (33%)	10 (67%)	15
3	9 (53%)	8 (47%)	17
4	5 (31%)	11 (69%)	16
5	8 (32%)	17 (68%)	25
Overall	36 (41%)	51 (59%)	87

Table 6.38 - Results of combined left/right, upper/lower and anterior/posterior location comparisons between lesions seen on ultrasound and those seen on SPECT images
Number and percentage of lesions seen in the same and different overall location for each observer and for the combined for all observers.

It can be seen that both observer 1 and observer 3 gave >50% of lesions at the same overall location as were reported from ultrasound scanning. However, the other observers only gave around 30% of lesions at the same location.

Table 6.39 shows the calculated sensitivity and specificity values for each individual observer and for all the observers combined when the ultrasound results are taken to be the comparison standard. The results clearly show good sensitivity in general, with observer 4 having 100% sensitivity. However, the specificity is more variable with observer 2 having a value of 73% whilst observer 3 has just 36%. When compared with the results in Table 6.19, the sensitivity shows a general improvement, whilst the specificity is poorer. This is the same situation as was seen when the Phase 1 and 2 observer study results were compared with the surgical findings (Section 6.2.2.1), indicating that more true lesions are seen on the SPECT images than the planar but that there are also more false positive reports being given by the observers.

Observer	Sensitivity (%)	Specificity (%)
1	91	63
2	60	73
3	67	36
4	100	38
5	94	42
Overall	81	48

Table 6.39 - Calculated sensitivity and specificity values for comparison of US and SPECT imaging results
Percentage sensitivity and specificity values are given for each observer and for the combined results of all observers

6.2.3 Phase 3 versus Surgical and US Findings Comparison

6.2.3.1 Surgical Results Comparison

For each of the 17 patients, the difference between the number of samples resected during parathyroidectomy and the number seen by each of the 5 observers on the Sestamibi (planar + SPECT) images in phase 3 of the observer study was calculated. Table 6.40 shows the results categorised in the same way as the previous analyses involving the results from phases 1 and 2 of the observer study.

Observer	Sur > M	Sur < M	Sur = M	Total
1	6	0	11	17
2	9	0	8	17
3	5	0	12	17
4	7	2	8	17
5	1	5	11	17
Total	28	7	50	85

Table 6.40 - Comparison of number of samples resected at surgery and number of lesions seen in phase 3 (Sestamibi only)

Sur>M = number of times more lesions were resected than were seen on Sestamibi images, Sur<M = number of times fewer lesions were resected than were seen on Sestamibi images, Sur=M = number of times same number of lesions were resected as were seen on Sestamibi images.

The results show that there were only a very small number of occasions in which there were more lesions seen on the Sestamibi images than were resected at surgery, whilst there were 4 times as many occasions on which there were fewer lesions seen than were sampled. The largest category is once again that in which there were equal numbers of surgical samples and lesions reported from the images.

Table 6.41 shows the results of the non-parametric Wilcoxon Signed Ranks test being applied to these data. The results for 2 of the observers (1 & 2) show statistically significant differences with $p < 0.05$ but this is not the case for the other 3 observers. The result of the test applied to the data from all the observers is also statistically significant. Interestingly, only observer 5 has a 95% CI that is ≤ 0 , which indicates that this observer generally saw more lesions on the Sestamibi images than were sampled at surgery, whereas the opposite was true for all the other observers.

Observer	p-value	Estimated Median	95% CI
1	0.036	0.5	(0.0, 0.5)
2	0.009	0.5	(0.0, 1.0)
3	0.059	0.0	(0.0, 0.5)
4	0.155	0.5	(0.0, 0.5)
5	0.173	0.0	(-0.5, 0.0)
Overall	0.001	0.5	(0.0, 0.5)

Table 6.41 - Results from Wilcoxon Signed Ranks test on differences in number of lesions seen (surgery vs phase 3)

Output from Minitab software applied to the differences in the number of lesions resected at surgery and the number seen on Sestamibi only imaging.

The reported positive/negative results for each sample resected and each lesion seen on phase 3 of the observer study were then compared and the results are shown in Table 6.42.

Observer	No. Same +/- (%)	No. Different +/- (%)	Total
1	7 (35%)	13 (65%)	20
2	6 (30%)	14 (70%)	20
3	9 (45%)	11 (55%)	20
4	13 (59%)	9 (41%)	22
5	20 (69%)	9 (31%)	29
Overall	55 (49%)	56 (51%)	111

Table 6.42 - Results from comparison of positive/negative findings (surgery vs phase 3) Number of comparisons between the overall given positive/negative report for a lesion that were the same and different between the surgically resected lesions and those seen on the Sestamibi only images. Percentages of the total in each category for each observer and overall are given in brackets.

In contrast to the results for the comparisons of surgical results with those from phases 1 and 2 of the observer study, 3 of the individual observers as well as the combined result for all the observers have <50% in the “same” category. Given that 18 of the 20 samples from surgery were given a positive histological report for parathyroid adenoma or hyperplasia, this suggests that the observers were either not seeing some true lesions on the Sestamibi images or that they are not confident that the lesion they are seeing is a true adenoma and so are reporting it as equivocal.

The Wilcoxon Signed Ranks test was then applied to these data and the results are given in Table 6.43. None of the results are statistically significant as $p > 0.05$ in every case. However, the 95% CI values for observers 1-3 are all ≤ 0 whilst those for observers 4 & 5 are ≥ 0 . This supports the results in Table 6.42 by showing that observers 1-3 tend to give a different report from the surgical report whilst observers 4 & 5 generally give the same report.

Observer	p-value	Estimated Median	95% CI
1	0.247	0.0	(-1.0, 0.0)
2	0.121	-0.5	(-1.0, 0.0)
3	0.709	0.0	(-1.0, 0.0)
4	0.465	0.0	(0.0, 1.0)
5	0.076	0.0	(0.0, 1.0)
Overall	0.936	0.0	(0.0, 0.0)

Table 6.43 - Results from Wilcoxon Signed Ranks Test on positive/negative comparison (surgery vs phase 3)

Output from statistical test applied to comparison between the positive/negative report findings for surgical results and those given from review of the Sestamibi only images.

A comparison of the given location of each lesion for each patient was then carried out in the same way as has been previously discussed. The results for the left/right comparison between the surgically resected samples and those seen on Sestamibi images are shown in Table 6.44. As has been the case previously, observer 5 has the highest number of comparisons, meaning that this observer generally saw a greater number of lesions on the Sestamibi images than did the other observers. It can also be seen from the results that observer 2 saw the smallest proportion of lesions at the same left/right position as those sampled at surgery at only 35%. All the other observers saw >50% at the same position, with observer 1 having the highest fraction at 76%.

Observer	No. Same (%)	No. Different (%)	Total
1	13 (76%)	4 (24%)	17
2	6 (35%)	11 (65%)	17
3	12 (71%)	5 (29%)	17
4	12 (63%)	7 (37%)	19
5	18 (75%)	6 (25%)	24
Overall	61 (65%)	33 (35%)	94

Table 6.44 - Results of comparison in left/right location between lesions resected at surgery and those seen on Sestamibi only images

Number and percentage of lesions seen in the same and different left/right location for each observer and combined for all observers.

The results of the upper/lower location comparison are shown in Table 6.45. In this instance, only observer 3 gave the same upper/lower location as the surgical report in more than half of cases (53%). The lowest proportion of reports at the same site was given by observer 2 with only 29%.

The left/right and upper/lower comparisons were then combined and the results are shown in Table 6.46. Once again, only observer 3 saw >50% of lesions on the

Sestamibi images at the same overall location as those which were sampled at surgery.

Observer	No. Same (%)	No. Different (%)	Total
1	8 (47%)	9 (53%)	17
2	5 (29%)	12 (71%)	17
3	9 (53%)	8 (47%)	17
4	9 (47%)	10 (53%)	19
5	10 (42%)	14 (58%)	24
Overall	41 (44%)	53 (56%)	94

Table 6.45 - Results of comparison in upper/lower location between lesions resected at surgery and those seen on Sestamibi only images
Number and percentage of lesions seen in the same and different upper/lower location for each observer and combined for all observers.

Observer	No. Same (%)	No. Different (%)	Total
1	7 (41%)	10 (59%)	17
2	4 (24%)	13 (76%)	17
3	9 (53%)	8 (47%)	17
4	8 (42%)	11 (58%)	19
5	8 (33%)	16 (67%)	24
Overall	36 (38%)	58 (62%)	94

Table 6.46 - Results of combined left/right and upper/lower location comparisons between lesions resected at surgery and those seen on Sestamibi only images
Number and percentage of lesions seen in the same and different overall location for each observer and for the combined for all observers.

As SPECT image data was included in this phase of the study, a comparison was also made of the reported anterior/posterior location of each lesion, and the results are given in Table 6.47. There are significant variations in the results for the different observers with observer 1 having the same proportion (81%) given at the same location as observer 2 has given at a different location. The overall combined results for all the observers show little difference between the two categories.

Observer	No. Same (%)	No. Different (%)	Total
1	13 (81%)	3 (19%)	16
2	3 (19%)	13 (81%)	16
3	11 (69%)	5 (31%)	16
4	6 (33%)	12 (67%)	18
5	15 (68%)	7 (32%)	22
Overall	48 (54%)	40 (46%)	88

Table 6.47 - Results of comparison in anterior/posterior location between lesions resected at surgery and those seen on Sestamibi only images
Number and percentage of lesions seen in the same and different anterior/posterior location for each observer and combined for all observers.

The final analysis on the location data was to combine the left/right, upper/lower and anterior/posterior comparison information to give an overall location comparison in 3 dimensions for each reported lesion. The results are shown in Table 6.48.

Observer	No. Same (%)	No. Different (%)	Total
1	6 (35%)	11 (65%)	17
2	2 (12%)	15 (88%)	17
3	7 (41%)	10 (59%)	17
4	4 (21%)	15 (79%)	19
5	6 (25%)	18 (75%)	24
Overall	25 (27%)	69 (73%)	94

Table 6.48 - Results of combined left/right, upper/lower and anterior/posterior location comparisons between lesions resected at surgery and those seen on Sestamibi only images
Number and percentage of lesions seen in the same and different overall location for each observer and for the combined for all observers.

It is clear from these results that, in general, there are a much larger number of cases in which the location given from Sestamibi images is different from that given in the surgical report. This suggests that there is either insufficient information available to the observers without the ^{123}I -iodide and subtraction images or that there is poor differentiation of true lesions on the Sestamibi images.

The given positive/negative findings and left/right locations for each lesion were then used to calculate the sensitivity and specificity of lesion detection for each of the observers and for the overall combined results. The results are shown in Table 6.49. The sensitivity and specificity of the ultrasound imaging results is also shown to provide a comparison between the two imaging methods.

Observer	Sensitivity (%)	Specificity (%)
1	25	100
2	25	100
3	44	100
4	57	20
5	72	0
Overall	45	29
US	72	33

Table 6.49- Calculated sensitivity and specificity values for comparison of surgical and Sestamibi only imaging
Percentage sensitivity and specificity values are given for each observer and for the combined results of all observers as well as for US imaging to provide a comparison

Both the sensitivity and specificity are very variable between the different observers with a higher sensitivity tending to be accompanied by a low specificity and vice versa. For example, observer 5 has a comparable sensitivity to ultrasound imaging of 72% but a specificity of 0%. In contrast, observers 1 & 2 have poor sensitivity at just 25% but have 100% specificity. These results indicate that observers 1 & 2 were less likely to designate a possible lesion seen on the ^{99m}Tc -Sestamibi-only images as positive and, in so doing, gave no false positive reviews but also missed true positive lesions. Observer 5, however, tended to give a positive result to all lesions seen, meaning that the sensitivity was high but the specificity was low because of many false positive reports.

The tradeoff between sensitivity and specificity can be characterised by a receiver operating characteristic (ROC) curve. This is a plot of sensitivity against 1-specificity and demonstrates how the sensitivity and specificity vary relative to one another as the decision threshold varies. For example, an operator using a conservative measure of a positive lesion would achieve good specificity due to few false positive results but this would result in poorer sensitivity due to true positive lesions being classified as false negative. In contrast, an operator using a liberal measure of a positive lesion would have good sensitivity but poorer specificity. Thus, from the results in Table 6.49, it can be seen that observers 1-3 were using a conservative threshold, whilst observers 4 & 5 were using a more liberal measure of a positive lesion.

The sensitivity and specificity results for phase 3 of the observer study were much more variable than those for phases 1 & 2, which are given in Table 6.11 and Table 6.29, respectively. The observers openly stated that they were not comfortable reviewing the ^{99m}Tc -Sestamibi images in the absence of the ^{123}I -iodide images, which provided an indication of the position and shape of the thyroid gland as well as subtraction images, and so this is not a surprising finding.

6.2.3.2 Ultrasound Results Comparison

The difference between the number of lesions seen by each observer on phase 3 of the observer study and that reported from ultrasound scanning was calculated for each of the 25 patients. The results were then categorised in the same

manner as previously and the results are shown in Table 6.50. The Wilcoxon Signed Ranks test was also applied to these data and the results of this analysis are shown in Table 6.51.

The results show a more even spread between the categories than was seen when the surgical results were compared to those from phase 3 of the observer study. The largest category is once again that in which the number of lesions seen by the observers is the same as that seen on ultrasound scanning but the other two categories both have a significant number of entries. There were, however, more occasions in which the observer saw more lesions on the Sestamibi only images than were reported from ultrasound than when the opposite was the case. In particular, observer 5 had more observations in this category than in either of the others.

Observer	US > M	US < M	US = M	Total
1	5	9	11	25
2	8	3	14	25
3	5	8	12	25
4	4	7	14	25
5	2	14	9	25
Total	24	41	60	125

Table 6.50 - Comparison of number of lesions seen on ultrasound and in phase 3 (Sestamibi only)

US>M = number of times more lesions were seen on ultrasound than on Sestamibi images, US<M = number of times fewer lesions were seen on ultrasound than on Sestamibi images, US=M = number of times same number of lesions were seen on ultrasound as on Sestamibi images.

Observer	p-value	Estimated Median	95% CI
1	0.363	0.0	(-0.5, 0.0)
2	0.197	0.0	(0.0, 0.5)
3	0.485	0.0	(-0.5, 0.0)
4	0.351	0.0	(-0.5, 0.0)
5	0.004	-0.5	(-1.0, -0.5)
Overall	0.021	0.0	(-0.5, 0.0)

Table 6.51 - Results from Wilcoxon Signed Ranks test on differences in number of lesions seen (ultrasound vs phase 3)

Output from Minitab software applied to the differences in the number of lesions seen on ultrasound and those seen on Sestamibi only imaging.

The results of the Wilcoxon Signed Ranks test support those given in Table 6.50 in that only the results from observer 5 show a statistically significant difference with $p < 0.05$. As expected, the estimated median and 95% CI for this observer are both < 0 , indicating that more lesions were seen on the Sestamibi images

than were highlighted in the ultrasound report. The result from the statistical test applied to the data from all 5 observers combined is also statistically significant with $p < 0.05$, which is most likely due to the increased power of the test when a larger sample size is used.

Table 6.52 gives the results of the comparison between the positive/negative reports from ultrasound and Sestamibi imaging. It can be seen that only observer 1 has <50% in the “same” category at 36%, whilst all the others have >50% in this category with the highest being 64% for observer 3.

Observer	No. Same +/- (%)	No. Different +/- (%)	Total
1	9 (36%)	16 (64%)	25
2	14 (56%)	11 (44%)	25
3	16 (64%)	9 (36%)	25
4	14 (54%)	12 (46%)	26
5	19 (54%)	16 (46%)	35
Overall	72 (53%)	64 (47%)	136

Table 6.52 - Results from comparison of positive/negative findings (ultrasound vs phase 3) Number of comparisons between the overall given positive/negative report for a lesion that were the same and different between those seen on ultrasound imaging and those seen on the Sestamibi only images. Percentages of the total in each category for each observer and overall are given in brackets.

Once again, the Wilcoxon Signed Ranks test was applied to these data and the results are shown in Table 6.53. In this case, there were no statistically significant results with $p > 0.05$ in all cases. The 95% CI for observer 1 is ≤ 0 , which is as expected, given the findings in Table 6.52.

Observer	p-value	Estimated Median	95% CI
1	0.226	0.0	(-1.0, 0.0)
2	0.609	0.0	(0.0, 1.0)
3	0.226	0.0	(0.0, 1.0)
4	0.741	0.0	(0.0, 1.0)
5	0.664	0.0	(0.0, 0.0)
Overall	0.552	0.0	(0.0, 0.0)

Table 6.53 - Results from Wilcoxon Signed Ranks Test on positive/negative comparison (ultrasound vs phase 3) Output from statistical test applied to comparison between the positive/negative report findings from ultrasound imaging and those given from review of the Sestamibi only images.

The same comparisons were then made of the reported locations of each lesion from the ultrasound images and by the observers from the Sestamibi images. The results of the left/right comparison are shown in Table 6.54 and it can be

Observer	No. Same (%)	No. Different (%)	Total
1	7 (50%)	7 (50%)	14
2	4 (29%)	10 (71%)	14
3	8 (57%)	6 (43%)	14
4	8 (57%)	6 (43%)	14
5	13 (68%)	6 (32%)	19
Overall	40 (53%)	35 (47%)	75

Table 6.54 - Results of comparison in left/right location between lesions seen on ultrasound and those seen on Sestamibi only images
Number and percentage of lesions seen in the same and different left/right location for each observer and combined for all observers.

seen that once again observer 2 has the lowest proportion in the “same” category at 29%, whilst all the others have $\geq 50\%$ in this category.

The same analysis was applied to the give upper/lower location of each observed lesion and the results are shown in Table 6.55. As was the case when the surgical results were compared to those from phase 3 of the observer study, only observer 3 gave a higher proportion of lesions in the same upper/lower location than in a different position.

Observer	No. Same (%)	No. Different (%)	Total
1	5 (39%)	8 (61%)	13
2	4 (31%)	9 (69%)	13
3	7 (54%)	6 (46%)	13
4	4 (31%)	9 (69%)	13
5	8 (44%)	10 (56%)	18
Overall	28 (40%)	42 (60%)	70

Table 6.55 - Results of comparison in upper/lower location between lesions seen on ultrasound and those seen on Sestamibi only images
Number and percentage of lesions seen in the same and different upper/lower location for each observer and combined for all observers.

The results of the combined analysis of the left/right and upper/lower locations are shown in Table 6.56. As expected from the results in Table 6.54 and Table 6.55, only observer 3 gave more lesions as being in the same combined location as being at a different site. The lowest proportion of lesions reported at the same site from the Sestamibi images as were seen on ultrasound scanning was from observer 2 at just 29%.

Observer	No. Same (%)	No. Different (%)	Total
1	5 (36%)	9 (64%)	14
2	4 (29%)	10 (71%)	14
3	8 (57%)	6 (43%)	14
4	5 (36%)	9 (64%)	14
5	9 (47%)	10 (53%)	19
Overall	31 (41%)	44 (59%)	75

Table 6.56 - Results of combined left/right and upper/lower location comparisons between lesions seen on ultrasound and those seen on Sestamibi only images
Number and percentage of lesions seen in the same and different overall location for each observer and for the combined for all observers.

A similar comparison was then carried out on the reported anterior/posterior location of each lesion and on an overall combined left/right, upper/lower and anterior/posterior location. The results are shown in Table 6.57 and Table 6.58 respectively.

Observer	No. Same (%)	No. Different (%)	Total
1	9 (64%)	5 (36%)	14
2	4 (29%)	10 (71%)	14
3	9 (64%)	5 (36%)	14
4	3 (21%)	11 (79%)	14
5	10 (53%)	9 (47%)	19
Overall	35 (47%)	40 (53%)	75

Table 6.57 - Results of comparison in anterior/posterior location between lesions seen on ultrasound and those seen on Sestamibi only images
Number and percentage of lesions seen in the same and different anterior/posterior location for each observer and combined for all observers.

The results of the comparison of the anterior/posterior position are similar to those of the left/right comparison (Table 6.54) with the exception of observer 4 seeing a very low proportion (21%) at the same location as was reported from ultrasound imaging.

Observer	No. Same (%)	No. Different (%)	Total
1	5 (36%)	9 (64%)	14
2	2 (14%)	12 (86%)	14
3	8 (57%)	6 (43%)	14
4	1 (7%)	13 (93%)	14
5	6 (32%)	13 (68%)	19
Overall	22 (29%)	53 (71%)	75

Table 6.58 - Results of combined left/right, upper/lower and anterior/posterior location comparisons between lesions seen on ultrasound and those seen on Sestamibi only images
Number and percentage of lesions seen in the same and different overall location for each observer and for the combined for all observers.

Finally, the comparisons of the overall given location for the lesions shows that again, observer 3 is the only individual with >50% in the “same” category. Observer 4 saw only a single lesion (7%) at the same overall location as was reported from the ultrasound imaging, which is the lowest proportion seen on any of the location comparisons in this report.

The sensitivity and specificity for each observer taking the ultrasound result as the comparison standard and considering only the given positive/negative and left/right findings are shown in Table 6.59.

As was the case when the phase 3 findings were compared to the surgical results (see Table 6.49), there is considerable variation in the sensitivity and specificity for the different observers. However, the sensitivity is generally low, indicating that there were a number of lesions seen on ultrasound imaging that were not noted by the observers on the ^{99m}Tc -Sestamibi planar + SPECT images. The specificity values are better, but are still very variable with observer 3 demonstrating high specificity at 82% whilst observer 5 was poor with a value of just 44%. The variable results once again demonstrate that the observers were not confident in reviewing the ^{99m}Tc -Sestamibi images in the absence of the ^{123}I -iodide images.

Observer	Sensitivity (%)	Specificity (%)
1	8	55
2	17	75
3	46	82
4	46	64
5	53	44
Overall	35	62

Table 6.59- Calculated sensitivity and specificity values for comparison of US and Sestamibi only imaging results
Percentage sensitivity and specificity values are given for each observer and for the combined results of all observers

6.2.4 Phase 4 versus Surgical and US Findings Comparison

6.2.4.1 Surgical Results Comparison

The final comparison involving the findings from parathyroidectomy surgery on the study participants was carried out with the results of phase 4 (all images) of the observer study. As before, the difference between the number of lesions

sampled at surgery and the number seen by each individual observer when reviewing all the available images together was calculated. The results of the analysis are shown in Table 6.60.

It is clear from the data that the largest category for each individual observer and also overall is that in which the same number of samples were taken at surgery as lesions were seen on the nuclear medicine images. These account for 67% of the total, indicating that there is good agreement between the number of lesions suggested on nuclear medicine planar + SPECT subtraction imaging and the number of suspicious samples noted by the surgeon.

Observer	Sur > A	Sur < A	Sur = A	Total
1	4	2	11	17
2	4	0	13	17
3	5	1	11	17
4	3	3	11	17
5	1	5	11	17
Total	17	11	57	85

Table 6.60 - Comparison of number of samples resected at surgery and number of lesions seen in phase 4 (all images)

Sur>A = number of times more lesions were resected than were seen on review of all available images, Sur<A = number of times fewer lesions were resected than were seen on review of all available images, Sur=A = number of times same number of lesions were resected as were seen on review of all available images.

Table 6.61 gives the results of the Wilcoxon Signed Ranks test that was applied to the difference data. It is immediately apparent that there are no instances in which $p < 0.05$, meaning that no statistically significant differences exist between the number of lesions resected and the number seen by the observers. This supports the conclusions drawn from the data in Table 6.60.

Observer	p-value	Estimated Median	95% CI
1	0.402	0.0	(0.0, 0.5)
2	0.100	0.0	(0.0, 1.0)
3	0.142	0.0	(0.0, 0.5)
4	1.000	0.0	(-0.5, 0.5)
5	0.173	0.0	(-0.5, 0.0)
Overall	0.139	0.0	(0.0, 0.0)

Table 6.61 - Results from Wilcoxon Signed Ranks test on differences in number of lesions seen (surgery vs phase 4)

Output from Minitab software applied to the differences in the number of lesions resected at surgery and the number seen on review of all images.

The positive/negative report information given for each lesion from histology after surgery and that given by the observers from the subtraction imaging were then compared, and the results are shown in Table 6.62. All the observers gave a significant majority of reports that were the same as those from surgery, with observer 4 having the highest proportion in this category at 74%. Once again, the tendency for observer 5 to report more lesions is demonstrated by the higher number of overall comparisons for this observer compared to the others.

Observer	No. Same +/- (%)	No. Different +/- (%)	Total
1	14 (64%)	8 (36%)	22
2	12 (60%)	8 (40%)	20
3	14 (67%)	7 (33%)	21
4	17 (74%)	6 (26%)	23
5	18 (62%)	11 (38%)	29
Overall	75 (65%)	40 (35%)	115

Table 6.62 - Results from comparison of positive/negative findings (surgery vs phase 4)
Number of comparisons between the overall given positive/negative report for a lesion that were the same and different between the surgically resected lesions and those seen when all images were reviewed together. Percentages of the total in each category for each observer and overall are given in brackets.

These data were then subjected to the non-parametric Wilcoxon Signed Ranks statistical test. The results are shown in Table 6.63 and it can be seen that statistically significant differences exist only for observer 4 - who had the highest proportion in the “same” category - and the overall combined data for all 5 observers. The 95% CI for each observer are, however, ≥ 0 , indicating that there is a general tendency for the observers to give the same rather than a different positive/negative report when compared to the surgical findings. Once again, this is as expected, given the findings shown in Table 6.62.

Observer	p-value	Estimated Median	95% CI
1	0.270	0.0	(0.0, 1.0)
2	0.444	0.0	(0.0, 1.0)
3	0.187	0.0	(0.0, 1.0)
4	0.046	1.0	(0.0, 1.0)
5	0.261	0.0	(0.0, 1.0)
Overall	0.005	0.0	(0.0, 1.0)

Table 6.63 - Results from Wilcoxon Signed Ranks Test on positive/negative comparison (surgery vs phase 4)
Output from statistical test applied to comparison between the positive/negative report findings for surgical results and those given from review of all images.

A similar analysis to that carried out previously (see Sections 6.2.1.1, 6.2.2.1 & 6.2.3.1) was then performed on the given information relating to the location of each lesion. The results of the left/right comparison are shown in Table 6.64.

For each observer, the majority of lesions were given to be at the same left/right location as those that were sampled at surgery. The lowest proportion at the same site was reported by observer 5 with 65%.

Observer	No. Same (%)	No. Different (%)	Total
1	14 (78%)	4 (22%)	18
2	12 (71%)	5 (29%)	17
3	13 (77%)	4 (23%)	17
4	13 (68%)	6 (32%)	19
5	15 (65%)	8 (35%)	23
Overall	67 (71%)	27 (29%)	94

Table 6.64 - Results of comparison in left/right location between lesions resected at surgery and those seen on review of all images
Number and percentage of lesions seen in the same and different left/right location for each observer and combined for all observers.

The same analysis was then carried out on the upper/lower position information and the results are shown in Table 6.65. The results are more variable than those from the left/right comparison with observer 2 giving only 47% of reported lesions given at the same upper/lower site, whilst observers 1 & 5 saw 61% at the same position.

Observer	No. Same (%)	No. Different (%)	Total
1	11 (61%)	7 (39%)	18
2	8 (47%)	9 (53%)	17
3	9 (53%)	8 (47%)	17
4	11 (58%)	8 (42%)	19
5	14 (61%)	9 (39%)	23
Overall	53 (56%)	41 (44%)	94

Table 6.65 - Results of comparison in upper/lower location between lesions resected at surgery and those seen on review of all images
Number and percentage of lesions seen in the same and different upper/lower location for each observer and combined for all observers.

The left/right and upper/lower comparisons were then combined and the results are shown in Table 6.66. Again, there is considerable variation between the observers with observer 1 seeing as many as 56% of lesions at the same overall site but observer 4 giving only 37% at the same location. It is interesting to note that observer 4 had proportions in the “same” category of >50% for each of the

left/right and upper/lower comparisons independently but a much lower fraction for the combined analysis. This suggests that this observer tends to give one or other of these positions as the same as the surgical findings, but not both for an individual patient.

Observer	No. Same (%)	No. Different (%)	Total
1	10 (56%)	8 (44%)	18
2	8 (47%)	9 (53%)	17
3	9 (53%)	8 (47%)	17
4	7 (37%)	12 (63%)	19
5	11 (48%)	12 (52%)	23
Overall	45 (48%)	49 (52%)	94

Table 6.66 - Results of combined left/right and upper/lower location comparisons between lesions resected at surgery and those seen on review of all images
Number and percentage of lesions seen in the same and different overall location for each observer and for the combined for all observers.

As SPECT data was presented to the observers during phase 4 of the observer study, an analysis of the anterior/posterior position of each lesion was possible. The results of the comparison between the surgical position and that reported by the observers are shown in Table 6.67.

Observer	No. Same (%)	No. Different (%)	Total
1	12 (71%)	5 (29%)	17
2	8 (50%)	8 (50%)	16
3	12 (75%)	4 (25%)	16
4	14 (78%)	4 (22%)	18
5	19 (86%)	3 (14%)	22
Overall	65 (73%)	24 (27%)	89

Table 6.67 - Results of comparison in anterior/posterior location between lesions resected at surgery and those seen on review of all images
Number and percentage of lesions seen in the same and different anterior/posterior location for each observer and combined for all observers.

The results show that each of the observers gave $\geq 50\%$ of lesions at the same anterior/posterior position as was recorded in the surgical notes for each resected sample. The highest proportion in the “same” category was for observer 5 with 86%, whilst the lowest was for observer 2 with 50%.

An overall comparison of given location was then carried out by combining all the information from the individual left/right, upper/lower and anterior/posterior comparisons. The results of this analysis are shown in Table 6.68.

Observer	No. Same (%)	No. Different (%)	Total
1	9 (50%)	9 (50%)	18
2	5 (29%)	12 (71%)	17
3	8 (47%)	9 (53%)	17
4	5 (26%)	14 (74%)	19
5	10 (44%)	13 (56%)	23
Overall	37 (39%)	57 (61%)	94

Table 6.68 - Results of combined left/right, upper/lower and anterior/posterior location comparisons between lesions resected at surgery and those seen on review of all images
Number and percentage of lesions seen in the same and different overall location for each observer and for the combined for all observers.

Only observer 1 gave as many as 50% of lesions at the same overall location as the surgical report, whilst observer 4 saw only 26% at the same site. Although the results from all the individual comparisons were positive, the combined results are somewhat poorer, again suggesting that the observers are often giving one position parameter as the same as the surgical report but the other 2 parameters are rarely also the same for an individual patient.

Table 6.69 shows the sensitivity and specificity values for each observer and for the combined results from all 5 observers. The sensitivity and specificity of the ultrasound imaging results is also given for comparison.

Observer	Sensitivity (%)	Specificity (%)
1	67	50
2	60	33
3	67	25
4	80	29
5	69	13
Overall	64	27
US	72	33

Table 6.69 - Calculated sensitivity and specificity values for comparison of surgical and all dual-isotope subtraction imaging
Percentage sensitivity and specificity values are given for each observer and for the combined results of all observers as well as for US imaging to provide a comparison

When compared with the sensitivity and specificity values for the other phases of the observer study (see Table 6.11, Table 6.29 & Table 6.49), it can be seen that the sensitivity values are generally less variable between the observers and are comparable to the result for ultrasound imaging. The specificity values are, however, more variable with a range of 13% (observer 5) to 50% (observer 1). The sensitivity is generally slightly poorer than for phase 2 (SPECT only) but the specificity is improved for 3 of the 5 observers (see Table 6.29). Once again,

observer 5 shows good sensitivity but the poorest specificity, highlighting this observer's tendency to see more lesions than the others.

6.2.4.2 Ultrasound Results Comparison

The findings from the ultrasound scans and the observers' reading of the phase 4 images were then compared. The results of the difference in the number of lesions seen are shown in Table 6.70, with all 25 patients who had ultrasound scanning taken into account. The Wilcoxon Signed Ranks test was also applied to these data and the results are shown in Table 6.71.

Observer	US > A	US < A	US = A	Total
1	0	8	17	25
2	2	3	20	25
3	1	7	17	25
4	0	10	15	25
5	0	13	12	25
Total	3	41	81	125

Table 6.70 - Comparison of number of lesions seen on ultrasound and in phase 4 (all images)

US>A = number of times more lesions were seen on ultrasound than on review of all available SPECT and planar images, US<A = number of times fewer lesions were seen on ultrasound than on review of all images, US=A = number of times same number of lesions were seen on ultrasound as on review of all images.

It can immediately be seen that there are almost no occasions in which the observer saw fewer lesions on review of all the planar and SPECT images together than were reported from the ultrasound scan. The largest category is that in which the same number of lesions were seen on each type of imaging, which is the case both overall and for 4 of the 5 observers. Only observer 5 had more instances where more lesions were seen on the nuclear medicine images than the ultrasound. This is in keeping with the findings throughout this study, whereby observer 5 tended to see more lesions than any of the other observers.

The Wilcoxon Signed Ranks test demonstrates that statistically significant differences exist for 3 of the 5 observers (observers 1, 4 & 5) individually as well as for the combined data for all observers. In each case, the estimated median and 95% CI returned by the statistical software are ≤ 0 , meaning that there was a tendency for the observers to see more lesions in the phase 4 images than were reported from ultrasound.

Observer	p-value	Estimated Median	95% CI
1	0.014	-0.5	(-0.5, 0.0)
2	0.787	0.0	(0.0, 0.0)
3	0.059	0.0	(-0.5, 0.0)
4	0.006	-0.5	(-1.0, 0.0)
5	0.002	-0.5	(-1.0, -0.5)
Overall	<0.001	-0.5	(-0.5, 0.0)

Table 6.71 - Results from Wilcoxon Signed Ranks test on differences in number of lesions seen (ultrasound vs phase 4)

Output from Minitab software applied to the differences in the number of lesions seen on ultrasound and those seen on review of all images.

The final results in terms of the positive/negative report given for each lesion seen on ultrasound and planar + SPECT imaging were then compared. The results are given in Table 6.72. There is a clear distinction between the number of times a different report was given to the number of times the same result occurred, with the “same” category being significantly larger. The highest proportion in this category was for observer 1 with 79%, whilst the lowest was for observers 2 & 5 with 72%. The proportions given the same report here are slightly higher than those for the comparison of the lesions resected at surgery and those seen on the planar + SPECT images.

Observer	No. Same +/- (%)	No. Different +/- (%)	Total
1	22 (79%)	6 (21%)	28
2	18 (72%)	7 (28%)	25
3	20 (77%)	6 (23%)	26
4	24 (77%)	7 (23%)	31
5	26 (72%)	10 (28%)	36
Overall	110 (75%)	36 (25%)	146

Table 6.72 - Results from comparison of positive/negative findings (ultrasound vs phase 4)
Number of comparisons between the overall given positive/negative report for a lesion that were the same and different between those seen on ultrasound imaging and those seen on review of all images. Percentages of the total in each category for each observer and overall are given in brackets.

Once again, the Wilcoxon Signed Ranks test was applied to the data and the results are shown in Table 6.73. In this case, only the result for observer 2 has $p > 0.05$, meaning that all the others are statistically significant. All the estimated median and 95% CI values are ≥ 0 , meaning that more lesions are given the same positive/negative report than are given a different report. These results support the conclusions drawn from the data in Table 6.72.

Observer	p-value	Estimated Median	95% CI
1	0.009	1.0	(0.0, 1.0)
2	0.056	1.0	(0.0, 1.0)
3	0.017	1.0	(0.0, 1.0)
4	0.008	1.0	(0.0, 1.0)
5	0.020	1.0	(0.0, 1.0)
Overall	<0.001	1.0	(0.0, 1.0)

Table 6.73 - Results from Wilcoxon Signed Ranks Test on positive/negative comparison (ultrasound vs phase 4)

Output from statistical test applied to comparison between the positive/negative report findings from ultrasound imaging and those given from review of all images.

The reported left/right position of each lesion from ultrasound and planar + SPECT images was then compared and the results are shown in Table 6.74. More lesions were seen at the same position than at a different site by all the observers with observer 5 having the lowest proportion at 65%.

Observer	No. Same (%)	No. Different (%)	Total
1	11 (73%)	4 (27%)	15
2	10 (71%)	4 (29%)	14
3	11 (79%)	3 (21%)	14
4	11 (73%)	4 (27%)	15
5	11 (65%)	6 (35%)	17
Overall	54 (72%)	21 (28%)	75

Table 6.74 - Results of comparison in left/right location between lesions seen on ultrasound and those seen on review of all images

Number and percentage of lesions seen in the same and different left/right location for each observer and combined for all observers.

The given upper/lower locations were then compared in the same way and the results are shown in Table 6.75. Once again, more lesions were seen at the same position as that reported from ultrasound by all the observers, with the lowest proportion in this category being 61% for observer 3.

Observer	No. Same (%)	No. Different (%)	Total
1	10 (71%)	4 (29%)	14
2	10 (77%)	3 (23%)	13
3	8 (61%)	5 (39%)	13
4	11 (77%)	3 (23%)	14
5	10 (62%)	6 (38%)	16
Overall	49 (70%)	21 (30%)	70

Table 6.75 - Results of comparison in upper/lower location between lesions seen on ultrasound and those seen on review of all images

Number and percentage of lesions seen in the same and different upper/lower location for each observer and combined for all observers.

Table 6.76 shows the results of the combined left/right and upper/lower comparisons. It is immediately clear that, on this occasion, all the observers saw >50% of lesions at the same overall site, which is considerably higher for some of the observers than the comparison with the surgical results presented in Table 6.66.

Observer	No. Same (%)	No. Different (%)	Total
1	10 (67%)	5 (33%)	15
2	9 (64%)	5 (36%)	14
3	9 (64%)	5 (36%)	14
4	10 (67%)	5 (33%)	15
5	10 (59%)	7 (41%)	17
Overall	48 (64%)	27 (36%)	75

Table 6.76 - Results of combined left/right and upper/lower location comparisons between lesions seen on ultrasound and those seen on review of all images
Number and percentage of lesions seen in the same and different overall location for each observer and for the combined for all observers.

As all the acquired SPECT data was included in phase 4 of the observer study, a comparison was also made of the given anterior/posterior location for each lesion on ultrasound and SPECT. The results of this analysis are shown in Table 6.77.

Observer	No. Same (%)	No. Different (%)	Total
1	13 (87%)	2 (13%)	15
2	11 (79%)	3 (21%)	14
3	12 (86%)	2 (14%)	14
4	12 (80%)	3 (20%)	15
5	15 (88%)	2 (12%)	17
Overall	63 (84%)	12 (16%)	75

Table 6.77 - Results of comparison in anterior/posterior location between lesions seen on ultrasound and those seen on review of all images
Number and percentage of lesions seen in the same and different anterior/posterior location for each observer and combined for all observers.

As was the case for the left/right and upper/lower comparisons, a significantly higher proportion of lesions were seen at the same anterior/posterior location than were seen at a different position.

These data were then combined with the left/right and upper/lower comparison results to give a comparison of the overall 3-dimensional location of each lesion and the results are given in Table 6.78. For the first time in this analysis, >50% of the comparisons of the overall location of each lesion fell into the “same”

Observer	No. Same (%)	No. Different (%)	Total
1	10 (67%)	5 (33%)	15
2	8 (57%)	6 (43%)	14
3	9 (64%)	5 (36%)	14
4	9 (60%)	6 (40%)	15
5	10 (59%)	7 (41%)	17
Overall	46 (61%)	29 (39%)	75

Table 6.78 - Results of combined left/right, upper/lower and anterior/posterior location comparisons between lesions seen on ultrasound and those seen on review of all images
Number and percentage of lesions seen in the same and different overall location for each observer and for the combined for all observers.

category for each of the 5 observers. This indicates that similar information is being gained from the anatomical ultrasound imaging and the functional nuclear medicine imaging when both subtraction planar and subtraction SPECT are considered by the reporting observer.

The calculated sensitivity and specificity values for the observer findings compared to the ultrasound report as the comparison standard are shown in Table 6.79.

Observer	Sensitivity (%)	Specificity (%)
1	75	75
2	62	75
3	69	83
4	100	45
5	83	57
Overall	73	64

Table 6.79- Calculated sensitivity and specificity values for comparison of US and all dual-isotope subtraction imaging
Percentage sensitivity and specificity values are given for each observer and for the combined results of all observers

The sensitivity is high for all observers, with observer 4 demonstrating a sensitivity of 100%. However, the specificity is more variable with high sensitivity coupled to lower specificity again demonstrated. As has been the case throughout this study, the sensitivity and specificity values for the comparison with ultrasound imaging are better than those for the comparison with the surgical findings (see Table 6.69). However, this is not a surprising result, as the report from nuclear medicine imaging is almost always available before ultrasound imaging is undertaken, meaning that the anatomical ultrasound imaging is often heavily influenced by the functional nuclear medicine imaging.

6.2.5 Summary of Observer Study and Surgical Comparison Results

In a similar way to Sections 5.4.6 & 5.5.7, graphical plots were created to summarise the findings of the comparison between the results of the observer study and the report from surgery. In each case, differences in the number of lesions seen are quoted as the result from surgery minus the result from the observer study.

A plot of the differences in the number of lesions seen between surgery and each phase of the observer study is shown in Figure 6.1. In each case “more” indicates that more lesions were resected at surgery than were seen by the observers and “less” means that fewer lesions were removed than were reported from the images.

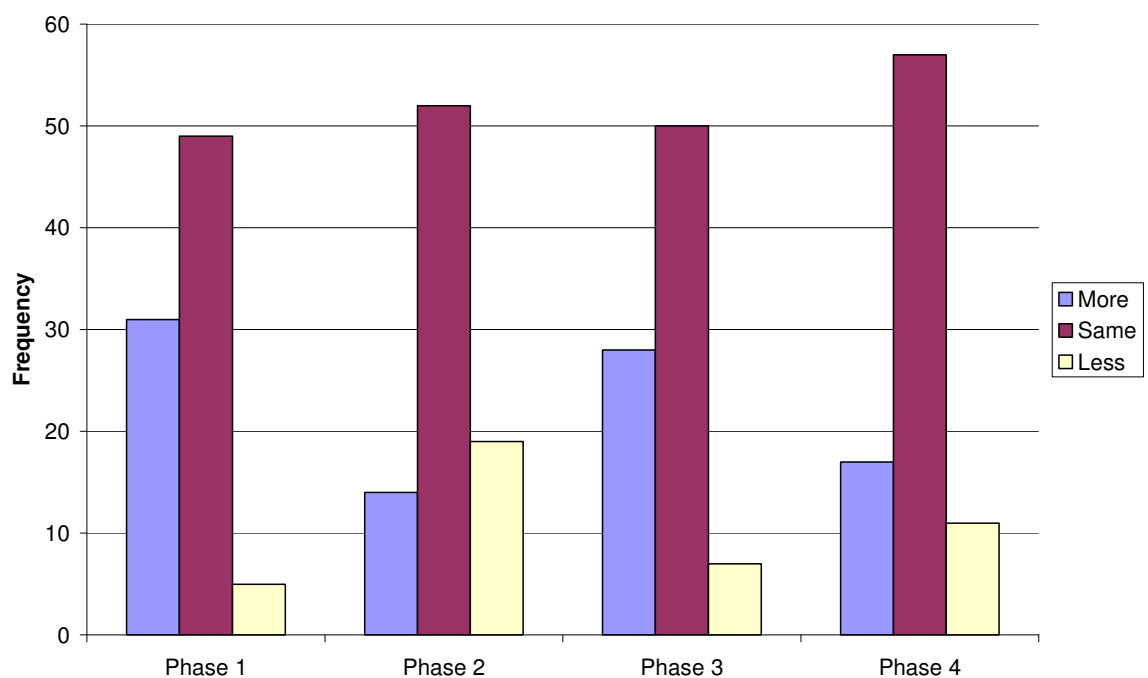


Figure 6.1 - Bar chart of differences in number of lesions
Frequency of “more”, “same” and “less” findings for comparison of number of lesions removed at surgery versus the number reported on each phase of the observer study.
Phase 1 = planar images only, Phase 2 = SPECT images only, Phase 3 = Sestamibi images only (planar & SPECT), Phase 4 = all images.

It is immediately clear that the largest category in each case is “same”, meaning that the surgeon removed the same number of suspicious lesions as had been seen by the observers on the nuclear medicine images. The highest overall

number in this category occurred for phase 4 with the lowest for phase 1. In addition, the results from phase 2 show a larger number in the “less” category than in “more”. This indicates that there are more instances where fewer lesions were resected by the surgeon than had been seen by the observers on the SPECT images than instances where a greater number of lesions were resected than had been seen. The opposite is true for all of the other phases. This suggests that there was a degree of over-reporting by the observers when reviewing the SPECT only images, which was less prevalent on the other phases.

The number of times that the same positive/negative result for adenoma was found after surgery as was given by the observers from the images in each phase of the study is shown in graphical form in Figure 6.2.

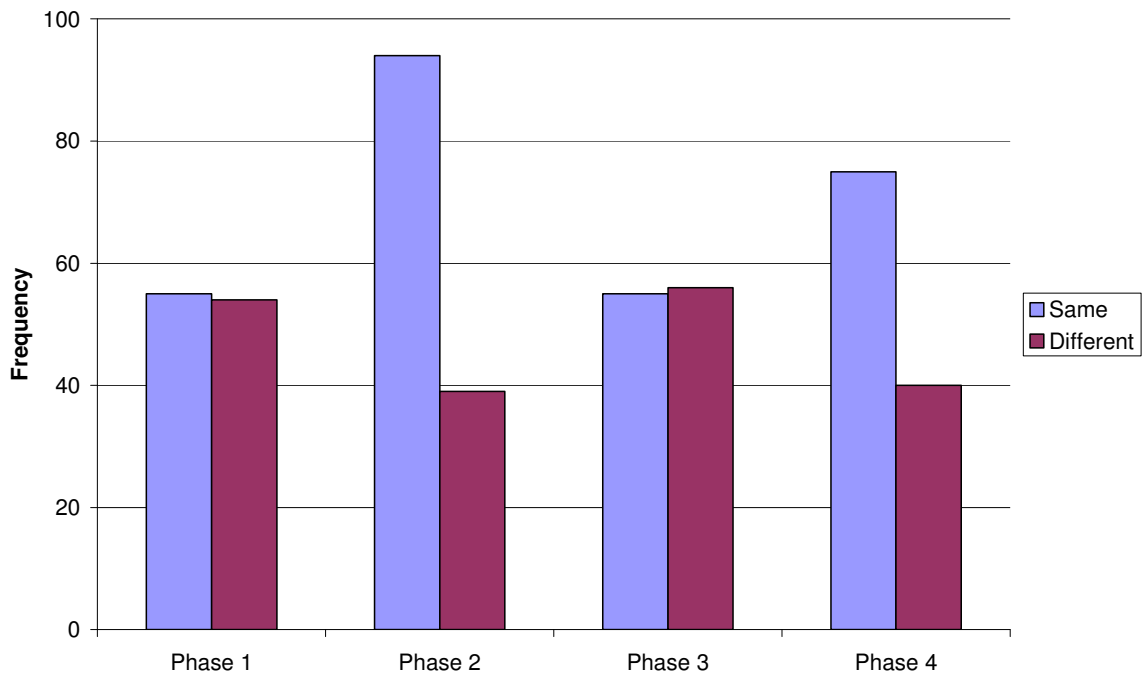


Figure 6.2 - Bar chart of comparisons in positive/negative findings
 Frequency of “same” and “different” findings for comparison of the positive/negative findings for each lesion resected at surgery compared to those seen on each phase of the observer study. Phase 1 = planar images only, Phase 2 = SPECT images only, Phase 3 = Sestamibi images only (planar & SPECT), Phase 4 = all images.

The chart clearly shows that the number of “same” and “different” findings for phases 1 & 3 are similar, whereas there are considerably more in the “same” category for phases 2 & 4. The results for phase 2 demonstrate both the highest number in the “same” category and the lowest number in the “different” category. Given that there were only two negative results reported from

surgery, the results in the graph show that more true positive lesions were identified by the observers when the dual-isotope subtraction SPECT images were available for review than when they were not.

A graphical comparison of the given left/right locations of the lesions resected at surgery and those seen on each phase of the observer study is shown in Figure 6.3. The given location of each lesion seen on the observer studies was defined as “same” or “different” with respect to the position of removed samples recorded in the surgical report.

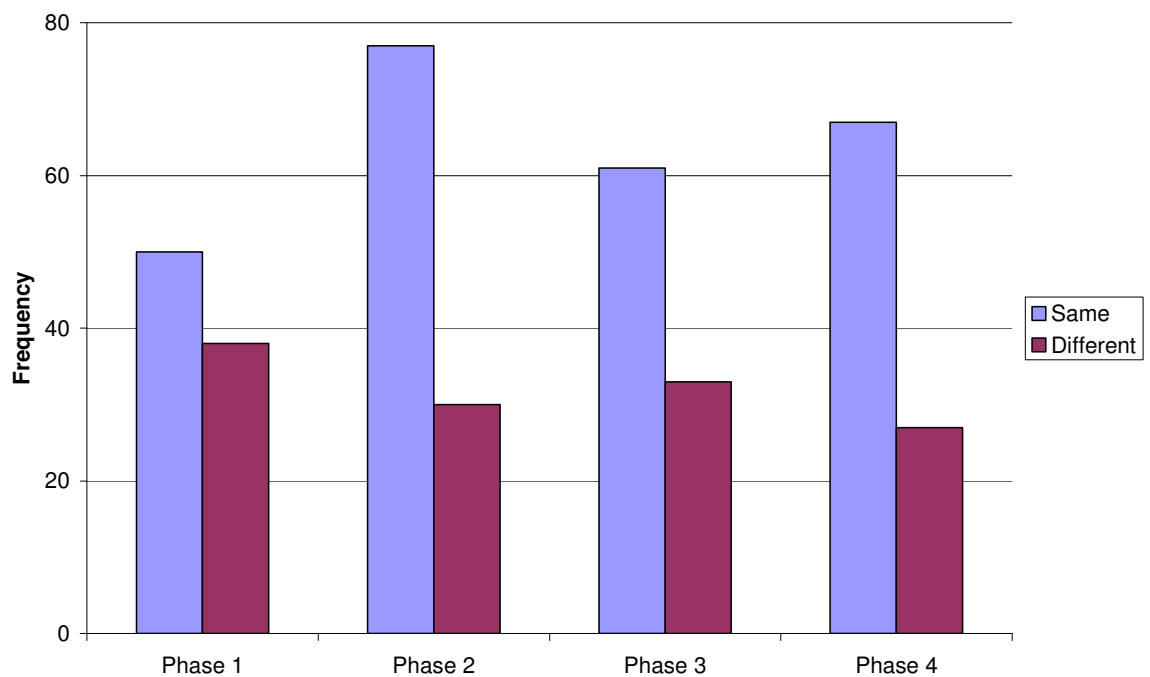


Figure 6.3 - Bar chart of comparisons in left/right locations
Frequency of “same” and “different” findings for comparison of the given left/right location for each lesion resected at surgery compared to those seen on each phase of the observer study. Phase 1 = planar images only, Phase 2 = SPECT images only, Phase 3 = Sestamibi images only (planar & SPECT), Phase 4 = all images.

The chart shows that on each phase of the study, the observers were seeing more lesions at the same left/right position than on the contra-lateral side when the results were compared to the surgical findings. The highest number of “same” comparisons was for phase 2 of the observer study, whilst the lowest number was for phase 1. The number of lesions given on the “different” side was roughly the same for phases 2, 3 & 4, with phase 4 having slightly the lowest value.

The overall location of each lesion seen on the observer study, taking into account the given left/right, upper/lower and anterior/posterior positions, was also compared to the surgical report. The results are plotted in Figure 6.4. Once again, it should be noted that no anterior/posterior information was included in the assessment of results for phase 1 (planar only) of the observer study.

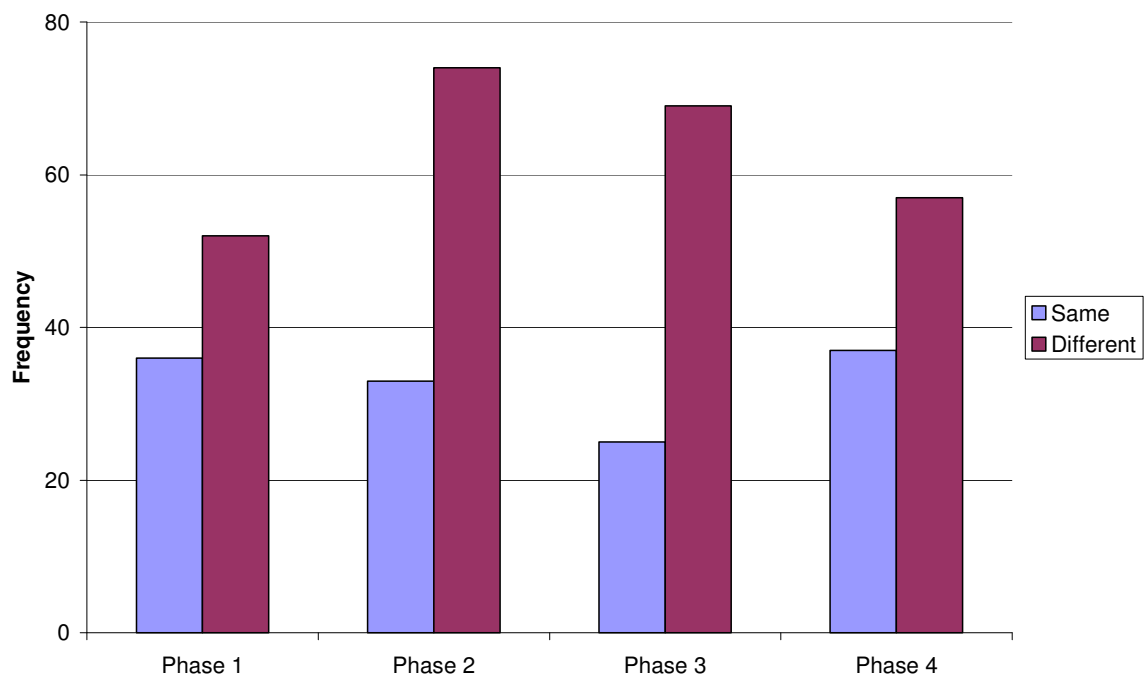


Figure 6.4 - Bar chart of comparisons in overall given location

Frequency of “same” and “different” findings for comparison of the overall given location for each lesion resected at surgery compared to those seen on each phase of the observer study. Phase 1 = planar images only, Phase 2 = SPECT images only, Phase 3 = Sestamibi images only (planar & SPECT), Phase 4 = all images.

In contrast to the results displayed in Figure 6.3, every phase has a higher frequency of “different” results in relation to “same”. The reason for these differences is most likely to be the different way in which the image observers and the surgeon define the position of a lesion. The observers will always define a lesion’s location with respect to the thyroid gland, meaning that “upper” will relate to a lesion seen superior to the thyroid isthmus and “lower” will define a lesion inferior to the isthmus. However, the surgeon will define the position of the resected parathyroid gland with respect to other glands seen at surgery, or possibly even some other anatomical landmark. Given the significant variation in the location of parathyroid glands (see Section 1.1.2, Figure 1.5), this could

lead to the same gland being given a different location by the surgeon when compared to the image observer.

Further and more detailed discussion of all the results in Chapters 5 & 6 is carried out in Chapter 7 of this thesis.

Chapter 7 – Parathyroid Study – Discussion, Conclusions and Suggestions for Further Work

7.1 Discussion

7.1.1 Study Participants

All patients referred to the Nuclear Medicine Department at Glasgow Royal Infirmary (GRI) for parathyroid imaging between February 2006 and October 2008 were invited to take part in this study. The eventual 32 study participants were those patients who provided informed consent that they were willing to take part in the study. The demographics show that there were more female participants than male (19:13), which is as expected due to the higher prevalence of parathyroid disorders among women (Sorva *et al.*, 1992, Robin, 1996, Jensen, 1999, Adami *et al.*, 2002, Judson & Shaha, 2008, Rodgers *et al.*, 2008, Sathe *et al.*, 2009). All participants tolerated the SPECT scan acquisition well with a minimal level of movement artefact visible on only a small number of the acquisitions. Only a single patient complained of slight claustrophobia but, after reassurance, was able to tolerate the acquisition to completion.

7.1.2 SPECT Reconstructions

The parameters chosen in this study for the reconstruction of the SPECT images were as a result of direct advice taken from the company supplying the reconstruction software and a trial-and-error process to optimise the final viewed images. The software suppliers, Nuclear Diagnostics Ltd., recommended that the iterative Ordered Subsets Expectation Maximisation (OSEM) reconstruction algorithm be used in preference to the traditional filtered back-projection (FBP) option. Evidence in the literature suggests that the OSEM technique improves spatial resolution (Brambilla *et al.*, 2005) and that reconstructed images of equal quality to those from FBP can be achieved with fewer acquisition projections or a lower number of acquired counts per projection (Takahashi *et al.*, 2003). The chosen number of subsets and iterations used for the reconstructions was also as a result of advice from

Nuclear Diagnostics Ltd. They recommended that, from their experience, the number of subsets should be $\frac{1}{4}$ of the total number of acquisition frames (in this case 60, meaning 15 subsets were used) and that 4 iterations would allow convergence to an accurate representation of the true radionuclide distribution within the body without requiring excessive processing time. These parameters were therefore adopted.

The choice of post-reconstruction filter was largely as a result of trial-and-error. Each of the 9 different filters available with the reconstruction software was trialled with a number of different values of the variable parameters for each filter on a number of different patient image data sets (see Section 5.3 for a list of the filters and the variable parameters for each). Those images felt by the researcher to provide a reasonable compromise between smoothness and excessive noise were then shown to some of the observers of this study (2 clinicians and 2 clinical scientists) and they were asked to pick their preferred images in each case. The final choice of filter used for all images in this study was therefore chosen by consensus of subjective opinion from several experienced members of staff on optimal image quality.

The fact that the same post-reconstruction filter was chosen as the optimum for both the ^{99m}Tc -Sestamibi and ^{123}I -iodide images was surprising. The total counts in the ^{99m}Tc and ^{123}I energy windows are very different due to the different injected activities and the relative affinity of organs in the neck region to each radiopharmaceutical. The total counts in the ^{99m}Tc window were higher in almost all cases due to the higher level of background activity in other tissues of the neck but the counts in the thyroid gland itself was more variable for the two radiopharmaceuticals, with some patients demonstrating higher counts in the ^{99m}Tc window, some showing higher counts in the ^{123}I window and others showing similar counts in each. Also, the target to background ratio of the thyroid gland in the two different energy windows are significantly different, with the ratio being low for ^{99m}Tc but very high for ^{123}I . It would therefore be expected that a different filter would be required to give the best contrast between the thyroid and the background activity. However, the consensus opinion from the observers was that the same Hanning filter (cutoff 3.0 cycles/cm) was the best compromise for both sets of images and so this was used for all reconstructions.

7.1.3 General Observer Comments

The 5 observers that took part in this study were two consultant nuclear medicine physicians, 1 consultant radiologist and 2 experienced clinical scientists in nuclear medicine physics. None had viewed parathyroid SPECT images before this study and so all the observers required some time to become familiar with the new image data sets at the start of the study. They all commented that the ^{99m}Tc -Sestamibi SPECT images in particular were difficult to interpret due to the high levels of non-specific uptake within the neck. As the study progressed, however, they all became more comfortable and confident in reviewing the SPECT images and indeed by the end of the study, all commented that they preferred the SPECT images to be available as they felt they could better characterise any lesions seen on the planar images.

All the observers also commented that they preferred the availability of the ^{123}I -iodide images in order to visualise the thyroid anatomy rather than viewing the ^{99m}Tc -Sestamibi images alone. This is most likely due to the fact that the standard protocol used at GRI is a dual-isotope planar subtraction technique and the observers are all used to presence of the ^{123}I images. This may have affected the results of this study slightly, but it is recognised that subtraction imaging can, on occasion, confirm the presence of lesions that are either equivocal or not visible on single-tracer imaging or the presence of thyroid disease (e.g. hot/cold thyroid nodule) that may be uncertain from imaging with ^{99m}Tc -Sestamibi only (Jeanguillaume *et al.*, 1997, Krausz *et al.*, 2001, Profanter *et al.*, 2003, Wong *et al.*, 2009). Imaging of the thyroid independently also reduces the risk of false-positive results, which can occur in the presence of a thyroid adenoma (Kresnik *et al.*, 1997).

When carrying out the final phase of the study, when all images were made available to the observers, they commented that there were some lesions that were not visible on the planar images that were very clear on the SPECT views. This indicates that there is some degree of under-reporting occurring with subtraction planar imaging that may be reduced with the introduction of subtraction SPECT imaging.

The number of lesions seen by each individual observer and in total was highest for phases 2 & 4 of the study, when the dual-isotope subtraction SPECT images were included in the review. The lowest total number of lesions seen as well as the highest number of negative reports was found for phase 1, in which only planar images were available for review. This demonstrates that more possible lesions are visible on the SPECT images than on planar alone, but does not in itself confirm that SPECT imaging is better as the extra lesions seen may be image artefacts and not true parathyroid adenomas.

There was a clear difference in the total number of lesions reported by the individual observers throughout the study. Observer 2 saw fewer lesions than all the others on every phase, whilst observer 5 saw more than all the others on every phase. This demonstrates the highly subjective nature of image review, even amongst experienced nuclear medicine clinicians and scientists. Observer 5 had a tendency to report every potential lesion seen on the images, whereas, in contrast, observer 2 felt that many of the possible lesions were image artefacts and so ignored them. Therefore, observer 5 had a probable tendency to over-report the images, whilst observer 2 had a tendency to under-report possible lesions.

The observers also gave scores for image quality during each phase of the study. In general, the ^{99m}Tc -Sestamibi SPECT images gained the lowest scores for image quality and were also occasionally described as “poor” by the observers due to a lack of acquired counts in the images. Improvements to image quality can be made by increasing the administered activity of ^{99m}Tc -Sestamibi to provide a greater activity concentration in the area of interest, by increasing the length of each SPECT acquisition frame beyond the 30s used in this study, or by using a combination of both of these options.

7.1.4 Comparison of Phases of Observer Study

The most striking finding of the observer study was that all the observers tended to see a larger number of lesions when SPECT imaging was available than when reviewing only planar images. This is to be expected, since the planar images only give an anterior view whereas the SPECT images give a three-dimensional representation of the distribution of radiopharmaceutical in the neck area. Any

lesion situated immediately posterior to the thyroid may therefore not be visualised on a planar view but the SPECT images include this area, allowing the lesion to be visualised. However, the increase in the number of lesions reported by the observers may be due to image artefacts rather than true lesions and so the comparison with the surgical reports is necessary to determine the true clinical utility of the SPECT images.

From the planar images, the observers gave positive reports for half of the lesions seen. When reviewing the SPECT images in the absence of the planar views, however, a greater number of lesions were seen and a greater proportion of those lesions - 85% - were reported as positive. A similar proportion at 79% were deemed positive when both planar and SPECT dual-isotope images were available for review with the proportion dropping to 64% when only the ^{99m}Tc -Sestamibi images were reviewed. The Wilcoxon Signed Ranks tests carried out on the data confirmed the increase in observer confidence when SPECT images were available for review with $p < 0.05$ in the majority of cases. The exception was in phase 3 with only Sestamibi images being available to the observers, when the expressed confidence levels were not significantly different from the review of planar images. This strongly suggests that the dual-isotope subtraction SPECT is allowing the observers to more clearly see possible lesions on the images and therefore giving them more confidence in their reports.

The scores for image quality were consistently higher for the ^{123}I -iodide images, both planar and SPECT, than for the ^{99m}Tc -Sestamibi images. This is to be expected, however, due to the high non-specific background activity that characterises Sestamibi uptake in the neck region whilst iodine is selectively taken up in the thyroid gland only. The lowest image quality scores were given for ^{99m}Tc -Sestamibi SPECT images in phases 2 & 3 of the observer study. In contrast, the highest overall image quality and subtraction usefulness scores were given in phase 4, when both planar and SPECT dual-isotope images were available to the observers for review. This suggests that the combination of planar and SPECT dual-isotope images is the preferred system for reporting of parathyroid images by the observers in this study.

It is also clear from the results in Chapter 5 that there was a wide variation in the number of lesions being reported by the 5 observers. In particular, observer

5 consistently reported more lesions than each of the other observers. This may represent over-reporting by this observer or increased caution by the others in order to prevent false-positive reports. Observer 5 is an experienced clinical scientist and, although having many years' experience of viewing parathyroid images, is not responsible for issuing reports for imaging studies in the department. In contrast, observers 1, 2 & 3 are consultant clinicians who all routinely issue clinical reports for a wide variety of nuclear medicine investigations, including parathyroid imaging.

In other areas considered in this study, there was often considerable variation between the results for each of the 5 observers. This shows how subjective the reviewing and reporting of nuclear medicine images can be but is also certainly due in part to the fact that the observers were asked to review types of SPECT images which were entirely new to them and of which they had no experience. All commented towards the end of the study that they were becoming more comfortable with reviewing the dual-isotope subtraction images and so it is possible that the results from phase 2 were slightly affected by this general unfamiliarity. In order to assess the magnitude of the effect, the observers were asked to review the phase 2 SPECT images a second time, after all the other phases of the study were complete. The results of this 2nd review are discussed in Section 7.1.7 below.

In all comparisons with planar images, a similar number of lesions were seen on the same side (i.e. left/right) as on the opposite side, indicating that the lesions seen on the planar images were not always the same as those seen when SPECT images were available. The main reason for this is the significantly higher number of lesions seen on phases 2-4 of the study relative to phase 1, meaning that the comparisons being made are not always like-with-like and a single lesion seen on the planar images may have been compared to up to 4 lesions seen in a later phase of the study. Unfortunately, there was no way to design the study to remove this effect as it would have required the researcher to make judgements as to when a lesion reported by an observer from different phases of the study was the same lesion or a completely different lesion or artefact. This would have been an unacceptable level of subjective interference from one person on the results and so the method of comparing each individual lesion from each of the different phases of the observer study was used instead.

The number of lesions seen at the same upper/lower location was always lower than the number given at the same left/right site. This is most likely due to the fact that the planar images give only a single-angled view of the location of the lesion relative to the thyroid gland. The resultant image would be heavily influenced by any angulation of the gamma camera detector at the time of acquisition, which could lead to slight distortion in the final image. The three-dimensional nature of the SPECT images removes this dependency, meaning that a more accurate assessment of the location of a lesion with respect to the thyroid can be made.

When the phases of the study involving the use of at least one set of SPECT images were compared to each other, a clear distinction emerged. During phase 3 of the study, when the planar and SPECT ^{99m}Tc -Sestamibi images were reviewed in the absence of any ^{123}I -iodide images, fewer lesions were reported and the level of confidence expressed by the observers was lower than when iodine images were also available. This is a confirmation of the general comments made by the observers, who all stated that they were least comfortable reviewing the images in phase 3 of the study. Indeed, when a Wilcoxon Signed Ranks test was performed on the confidence levels expressed by the observers during the dual-isotope SPECT image review were compared to those from the Sestamibi-only review, values of $p < 0.05$ were found in every case. The differences were less clear-cut when the Sestamibi-only review was compared with that involving all dual-isotope planar and SPECT images, but the tendency was still towards higher confidence levels being expressed when the ^{123}I -iodide images were available to the observers. These findings are certainly partly attributable to the fact that all the observers in the study are used to having dual-isotope and subtraction images available to them in the reporting of parathyroid images. However, the significant level of the differences indicates that, at least at this institution, a change in practice to single-isotope, dual-phase imaging would not be a welcome step and would be likely to lead to a considerable increase in the number of equivocal reports being produced.

In the comparison of phases 2 & 4, there was less difference between the numbers of lesions seen and the expressed confidence levels than was seen in the other comparisons. This suggests that the observers were primarily using the SPECT images to report on phase 4 of the study, rather than relying heavily on

the planar views. This is a surprising finding, since the observers' current practice is to view planar images only, but it demonstrates that the observers found the amount of information on radiopharmaceutical distribution that is displayed in the SPECT images very useful in making decisions on the presence or otherwise of true parathyroid adenomas on the images.

When considering the given left/right location of each lesion, the number of times the same side was given was highest in the comparison of phases 2 & 4, with all observers giving >60% of lesions on the same side with the exception of observer 5, whose results are likely to be influenced by the larger number of lesions this observer reported on all phases, as discussed above. This once again confirms that the observers were relying heavily on the SPECT images for locating lesions when all planar and SPECT images were available to them during phase 4. Both the comparisons involving the Sestamibi-only images with the other SPECT phases resulted in a similar number of lesions reported on the same side at slightly more than 50% in all cases with the exception of observer 1 in the comparison of phases 3 & 4, who gave just under 50% at the same left/right location. These results suggest that there are still a significant number of occasions on which a different lesion is being reported from each of the two sets of images involved in the comparison.

The given upper/lower and anterior/posterior locations for each of phases 2-4 of the observer study were also compared. The results clearly show that, in these two planes, the same location was given considerably less frequently than was the case for the left/right location. This is a slightly surprising result and indicates that the presence or absence of ¹²³I-iodine and/or planar images had a significant impact on the exact reported location of each lesion. The fact that more lesions were seen on phase 2 of the study than on the other phases may also be a factor since, as was the case when comparisons were made with the findings from the planar images, more than one lesion reported from phases 3 & 4 will have been compared to a single lesion noted on phase 2, as was discussed in more detail above.

In summary, the comparisons of the results from the different phases of the observer study demonstrate that the inclusion of SPECT images in nuclear medicine parathyroid examinations results in a larger number of lesions being

reported and an increase in the confidence level that these lesions represent true parathyroid adenomas. Also, the inclusion of dual-isotope subtraction SPECT images increases the confidence level of the observers over the situation where only ^{99m}Tc -Sestamibi images were made available. The most similar results were seen when phases 2 & 4 of the study were compared, indicating that the observers were relying heavily on the information from the SPECT images during phase 4, when both planar and SPECT images were available. The given location of lesions often differed for a single patient data set between different phases of the study, although this is partly due to the comparison method used here, as discussed above. However, the most similar results were once again seen between phases 2 & 4, with an overall figure of 60% of lesions seen at the same left/right location on the two phases.

7.1.5 Comparison of Surgical and Ultrasound Findings

Surgery is the primary curative method of choice in cases of hyperparathyroidism (Serchuk *et al.*, 1997, Thomas & Wishart, 2003, Pelizzo *et al.*, 2008, Rodgers *et al.*, 2008) and the ability of an experienced endocrine surgeon to visually detect and then remove a parathyroid adenoma during bi-lateral neck exploration has been the main technique used for many years, with a high success rate of 95% or more (van Heerden & Grant, 1991, Udén *et al.*, 1992, Weber *et al.*, 2000, Thomas & Wishart, 2003, Russell *et al.*, 2006, Pelizzo *et al.*, 2008), with post-surgical histology definitively determining the presence or otherwise of a parathyroid adenoma. However, minimally invasive parathyroidectomy is becoming increasingly common (Greene *et al.*, 2009), as it requires only a small, unilateral incision to be made and results in shorter surgery, a shorter hospital stay and lower morbidity rate post-surgery (Bergenfelz *et al.*, 2002, Adler *et al.*, 2008 & 2009) with no significant decrease in the curative effect of the surgery (Sidhu *et al.*, 2003, Russell *et al.*, 2006, Westerdahl & Bergenfelz, 2007).

In order to perform unilateral surgery, it is necessary for the surgeon to have some information on the location of the suspected parathyroid adenoma and this is provided by pre-surgical imaging studies (Quiros *et al.*, 2004). Both anatomical ultrasound and functional nuclear medicine imaging are available and patients may undergo both types of imaging prior to surgery. Of the 32

participants in this study, a total of 13 patients had both ultrasound imaging and parathyroidectomy surgery. The findings from ultrasound imaging were compared to those from histological analysis of surgically resected samples so as to provide a baseline with which to compare the various phases of the nuclear medicine observer study.

Most commonly, a surgical sample resected from a site identified as that of a positive lesion on ultrasound imaging was confirmed to be a parathyroid adenoma or hyperplastic gland upon histological examination. This was the case for 7 of the 13 patients. However, there were also 3 examples of a negative ultrasound report being given for patients who had a positive sample removed at surgery as well as a patient with an ectopic parathyroid adenoma in the mediastinum, which was also not reported from ultrasound due to the difficulties in using this type of imaging in the mediastinum (Beierwaltes, 1991, Carlier *et al.*, 2008). The remaining 2 patients had positive samples resected at surgery from different sites than those suggested by the preoperative ultrasound imaging. Overall, when taking into consideration the positive/negative report and given left/right location of each lesion, the sensitivity and specificity of ultrasound imaging were found to be 72% and 33% respectively for the study participants. These figures are well below those reported by some other researchers, as discussed further in Section 7.1.9 below.

7.1.6 Comparison of Observer Study with Surgical Findings

In order to determine the true clinical utility of the various types of nuclear medicine images investigated for the present study, it was necessary to compare the results to those from surgery which, with histological analysis of resected samples, provides the true gold standard as to the presence or otherwise of a parathyroid adenoma.

The results of all 4 phases of the observer study were compared to the surgical results, which were taken from the patients' case notes. Unfortunately for the purposes of this study, only 17 of the 32 participants (53%) have undergone parathyroidectomy surgery up to the present time. This is partly due to the patient-pathway employed at GRI, whereby the results of imaging studies are taken into account in the decision making process for surgery. Normally, only

patients with positive results from imaging investigations are referred on to the endocrine surgeons, whilst those with negative results tend to be managed clinically. The literature indicates that this is a different referral process from that used at other institutions, whereby the patients are referred for localisation imaging only once the need for surgery has already been confirmed (e.g. Billotey *et al.*, 1996a, Hindié *et al.*, 1998, Sidhu *et al.*, 2003). The report from imaging then acts as a guide for the surgeon as to the most likely location for the parathyroid adenoma, rather than being used to definitively determine its presence or absence.

The surgical findings of the 17 patients were, nonetheless, compared to the results of the various phases of the observer study, with the surgical results acting as the gold standard. There was some variation in the results from individual observers, with the tendency for observer 5 to see more lesions than the others previously discussed, but general trends are still evident in the data. When the observers were presented only with planar views in phase 1 of the study, they tended to see fewer lesions than were resected at surgery. This was also the case when only ^{99m}Tc -Sestamibi images were available to the observers in phase 3. In contrast, when dual-isotope subtraction SPECT images were used in phases 2 & 4 of the study, there was no significant difference between the number of lesions seen by the observers and the number removed at surgery. The exception to this was observer 5 in phase 2 of the study, where the observer reported more lesions from the SPECT images than were resected by the endocrine surgeon, which is again evidence of this observer's tendency to over-report lesions on the images. All of these results show, however, that there are a number of true parathyroid adenomas that are not being reported from the planar and Sestamibi-only images, but that the inclusion of dual-isotope subtraction SPECT allows visualisation of at least some of these lesions.

When the given positive/negative reports from the observers were compared to the positive/negative histological results, a similar pattern appeared. More of the lesions seen by the observers during phases 2 & 4 of the study were given the same positive/negative report as was given on histological examination of the resected gland than was the case for phases 1 & 3. The results of the non-parametric Wilcoxon Signed Ranks test applied to the data comparing the number of "same" and "different" positive/negative reports given underline

this. No statistically significant differences were seen for any of the observers when the test was applied to the results from the review of the planar and Sestamibi-only images and no clear patterns were demonstrated in the 95% confidence intervals (95% CIs). In contrast, the results from the SPECT and all images phases of the study demonstrated several cases of statistical significance ($p < 0.05$) in the comparisons and a strong tendency for the number of “same” results to be higher than the number of “different”, demonstrated by the 95% CIs being > 1 .

Comparisons were also made of the location of each lesion reported by the observers during each phase of the study and the location of each resected sample given by the endocrine surgeon. The most important information for the surgeon wishing to perform minimally invasive surgery is whether the suspected parathyroid adenoma is on the left- or right-hand-side of the neck and so the focus of the comparison was on the given left/right location of each lesion.

Generally speaking, more lesions were seen by the observers at the same left/right location that was recorded in the surgical notes than were seen on the contralateral aspect of the neck. This is encouraging, as it indicates that the information being given to the surgeons to assist in performing minimally invasive surgery is reasonably accurate. However, the results once again demonstrate that the same side was most often given when the observers were viewing dual-isotope subtraction SPECT images in phases 2 & 4 of the study, with little difference in the results when planar images were and were not included. The lowest numbers of lesions seen on the same side was for the planar images. This will be due in part to the fact that there were a number of occasions in which no lesion was seen on the planar images when, in fact, a sample was resected at surgery.

A comparison was also made of the given upper/lower location relative to the thyroid gland of each observed lesion against each sample resected at surgery. In each phase of the observer study, the results were less consistent with those from surgery than was the case for the given left/right location of each lesion. The main reason for this is the difference in the way “upper” and “lower” are defined by the image observers and surgeons respectively. An image observer will tend to report a lesion as “upper” if it lies at or above the thyroid isthmus

and “lower” if it lies below this level. However, a surgeon will define a gland as “upper” or “lower” on the basis of other glands observed at surgery, which relate to the embryologic origin of the different glands (Taïeb *et al*, 2007). It is therefore possible that a surgeon may find a gland that lies inferior to the thyroid isthmus but superior to another parathyroid gland and so would designate this as an “upper” gland, whereas a gland in this location on imaging would always be defined as a “lower” gland. The two definitions are therefore very different and cannot be compared directly. Since the lateral (left/right) position of the observed lesion is the most important factor for successful minimally invasive surgery, the upper/lower information can be helpful but is not absolutely necessary for the surgeon.

The same is true of the anterior/posterior location information given for the phases of the observer study involving SPECT images. Parathyroid glands most often lie posterior to the thyroid but ectopic glands are not uncommon (Berne & Levy, 1993, Moore & Agur, 2007, Rodgers *et al.*, 2008) and so it is possible that an adenoma could lie anterior to the thyroid. The anterior/posterior information was not given for all glands resected at surgery (see Table 6.1) and so comparisons with the observer study were made only for those samples where this information was available. The results of the comparison showed wide variation between the observers with little clear pattern. Again, however, the location definition used by the observers and surgeons were not necessarily the same and direct comparison is therefore not feasible.

The sensitivity and specificity for each phase of the observer study were calculated using only the given positive/negative result for parathyroid adenoma and the left/right location of the observed lesion and comparing these to the surgical report for each patient. The overall sensitivity and specificity values for each phase of the study are shown in Table 7.1, along with the calculated values for the comparison of the ultrasound imaging reports with the surgical reports.

It is immediately clear from these results that the sensitivity is significantly higher when dual-isotope subtraction SPECT images are available to the observers. The highest sensitivity value is for phase 2 of the observer study, when the dual-isotope subtraction SPECT images were presented in the absence of any planar images. The lowest sensitivity is found for phase 3, when no ¹²³I-

iodide images were included, which again confirms the preference for the observers to have the thyroid images available to them. The sensitivity for ultrasound imaging is lower than for SPECT imaging but is slightly better than for phase 4 of the study, when dual-isotope subtraction SPECT and planar images were both available.

Study Phase	Sensitivity (%)	Specificity (%)
1 (planar)	49	61
2 (SPECT)	77	31
3 (Sestamibi)	45	29
4 (all images)	64	27
Ultrasound	72	33

Table 7.1 - Overall sensitivity and specificity values for comparison of results of observer study and ultrasound imaging with surgical results
Combined sensitivity and specificity results for all 5 observers for each phase of the observer study and those from the ultrasound imaging reports relative to surgery

The specificity values are low for ultrasound imaging and for phases 2-4 of the observer study, which is likely to be due to the fact that there were only 2 true negative results from surgery. Since the specificity is strongly dependent on the true negative rate (see Equation 4.3), any slight differences between the observer study and surgical results will be magnified. The relatively high specificity for phase 1 is due to the low number of positive results given by the observers overall, meaning that the false positive rate was very low.

These overall results do, however, obscure variations between observers. Observer 5 tended to have high sensitivity but relatively low specificity due to the tendency to report larger numbers of lesions overall, as has been discussed previously. In contrast, observers 1-3 tended to have lower sensitivity but higher specificity values, indicating that these observers are more cautious overall and are therefore less likely to report an artefact as being a positive lesion, but are also more likely to report a true lesion as negative.

All of the results from the comparison of the surgical results with those from the observer study clearly show an improvement in the detection of parathyroid adenomas when dual-isotope subtraction SPECT imaging is utilised. Also, there is an improvement in the left/right localisation of a true lesion when dual-isotope SPECT is available. There was little discernible difference between the phases of the study when dual-isotope subtraction SPECT was used alone and

when it was used in conjunction with dual-isotope subtraction planar imaging. The overall benefit when compared to planar imaging alone is, however, clear and it would therefore be recommended that the technique is employed routinely at GRI for parathyroid imaging.

7.1.7 Second Review of Phase 2 SPECT Images

As the observers had no previous experience of viewing dual-isotope subtraction SPECT images, it is possible that the results from phase 2 of the observer study were affected by this unfamiliarity. The observers were therefore asked to review the phase 2 images a second time in order to determine the magnitude of this effect. Unfortunately, only 3 of the original 5 observers - observers 2, 3 & 5 - were available to take part in the second phase 2 review. The same 32 patient image data sets, scoring sheets and methods were used as in the original review and the results were analysed in a similar fashion. This second review took place around 12 months after the other reviews were complete, by which time each of the observers had obtained around 18 months worth of experience in reading dual-isotope subtraction SPECT parathyroid images.

In total, 81 lesions were seen by the 3 observers with 29 (36%) being classed as definitely positive for parathyroid adenoma, 17 (21%) felt to be suggestive and 35 (43%) being defined as equivocal. In total, 24 (25%) of the 96 reviews were reported as negative. A comparison of the number of lesions seen by each of the 3 observers on the first and second review of the phase 2 images is shown in Figure 7.1. It can clearly be seen that all of the observers reported fewer lesions seen on the second review compared to the first. The largest difference was for observer 5, who reported 64 lesions from the first review and only 34 from the second. This observer commented that on the first review, they reported a large number of equivocal lesions that they were more confident were simply artefacts on the second review. In contrast, the number of lesions seen by observer 2 differed by only 1 (24 to 23), indicating a greater degree of consistency by this observer on the 2nd review.

The sensitivity and specificity for comparison with the surgical findings were also calculated for the second SPECT review and are shown in Table 7.2, alongside the results from the first phase 2 review. Once again, only the given

positive/negative status of each lesion and its given left/right location were taken into account in the calculation of the sensitivity and specificity. The quoted overall sensitivity and specificity for the original review are for these 3 observers only, with observers 1 & 4 excluded, and so are slightly different to those quoted in Table 6.29.

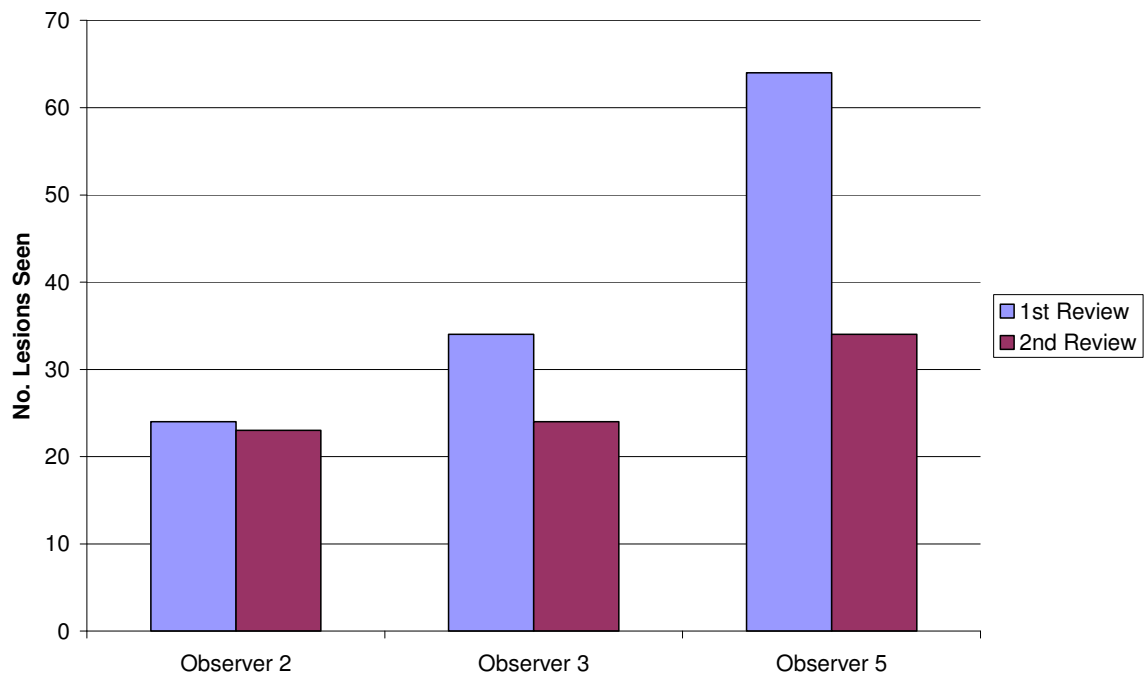


Figure 7.1 - Comparison of lesions seen on first and second reviews of SPECT data
Bar chart showing the total number of lesions seen by each observer on the first (blue) and second (purple) reviews of the phase 2 dual-isotope subtraction SPECT images.

Observer	Sensitivity 1 st review (%)	Sensitivity 2 nd review (%)	Specificity 1 st review (%)	Specificity 2 nd review (%)
2	57	57	25	25
3	75	60	60	75
5	84	67	40	50
Overall	73	61	42	50

Table 7.2 - Calculated sensitivity and specificity relative to surgical findings for first and second SPECT image reviews
Sensitivity and specificity calculated for each individual observer and overall relative to the surgical and histological reports for the 1st and 2nd phase 2 SPECT image review.

The sensitivity and specificity for observer 2 remained the same on the second review of the dual-isotope subtraction SPECT images, confirming this observer's consistency. However, the results for observers 3 & 5, as well as the overall results, demonstrate a reduced sensitivity and increased specificity on the second review. The increased specificity is to be expected since, as the

observers become more comfortable with reviewing the SPECT images, they will become more adept at distinguishing artefacts from true lesions. However, the reduction in sensitivity was not expected and is the result of some lesions that were previously correctly reported as positive now being felt to be artefacts.

Given the fact that patients at GRI are referred for imaging prior to any decision on surgery being made, the specificity is the more important measure, as discussed in Section 3.1.1. Although the overall specificity remains relatively low at 50%, the increase in specificity on the second review confirms that the observers are becoming more comfortable and confident in reading the dual-isotope subtraction SPECT images over time. Unfortunately, as noted previously, the small number of true negative lesions at surgery heavily influences the specificity and so it is not a reliable measure here. However, the overall sensitivity on the second review remains as good as any of the other phases of the observer study, meaning that the true positive rate remains high and many parathyroid adenomas are being visualised on the images. The relatively high sensitivity and increase in specificity on the second review confirms that dual-isotope subtraction SPECT imaging provides an improvement in parathyroid adenoma localisation over other nuclear medicine imaging methods.

7.1.8 Comparison of Observer Study with Ultrasound Findings

A total of 25 of the 32 study participants (78%) also had ultrasound imaging of the neck as an aid to localising any existing parathyroid adenomas. The results of the observer study were compared to the ultrasound results in order to determine any significant differences between the imaging modalities in detecting parathyroid adenomas. The comparison methods used were the same as those for comparing the observer study results with those from surgery, although on this occasion the reported ultrasound results were taken as the comparison standard.

In general, the results of the observer study were more similar to those of the ultrasound scanning than they were to those from surgery. At first glance, this may seem like a surprising result since ultrasound is an anatomical imaging modality whereas nuclear medicine gives images of physiological function. However, most of the participants that had an ultrasound scan of the neck for

suspected parathyroid adenoma were referred for the scan after having nuclear medicine imaging in order to confirm a possible or likely lesion seen on the planar dual-isotope subtraction images. The operator performing the ultrasound scan is aware of the reported result from the functional nuclear medicine imaging and so may be influenced. As a result, the two imaging modalities are not totally independent. The sensitivity and specificity of ultrasound scanning were also well below 100% - at 72% and 33%, respectively - and so using the ultrasound report as a gold standard is not truly accurate, but nevertheless gives an interesting comparison of the results from the two imaging modalities.

In the comparison of the number of lesions seen on ultrasound imaging and each of the 4 phases of the observer study, there was generally little difference to be seen. Indeed, for each of the 4 phases, there were more instances where the same number of lesions was reported than a different number. When the results from phase 1 of the observer study were used in the comparison, there was a general tendency for more lesions to be seen on ultrasound than on planar subtraction nuclear medicine imaging. In contrast, the opposite was true when the phase 2 results were compared to ultrasound, with statistically significant differences in the number of lesions seen demonstrated for 4 of the 5 observers on application of the Wilcoxon Signed Ranks test to the data. The 95% CI for the difference in number of lesions seen for all 5 observers was ≤ 0 , indicating that more lesions were being reported from the subtraction SPECT images than from ultrasound.

Phase 3 of the study gave the least significant differences between the reports from ultrasound and nuclear medicine imaging. There was a slight tendency for more lesions to be seen on the Sestamibi-only images, although the results were only statistically significant for observer 5 and the overall total. As has been mentioned previously, observer 5 was inclined to report more lesions than the other observers throughout this process and so this result is not surprising. The comparison of the results of phase 4 of the observer study with the ultrasound reports showed a more significant trend towards the observers seeing more lesions when all the nuclear medicine images were available to them. For 3 of the 5 observers as well as the overall combined results, a statistically significant difference in the number of lesions seen was demonstrated and the 95% CIs all being ≤ 0 shows that the observers tended to see more lesions on the combined

planar and SPECT subtraction nuclear medicine images than were reported at ultrasound scanning. These results all suggest either a tendency for over-reporting of lesions from nuclear medicine images or a lack of sensitivity on ultrasound imaging.

The given positive/negative results from the ultrasound scanning report were then compared to those from the 4 phases of the observer study and a similar pattern to that seen on comparison of the surgical and observer study results was observed. For the results of phases 1 & 3 of the study, there were no significant differences found, with the same positive/negative report being given in most cases. However, phases 2 & 4 of the observer study showed different reports being given in many cases, with most observers individually as well as the combined totals showing a statistically significant difference ($p < 0.05$) on application of the Wilcoxon Signed Ranks test. The fact that the 95% CIs are all ≥ 0 indicates that the nuclear medicine observers are more inclined to report a lesion as positive than is the case on the ultrasound reports.

As was the case when the observer study results were compared with the surgical findings, comparisons were also made of the reported location of each lesion during each phase of the observer study and the site of each lesion given in the ultrasound report. As before, the main focus of the comparison was on the given left/right location of each lesion (see Section 7.1.6 above), although the upper/lower and anterior/posterior locations were also considered.

The results of the left/right location comparison showed that in the majority of cases in all 4 phases of the observer study, the same left/right site was given as had been reported from ultrasound. Only observer 2 saw more lesions at a different site from ultrasound imaging than at the same site, and then only in phases 1 (planar) and 3 (Sestamibi-only). This again demonstrates the similarities between the findings from the 2 types of preoperative imaging, despite the fact that ultrasound is an anatomical imaging modality whilst nuclear medicine produces functional images.

As discussed in Section 7.1.6 above, the definitions of “upper”, “lower”, “anterior” and “posterior” as applied to a parathyroid lesion can differ between an observer reviewing an imaging study and an endocrine surgeon resecting

suspicious samples during parathyroidectomy. However, these differences do not exist when considering a comparison of different types of imaging since all location definitions will be given relative to the observed thyroid gland. It was therefore expected that the comparisons of the given upper/lower and anterior/posterior sites for each lesions on ultrasound and the various phases of the observer study would be more similar than when the observer study results were compared with surgery.

This was, however, not the case for all phases. The results were very variable between observers but general overall trends could be determined. The comparison of phase 1 with the ultrasound findings included only the upper/lower information as it is not possible to determine the anterior/posterior position of a lesion from an anterior planar projection image. The numbers of lesions seen at the same and different upper/lower locations were similar with no obvious trend seen. Phase 2 gave similar results for the upper/lower comparison, although there was a slight tendency for more lesions to be given at the same location than at a different site. In complete contrast, the anterior/posterior comparison results for phase 2 clearly showed more lesions being given at the same site than at a different position for all observers, with observer 1 giving as many as 93% at the same location as was reported at ultrasound.

The results for phase 3 were less clear cut with generally slightly fewer lesions being given at the same upper/lower location from Sestamibi-only images as from ultrasound. The results for the anterior/posterior comparison were very variable with 3 of the 5 observers seeing more lesions at the same site, whilst the others saw more at a different position. This again demonstrates that the observers were not entirely comfortable reporting from the Sestamibi-only images and preferred to have ^{123}I -iodide images available to give a clear image of thyroid uptake. Phase 4 was the only part of the observer study that gave the expected results for the upper/lower and anterior/posterior location comparisons, with all observers reporting more lesions at the same site than at a different position when compared to the findings of ultrasound imaging. This suggests that the combination of planar and SPECT subtraction images gives the most consistent location information when compared to ultrasound than do any of the other combinations of nuclear medicine images.

The overall sensitivity and specificity values for the comparison of the various phases of the observer study with the ultrasound results are shown in Table 7.3. When compared to those in Table 7.1, it is immediately clear that the sensitivity and particularly the specificity are higher when taken relative to ultrasound rather than the surgical results. This is to be expected since, as discussed above, the ultrasound and nuclear medicine imaging for parathyroid disease at GRI are not totally independent.

Study Phase	Sensitivity (%)	Specificity (%)
1 (planar)	46	72
2 (SPECT)	81	48
3 (Sestamibi)	35	62
4 (all images)	73	64

Table 7.3 - Overall sensitivity and specificity values for comparison of results of observer study with ultrasound imaging results
Combined sensitivity and specificity results for all 5 observers for each phase of the observer study compared with those from the ultrasound imaging reports

The results also demonstrate that the sensitivity is once again higher for those phases of the observer study that included dual-isotope subtraction SPECT images than for those phases that did not. The highest sensitivity, as was the case for the comparison with the surgical results, was for phase 2, but this was combined with the lowest specificity. In contrast, both phases 1 & 3 had low sensitivity but higher specificity. The results for phase 4 show relatively high sensitivity and specificity, suggesting that the combination of dual-isotope subtraction planar and SPECT images gives results most similar to those from ultrasound imaging.

7.1.9 Comparison with Results from Other Researchers

A detailed description of the history of nuclear medicine imaging of the parathyroid glands and the many available radiopharmaceuticals and techniques is given in Section 1.3.2 of this thesis. A 1998 review of the available literature (Pattou *et al.*, 1998) clearly demonstrated the large number of different techniques in use and the relative success with which they were used at different centres. The measured sensitivity in parathyroid adenoma detection from a large number of studies was collated and the results showed wide variation, with a range of 55% - 100%, for planar imaging techniques. Indeed, the first study into the use of the ^{99m}Tc -Sestamibi dual-phase technique

(Taillefer *et al.*, 1992) found a sensitivity of 90%, whilst a much later study using the same technique reported a sensitivity of just 55% (Neumann *et al.*, 1997a & 1997b).

The main premise behind the dual-phase technique - that the washout rate of Sestamibi from a parathyroid adenoma is slower than that of thyroid tissue - has also been shown to be non-universal (Calendini-Viallet, 1997, Krausz *et al.*, 2001). Further work has demonstrated increased sensitivity from dual-isotope techniques when compared to the use of dual-phase washout (Hindié *et al.*, 1998, Leslie *et al.*, 2002, Wakamatsu *et al.*, 2003) and a sensitivity of 100% in relation to preoperative localisation of a single diseased gland prior to unilateral surgery has been reported with dual-isotope planar imaging (Hindié *et al.*, 2000). Pattou's review (1998) also demonstrated a tendency for increased sensitivity when ^{123}I was used to define the thyroid gland in subtraction imaging, as opposed to the use of $^{99\text{m}}\text{Tc}$ -pertechnetate. This has been confirmed by more recent work (Kettle & O'Doherty, 2006).

The findings of the present study show much lower sensitivity values than most of the analysis presented in the literature, with the sensitivity varying between 46% and 60% for the 5 observers reviewing dual-isotope subtraction planar images. These values are, however, comparable with the 55% found by Neumann (Neumann *et al.*, 1997a & 1997b), who used the same parameters to determine the sensitivity. Other studies are less clear on how sensitivity is defined and so may be measuring a different quantity and a direct comparison may not be valid. Another factor which could affect the sensitivity of this study is the standard referral pattern at GRI. As previously noted, at other centres, patients undergo imaging only after the need for surgery has been confirmed, whereas the results of imaging at GRI will affect the clinical decision on whether or not to operate. The clinicians reporting images at other centres are therefore simply providing guidance to the surgeon as to the most likely position of an adenoma or hyperplastic parathyroid gland. In contrast, at GRI the purpose of imaging is to confirm the presence of an overactive gland to assess the requirement for surgery. Clinicians at other centres are therefore more likely to class a lesion as positive than would be the case at GRI, meaning that the sensitivity for parathyroid imaging at other centres is higher than at GRI.

Differences in the detection rates of lesions between primary and secondary hyperparathyroidism and between single- and multi-gland disease have also been demonstrated by a number of groups. For example, one group found a sensitivity of 96.2% for adenoma detection in primary hyperparathyroidism, but just 48.5% in secondary hyperparathyroidism (Suehiro & Fukuchi, 1992). Another group determined a sensitivity of 89% for the detection of single adenomas but only 47% for hyperplastic glands (Chen *et al.*, 1997). However, another study found good sensitivity for the detection of hyperplasia at 96% (Gordon *et al.*, 2002). The size of the adenoma has also been found to affect the sensitivity of imaging with ^{99m}Tc -Sestamibi, with sensitivity for detection of large and small adenomas of 81% and 56% respectively, although the mechanism for this is not well understood (Moka *et al.*, 2000b).

There was no segregation between participants with primary and secondary hyperparathyroidism or between single- and multi-gland disease in the present study due to the relatively small sample size available. However, the inclusion of all participants in a single group is likely to be contributing to the relatively low sensitivity found in this study when compared to others in the literature. Indeed, the sensitivity found here for planar imaging is not dissimilar to that found in studies where no distinction was made between groups of patients (e.g. Thomas *et al.*, 2009).

Three-dimensional single-isotope SPECT imaging with ^{99m}Tc -Sestamibi has also been studied widely, again with varying reported sensitivity. Some groups found that the use of SPECT increased sensitivity significantly over planar imaging (Billotey *et al.*, 1996a & 1996b, Moka *et al.*, 2000b, Lorberboym *et al.*, 2003, Schachter *et al.*, 2004, Spanu *et al.*, 2004, Slater & Gleeson, 2005, Ansquer *et al.*, 2008, Carlier *et al.*, 2008, Thomas *et al.*, 2009), whilst others found little or no improvement (Torres *et al.*, 1996, Chen *et al.*, 1997, Ho Shon *et al.*, 2008, Nichols *et al.*, 2008). The quoted sensitivities for ^{99m}Tc -Sestamibi SPECT imaging in these studies range from 54% (Ho Shon *et al.*, 2008) to 98% (Spanu *et al.*, 2004) with the majority being well above 80%. It should be noted, however, that some of these studies differentiate between different types of parathyroid disease whereas others, which tend to have lower overall sensitivity, do not. Also, some studies involved the reviewing of SPECT images only, whilst others used a combination of ^{99m}Tc -Sestamibi SPECT and planar images.

This study found sensitivity values for ^{99m}Tc -Sestamibi planar + SPECT imaging of between 25% and 72% for the 5 observers. Although the values found in different studies in the literature have a similar overall range, the sensitivities found here are generally lower than these other studies. This is most likely due to the fact that the routine practice at GRI is to perform dual-isotope imaging and so the observers are unused to reviewing Sestamibi images without the accompanying ^{123}I -iodide thyroid images. This unfamiliarity resulted in a lack of confidence from the observers in defining possible lesions as positive, leading to a significant reduction in the sensitivity.

Numerous comparisons have also been made of the relative sensitivities of nuclear medicine and ultrasound imaging. Again, there are differences of opinion, with some groups finding ultrasound to be equally or more sensitive when compared to planar imaging (Wakamatsu *et al.*, 2001 & 2003, Berber *et al.*, 2008, Siperstein *et al.*, 2008, Wong *et al.*, 2009), whilst others found it to be less sensitive (Heller *et al.*, 1993) and still others concluded that a combined imaging protocol provided the maximum useful clinical information (Kara Gedik *et al.*, 2008). Comparisons have also been made with SPECT imaging, once more with conflicting results. One study found that ultrasound had a significantly higher sensitivity at 74% than SPECT at 58% (Tublin *et al.*, 2009), whereas others found SPECT to provide improved sensitivity over ultrasound at 91% to 71% (Hara *et al.*, 2007), 82% to 51% (Carlier *et al.*, 2008) and 75% to 56% (Quiros *et al.*, 2004). The present study found a comparable sensitivity from ultrasound imaging at 72%, although this was considerably higher than the sensitivity for ^{99m}Tc -Sestamibi planar + SPECT imaging, for the reasons discussed in the preceding paragraph.

Despite there being a large number of publications relating to the use of SPECT in nuclear medicine parathyroid imaging, the research group led by Donald R. Neumann in Cleveland, Ohio, is the only team to have published work focussing on dual-isotope subtraction SPECT using ^{99m}Tc -Sestamibi and ^{123}I -iodide in the investigation of parathyroid disease. This group has published several studies on the topic (Neumann *et al.*, 1997b, 1998, 2000, 2008), with each study focussing on a different patient sample. For example, the work published in 1997 considered only patients with primary hyperparathyroidism and found an overall sensitivity of 88% in the detection of hyperfunctioning parathyroid glands. The

1998 study concerned only patients with secondary hyperparathyroidism, none of whom had previously undergone parathyroidectomy surgery. On this occasion, the sensitivity of the dual-isotope SPECT was found to be slightly lower at 77%. When only reoperative patients were considered in the 2000 paper, the sensitivity in this group was found to be 100%. A further study in 2008 once again included only patients with primary hyperparathyroidism, although this was a larger sample size than in the 1997 work. The sensitivity reported from the 1998 Neumann study was 71% and the criteria for determining sensitivity were the same as those used in this study.

The present study included all these categories of patients, with primary and secondary hyperparathyroidism and reoperative patients all represented. The sensitivity for dual-isotope SPECT alone ranged from 57% to 85% for the 5 observers, whilst that for dual-isotope planar and SPECT together ranged from 60% to 80%. These values are consistent with those found in the larger sample size study performed by Neumann *et al* in 2008, which were calculated using the same conditions. This confirms that the results of this study are valid and that the significant increase in sensitivity seen when dual-isotope SPECT images are included in the observer review demonstrates a true improvement.

Multi-modality imaging systems are now becoming more common in many centres, and the introduction of SPECT/CT into routine use has provided a new avenue for the investigation of parathyroid disease. Various groups have utilised ^{99m}Tc -Sestamibi SPECT/CT and have found improvements in sensitivity and particularly in specificity in patients who have an ectopic parathyroid adenoma or who have previously undergone neck surgery (Even-Sapir *et al.*, 2001, Gayed, *et al.*, 2005, Krausz, *et al.*, 2006, Lavelly *et al.*, 2007, Papathanassiou *et al.*, 2008, Akram *et al.*, 2009). Once again, only one group has considered dual-isotope subtraction SPECT/CT (Neumann *et al.*, 2008) and found a similar sensitivity when compared with dual-isotope SPECT at 70% vs 71%, but a significantly increased specificity at 96% vs 48%. A SPECT/CT system is now in place at GRI but, unfortunately, was not available in time for any work in this area to be included in this thesis. However, work has now begun in the department to evaluate the utility of dual-isotope subtraction SPECT/CT for parathyroid imaging.

7.1.10 Results with Equivocal Reports Taken as Positive

The different referral pattern for imaging used at GRI compared to many other institutions for patients with hyperparathyroidism and how this may affect the reports given by the nuclear medicine clinicians was outlined in Section 3.1.1. It is acknowledged that, at GRI, there is a greater likelihood of images being reported as equivocal or negative than at many other centres in order to prevent patients undergoing unnecessary surgery. In this study, equivocal reports from the observers were regarded as being negative as there was no definitive localisation of an adenoma. However, the observers were still seeing something they regarded as suspicious on these images, and it is possible that such investigations would be treated as positive at another institution where the patient would be undergoing surgery regardless of imaging results, and that this may account for the differences in sensitivity found in this study when compared to those published in the literature, as discussed in Section 7.1.9 above. In order to assess how this may affect the results of the observer study, the analysis was repeated taking all equivocal results to be positive.

Figure 7.2 shows a comparison of the total number of lesions regarded as positive for adenoma on each phase of the observer study when equivocal results were taken as being firstly negative and then positive. It is clear that the number of positive lesions seen on all 4 phases increases significantly when an equivocal report is regarded as positive. This is to be expected as there were equivocal results given by the observers on all the phases. The greatest percentage increase in the number of positive lesions was for phase 3 at 87%. This confirms that there was a high proportion of equivocal results for this phase, due to the observers' discomfort with reviewing ^{99m}Tc -Sestamibi images in the absence of the ^{123}I -iodide thyroid images.

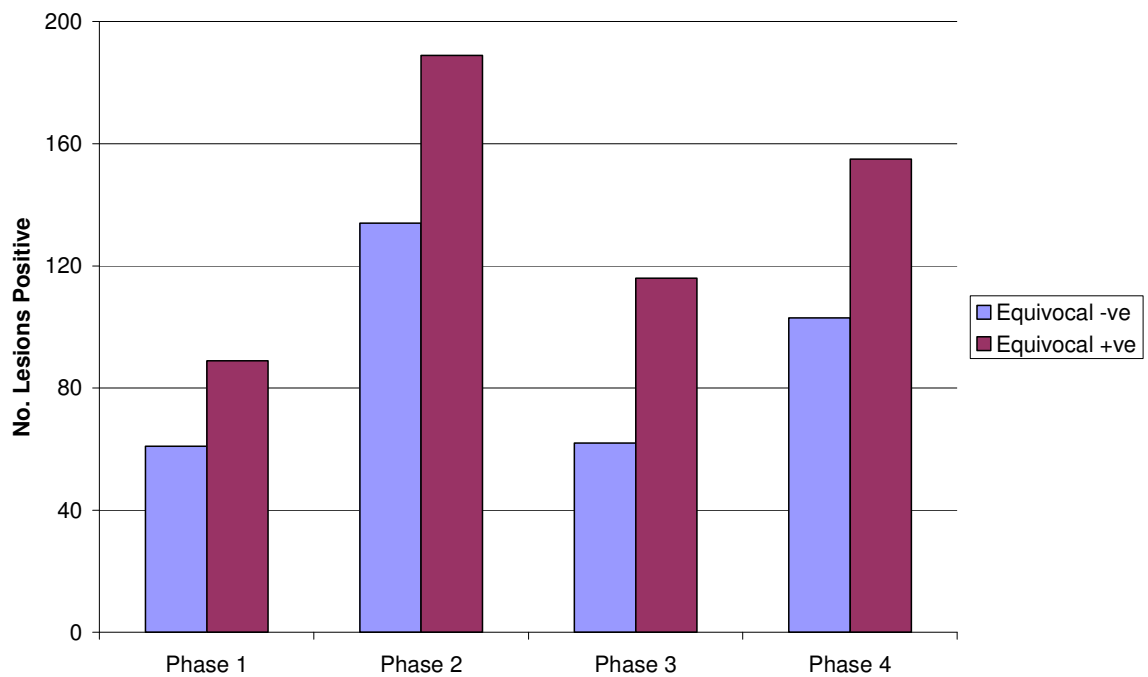


Figure 7.2 - Comparison of number of positive lesions seen when equivocal taken as negative and positive

Bar chart showing the number of lesions given as positive for adenoma by the observers on each of the 4 phases of the observer study (Phase 1 = planar, Phase 2 = SPECT, Phase 3 = Sestamibi only, Phase 4 = all images) when equivocal reports were regarded as negative (blue) and positive (purple).

The given positive/negative report from histological assessment of each gland resected at surgery was then compared to the positive/negative findings from the observer study. Figure 7.3 shows a comparison of the number of times the same positive/negative report was given from surgery and imaging when the equivocal results from the observers were taken to be firstly negative and then positive. The number of times the same conclusion on the status of a gland was reached can clearly be seen to be higher on every phase when the equivocal reports were taken to be positive for the presence of an adenoma.

These findings suggest that regarding lesions reported as equivocal by the observers to be positive for the presence of parathyroid adenoma can significantly affect the results of the comparison of imaging findings with surgical findings. In order to further assess this effect, the sensitivity and specificity for each phase of the study was re-calculated taking equivocal reports as positive and the results were compared to the original values given in Table 7.1. As before, only the given positive/negative and left/right findings were used to calculate the sensitivity and specificity, and the results are shown

in Table 7.4, with those from the original analysis with equivocal taken as negative also shown for comparison.

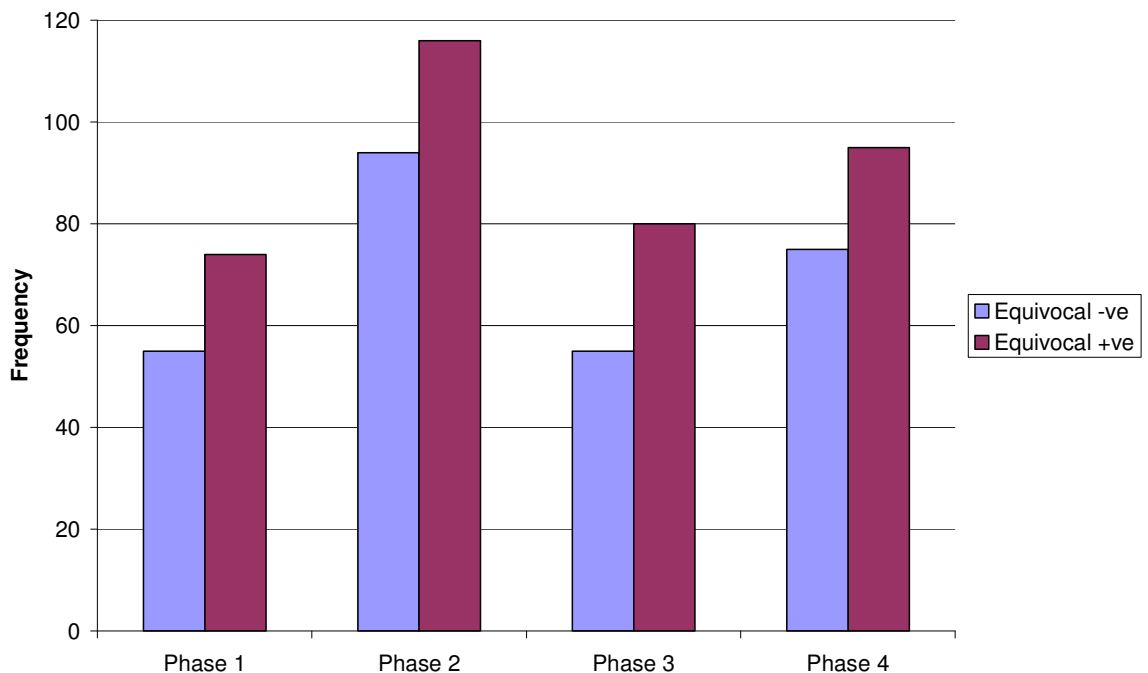


Figure 7.3 - Comparison of number of same positive/negative reports when equivocal taken as negative and then positive

Bar chart showing the number of times the same positive/negative report was given for each gland removed at surgery as compared to each lesion reported by the observers on the 4 phases of the observer study (Phase 1 = planar, Phase 2 = SPECT, Phase 3 = Sestamibi only, Phase 4 = all images) when equivocal reports were regarded as negative (blue) and positive (purple).

Study Phase	Sensitivity (%) Equi -ve	Sensitivity (%) Equi +ve	Specificity (%) Equi -ve	Specificity (%) Equi +ve
1 (planar)	49	67	61	25
2 (SPECT)	77	87	31	3
3 (Sestamibi)	45	69	29	9
4 (all images)	64	82	27	8

Table 7.4 - Sensitivity and specificity results for equivocal taken as negative and positive
Calculated overall sensitivity and specificity relative to the surgical gold standard for each phase of the observer study firstly taking equivocal reports as negative (Equi -ve) and then positive (Equi +ve).

The calculated sensitivity and specificity values in Table 7.4 clearly show that taking equivocal reports as positive leads to a significant increase in the sensitivity but with an associated decrease in the specificity. The former is due to an increase in the true positive rate for lesions that were previously classed as false negative, whereas the latter is due to an increase in the number of false positive reports that were previously true negatives. The sensitivity values when

taking equivocal reports as positive, particularly for phases 2 & 4 which included the dual-isotope subtraction SPECT images at 87% and 82% respectively, are more similar to the values found by other research groups, as discussed in Section 7.1.9 above. Although the specificity is very poor, it is important to note that, as discussed previously, the specificity is highly dependent on the true negative rate. Since there were only 2 true negatives recorded at surgery, the calculated specificity values are likely to be unreliable.

These results confirm that the standard patient pathway and referral pattern used at GRI has a strong influence on the way that imaging studies are reported. Lesions which may be reported as positive at other centres that use a different referral pattern are given as equivocal at GRI. Taking these equivocal reports to be positive gives similar sensitivity values to those seen in studies carried out at other institutions. However, the specificity is considerably reduced due to an increase in the number of false positive reports. In a situation where it has already been confirmed that the patient will undergo surgery, a false positive report is of little consequence as the surgeon will simply look elsewhere in the neck if a suspicious gland is not seen at the location suggested by the imaging report. In contrast, if the decision to perform surgery is dependent on the result of the imaging investigation, a false positive report could lead to unnecessary surgery being carried out and so is therefore undesirable. Should the referral pattern at GRI change in the future, it will be necessary for the nuclear medicine clinicians to modify their reporting techniques to reflect the different emphasis required from the results.

7.2 Conclusions

The inclusion of dual-isotope subtraction SPECT images in the investigation of parathyroid disease gave an increase in the number of observed lesions over the use of planar imaging alone. This was coupled with an increase in the confidence level expressed by the observers taking part in the study. Single isotope ^{99m}Tc -Sestamibi imaging including both planar and SPECT imaging provided no significant benefit over dual-isotope planar imaging for the observers. This is mainly due to the fact that standard practice at GRI is to carry out dual-isotope subtraction imaging, and so the observers involved in this

study are not comfortable reporting parathyroid studies without the presence of ^{123}I -iodide thyroid images.

Surgical findings represent the gold standard for parathyroid studies, since histology is the only way to confirm or deny the presence of a true parathyroid adenoma or hyperplastic gland. The phases of the observer study that included dual-isotope subtraction SPECT showed an increase in sensitivity for detecting true parathyroid adenomas at the correct lateral location in the neck over the other phases. This indicates that dual-isotope subtraction SPECT is the preferred method of those considered in this study for parathyroid imaging.

The sensitivity and specificity values found during this study were lower than those found in the literature. The reason for this is not entirely clear but may be due to the methods for determining sensitivity used by other groups. Also, some of the other studies included information from surgery about parathyroid glands that were not resected, giving a larger number of true negative results that would influence the specificity particularly. However, the increase in sensitivity with dual-isotope subtraction SPECT over planar imaging is sufficiently significant to conclude that this is the method of choice for pre-operative localisation of parathyroid lesions.

The results of the comparison between ultrasound imaging and the various phases of the observer study are affected by the fact that, due to standard practice at GRI, the two modalities are not entirely independent for parathyroid imaging. However, it was demonstrated that the inclusion of dual-isotope subtraction SPECT images increases the sensitivity relative to ultrasound imaging, as was the case for the comparison with the surgical findings.

Since the work for this study was carried out, the standard protocol for parathyroid imaging in the Department of Nuclear Medicine at GRI has been altered to include dual-isotope subtraction SPECT. The clinicians felt strongly that the results of this study demonstrated that there were clear benefits in terms of the accuracy of reporting to be gained from including SPECT imaging. Since late 2008, all patients presenting for parathyroid imaging in the department have therefore undergone dual-isotope subtraction SPECT at 15 minutes post-injection of $^{99\text{m}}\text{Tc}$ -Sestamibi and dual-isotope subtraction planar

imaging 2 hours later. All patients are now administered with a standard activity of 900MBq of ^{99m}Tc -Sestamibi, which is considerably higher than the average of 621.9MBq administered to the participants of this study, as well as 20MBq ^{123}I -iodide for the dual-isotope acquisition. The acquisition time for each frame of the SPECT image acquisition has also been increased from 30s to 40s to provide a higher total number of counts and therefore better image quality than was available for this study. Indeed, the second review of the phase 2 SPECT data (Section 7.1.7) took place after this change in routine practice had been implemented, and the observers all commented on the relatively poor image quality of the images for this study in comparison to those now routinely acquired according to the new standard procedure. The clinicians are therefore confident that this new protocol allows them to provide the maximum level of useful clinical information to both the referring clinicians and the endocrine surgeons.

7.3 Suggestions for Further Work

The relatively small number of participants who underwent parathyroidectomy surgery is the main weakness of this study. The main reason for this problem occurring is the way the standard patient pathway is laid out at GRI, meaning that a patient with negative imaging results will most often be managed clinically and not undergo surgery. A researcher carrying out a prospective imaging study can therefore not be certain that any individual patient will be referred for surgery after imaging. This problem could be overcome either by collecting patient image data over a longer time period, resulting in a larger number of participants and more surgical examples, or by extending the study to other centres to include a larger number of patients, some of whom will undergo surgery regardless of the results of imaging examinations.

The work of the group led by Neumann (Neumann, 1992, Neumann *et al.*, 1997b, 1998, 2000, 2008) was carried out with segregation of the different types of hyperparathyroidism, whereas this study included patients with all types of hyperparathyroidism, although primary hyperparathyroidism was most common. Neumann and his team found differences in the detection sensitivity and specificity between patients with primary and secondary hyperparathyroidism

(Neumann *et al.*, 1997b, 1998, 2000), with lesions due to secondary hyperparathyroidism being generally harder to detect than primary parathyroid adenomas. The inclusion of participants with both types of disease in this study may have influenced the results slightly and so, if a larger sample was to be taken to extend this work, segregation of participants would be recommended. The results could then be more directly compared to those from Neumann's various studies published in the literature.

Another problem encountered in this study was the lack of true negative results from surgery, which is mainly attributable to the high specificity of the experienced endocrine surgeon in identifying parathyroid adenomas or hyperplastic glands and the fact that the decision to send a patient for surgery is based on the results of imaging studies. This meant, however, that the specificity results from the comparison of the observer study findings with those from surgery are somewhat unreliable, as the specificity is so heavily dependent on the true negative rate. Again, a larger study sample would go some way to improving the situation, but it is recognised that the problem is likely to remain to some extent because of the aforementioned high specificity of the endocrine surgeons.

There were also sometimes significant differences in the results for each of the individual observers. Further work involving consensus reporting by two or more observers may be useful in determining why these differences exist and if improvements to the sensitivity and/or specificity can be made. Standard practice at GRI is for an individual consultant physician or radiologist (observers 1-3) to report images, usually in the presence of an experienced nuclear medicine clinical scientist (observers 4 & 5).

A further development that would be interesting to study would be the use of dual-isotope subtraction SPECT/CT in parathyroid imaging. Indeed, the group led by Neumann has carried out some preliminary work on this topic (Neumann *et al.*, 2008), which suggests that the inclusion of the registered CT data in conjunction with $^{123}\text{I}/^{99\text{m}}\text{Tc}$ -Sestamibi subtraction SPECT increases the specificity of parathyroid imaging. As mentioned previously, the department at GRI is now using dual-isotope subtraction SPECT routinely but also now has a SPECT/CT system and work is now being carried out to assess the utility of SPECT/CT for

parathyroid patients. This work is not well enough advanced to be discussed here, but it is hoped that a sufficient body of data will be built up to allow reasonable assessments of the relative merits of imaging with and without CT to be made.

Chapter 8 – Thyroid Uptake Calculations from SPECT Images

8.1 Introduction

8.1.1 Nuclear Medicine Thyroid Studies

It has been known for many years that the thyroid gland is responsible for the production of various hormones which regulate metabolism (Martini, 2001, Moore & Agur, 2007). These hormones contain iodine as an important component and it was quickly realised that iodine from the bloodstream accumulates in the thyroid via an ion-concentrating mechanism. The thyroid then metabolises trapped iodide ions to create the thyroid hormones. Since the introduction of nuclear medicine imaging, this tendency to accumulate iodine has been utilised to assess the function of the thyroid gland. Although ultrasound imaging is still used extensively to assess the anatomy and morphology of the thyroid, it cannot provide functional information in the way that nuclear medicine is able to (Sharp *et al*, 1998).

Initial work on nuclear medicine studies of the thyroid was carried out using the fission product ^{131}I -iodide and a scintillation detector connected to a multi-channel analyser to measure the total counts detected and hence calculate a percentage uptake value for the thyroid. However, ^{131}I has a long half-life of 8.04 days and produces beta radiation as well as high energy gamma emissions (364keV). Patients therefore received a high radiation dose, particularly to the thyroid itself, and the gamma photons produced were of a higher energy than is ideal for detection. The radiation burden for the patient could be reduced by chemically blocking the metabolism of iodine in the thyroid using drugs such as methimazole or propylthiouracil (Andros *et al*, 1965, Esser *et al*, 1973), but the problems with detection of the emitted photons remained. Images could be acquired using a rectilinear scanner or a gamma camera, but the quality was poor.

The radioactive iodine uptake (RAIU) measurement quickly became an important tool in the diagnosis of thyroid disorders as it gave a direct measure of the thyroid function. However, good quality images of the gland were also becoming increasingly important to clinicians, especially in cases of nodular thyroids (Sharp *et al*, 1998). The functional nuclear medicine images were able to distinguish between nodules that had increased function relative to the surrounding thyroid tissue (“hot” nodules) and those that had decreased function (“cold” nodules). Other thyroid diseases also produce characteristic abnormal patterns (Smith & Oates, 2004) which can aid in diagnosis. Isotopes that would give higher quality images than ^{131}I were therefore sought.

Other radioactive isotopes of iodine, such as ^{123}I and ^{125}I , soon became available and were considered as possible replacements for ^{131}I in thyroid studies. However, although ^{123}I has an acceptably short half-life of 13 hours and a gamma emission in the ideal energy range for scintillation detection and hence gamma camera imaging at 159keV, it can only be produced by a cyclotron and is therefore considerably more expensive than products containing $^{99\text{m}}\text{Tc}$ as the radioisotope. Similarly, although ^{125}I is reactor produced and is therefore less expensive, it also has disadvantages as it has a very long half-life of 59.9 days and low gamma energy of 27 - 36keV (Delacroix *et al*, 2002) and so again will give a large radiation dose to the patient with poor detection capabilities.

By the mid-1960s, it had been discovered that the pertechnetate ion was also concentrated in the thyroid gland (Andros *et al*, 1965). In fact, the initial distribution of pertechnetate throughout the body is similar to that of iodine, with concentration in the thyroid, the salivary glands and the stomach. Although the thyroid does not metabolise the pertechnetate, it appears to accumulate the ion using the same ion-concentrating mechanism that takes iodine into the gland (Andros *et al*, 1965), giving uptake results similar to those found with a blocked thyroid gland, but the exact mechanism for pertechnetate trapping within the thyroid remains unknown (Sharp *et al*, 1998). The radioactive isotope $^{99\text{m}}\text{Tc}$ was already commonly used in nuclear medicine because of its short half-life and ideal gamma photon energy of 140keV for detection using a scintillation device, and so radioactive pertechnetate was easy to acquire. Indeed, the standard eluate from a $^{99\text{m}}\text{Tc}$ generator flushed with

sterile saline is sodium pertechnetate and so substantial amounts of this radiopharmaceutical can be readily and cheaply obtained.

Although ^{99m}Tc -pertechnetate has been used in nuclear medicine studies for many years, there are relatively few models that describe the distribution of the radiopharmaceutical in the body. Several authors have described compartmental models of pertechnetate distribution and uptake within the thyroid (Andros *et al*, 1965, Atkins & Richards, 1968, Shimmins *et al*, 1968, Hays & Berman, 1977, Hays, 1978, Hilditch & Alexander, 1980, Okada *et al*, 2003) with various methods of introducing pertechnetate into the body and measuring its distribution.

In 1988, the International Commission on Radiological Protection published a report (ICRP, 1988) giving biokinetic data for a wide range of commonly used radiopharmaceuticals. For ^{99m}Tc -pertechnetate, the model for uptake in the thyroid takes the form of a bi-exponential with one rapid washout component of half-life 60 minutes and another, much slower, washout component of half-life 600 minutes. The rapid component accounts for 85% of the washout, whilst the slower component accounts for 15%. The model therefore takes the mathematical form:

$$A = A_0(0.85e^{-(t/60)} + 0.15e^{-(t/600)})$$

Equation 8.1

where A is the activity in the thyroid gland at time t, A_0 is the initial activity in the thyroid and t is the time since injection of the ^{99m}Tc -pertechnetate in minutes. The model assumes that the thyroid accumulates a total of 2% of the initial injected activity and therefore this is the value for A_0 . The uptake of the thyroid gland as a percentage of the initial injected activity can therefore be calculated at any subsequent time t using the model.

8.1.2 The Thyroid Uptake Measurement

The percentage uptake of radioactive iodine or pertechnetate is a useful diagnostic aid in thyroid diseases. Although it is not normally used as a

definitive diagnosis for hypo- or hyperthyroidism - biochemical markers of the levels of thyroid hormone in the blood are more accurate - the uptake is often used to differentiate different types of disease; for example, it is often used to distinguish between Graves' disease and other hyperthyroid conditions (Sharp *et al*, 1998).

A measurement of uptake of radioactive iodine rapidly became commonplace for patients with thyroid disorders after the introduction of routine nuclear medicine investigations in the 1960s. The patient was given an oral or intravenous administration containing ^{131}I (or later ^{123}I or ^{125}I) in the form of sodium iodide. The uptake measurement would then be carried out 24 hours later, when the uptake in the thyroid gland was approximately at its peak. The introduction of $^{99\text{m}}\text{Tc}$ -pertechnetate for thyroid imaging allowed the uptake to be measured in a same-day procedure, meaning that the patient was not required to attend for 2 appointments on consecutive days (Wagner *et al*, 1999).

For many years, the uptake measurement was carried out using a dedicated counter system. A single sodium iodide scintillation crystal of typically 5cm diameter was optically linked to a photomultiplier tube, which was in turn connected to a multichannel analyser (Sharp *et al*, 1998). In front of the crystal, a tapering lead collimator would be mounted to prevent extraneous counts from being measured in the detection system. The counter would be positioned a set distance from the neck of the patient and the counts in the neck area over a set period of time would be noted. The distance between the patient and the counter and also the acquisition time varied between institutions (e.g. Andros *et al*, 1976, Atkins & Richards, 1968, Hays & Berman, 1977) but the technique was consistent at each individual institution. A standard of known activity was also counted in the same geometry in order to perform an absolute calculation of the percentage uptake in the thyroid. The standard activity was placed in a special neck phantom to simulate the attenuation of the gamma photons by the soft tissues of the neck between the thyroid gland and the detector.

Since the counter positioned over the neck would record counts that were not in the thyroid but were present in the extrathyroidal blood pool or other spaces, a background subtraction was required to obtain the true thyroid counts. Uptake measurements with radioactive iodine commonly used a second counter placed

over the thigh to measure the blood pool activity (Atkins & Richards, 1968, Sharp *et al*, 1998). However, initial measurements with pertechnetate found some difficulties with this technique, primarily due to the fact that the pertechnetate uptake must be carried out soon after injection as the pertechnetate is not organically bound in the thyroid and so is rapidly lost from the gland (Shimmins *et al*, 1969). This leads to a high background activity in the neck and a poorer target: background ratio than is achieved with iodine (Andros *et al*, 1976, Hays, 1978).

In order to overcome these problems, some groups began to acquire scanning images of the neck using a rectilinear scanner (Atkins & Richards, 1968, Shimmins *et al*, 1968 & 1969 Andros *et al*, 1976) or a multicrystal camera (Hays, 1978). The thyroid could then be visualised along with the activity surrounding it. A region of interest (ROI) could be applied around the thyroid, excluding most of the extrathyroidal activity. The counts within the ROI were then used to perform the uptake calculation. Background subtraction was still performed, but an ROI below the thyroid was used, rather than the thigh as was previously the case. The ROI below the thyroid would give a better estimation of the extrathyroidal activity in the neck whilst ensuring that the salivary glands - which also concentrate iodine and pertechnetate - were outwith the region.

From the early 1970s onwards, the gamma camera became more commonly used for the pertechnetate uptake measurement (Esser *et al*, 1973). The main advantage of the gamma camera was that good quality images of the thyroid could be acquired simultaneously, reducing the total examination time considerably. This technique does, however, require a larger activity to be given to the patient to ensure a sufficiently high count rate for imaging (Wagner *et al*, 1999). The uptake measurement is carried out by taking the counts in a thyroid ROI and a background ROI placed below the thyroid. A standard image must still be acquired to allow the absolute quantification to be carried out (Vahjen *et al*, 1992).

Several studies have been performed to determine the best time post-injection at which to carry out the uptake measurement. Atkins & Richards (1968) suggested that an uptake measurement at 20 minutes post-injection would give a result similar to a 24 hour iodine uptake. Esser *et al* (1973) created uptake

curves over a 30 minute period after injection and were unable to find any pattern linking the shape of the uptake curve with the underlying disease type. However, they noted that an uptake measurement at 20 minutes post-injection would give a result within 94.5% of the maximum value, on average. The uptake measurement is now routinely carried out at 20 minutes in most institutions, including Glasgow Royal Infirmary (GRI).

As mentioned previously, different institutions will use different geometries for acquiring the information for the uptake measurement. However, it is important that each institution is consistent in its own measurements, so that uptake values can be directly compared between patients and also between similar measurements carried out on the same patient at different time points. The normal range must also be defined independently by each institution as the measurement geometry and the phantom used for the standard acquisition can have a significant effect on the final result (Vahjen *et al*, 1992).

8.1.3 Glasgow Royal Infirmary Thyroid Clinic

The Nuclear Medicine department at GRI runs a thyroid clinic each Monday afternoon. Patients with known or suspected thyroid disease are referred to the clinic for imaging and an assessment by a nuclear medicine physician. Around 10 - 12 patients attend the clinic each week.

When a patient attends the clinic, they firstly undergo thyroid imaging with an associated uptake measurement. The patient is given an intravenous (IV) injection of ^{99m}Tc -pertechnetate and is imaged 20 minutes later. The first image is a 60 second (s) anterior planar view of the neck, with the patient at a standard distance from the face of the gamma camera collimator, which is used to calculate the percentage uptake of pertechnetate in the thyroid (see Section 8.2.2 for details of the uptake calculation). A second image with a marker denoting the sternal notch is then acquired, which gives the reporting physician information on the anatomical location of the thyroid and any unusual features within or around the gland. The third and final image is acquired for 5 minutes and encompasses a wider field of view to include the chest area and highlight any ectopic thyroid tissue or other abnormality.

After imaging, the patient is assessed by a consultant nuclear medicine physician. The physician reviews the images as well as the patient's clinical history and symptoms in order to diagnose any disease that is present and to determine the best course of treatment. Around 25 - 30% of the patients attending the clinic require radio-iodine treatment for thyrotoxicosis and will return to the department at a later date to be administered ^{131}I -iodide as a drink by one of the physicists.

An average clinic appointment will last for around 45 minutes, although the length of time can vary. For this study, patients were asked to remain in the department for a further 30 minutes after consulting the physician so that a SPECT acquisition could be carried out.

8.2 Materials and Methods

8.2.1 Study participants

The study received approval from the local research ethics committee (LREC) at GRI in combination with the parathyroid study discussed previously. Further details of the ethics application and approval granted can be found in Section 3.1.3.1 and Appendix A of this thesis.

All patients referred to the thyroid clinic between February 2006 and October 2008 were sent a copy of the patient information sheet and consent form for the study (see Appendix B). Patients who expressed an interest in the study were given the opportunity to speak to the principal researcher or another member of staff privately. Those who were willing to take part were then asked to sign the consent form. Time constraints on the clinical service in the department meant that the number of study patients that could be accommodated each week ranged from 0 to a maximum of 3. Once the maximum number of patients for a session had consented to take part, consent was not sought from any others, even if they had initially expressed an interest in taking part.

The SPECT acquisitions were performed after the patients had completed their appointments in the thyroid clinic in order to prevent disruption to the routine provision of the clinic service. As waiting times between planar imaging and the

consultation with a clinician as well as the length of the consultation for each patient varied, this resulted in a wide spread of times between injection and SPECT scanning. In contrast, the injection to planar scanning time was constant at as close to 20 minutes as possible, as per the departmental protocol for the thyroid clinic.

A total of 60 patients initially gave consent to take part in the study. However, time constraints within the thyroid clinic meant that 3 of the patients did not undergo SPECT scanning. Therefore, 57 thyroid SPECT acquisitions were performed.

From February 2006 to April 2007, each patient attending the thyroid clinic received an intravenous injection of around 180MBq ^{99m}Tc -sodium pertechnetate 20 minutes prior to planar imaging. This injected activity is considerably higher than the usual limit of 80MBq set by the Administration of Radioactive Substances Advisory Committee (ARSAC). However, specific approval had been given by ARSAC to the department at GRI to give the higher activity, provided that a drink of 20mg sodium perchlorate solution was given to each patient after imaging to wash the pertechnetate out of the thyroid gland and reduce the radiation dose to the same level as that for an administration of 80MBq. From May 2007 onwards, each patient received an intravenous injection of 80MBq ^{99m}Tc -sodium pertechnetate, which is the ARSAC limit for thyroid imaging. Of the study participants, 37 therefore received an injected activity of 180MBq and 20 received an injected activity of 80MBq. Those participants scanned before May 2007 had their sodium perchlorate drink delayed for the 15 minute period required for the SPECT acquisition.

The activity in the syringe before the injection and the residual activity in the syringe after injection were measured using a Capintec isotope calibrator and were recorded for all patients to allow an absolute measure of thyroid uptake to be calculated.

8.2.2 Planar Uptake Measurements

The thyroid uptake was calculated from an anterior planar image at 20 minutes post injection for every patient. This is part of the standard protocol for

patients attending the thyroid clinic. The patients are seated in front of a gamma camera with the neck a standard distance (12cm) from the face of a low energy, high resolution collimator. A 60s anterior planar image is then taken. A 60s standard image of a known activity is also acquired in order to determine the sensitivity of the gamma camera in counts/s/MBq. The percentage uptake of ^{99m}Tc -pertechnetate in the thyroid gland is then calculated using a program supplied with the department's HERMES computer system (Nuclear Diagnostics Ltd.), which applies a decay correction for the physical decay of the ^{99m}Tc between the time of injection and imaging.

The departmental normal range for thyroid uptake is 0.5% - 4.0%. If a patient has a calculated uptake of <0.5%, he or she is deemed to be hypothyroid. Similarly, patients with an uptake of >4% are classed as hyperthyroid.

8.2.3 SPECT Acquisition

All acquisitions were performed on a double headed Philips ADAC Forte gamma camera with the patient lying supine and using a head rest to ensure the head and neck remained still throughout the acquisition. As for the parathyroid imaging, the camera heads were placed at a relative angle of 90° . The initial SPECT acquisition protocol was established assuming an injected activity of 180MBq. The acquisition parameters were as follows: 128^2 matrix, energy window at $140\text{keV} \pm 10\%$, parallel hole high resolution (VXHR) collimators, 180° circular anterior rotation, 60 frames, 30s acquisition time per frame. A roving zoom of a 30cm square centred on the thyroid gland was also applied to the acquired frames.

The total imaging time for this protocol was felt to be long enough to allow reasonable counts to be acquired in each frame but short enough to be comfortable for the patients and to keep the risk of patient movement to a minimum.

When the injected activity was reduced to 80MBq in May 2007, the acquisition time per frame was increased from 30s to 40s to ensure adequate counts per frame were maintained for each acquisition giving a total imaging time of 20 minutes. This increase in time per frame was not in proportion to the decrease

in administered activity for two main reasons. The first was that it was felt unlikely that participants could lie still for significantly longer than 20 minutes, meaning that a longer scan time would lead to a considerable increase in the risk of motion artefacts in the SPECT images. The second reason was that this study was being carried out in a working clinical department, meaning that gamma camera time was at a premium and long scanning times were not possible. It was therefore felt that an increase in the acquisition time per frame from 30s to 40s would allow adequate counts to be acquired in each frame whilst keeping the total imaging time to an acceptable level.

In order to carry out a calculation of the absolute uptake, it was necessary to acquire an acquisition of a standard of known activity for each patient acquisition and use the images to determine the sensitivity of the gamma camera in counts/s/MBq. The thyroid phantom designed for this study (see Chapter 2 for further details) was used for the standard SPECT acquisition. A known activity in the region of 10MBq of ^{99m}Tc -pertechnetate was added to the phantom's thyroid insert and a SPECT acquisition was carried out using all the same parameters as for the patient acquisitions with the exception of the frame time. This was reduced to 10s per frame, meaning a total acquisition time of 5 minutes, to keep the imaging time to a minimum. When multiple patient acquisitions were performed on one day, a single standard was acquired and applied to all the patient data sets for that day.

Since the activity of ^{99m}Tc decays over time and also that the ICRP model of thyroid uptake (ICRP, 1988) depends upon time post injection, the time at which each SPECT acquisition began was noted. The times at which the standard activity was measured and the standard SPECT acquisition commenced were also noted so that a decay correction for the total activity in the phantom at the time of acquisition could be carried out. This would then allow an accurate measure of the gamma camera sensitivity to be made.

8.2.4 SPECT Image Reconstruction

All SPECT images - both patient and standard data - were reconstructed using the Ordered Subsets Expectation Maximisation (OSEM) iterative algorithm on the HERMES computer system. The reconstruction was performed using 15 subsets

and 4 iterations with no scatter correction applied. A post-reconstruction filter was then applied to smooth the data. This filter was chosen after a trial-and-error process to find a filter that gave the best compromise between sharpness and excessive image noise.

A further reconstruction that included attenuation correction (AC) was carried out on 20 of the patient data sets. The results of the uptake calculations from the two reconstructions could then be compared to determine if performing AC affects the uptake value. A uniform attenuation correction of $\mu=0.12\text{cm}^{-1}$ was included in the iterative reconstruction algorithm. Again, a post-reconstruction filter was applied to smooth the resulting SPECT images. The images of the standard for each of the 20 patient data sets were also attenuation corrected before the uptake calculation was performed. Since the thyroid lies very anterior in the neck with little overlying tissue to cause significant attenuation of the 140keV gamma photons from the $^{99\text{m}}\text{Tc}$ emission, performing the attenuation correction on the SPECT data was not expected to result in a significant difference in the calculated thyroid uptake. However, large thyroid glands may have a degree of self-attenuation associated with them, which may lead to significantly different results when an attenuation correction is applied.

8.2.5 Volume of Interest Definition

In order to calculate the uptake, it was necessary to determine the total number of counts in the thyroid for both the patient and standard data by creating a volume of interest (VOI) outlining the thyroid gland on each set of SPECT images. Several possible methods of VOI definition were examined. Ideally, the VOI would be defined as a whole from the full 3D data set using a threshold value, whereby all the pixels with a value greater than a certain percentage of the maximum counts are enclosed within the VOI. However, when this was attempted with the available HERMES software, it was not possible to outline the thyroid satisfactorily. An example data set with the poor VOI definition is shown in Figure 8.1, with the VOI shown in red on single reconstructed coronal (a), sagittal (b) and transverse (c) images. It can clearly be seen that the thyroid as a whole is not correctly outlined. When a lower threshold value was chosen, large amounts of background were included in the VOI, which is equally

unacceptable for an uptake calculation. This was the case for all the patient data sets and so a different method of VOI definition was required.

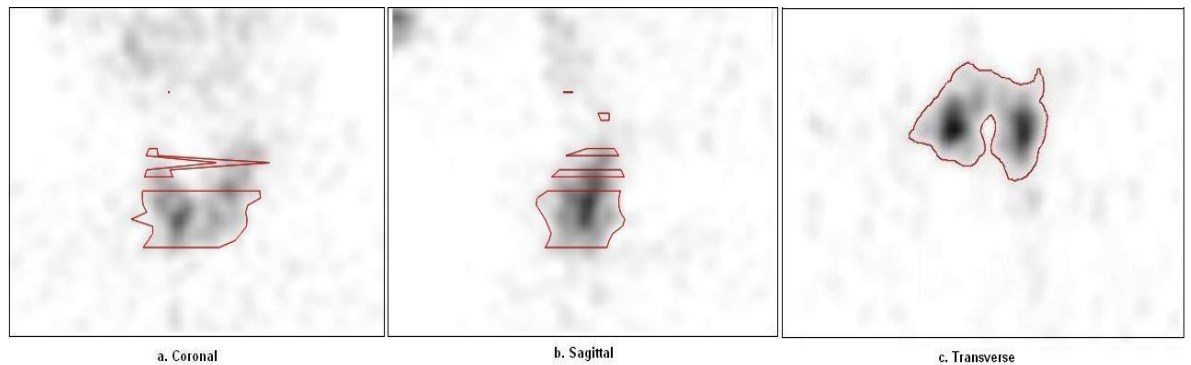


Figure 8.1 - Threshold VOI
Automatic VOI (shown in red) created on thyroid SPECT images using a threshold technique.

Instead of defining a full VOI, it is possible to achieve the same result by creating thyroid regions of interest (ROIs) on all the slices on which the thyroid is visible. Various methods of ROI definition can be used, including seed, threshold or hand-drawn regions. The seed method involves the selection of a “seed” pixel from which the ROI is grown along lines of equivalent counts until the necessary area is enclosed. The threshold method is similar to that described above for the definition of a VOI. The final method involves an operator manually drawing the ROI on each slice on which the thyroid is visible and so is more labour-intensive than the other methods. It should also be noted that any of the 3D projections (coronal, sagittal and transverse) can be used to create these ROIs.

The technique chosen for this study was to use the transverse slices to define the ROIs as it was felt that the thyroid was more readily distinguished from the background activity on this projection. Each of the methods of ROI definition were then tested on a number of patient and standard data sets to see which would give the most acceptable results.

An example ROI using the seed method is shown in Figure 8.2. The ROI produced by this method is too large and includes a significant amount of background area as well as the thyroid gland itself. If the ROI was grown to a lesser extent (i.e. not grown so far from the seed value), it would only encompass one thyroid lobe

and would also not be acceptable for the uptake calculation. This seed method was therefore rejected.

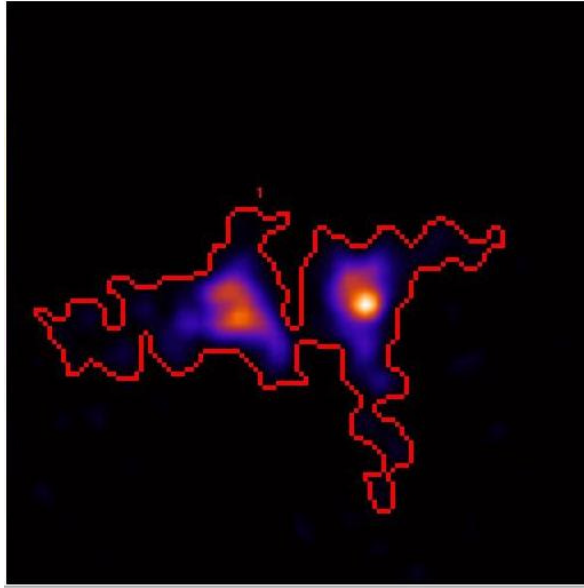


Figure 8.2 - Seed ROI
Example of ROI produced on transverse SPECT slice using the seed method

The threshold method, which allowed steps of 1% in the threshold value, was also investigated, and example ROIs defined using the method are shown in Figure 8.3. The slice shown is the same slice from the same patient data set that is shown in Figure 8.2. It can be seen that the higher threshold ROI (12%) only encloses one lobe of the thyroid whilst the lower threshold value (11%) produces an ROI that is too large and includes a significant area of background activity. This situation occurred on several slices on most of the patient data sets and so the threshold method was also rejected as being unsuitable for this study.

The major problem encountered with the seed and threshold values was the inability of the system to select both lobes of thyroid when they were separated on the image slice by an area of background activity. Since the isthmus is small and is only visible on a limited number of slices, this situation occurs on the majority of slices. It was therefore decided that, although more labour-intensive, the hand-drawn method of ROI definition would be used. An example of the ROI produced on the same image slice as those in Figure 8.2 and Figure 8.3 is shown in Figure 8.4. This ROI includes only the thyroid and does not encompass background activity.

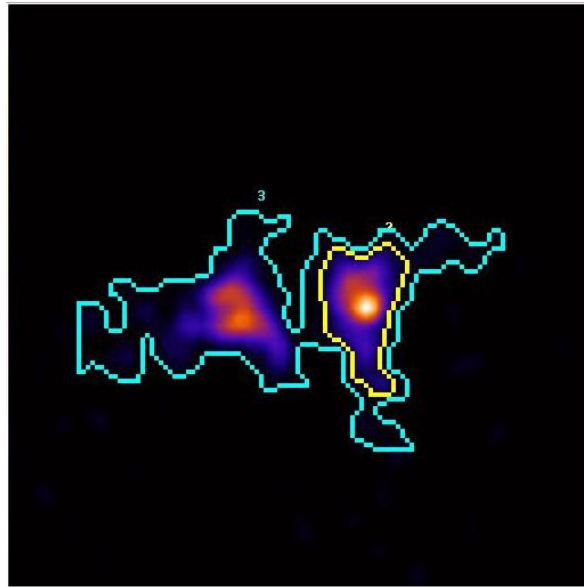


Figure 8.3 - Threshold ROIs

Two ROIs defined using the threshold method at 12% (yellow) and 11% (blue) of the maximum counts in the image

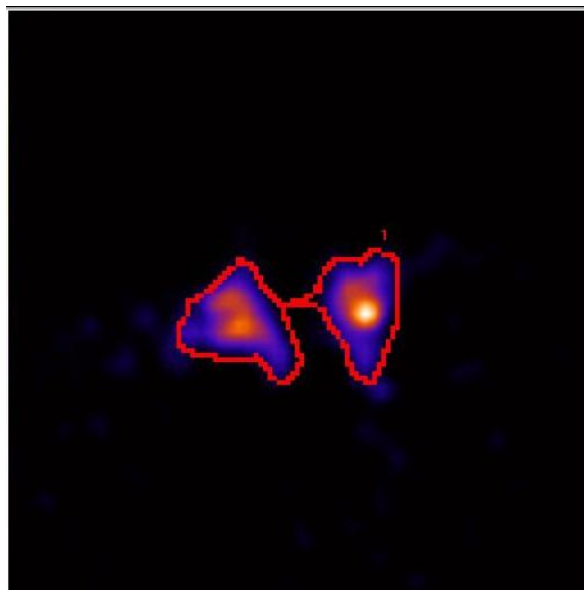


Figure 8.4 - Hand-drawn ROI

Example of ROI produced by an operator manually drawing around the image of the thyroid gland

An ROI outlining the thyroid was therefore hand-drawn on every transverse image slice on which the thyroid was visible for each patient data set. A background ROI was also applied to each slice so that background counts could be subtracted from those in the thyroid to give a more accurate value for each slice. The background region was drawn once for each patient data set and then applied to each slice on which the thyroid was visible. An example of a hand-drawn thyroid ROI with a typical background ROI is shown in Figure 8.5. Similar

ROIs were also drawn on all transverse slices of the standard image data on which the thyroid phantom was visible.

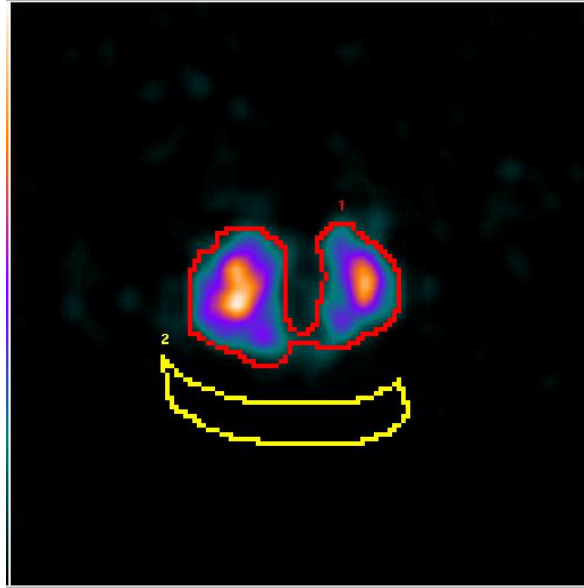


Figure 8.5 - Typical thyroid and background ROIs
Hand-drawn thyroid (red) and background (yellow) ROIs on a transverse image slice

8.2.6 Thyroid Uptake Calculation

The counts and total number of pixels in each ROI on each slice were stored electronically using the HERMES system. The data were then exported from the HERMES computer to a PC and entered into a spreadsheet program (Microsoft Excel) for analysis. A background correction, taking into account the relative areas of the thyroid and background ROIs, was performed on the counts in each thyroid ROI using the following equation:

$$C_{bc} = C_t - \left(\frac{A_t}{A_b} \right) C_b$$

Equation 8.2

where C_{bc} is the background corrected counts, C_t is the total counts in the thyroid ROI, C_b is the total counts of the background ROI, A_t is the area (total number of pixels) of the thyroid ROI and A_b is the area of the background ROI. The background corrected counts on all slices were then summed to obtain the total number of counts in the thyroid gland - that is the counts in the thyroid VOI.

The same background correction was applied to the data from the standard acquisition and the total counts were again summed. This value was then divided by the total acquisition time (5 minutes, 300s) and the known activity in the phantom at the time the SPECT acquisition was started, giving the sensitivity of the gamma camera in counts/s/MBq. This value was then used along with the total counts from the patient thyroid VOI and the known time of the patient SPECT acquisition (15 minutes, 900s, or 20 minutes, 1200s) to give a total thyroid activity in MBq as follows:

$$A_t = \frac{C_t}{S \times T}$$

Equation 8.3

where A_t is the total activity in the thyroid in MBq, C_t is the total counts in the thyroid VOI, S is the gamma camera sensitivity in counts/s/MBq and T is the total acquisition time in seconds.

The percentage uptake of ^{99m}Tc -pertechnetate was then calculated as:

$$U_{\%} = \left(\frac{A_t}{A_s - A_r} \right) \times 100\%$$

Equation 8.4

where $U_{\%}$ is the percentage uptake in the thyroid, A_t is the activity in the thyroid calculated using Equation 8.3, A_s is the activity in the syringe prior to injection and A_r is the residual activity in the syringe after injection. All activities were decay corrected to account for the time differences between the initial measurement of the activity prior to injection and the acquisition of the SPECT images. An identical method was used to find the uptake value from the attenuation corrected SPECT images.

An estimate of the error in the calculated SPECT uptake value was made by re-analysing a total of 15 patient data sets. The differences between the first and second uptake values were found and the error taken to be the standard deviation of these differences.

8.2.7 Uptake Calculation from Single SPECT Frame

A further calculation of the uptake was made using a single anterior frame of the patient and standard SPECT acquisition data. The acquisition frame was 30s long for the early participants in the study (prior to May 2007) and 40s for the later participants. The analysis carried out was identical to that used to calculate the uptake from a planar image. Since there was often a long time delay between injection and the SPECT scan due to the need for the patient to complete their thyroid clinic visit before the additional acquisition, it was hoped that this calculation would provide a more direct comparison between the uptake calculated from planar and SPECT images. For the purposes of clarity, this value will be referred to as the “frame SPECT” uptake throughout the results and discussion sections.

8.2.8 Comparison of Planar, SPECT, Attenuation Corrected SPECT and Model Uptake Values

The ICRP model (ICRP, 1988) was used to determine an expected uptake value at the time of the SPECT acquisition using the measured planar uptake at a known time as the standard value. That is, given the uptake value calculated from the planar images at around 20 minutes post injection, what would the model expect the uptake to be at the time of the SPECT acquisition? The expected value was calculated as follows:

$$U_E = U_p \times \frac{0.85e^{-(t_s/60)} + 0.15e^{-(t_s/600)}}{0.85e^{-(t_p/60)} + 0.15e^{-(t_p/600)}}$$

Equation 8.5

where U_E is the expected percentage uptake based on the model, U_p is the percentage uptake calculated from the planar image, t_s is the time of the SPECT acquisition in minutes post injection and t_p is the time of the planar acquisition post injection, also in minutes.

Comparisons of this expected value and the various calculated uptake values were then made using graphical plots produced using the spreadsheet program.

The method of least squares was used to find the best-fit straight line for each plot, with the equation:

$$y = ax + b$$

Equation 8.6

where a is the gradient and b is the intercept of the straight line.

A statistical software program (Minitab v13) was also used to assess any statistically significant differences between the various uptake values calculated from the image data and the ICRP model. Since, with each comparison, the data were not normally distributed, a non-parametric test was used. The difference between the percentage uptake determined from alternative methods was calculated and a Wilcoxon Signed Ranks test was applied to the results, giving a p -value, an estimated median and a 95% confidence interval (CI) for the difference between the two uptake values being compared. Statistical significance was taken to be a result with $p < 0.05$.

8.3 Results

8.3.1 Patient Demographics and SPECT Imaging Times

A total of 57 patients took part in the study, with 13 males (23%) and 44 females (77%). The average age of the participants was 49.9 ± 13.1 years (mean \pm 1SD) with a range of 20 to 77 years. From the results of the uptake calculated from the planar image as part of the visit to the thyroid clinic, 1 patient was classed as hypothyroid (uptake $< 0.5\%$), 31 patients were classed as euthyroid (uptake $0.5\% - 4.0\%$) and 25 were classed as hyperthyroid (uptake $> 4.0\%$).

All planar scans were taken as close to 20 minutes post injection as possible, with an average time of 24.5 ± 8.0 minutes (mean \pm 1SD) and a range of 5 - 42 minutes. The timing of the SPECT acquisition post injection varied more widely due to the differing times taken for patients to complete their visit to the thyroid clinic. The average scan time was 71.5 ± 17.5 minutes post injection with a range of 40 - 106 minutes. A histogram of the imaging times post

injection for both planar and SPECT acquisitions is shown in Figure 8.6. The wider spread of the time at which the SPECT acquisitions were commenced is clearly seen.

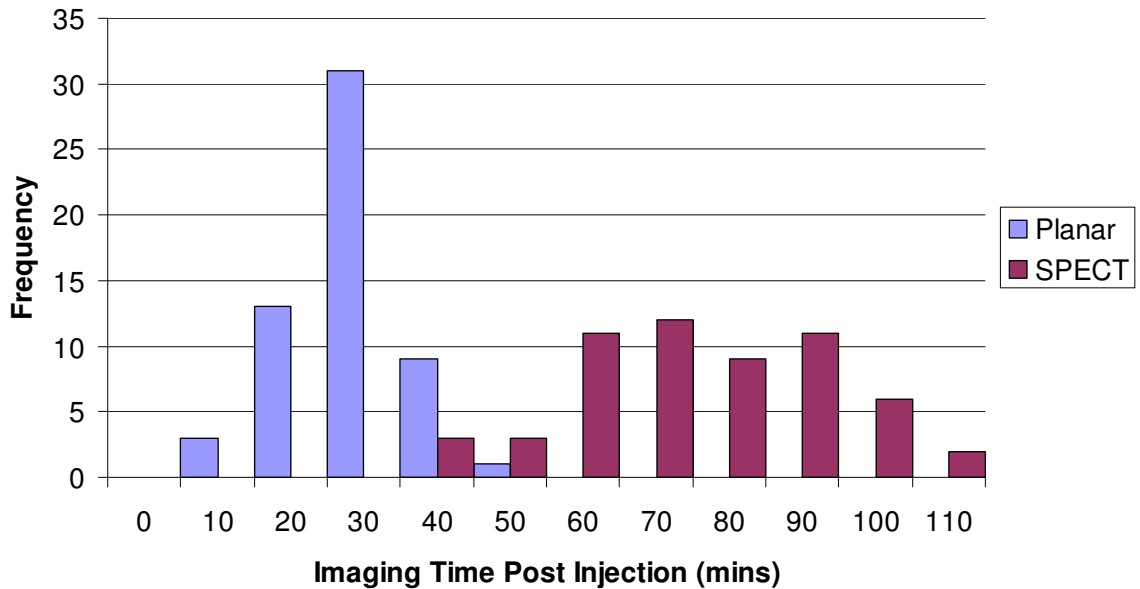


Figure 8.6 - Histogram of imaging time post injection
Histogram showing the time at which each acquisition commenced after injection of ^{99m}Tc -pertechnetate

8.3.2 SPECT Reconstruction

Although the SPECT image data were to be used primarily for uptake measurements and not for clinical evaluation, it was necessary to define parameters for the SPECT reconstruction that gave acceptable image quality. The number of subsets and iterations (15 and 4 respectively) were chosen to give rapid convergence to the physiological distribution of activity. After the iterative reconstruction was complete, the data were filtered to smooth the resultant images. The following filters, with the option to vary certain parameters, which are listed in Section 5.3, are available from the HERMES system: Butterworth, Hanning, Low Pass, Metz and 3x3x3 smoothing. All the filters were tested on a number of patient data sets. For each type of filter, a number of different image data sets were produced after varying the optional parameters. The goal was to produce images with the best compromise between sharpness and excessive image noise over a range of uptakes.

Figure 8.7 shows slices in 3 planes from a patient data set to which a post reconstruction filter that gives images which are too smooth has been applied. The structure of the thyroid cannot be defined from the images. A sharper filter is therefore required to give images of acceptable quality.

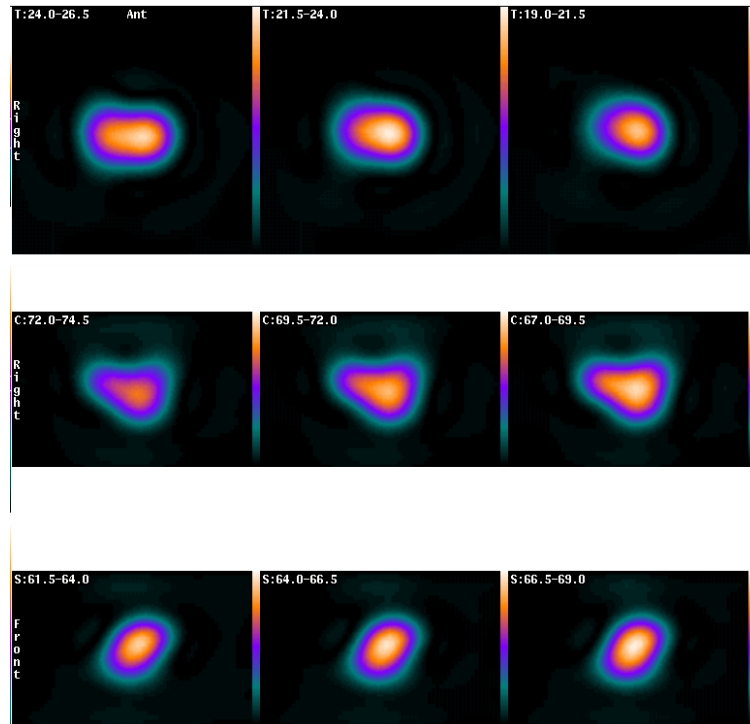


Figure 8.7 - Overly smoothed thyroid SPECT images
 Example of patient thyroid SPECT data that has been overly smoothed by the post reconstruction filter. Figure shows coronal (top), transverse (middle) and sagittal (bottom) slices

In contrast, the same slices are shown in Figure 8.8, but these were produced using a different filter which smoothed the images much less. The resulting images are excessively noisy and so a filter giving a result between those shown in Figure 8.7 and Figure 8.8 was required.

The same slices are shown again in Figure 8.9, showing the images produced when the best compromise post reconstruction filter is applied to the SPECT data. The final choice of filter that was then applied to all data sets prior to the uptake calculation being performed was a Butterworth filter of order 5 and with a cut-off frequency of 2.5 cycles/cm. The choice was made by asking experienced physicians and clinical scientists to review a number of SPECT image

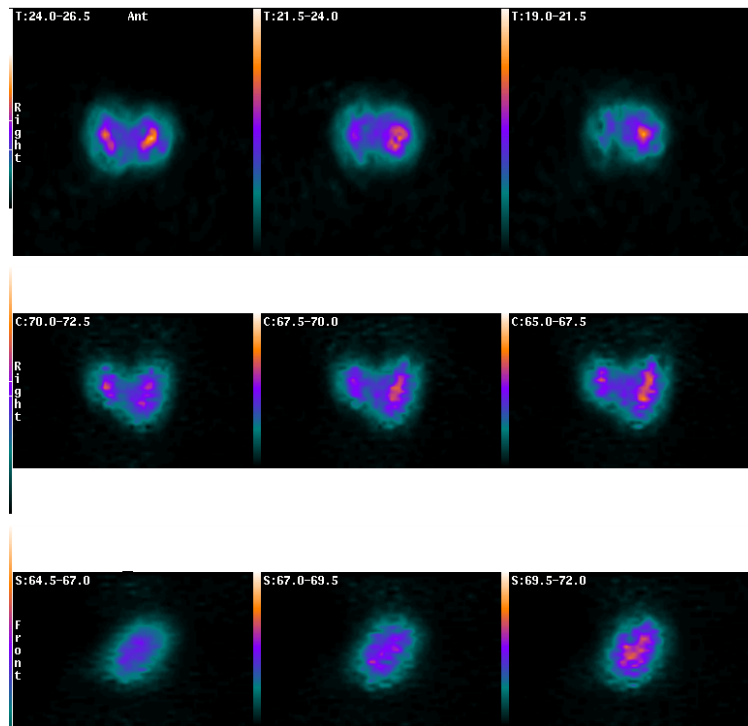


Figure 8.8 - Overly sharp thyroid SPECT images

Example of patient thyroid SPECT data that is too noisy after the application of the post reconstruction filter. Slices are the same as those shown in Figure 8.7.

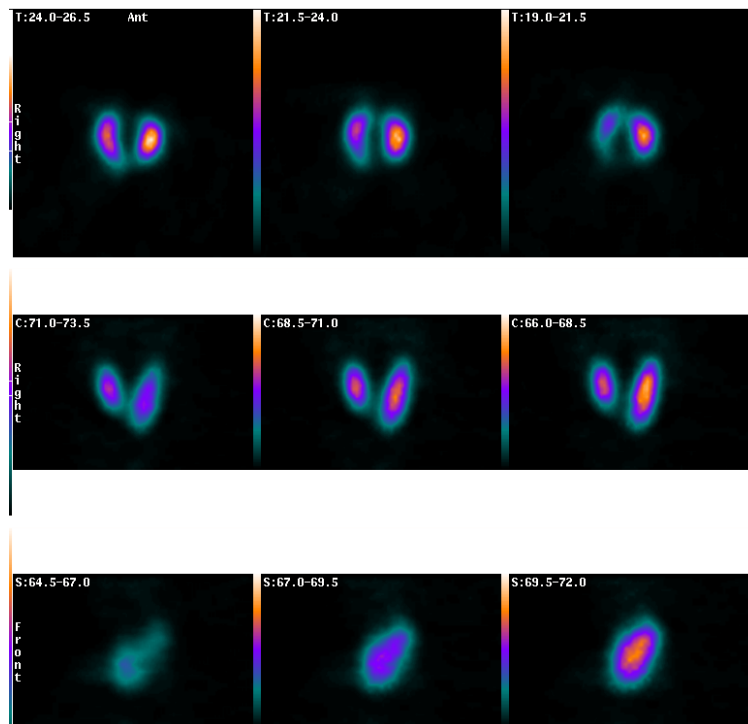


Figure 8.9 - Best compromise thyroid SPECT images

Example of patient thyroid SPECT data with the best compromise post reconstruction filter applied. Slices are the same as those shown in Figure 8.7 and Figure 8.8.

data sets with different post-reconstruction filters applied for each of several different patient acquisitions. The reviewers were asked to assess which images

gave the best compromise between sharpness and excessive noise and the consensus view was taken to be the most appropriate filter for use in this study. The same filter was also applied to all the reconstructed standard data before the ROIs were defined for the sensitivity calculation.

8.3.3 Comparison of Calculated and Modelled Uptake Values

8.3.3.1 Basic Statistics

A basic statistical analysis was carried out on each of the calculated uptake values to give some indication of any differences that may exist before a more thorough analysis was performed. The mean, median, standard deviation, minimum, maximum and 1st and 3rd quartile values were assessed for each type of uptake calculation, and the results are shown in Table 8.1. The data were then analysed in more detail, and the results are given in the following sections.

It is apparent from these results that the mean percentage uptake as measured from SPECT imaging is higher than that measured from planar imaging or calculated from the ICRP model. The minimum, maximum and standard deviation values are also higher for SPECT uptakes. For each parameter considered, the ICRP model gave the lowest value, which was often significantly different from all the others.

Uptake Type	Mean %	Median %	SD %	Min %	Max %	Q1 %	Q3 %
Planar	4.84	3.54	4.40	0.15	18.63	1.40	6.93
SPECT	6.29	4.46	6.22	0.25	26.68	1.79	8.81
Frame SPECT	6.39	4.63	5.89	0.20	25.59	1.71	9.45
AC SPECT	6.45	2.12	9.79	0.97	36.65	1.21	6.90
ICRP Model	2.71	1.76	2.55	0.08	11.10	0.86	3.49

Table 8.1 - Basic descriptive statistics for thyroid uptake results calculated with different methods

SD = standard deviation, min = minimum value, max = maximum value, Q1 = first quartile, Q3 = third quartile.

8.3.3.2 Planar versus SPECT Uptake Values

A spreadsheet program (Microsoft Excel) was used to produce plots to compare the various calculated uptake values. As the uptake of pertechnetate within the thyroid gland is known to vary with time (Andros *et al*, 1965, Atkins & Richards,

1968, Shimmins *et al*, 1968, Hays & Berman, 1977, Hays, 1978, Hilditch & Alexander, 1980, ICRP, 1988, Okada *et al*, 2003), a direct comparison of the uptake values calculated from a planar image using the departmental standard method and a SPECT data set is not strictly valid. Also, the values would not be expected to be exactly the same due to the fact that there will be some self-attenuation of gamma rays within the thyroid gland. This will have the greatest effect on the uptake calculated from a planar image as only a single projection is acquired. SPECT reduces the effect by acquiring data from many different projections, meaning that the self-attenuation is minimised. This effect would be expected to be most pronounced in a large gland due to the greater amount of attenuating material present. However, in order to give a rough indication of the accuracy of the SPECT method - that is, to ensure the method was giving results within the same ballpark - the calculated SPECT value for each patient was plotted against the calculated planar value. The method of least squares was then used to find the best fit straight line to the data. The results are shown in Figure 8.10, with the line of identity shown in pink. All error bars denote $\pm 1SD$. The thyroid uptake value calculated from the SPECT data can be seen to be generally higher than that calculated from the planar image as most of the points on the plot lie above the line of identity. The data do, however, form a good straight line with $r^2 > 0.9$ and gradient > 1 , which again indicates that the SPECT uptake tends to be higher than the planar uptake.

The difference in the percentage uptake value calculated from the two sets of images (planar - SPECT) was also calculated. The Wilcoxon Signed Ranks test was then applied to the difference values. The test gave a statistically significant result with $p < 0.001$, an estimated median of -0.86% and a 95% CI of (-1.61%, -0.43%). The negative estimated median and CI support the finding that the uptake value calculated from the SPECT images for the same patient tends to be higher than that calculated from the planar image.

In order to determine if there was any relationship between the time difference between planar and SPECT image acquisition and the difference in the calculated uptake, the data were plotted and the result is shown in Figure 8.11. The plot shows no obvious trend towards an increasing or decreasing difference

in calculated uptake as the time difference between image acquisitions increases.

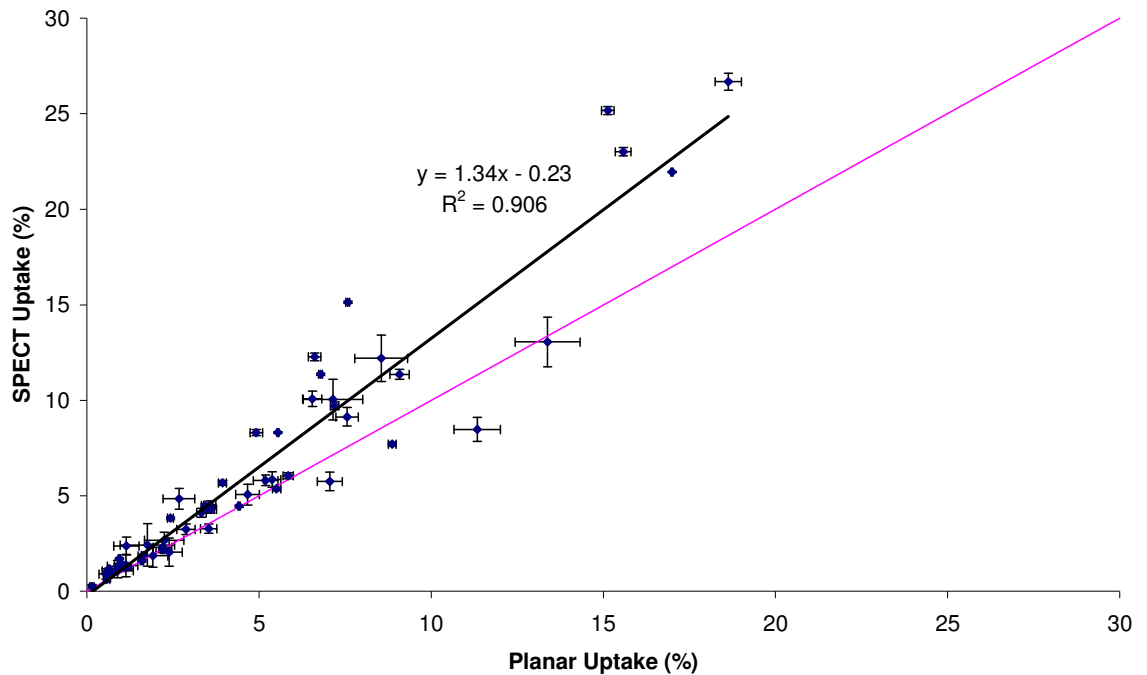


Figure 8.10 - Uptake from SPECT versus uptake from planar images

Plot showing the uptake calculated from the SPECT data against the uptake from the anterior planar image with a straight line fit added. The line of identity is shown in pink.

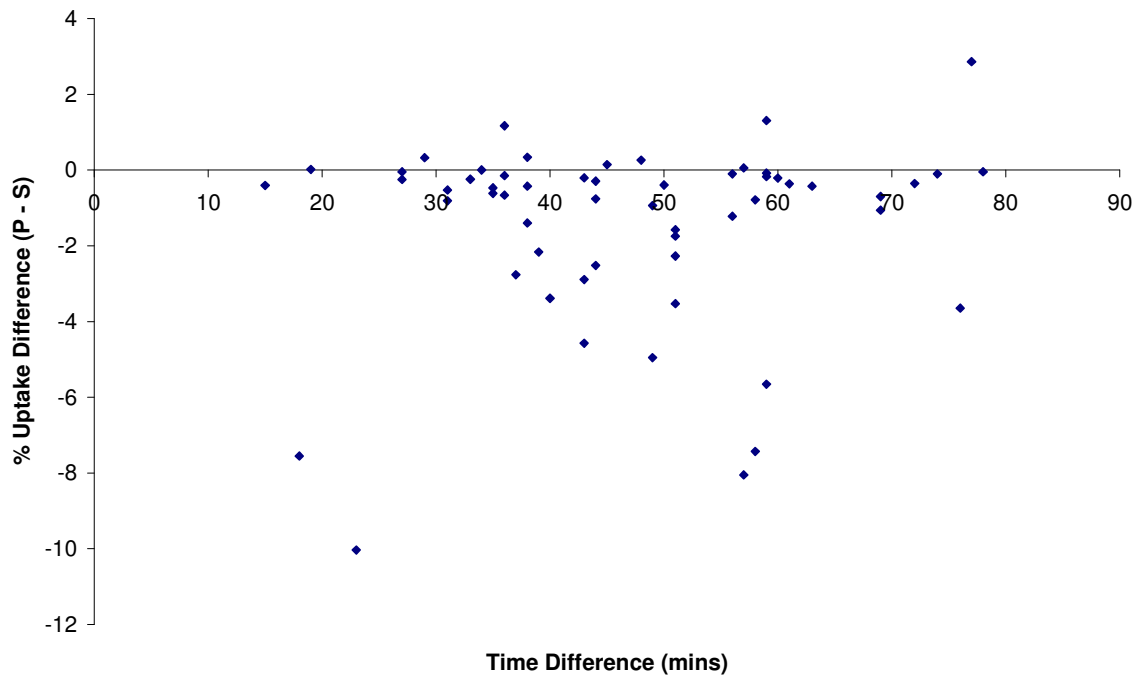


Figure 8.11 - Difference in calculated uptake (P - S) versus acquisition time difference
Plot showing the difference between the uptake values calculated from the planar and SPECT images against the difference in acquisition start time post injection

8.3.3.3 Single SPECT Frame Uptake Values

By extracting a single acquisition frame from the patient and standard SPECT data that was taken in an anterior position (with the gamma camera head at 0°), it was possible to calculate a “planar” uptake from the SPECT data. This measurement of thyroid uptake would be made at the same time as the SPECT acquisition and so a direct comparison with the value calculated from the SPECT data can be made. The single frame for the patient data set was acquired for a period of 30s (prior to May 2007) or 40s (May 2007 onwards) and the standard frame was 10s.

A plot of the frame SPECT uptake against the planar uptake value is shown in Figure 8.12. As with the plot of the SPECT against planar uptake values, the points all tend to lie above the line of identity, indicating that the frame SPECT uptake values are generally higher than those from the planar images.

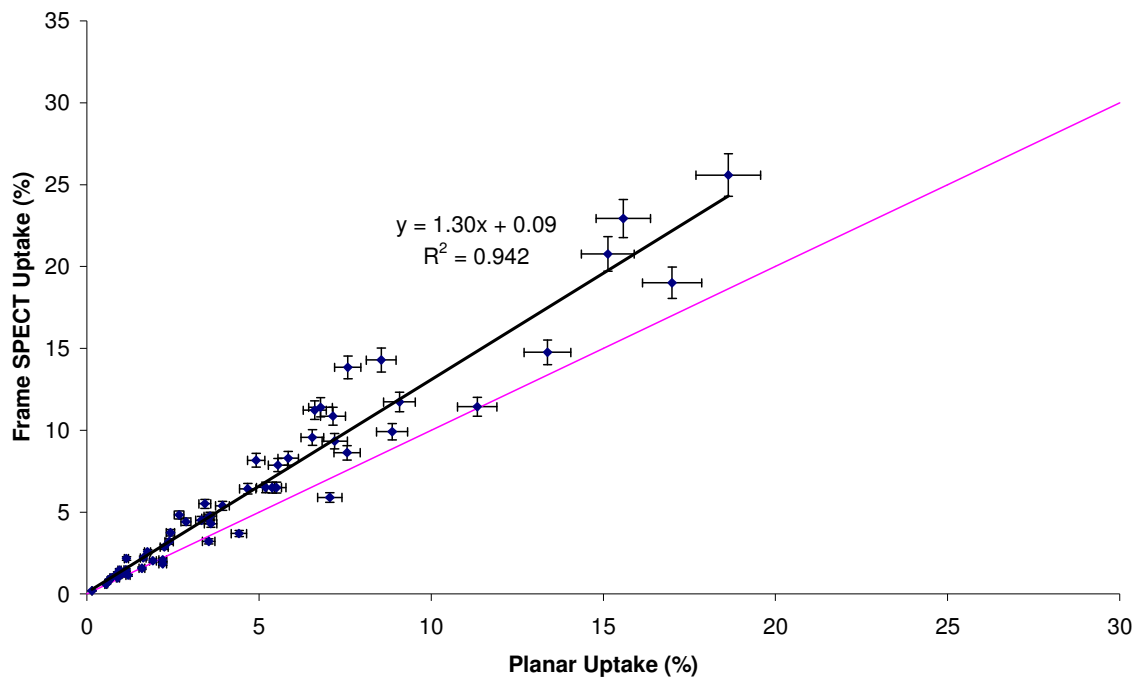


Figure 8.12 - Uptake from frame SPECT versus uptake from planar images
 Plot showing the uptake calculated from the single anterior SPECT frame against the uptake from the anterior planar image with a straight line fit added. The line of identity is shown in pink.

The Wilcoxon Signed Ranks test applied to the difference between the uptake measured from the planar image and that from the frame SPECT image returned

a statistically significant result with $p < 0.001$, an estimated median of -1.16% and a 95% CI of $(-1.70\%, -0.76\%)$. This again emphasises that the uptake calculated using counts from the frame SPECT image tends to be a higher value than that calculated from the planar image.

As with the comparison of planar and SPECT uptake values, a plot was made of the difference between the calculated uptake from the planar and frame SPECT methods against the time difference between the image acquisitions. The resultant plot is shown in Figure 8.13 and allows the affect of the time difference on the measured uptake to be assessed. It can clearly be seen from the plot that there is no obvious trend in increasing or decreasing difference in the measured percentage uptake value with increasing time, meaning that the time of the measurement appears to have little effect on the result.

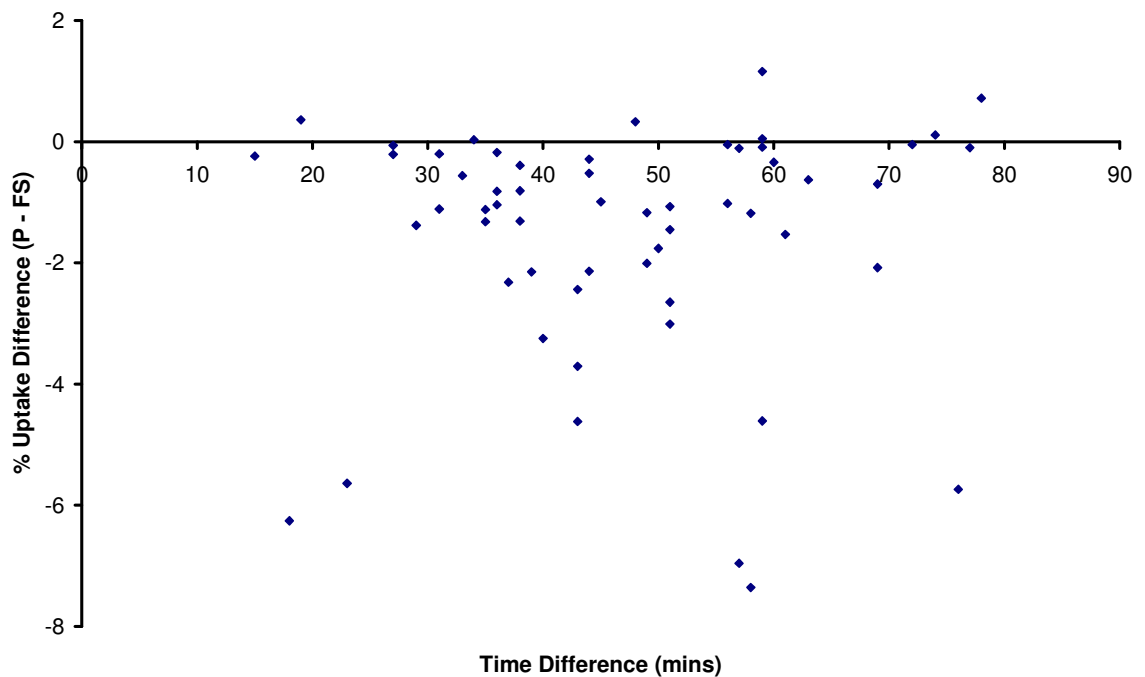


Figure 8.13 - Difference in calculated uptake (P - FS) versus acquisition time difference
Plot showing the difference between the uptake values calculated from the planar and frame SPECT images against the difference in acquisition start time post injection

When the frame SPECT uptake values were compared to those calculated from the full SPECT data, an altogether different result was obtained. The resultant plot is shown in Figure 8.14, from which it can clearly be seen that all the points lie much closer to the line of identity with a more even spread above and below than is seen in Figure 8.12.

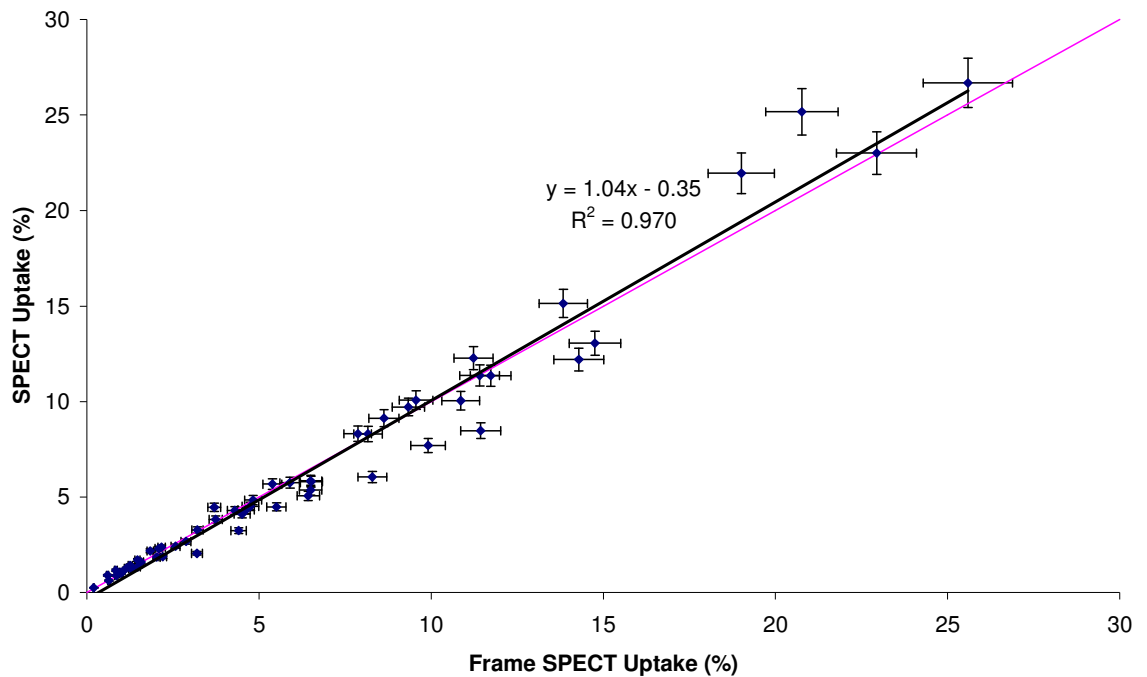


Figure 8.14 - Uptake from SPECT images versus uptake from frame SPECT image
 Plot showing the uptake calculated from the full reconstructed SPECT data set against the uptake from a single anterior SPECT frame with a straight line fit added. The line of identity is shown in pink.

The straight line fit determined from the method of least squares is very close to the line of identity ($y = x$). The non-parametric Wilcoxon Signed ranks statistical test applied to the data gave $p=0.61$ with an estimated median of -0.04% and a 95% CI of $(-0.29\%, 0.10\%)$. This indicates that no significant difference exists between the two uptake values calculated from planar and SPECT data acquired at the same time post injection. This is in contrast to the comparison of the SPECT and planar uptakes. The reason for this is not immediately clear, although possible causes include the shorter total acquisition time of the anterior SPECT frame (30s or 40s) relative to the 60s planar acquisition or an unexpected variation in the thyroid uptake over the period between the planar and SPECT acquisitions.

8.3.3.4 Attenuation Corrected SPECT Uptake Values

A total of 20 patient data sets were re-analysed after an attenuation correction was added to the reconstruction algorithm. A simple Chang attenuation correction with a linear attenuation coefficient of $\mu = 0.120\text{cm}^{-1}$ was included in the iterative reconstruction after the patient outline had been traced to define

the attenuation correction volume. The same process was then carried out on the attenuation corrected SPECT (AC SPECT) images as had already been performed on the non-AC SPECT data to calculate the thyroid uptake. The resulting values were compared with those from the planar, SPECT and frame SPECT images. It should be noted that the smaller sample of data used in this analysis means that the power of the statistical test is reduced when compared to its use for the larger sample of non-attenuation corrected image data.

When compared with the uptake from the planar images, the AC SPECT uptake tended to give a higher value, as is demonstrated in the plot in Figure 8.15. The Wilcoxon Signed Ranks Test performed on the difference between the planar and AC SPECT values supported this conclusion, giving $p < 0.001$, an estimated median of -0.59% and a 95% CI of $(-3.63\%, -0.25\%)$. This is similar to the result obtained when the planar uptake was compared with that from the non-AC SPECT images.

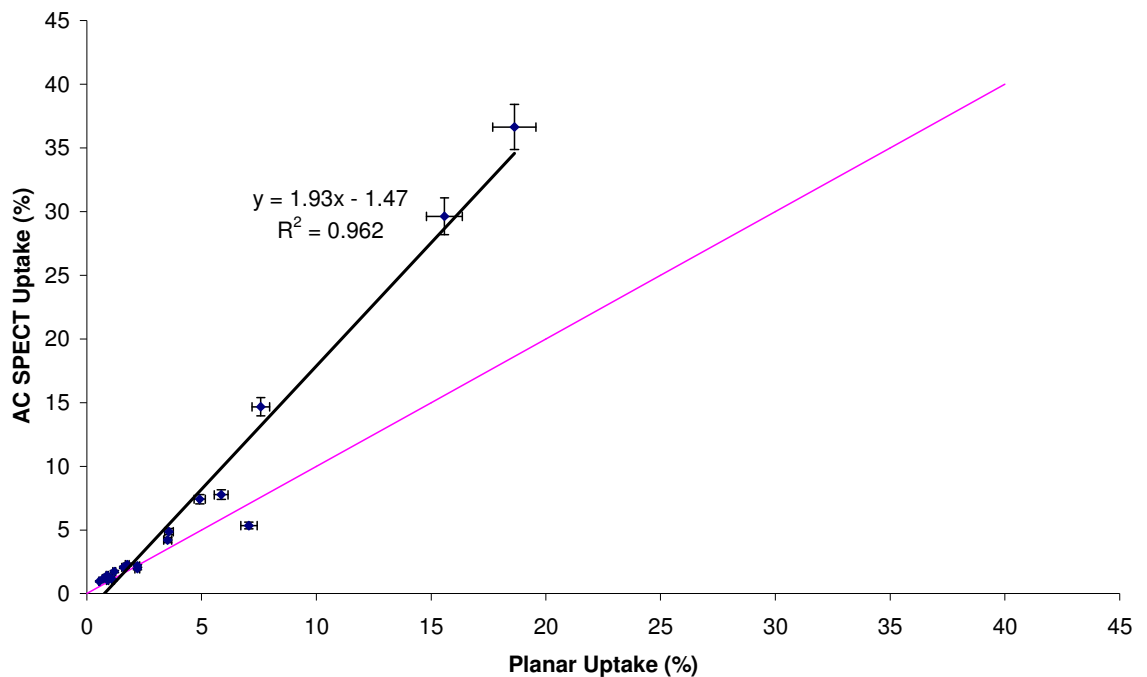


Figure 8.15 - Uptake from AC SPECT images versus uptake from planar image
Plot showing the uptake calculated from the attenuation corrected SPECT data set against the uptake from an anterior planar image with a straight line fit added. The line of identity is shown in pink.

Indeed, the gradient of the best-fit straight line of AC SPECT vs planar uptake is larger than that for SPECT vs planar uptake (1.93 vs 1.34). This indicates that uptake calculated from the AC SPECT data is more different from the planar

uptake value than is the uptake calculated from the normal SPECT data. A direct comparison of the AC SPECT and SPECT calculated uptake values was then made to assess the impact of the attenuation correction on the final thyroid uptake value.

The plot of AC SPECT uptake vs SPECT uptake is shown in Figure 8.16, from which it can be seen that the uptake values are similar at low uptakes (lying close to the line of identity). However, at the highest uptakes, the results diverge with the AC SPECT yielding a higher value, which would be expected if there was a degree of self-attenuation in the largest thyroids. The Wilcoxon Signed Ranks test gave $p=0.83$ with an estimated median of 0.04% and a 95% CI of (-0.27%, 0.23%), meaning that no statistically significant differences exist between the two sets of uptake calculations.

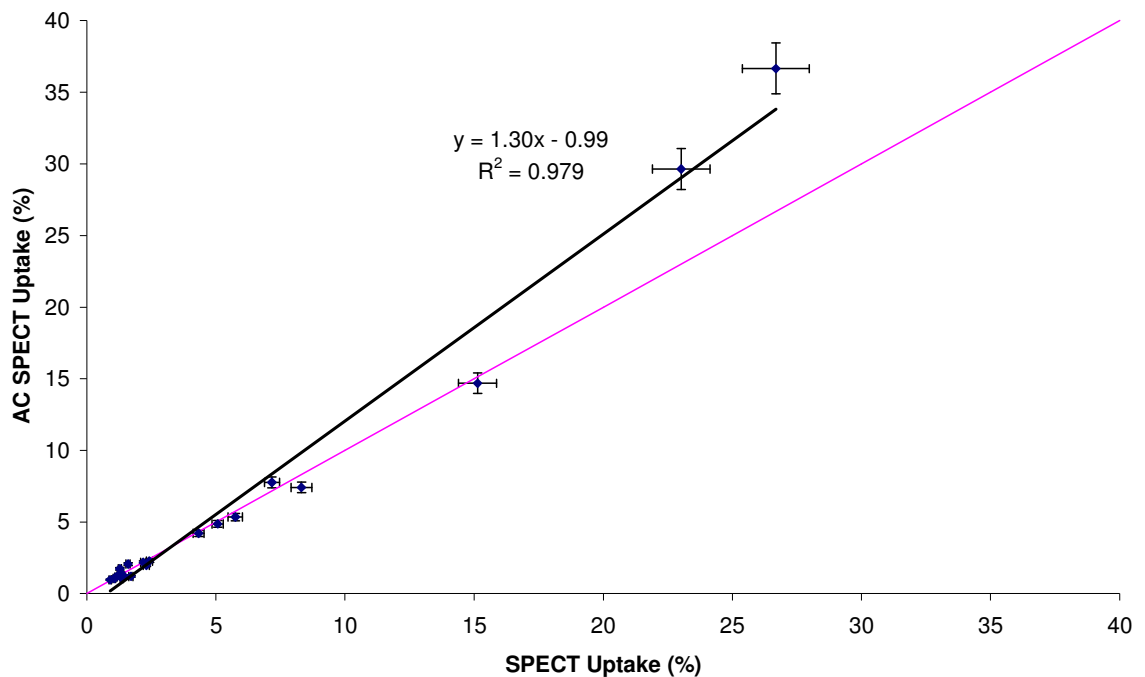


Figure 8.16 - Uptake from AC SPECT images versus uptake from SPECT images
Plot showing the uptake calculated from the attenuation corrected SPECT data set against the uptake from the SPECT data reconstructed without attenuation correction with a straight line fit added. The line of identity is shown in pink.

Finally, the AC SPECT data were compared to the frame SPECT uptake results to assess the differences between attenuation corrected SPECT and planar calculations carried out on data acquired at the same time post injection. The plot produced from these data is shown in Figure 8.17. As with the comparison

with the SPECT uptake values, all points lie close to the line of identity at low uptake values but at higher values, the AC SPECT gives a higher result from the calculation of the thyroid uptake.

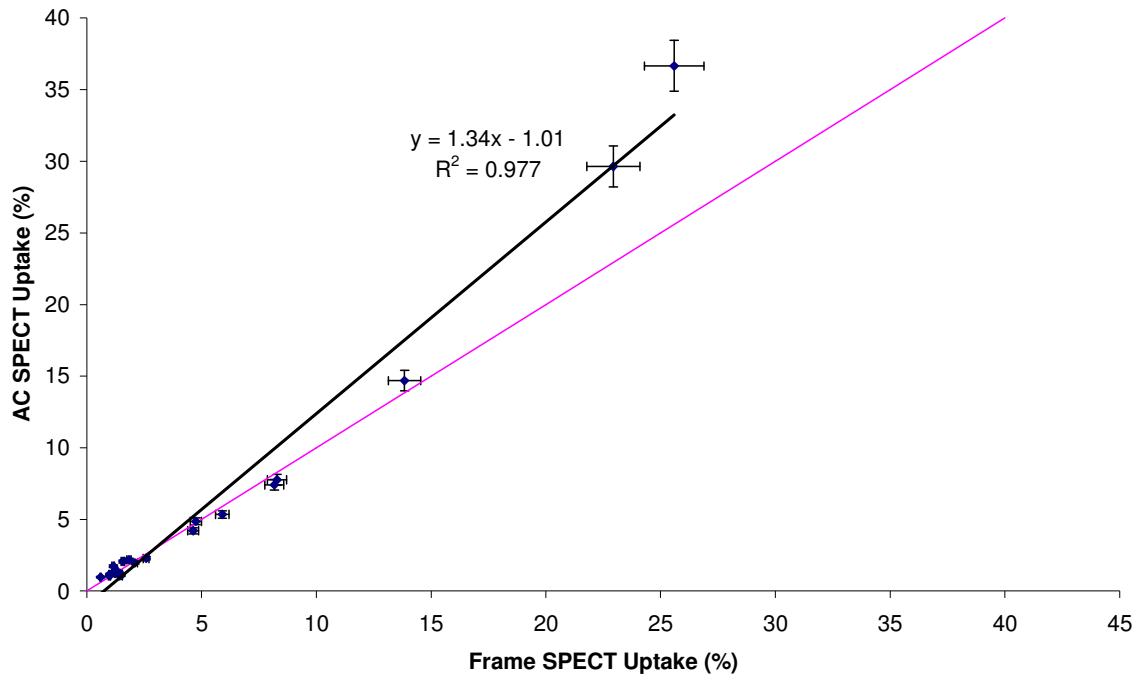


Figure 8.17 - Uptake from AC SPECT images versus uptake from frame SPECT image
Plot showing the uptake calculated from the attenuation corrected SPECT data set against the uptake from a single anterior SPECT frame with a straight line fit added. The line of identity is shown in pink.

The statistical analysis on the comparison of the AC SPECT and frame SPECT uptakes gave $p=0.55$, with an estimated median of 0.08% and a 95% CI of (-0.19, 0.46). No statistically significant difference was therefore found.

8.3.3.5 ICRP Thyroid Uptake Model

The ICRP model of thyroid uptake (ICRP, 1988) was used to calculate the expected uptake at the time of the SPECT acquisition given the uptake value calculated from the planar image at around 20 minutes post injection, using Equation 8.5. The resultant percentage uptake value was compared with those calculated from the SPECT, frame SPECT and AC SPECT images. The error in the expected uptake value was taken to be the difference between the value the model would give at the time post injection at which the SPECT data was

acquired and the value it would give at 20 minutes post injection, assuming the initial uptake was 0.

The plot showing the comparison of the expected and measured SPECT uptake values is shown in Figure 8.18. It can clearly be seen that the calculated value from the SPECT images is higher than that predicted by the ICRP model as most points lie above the line of identity, and the best-fit straight line has a gradient considerably greater than 1. Indeed, the Wilcoxon Signed Ranks test supports this finding with $p < 0.001$, an estimated median of 2.71% and a 95% CI of (1.93%, 3.82%), indicating that a significant difference exists between the expected and calculated uptake values, with the SPECT uptake tending to be higher than the value expected from the model.

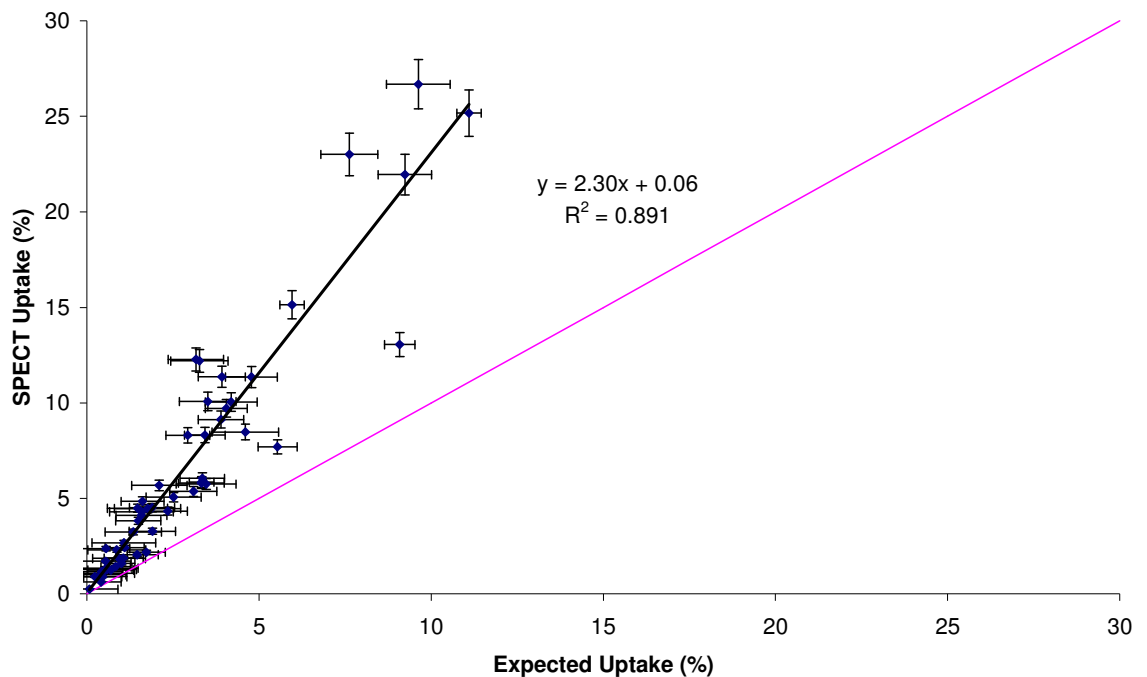


Figure 8.18 - Uptake from SPECT images versus expected SPECT uptake from ICRP model
Plot showing the uptake calculated from the SPECT data set against the uptake predicted by the ICRP model with a straight line fit added. The line of identity is shown in pink.

The same analysis was applied to the differences between the calculated frame SPECT and AC SPECT uptake values and those predicted by the model. The plots produced are shown in Figure 8.19 and Figure 8.20. Again, it is clear that the thyroid uptake calculated from the image data, both for the frame SPECT and AC SPECT images, is higher than that predicted by the ICRP model, as the gradients

for both best-fit straight lines are much greater than 1 and most points on both plots lie above the line of identity.

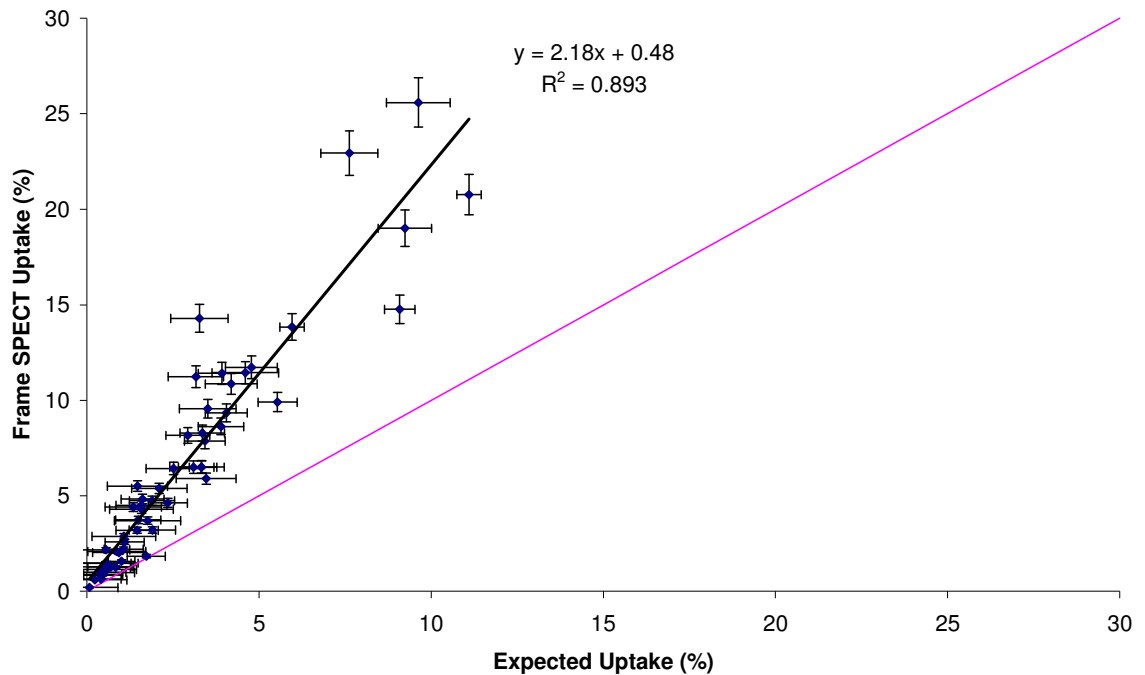


Figure 8.19 - Uptake from frame SPECT image versus expected uptake from ICRP model
Plot showing the uptake calculated from a single anterior SPECT frame against the uptake predicted by the ICRP model with a straight line fit added. The line of identity is shown in pink.

These findings are again strongly supported by the results of the statistical test. For the comparison of the frame SPECT and expected values, the test returned $p < 0.001$, an estimated median of 3.14% and a 95% CI of (2.30%, 4.14%), meaning that the differences between the expected and calculated values are statistically significant and that the calculated uptake from the frame SPECT tends to be higher than the predicted uptake. Similarly, the results of the statistical test for the difference between the AC SPECT and expected values showed statistical significance with $p < 0.001$ and an estimated median of 1.77% and a 95% CI of (0.88%, 4.69%), both of which indicate that the AC SPECT gives a higher thyroid uptake than would be expected from the ICRP model.

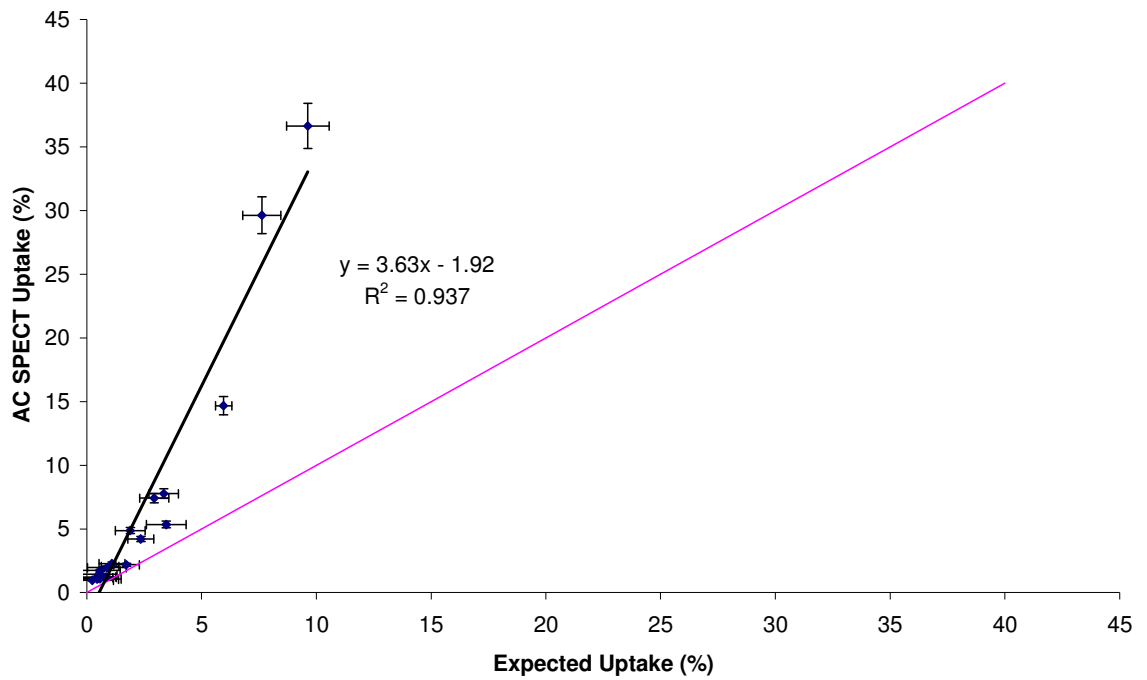


Figure 8.20 - Uptake from AC SPECT images versus expected uptake from ICRP model
Plot showing the uptake calculated from the attenuation corrected SPECT data set against the uptake predicted by the ICRP model with a straight line fit added. The line of identity is shown in pink.

8.3.3.6 Summary of Statistical Test Results

A summary of the results of the Wilcoxon Signed Ranks test for each of the comparisons of thyroid uptake is given in Table 8.2. The gradient of the best-fit straight line to the plotted data is also included in the table.

Difference comparison	p	Estimated median difference (%)	95% CI for difference (%)	Gradient of best-fit line
P - S	<0.001	0.86	(-1.61, -0.43)	1.35
P - FS	<0.001	-1.16	(-1.70, -0.76)	1.30
S - FS	0.61	-0.04	(-0.29, 0.10)	1.04
P - ACS	<0.001	-0.59	(-3.63, -0.25)	1.93
S - ACS	0.83	0.04	(-0.27, 0.23)	1.30
ACS - FS	0.55	0.08	(-0.19, 0.46)	1.34
S - E	<0.001	2.71	(1.93, 3.82)	2.30
FS - E	<0.001	3.14	(2.30, 4.14)	2.18
ACS - E	<0.001	1.77	(0.88, 4.69)	3.63

Table 8.2 - Summary of results from Wilcoxon Signed Ranks statistical test applied to differences in calculated uptake from each alternative imaging method
P = planar, S = SPECT, FS = frame SPECT, ACS = AC SPECT, E = expected from ICRP model

8.4 Discussion

The ability to acquire 3-dimensional nuclear medicine SPECT images can be of considerable use in identifying lesions not visible on planar projections due to the ability to increase contrast by separating activity distributions in overlying and underlying structures on planar imaging (Sharp *et al.*, 1998, Wagner *et al.*, 1999, Bruyant, 2002). Quantitative or semi-quantitative measurements are often performed in nuclear medicine imaging (Sharp *et al.*, 1998), giving a numerical value to some physiological function that is being imaged. Combining SPECT and quantitative imaging could potentially result in more accurate quantitative measures of radiopharmaceutical uptake by ensuring that photons from all parts of the target organ are acquired as part of the image and hence are used in the uptake calculation.

This study aimed to assess the practicality of measuring uptake of ^{99m}Tc -pertechnetate in the thyroid gland using SPECT imaging and any differences that exist in the measured uptake from planar and SPECT imaging. Both standard and attenuation-corrected SPECT images were considered, with a linear Chang attenuation correction with $\mu=0.12\text{cm}^{-1}$ being used. Comparisons were also made of the measured SPECT uptake values against a model of thyroid uptake produced by the ICRP (ICRP, 1988) to determine the accuracy of the model.

Ideally, the planar and SPECT images would be acquired at the same or a very similar time-point post-injection of ^{99m}Tc -pertechnetate due to the fact that pertechnetate uptake in the thyroid is known to vary over time (Andros *et al.*, 1965, Atkins & Richards, 1968, Shimmins *et al.*, 1968, Hays & Berman, 1977, Hays, 1978, Hilditch & Alexander, 1980, ICRP, 1988, Okada *et al.*, 2003).

Unfortunately, this study had to be carried out within the demands of the routine clinical service of the department at GRI and so in most cases it was not possible to carry out SPECT imaging immediately after planar imaging. Indeed, the time difference between the two acquisitions was usually greater than 30 minutes and was over 1 hour in a number of cases, meaning that the time between injection and SPECT imaging was sometimes well over 60 minutes. Published data from the literature (Andros *et al.*, 1965, Atkins & Richards, 1968, Shimmins *et al.*, 1968, Hays & Berman, 1977, Hays, 1978, Hilditch & Alexander,

1980, ICRP, 1988, Okada *et al*, 2003) includes studies of thyroid uptake up to and including 60 minutes post-injection but no information could be found on uptake behaviour beyond this time. It is therefore not possible to directly assess the impact of changing uptake on the results of this study. Further work to determine the pattern of uptake over a longer time period is required to perform a full analysis on the data.

The method of calculating thyroid uptake from SPECT images that was used in this study was very time-consuming and labour-intensive. The whole analysis process from reconstructing the SPECT images and drawing regions of interest (ROIs) to analysing the counts within the ROIs in a spreadsheet took a minimum of 60 minutes for each individual patient. This is an unrealistic time-frame for use in the clinical setting. Allied to the fact that the acquisition time for the SPECT images was considerably longer than for the planar images used routinely for thyroid imaging at GRI, the SPECT method of uptake calculation is unlikely to be used on a routine basis. However, this study has proved that it is possible to perform the measurement on patient data.

The study produced some unexpected results, with the calculated uptake value between the planar and single SPECT frame images being significantly different - the uptake measured from the frame SPECT image tending to be higher than that from the planar. Since the calculation method for the uptake from these types of image is essentially the same, some other effect must be responsible for the observed differences in measured uptake. However, there was no significant trend observed in the difference in the calculated uptake value from these two sets of images with the time difference between the image acquisitions. The reason for the observed differences is therefore unclear but could be related either to the different total acquisition time of the images or to the fact that the pertechnetate uptake had varied between the two acquisitions in an unknown way. Further work is needed to clarify the situation.

The same relationship was seen between the measured planar and SPECT uptakes, with the SPECT value tending to be higher. This may be because the calculation method is significantly different or once again because of an unknown variation in uptake with time. The frame SPECT and SPECT uptake

values were similar, however, which indicates that the cause is unlikely to be the different calculation method.

The fact that the attenuation corrected SPECT images produced uptake values higher than those measured from the standard SPECT images was as expected. The application of linear attenuation correction provides an adjustment in the measured photon counts to account for the attenuation of photons originating from greater depth within the thyroid gland and therefore having to pass through a greater thickness of tissue before reaching the gamma camera detector. Sections of the thyroid gland lying at greater depth within the neck therefore account for a greater proportion of the overall counts in the final attenuation corrected SPECT image than in the standard SPECT image and the measured uptake is correspondingly increased.

The ICRP model of ^{99m}Tc -pertechnetate in the thyroid gland (ICRP, 1988) has been shown here to be inadequate to describe the change in uptake with time. It is a simple model of bi-exponential reduction with time but the measured uptake from the SPECT images in this study varied significantly from the expected values from the model based on the initial 20 minute planar uptake. Although using the planar uptake as a starting point is not entirely accurate, the true thyroid uptake at any given time is not known and so the 20 minute uptake was taken to be the standard as it was measured for all patients participating in the study.

8.5 Conclusions and Suggestions for Further Work

This work has demonstrated that it is possible to determine the percentage uptake of ^{99m}Tc -pertechnetate in the thyroid gland from 3-dimensional SPECT images. However, the technique is both time-consuming and labour-intensive and so is unlikely to be implemented on a routine basis. The standard method of calculating uptake from anterior planar images will continue to be used at GRI.

This study has also shown that the ICRP model of ^{99m}Tc -pertechnetate uptake in the thyroid gland (ICRP, 1988) is not an accurate model, with significant differences existing between measured and expected uptake values from patient image data. The model does not take into account the known increase to a

plateau level in the first 15-20 minutes post injection (Atkins & Richards, 1968, Esser *et al.*, 1973, Meller & Becker, 2002), although it does include the fast and slow compartments modelled by Hays (Hays, 1978). In order to more accurately test the model, a known uptake value would be required, which is not possible with patient data. However, the results of this study suggest that the ICRP model should be used with caution.

The observed differences between the measured uptakes from the various images used in this study could not be easily explained with the information available from this patient study. The two main problems are the lack of knowledge of the true uptake in the thyroid gland at any given time and the unknown change in uptake over time. The first of these can be studied using a phantom into which a known “uptake” activity has been introduced. The second would require further acquisitions of patient data over an extended period of time post-injection of ^{99m}Tc -pertechnetate to determine the changing uptake.

The phantom designed and built for this study (see Chapter 2) is an ideal instrument for assessing the measured uptake value when a known “uptake” is present. Various acquisitions with the phantom were therefore performed to this end and the results are described in Chapter 9. Unfortunately, acquiring data on thyroid uptake over an extended period post-injection of ^{99m}Tc -pertechnetate was beyond the scope of this study but it is recommended that such work be carried out to fully assess the results presented here.

Chapter 9 – Accuracy of the Thyroid Uptake Calculation

9.1 Introduction

When measuring the uptake of a radioactive material in the thyroid gland, an absolute calculation is performed. However, there will still be errors and uncertainties in the final calculated uptake due to the imaging conditions. Since the sensitivity of the gamma camera is low due to the use of the collimator (Sharp *et al*, 1998), only a small fraction of the photons - around 1 in 10,000, or 0.01% - emitted from the thyroid will be recorded in the resultant image. Image statistics can therefore be poor, especially in cases of low thyroid uptake. Since the uptake measurement relies on the number of counts within a region of interest (ROI) defining the thyroid, low counts leads to large uncertainties in the final calculation.

For a planar image of the thyroid acquired in the anterior projection, only part of the gland is visualised directly. Photons that arise in the posterior portion of the thyroid need to pass through more tissue (both the thyroid itself and overlying tissue) before reaching the gamma camera crystal than do those that originate in the anterior portion of the gland. They are therefore attenuated more and the total number of counts recorded by the camera is reduced. Since the thyroid lies very anterior in the neck and is thin in the anterior-posterior dimension at 1-2.5cm (ICRP, 1975), the effect of the attenuation will be small but it will still exist. It may also be more significant for larger thyroids which may produce more self-attenuation due to greater thickness of thyroid tissue.

The 3-dimensional (3D) reconstructions from a single photon emission computed tomography (SPECT) acquisition remove the problem of the posterior part of the gland not being visualised. Image frames are collected from all angles around the patient and so counts from the posterior and lateral aspects of the thyroid are included directly in the acquisition. However, because the counts still have to pass through a certain depth of tissue to reach the gamma camera crystal, the problem of attenuation remains. SPECT images may therefore give better

visualisation of all parts of the thyroid gland but may not increase the accuracy of the uptake measurement.

Performing an attenuation correction on the SPECT data should reduce the dependency of the number of counts recorded on the depth of the origin of the photons within the patient. Various methods for attenuation correction exist (Webb *et al.*, 1983, Sharp *et al.*, 1998), ranging from a simple linear method that assumes uniform attenuation throughout the patient volume to the use of a CT acquisition to map the actual attenuation at all points in the image.

In order to directly compare the accuracy of the different methods for calculating thyroid uptake, it is necessary to first know the true uptake. Since it is never possible to know the true value for a patient, a phantom must be used to provide a simulation of a patient thyroid. A known activity of a radioactive material corresponding to a particular “uptake” can be introduced into the phantom. The phantom can then be imaged using a variety of different acquisition parameters and the uptake can be calculated from the resultant images. A direct comparison of the calculated value from each set of image data can then be made with the known true uptake. The relative accuracy of the different methods can then be assessed.

9.2 Materials and Methods

The new phantom custom designed and built for the work of this thesis (see Chapter 2 for further details) was used with its thyroid insert to directly compare the calculated thyroid uptake value from a variety of different image types. Planar and SPECT acquisitions were performed with a variety of activities added to the phantom along with acquisitions of a standard activity in order to calculate the absolute “uptake” within the thyroid phantom.

For each set of acquisitions, the main body of the phantom was filled with water and contained no radioactivity. The three hollow chambers within the phantom - which can be filled with activity if necessary to simulate hot nodules - were also filled with water but no radioactivity. In contrast, the main body of the thyroid insert was filled with water to which a known amount of activity had been added. It was this activity which was used to simulate thyroid uptake.

A vial containing a known activity (around 100MBq) of ^{99m}Tc -pertechnetate in a 10ml volume was used as the starting point for each measurement. The exact activity in the vial was measured using the department's Capintec isotope calibrator and the time of the measurement was noted. This was taken to be the initial injected activity, as would be the case for a patient study. A known volume (therefore corresponding to a known activity) was then drawn out of the vial and added to the main thyroid chamber of the phantom to simulate the uptake within the thyroid of a small percentage of the total injected activity. The residual activity in the syringe after injecting the pertechnetate into the phantom was measured and the time of this measurement was also noted. The phantom therefore contained a known activity of ^{99m}Tc at a reference time. The volume, and therefore percentage of the activity in the phantom, was varied for each set of acquisitions to simulate different thyroid uptakes within the range of 0.7% to 20%, which is a typical range of thyroid percentage uptakes seen at Glasgow Royal Infirmary (GRI).

A vial containing a known activity of ^{99m}Tc in the range 15MBq - 30MBq in a 10ml volume was used as a standard for each set of image acquisitions. The activity in the vial was measured using the isotope calibrator and the activity and time of measurement were recorded. The vial was then placed into the department's standard phantom for thyroid imaging, which consists of a Perspex cylinder of diameter 15cm and a 3cm diameter slot for a vial which lies 0.5cm from the front face of the phantom, and planar and SPECT images were acquired. These images could then be used to determine the sensitivity of the gamma camera (in counts/second/MBq) to allow an absolute measurement of the activity in the other phantom to be made.

Planar images of the phantom and standard were acquired using the normal departmental protocol. Each phantom was placed 12cm from the face of the LEHR collimator on the GE Camstar gamma camera in turn and a 60 second (s) image was acquired. The percentage uptake in the thyroid phantom was then calculated using the analysis program provided on the HERMES computer system.

Firstly, a region of interest (ROI) was drawn around the vial on the standard image and the counts within the ROI and the known activity in the vial at the time of measurement (decay corrected from the measurement made on the

isotope calibrator) were used to calculate the gamma camera sensitivity in counts/s/MBq.

This sensitivity was then entered into the program, along with the activity initially measured in the vial prior to the phantom activity being drawn out of it (simulating the injected activity into the patient) and the residual activity in the syringe. The time since the measurement of the vial activity was also entered to allow the program to perform a decay correction for the physical decay of the ^{99m}Tc between the activity measurement and the image acquisition.

Two ROIs were then drawn by hand on the image of the thyroid phantom. The first outlined the image of the thyroid whilst the second was a background ROI drawn below the thyroid. The program then used the counts in these ROIs to perform a background correction and to calculate the percentage “uptake” in the thyroid phantom insert at the time of imaging.

A SPECT acquisition was also carried out for both the thyroid phantom and the standard. The parameters used for the acquisition phantom images were identical to those used for patient acquisitions: VXHR collimators on the double-headed Philips Forte gamma camera with the heads in the 90° orientation, 180° anterior circular acquisition, a 10% energy window centred on 140keV, 60x40s frames with a 3° rotation between frames, giving a total acquisition time of 20 minutes and a 30cm square roving zoom applied.

The standard images were acquired in exactly the same way except that the acquisition time for each frame was reduced to 10s, giving a total acquisition time of 5 minutes. This was due to the fact that, on most occasions, the activity in the standard was considerably higher than that in the thyroid phantom and so an acceptable number of counts could be acquired in each frame in a shorter time. Reducing the standard acquisition time also mimicked the procedure used for the patient thyroid uptake study (see Section 8.2.3) and kept the total time required for study acquisitions to a minimum so as to reduce the impact on the clinical work of the department.

The SPECT images were then reconstructed using the same algorithm, parameters and post-reconstruction filter as those used for the patient thyroid

uptake study (Section 8.3.2). Attenuation corrected images were also produced using a uniform linear attenuation coefficient of $\mu=0.12\text{cm}^{-1}$ to allow a direct comparison of the accuracy of the calculated uptake from SPECT data with and without an attenuation correction applied. The final reconstructed SPECT images were in the transverse, coronal and sagittal planes.

As with the patient SPECT images, ROIs were drawn by hand around the visible thyroid on the transverse slices of the reconstructed SPECT images for both the attenuation corrected (AC) and non-attenuation corrected data sets for both thyroid phantom and standard acquisitions. A background ROI was also placed on each slice. A file containing the counts in the two ROIs for each slice was exported to a spreadsheet program. The “uptake” within the thyroid phantom was then calculated using Equation 8.2, Equation 8.3 & Equation 8.4.

As was the case with the patient thyroid SPECT data, a “planar” uptake was also calculated from the anterior frame of the SPECT acquisition data. The normal planar processing procedure using the HERMES system was followed to produce a “frame SPECT” uptake value.

The calculated planar, frame SPECT, SPECT and AC SPECT uptake values were then compared to the known uptake by plotting the values on a graph and finding the best fit straight line to the data using the least squares method. A non-parametric Wilcoxon Signed Ranks statistical test was also applied to the difference between the known and calculated uptake values to give a p-value, estimated median difference and a 95% confidence interval (CI) for the difference. A p-value of <0.05 was taken to be statistically significant.

An alternative to plotting one measured value against another would be to create Bland-Altman plots, whereby the difference between the two measured values is plotted against their mean. This type of plot demonstrates any underlying trend in the differences changing as the actual measured value changes - for example, increasing differences with increasing measured value. However, in this case the straight line plots were chosen to allow a more direct comparison with the patient data discussed in Section 8.3.

During the period of this study, a SPECT/CT system (Siemens Symbia T) was installed in the department at GRI. A small number of acquisitions were performed on this system to allow a non-uniform attenuation correction to be carried out using the CT data to create a mu-map of densities. Theoretically, this should give a more accurate attenuation correction than the uniform method applied to the data acquired on the dual-headed gamma camera and so should give a calculated percentage uptake which is closer to the known value. The SPECT acquisition parameters were similar to those used with the dual-headed gamma camera except that the Symbia is able to perform a non-circular acquisition but has no roving zoom facility. A non-circular acquisition with no zoom and all other parameters as listed above was therefore carried out for both the thyroid phantom and the standard.

SPECT images were acquired simultaneously in a second energy window at 108.5keV - 129.5keV, as shown in Figure 9.1, in order for scatter correction to be performed during reconstruction of the images. This acquisition of data in a scatter window is standard practice for SPECT/CT acquisitions at GRI, although it is not used with the other gamma camera systems.

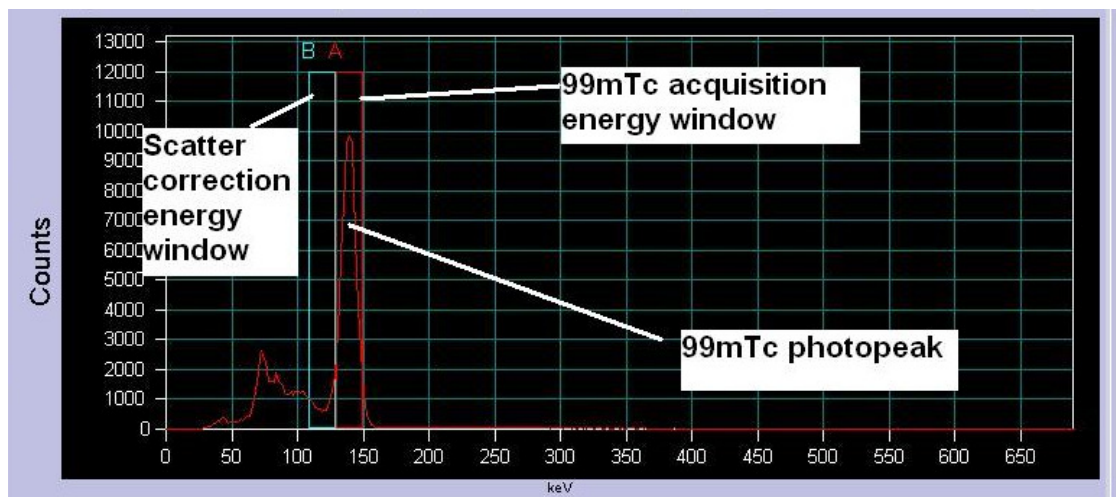


Figure 9.1 - Energy spectrum of ^{99m}Tc acquisition showing image and scatter correction acquisition windows

Gamma camera energy spectrum of ^{99m}Tc acquisition showing ^{99m}Tc image acquisition energy window A (red) and scatter correction energy window B (blue).

The mu-map from the CT acquisition was then loaded into the HERMES OSEM SPECT reconstruction program along with the SPECT data and the non-linear attenuation correction was applied as part of the iterative reconstruction. All

other reconstruction parameters were the same as those for the SPECT and AC SPECT reconstructions described above. The same ROI analysis was carried out on the resultant transverse image slices in order to calculate the “uptake” of the thyroid phantom.

A further CT attenuation corrected SPECT data set was also created using the Siemens Symbia system’s own software (MI Apps) to perform the SPECT reconstruction. The Siemens FLASH3D iterative reconstruction method was used with both attenuation correction from the CT mu-map and scatter correction applied. This method allows only a single type of post-reconstruction filter to be applied to the data, which is of the Gaussian form. Several reconstructions were carried out with different filters applied in order to determine which gave images most similar in appearance to those from reconstructions on the HERMES system. The parameters for the reconstruction were as follows: 15 subsets, 4 iterations, Gaussian 5.0 filter. The reconstructed images were then transferred to the HERMES system and the ROI analysis was carried out in the same way as for the other SPECT data.

The results from the SPECT/CT acquisitions were then compared to the uptakes calculated from the planar, frame SPECT, SPECT and AC SPECT images as well as the known value.

9.3 Results

9.3.1 Comparison with Known “Uptake” Value

Images were acquired of a total of 17 different “uptakes”, ranging from 0.78% to 19.16%, simulating a range of observed patient uptake values. A plot of the measured percentage uptake versus the known value was then created for the planar, frame SPECT, SPECT and AC SPECT uptakes and a straight line fit was performed on each set of data using the method of least squares. The resultant graph is shown in Figure 9.2 with the line of identity shown in black.

Theoretically, all points should lie upon this line of known uptake. The error in the known uptake was taken to be $\pm 5\%$ of the uptake value and the error bars in

the measured uptakes represent $\pm 1SD$, calculated in the same way as for the patient data sets in Section 8.3.3.

It is immediately clear that all of the points and best fit straight lines lie below the line of identity, indicating that all the methods of measuring the percentage uptake tend to underestimate the true uptake value. All the lines lie close together with gradients of between 0.70 and 0.78, suggesting that there is little true difference between the uptake calculated using each of the different methods. The quoted r^2 values from each of the straight line fits are all >0.96 , suggesting that each data set does correspond to a straight line with gradient <1 .

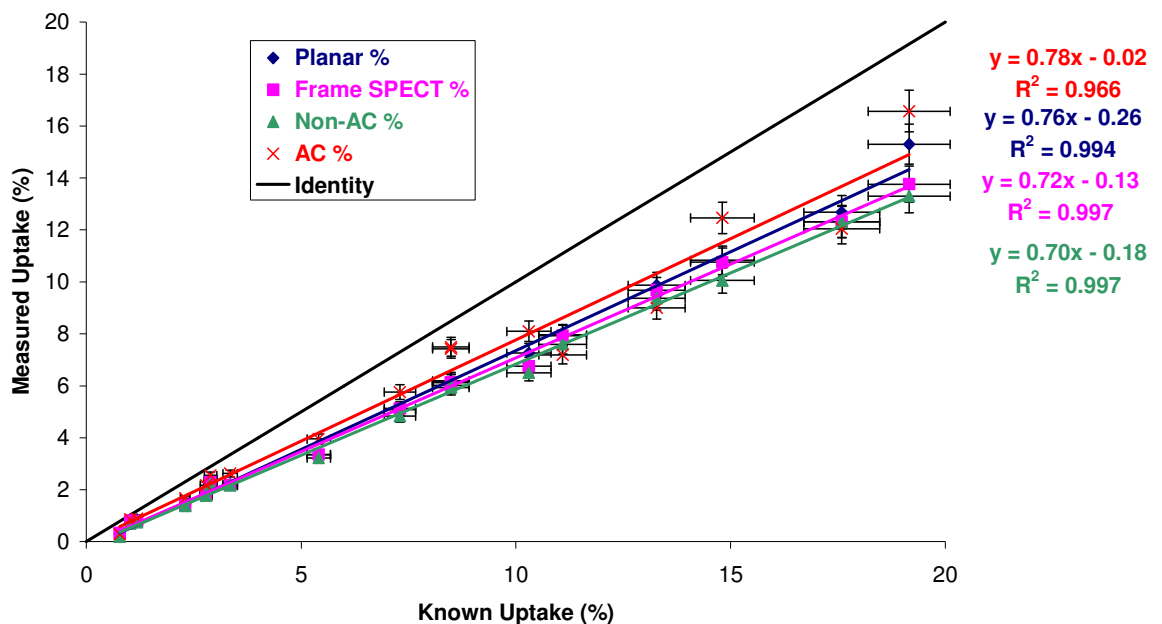


Figure 9.2- Measured uptake versus known uptake for phantom acquisitions
 Plot of measured uptake from planar (blue), frame SPECT (pink), non-attenuation corrected SPECT (green) and attenuation corrected SPECT (red) against known uptake in the phantom. The line of identity is shown in black and the equations of the best fit straight lines are shown in the corresponding colour to the data points.

The line lying closest to the line of identity is that representing the uptake calculated from the attenuation corrected SPECT images. This would be expected as the attenuation correction should provide some correction for the reduction in counts from the deeper-lying parts of the thyroid gland and so give a more quantitatively accurate result. In contrast, the non-attenuation corrected SPECT images gave calculated uptake values furthest from the known value. This is surprising as it was expected that the uptake from SPECT would

be more accurate than that from planar imaging due to the possibility of significant self-attenuation occurring on the planar images. However, in each of the 17 analyses, the uptake calculated from the anterior planar view was higher than that calculated from the SPECT images.

A statistical analysis was then carried out on these results using a dedicated software package (Minitab v13). The difference between the known “uptake” and that measured from each of the different image data sets was calculated for each phantom acquisition and the non-parametric Wilcoxon Signed Ranks test was applied. The test produces a p-value indicating the likelihood of the data corresponding to a data set with median value 0, an estimated median and a 95% confidence interval (CI). The package gives the p-value to 3 decimal places and so if $p < 0.001$, no exact figure is given. Statistical significance was taken to be when $p < 0.05$. The results of this statistical analysis are shown in Table 9.1.

	P	Estimated Median	95% CI
Known - Planar	<0.001	2.10%	(1.30%, 2.96%)
Known - Frame SPECT	<0.001	2.21%	(1.31%, 3.11%)
Known - SPECT	<0.001	2.41%	(1.45%, 3.40%)
Known - AC SPECT	<0.001	1.47%	(0.78%, 2.47%)

Table 9.1 - Results of Wilcoxon Signed Ranks statistical test applied to differences between known and calculated uptake values
Results from applying statistical test to the differences between the known and calculated uptake values for each of the different types of image.

The values in Table 9.1 verify the findings of the plot, with $p < 0.001$ in each case, indicating that the results of the uptake analysis from each type of image data set are statistically significantly different from the known value. The estimated median and 95% CI values are all > 0 , indicating that the known value is higher than that measured. Also, the estimated median and 95% CI values are highest for “known - SPECT” and lowest for the “known - AC SPECT”, which is as expected, given that the plotted best fit straight lines for these data sets are furthest from and closest to the line of identity respectively.

9.3.2 Direct Comparison of Calculated Uptake Values

Since the analysis performed on patient data (see Section 8.3.3) had no known uptake to provide a comparison, the measured values were compared directly to each other. A similar comparison was made with the data from the phantom

acquisitions in order to determine if the same differences between the uptakes calculated from different image data sets existed. Plots were created to compare the calculated uptake values from each method of analysis. These plots are shown in Figure 9.3 to Figure 9.8 with the line of identity shown in black on each plot and the equation of the best fit straight line to the data obtained by the method of least squares also given. A Wilcoxon Signed Ranks test was also applied to the differences in calculated values from the different image data sets, giving a p-value, estimated median and 95% CI. Once again, a result of $p < 0.05$ was taken to be statistically significant.

The plot shown in Figure 9.3 demonstrates that the measured uptake from the frame SPECT and planar images is similar, with the best-fit straight line lying close to the line of identity. The high value of r^2 indicates that the data are a good fit to a straight line. This result is as expected, since the same analysis program is used to calculate the uptake and both images were acquired from a single fill of the phantom, meaning that the true “uptake” was identical in both cases. This result does, however, differ significantly from that demonstrated in Chapter 8 when patient image data was considered (see Figure 8.12). In that case, the frame SPECT method gave an uptake result considerably higher than the technique using planar imaging.

The Wilcoxon Signed Ranks test gave a result of $p = 0.003$, estimated median of 0.07% and a 95% CI of (0.03%, 0.23%). Although this is a statistically significant result, the estimated mean and 95% CI values are $\ll 1\%$ and so would not result in a clinically significant difference in the final calculated value. The reasons for the difference between these results from phantom data and those from patient acquisitions is not immediately clear but may be primarily related to the variation in uptake over time in a real thyroid, whereas the “uptake” in the phantom remains constant.

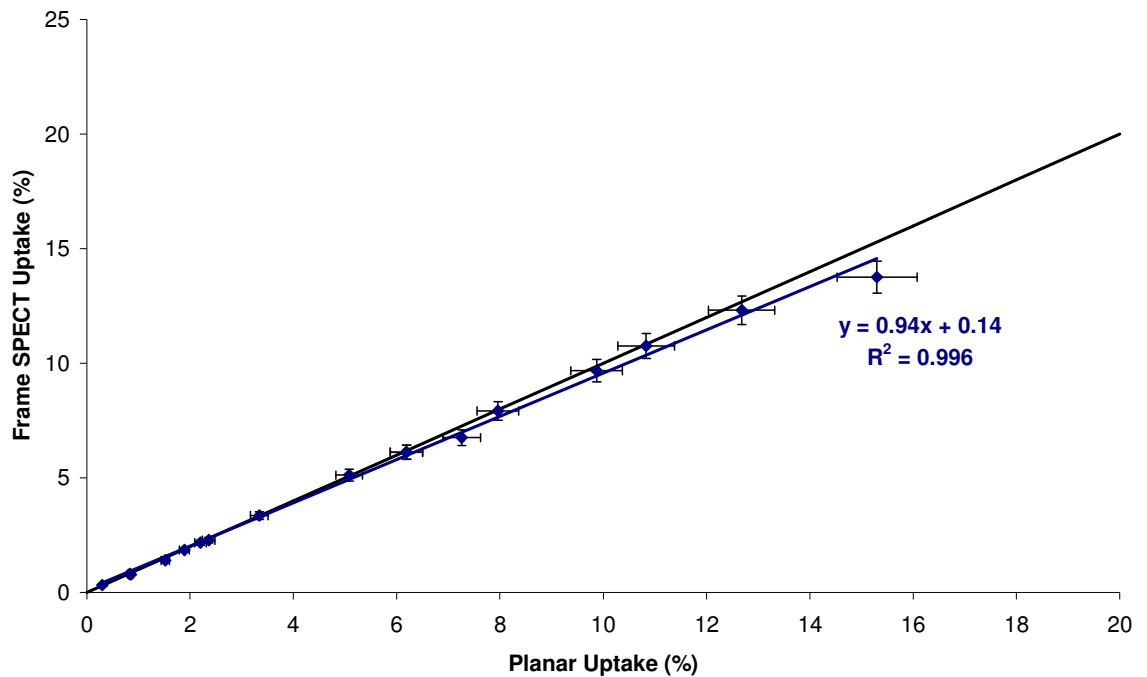


Figure 9.3 - Plot of uptake from frame SPECT image versus uptake from planar image
The line of identity is shown in black and the best fit straight line to the data is shown in blue with its equation and the r^2 value from the method of least squares also displayed.

Similarly, the plot of SPECT uptake versus planar uptake shown in Figure 9.4 shows the data lying close to the line of identity and demonstrating a good straight line fit. As in Figure 9.3, there is a slight tendency for the planar uptake value to be higher, which again is in contrast to the situation found when patient image data was considered (see Figure 8.10).

Applying the Wilcoxon Signed Ranks test to the data returned the following results: $p < 0.001$, estimated median of 0.25% and 95% CI of (0.14%, 0.46%). As for the difference between the planar and frame SPECT uptakes discussed above, although this is a statistically significant result, the magnitude of the estimated median and 95% CI values are $\ll 1\%$ and so would not be of significance in the clinical situation. The positive values also confirm the tendency for the planar result to be slightly higher than the SPECT uptake, which again is in contrast with the results from the patient image data.

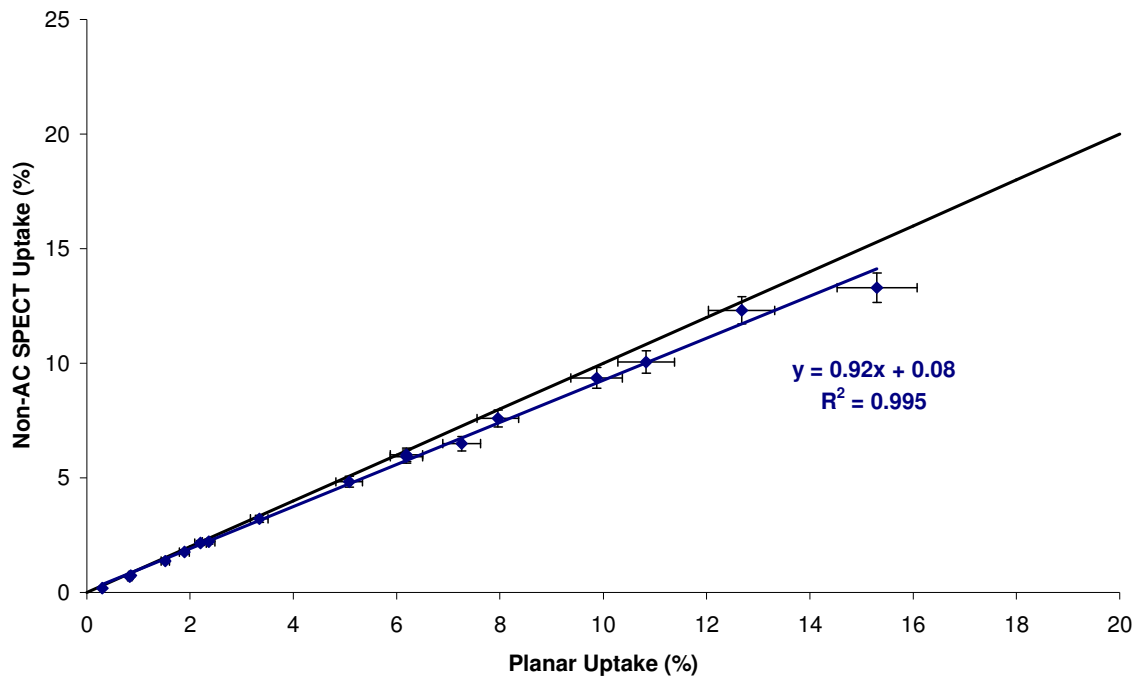


Figure 9.4 - Plot of uptake from SPECT images versus uptake from planar image
The line of identity is shown in black and the best fit straight line to the data is shown in blue with its equation and the r^2 value from the method of least squares also displayed.

Figure 9.5 shows a plot of the calculated uptake from the SPECT images versus that from the frame SPECT image. On this occasion, the best-fit straight line is very close to the line of identity with a gradient of 0.97 and an intercept very close to 0. This is similar to the result found from the patient data shown in Figure 8.14, although in that instance, the SPECT uptake tended to be slightly higher than the frame SPECT, whilst the opposite is true for the phantom data. The fact that these two uptake values are similar is to be expected as they are from the same raw acquisition data, meaning that there are no differences in the gamma camera or acquisition time to be taken into account.

Surprisingly, the Wilcoxon Signed Ranks test returned a statistically significant result for these data with $p < 0.001$, estimated median of 0.17% and 95% CI of (0.09%, 0.28%). The result from the test applied to the patient data was not statistically significant with $p = 0.61$. However, the very low estimated median and 95% CI values would once again be of no significance in the clinical setting.

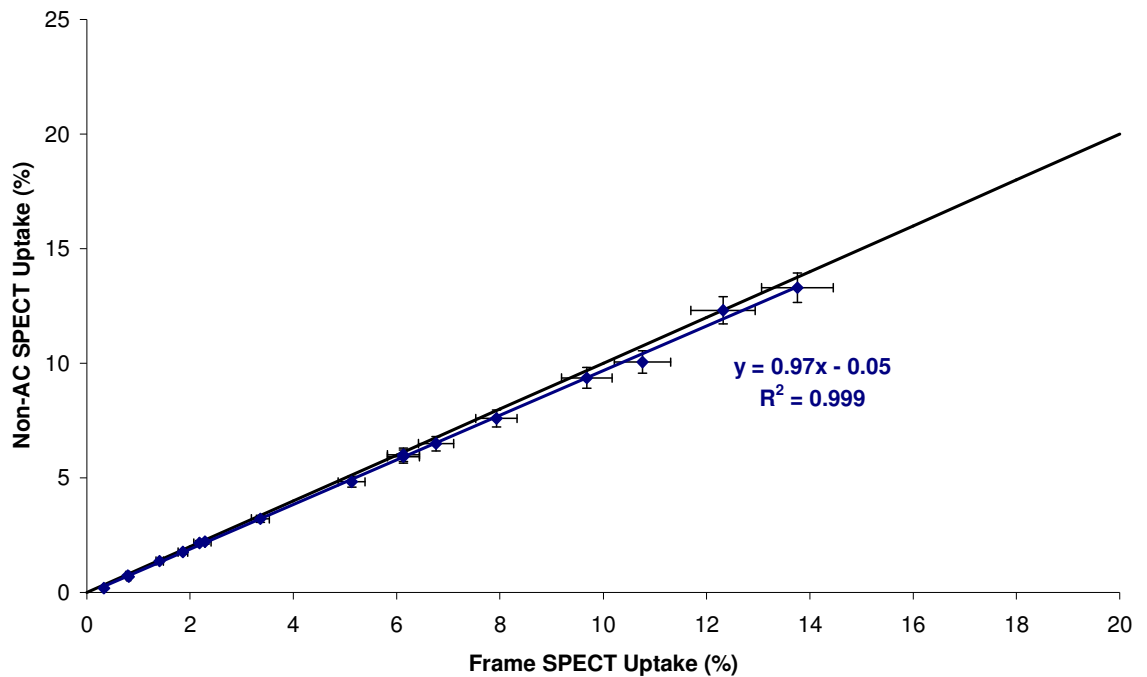


Figure 9.5 - Plot of uptake from SPECT images versus uptake from frame SPECT image
The line of identity is shown in black and the best fit straight line to the data is shown in blue with its equation and the r^2 value from the method of least squares also displayed.

As with the previous comparisons described above, the plot of uptake calculated from attenuation corrected SPECT images versus that from the planar image in Figure 9.6 shows the data lying close to the line of identity. Once again, the best-fit straight line has a high r^2 value and a gradient close to 1. When the same analysis was carried out on the results from the patient image data (see Figure 8.15), there was an obvious tendency for the AC SPECT uptake to be considerably higher than that from the planar analysis. On that occasion, the difference was statistically significant with $p < 0.001$. The results from the phantom data were also demonstrated to be statistically significant with $p = 0.047$, an estimated median of -0.36% and 95% CI of $(-0.77\%, -0.02\%)$.

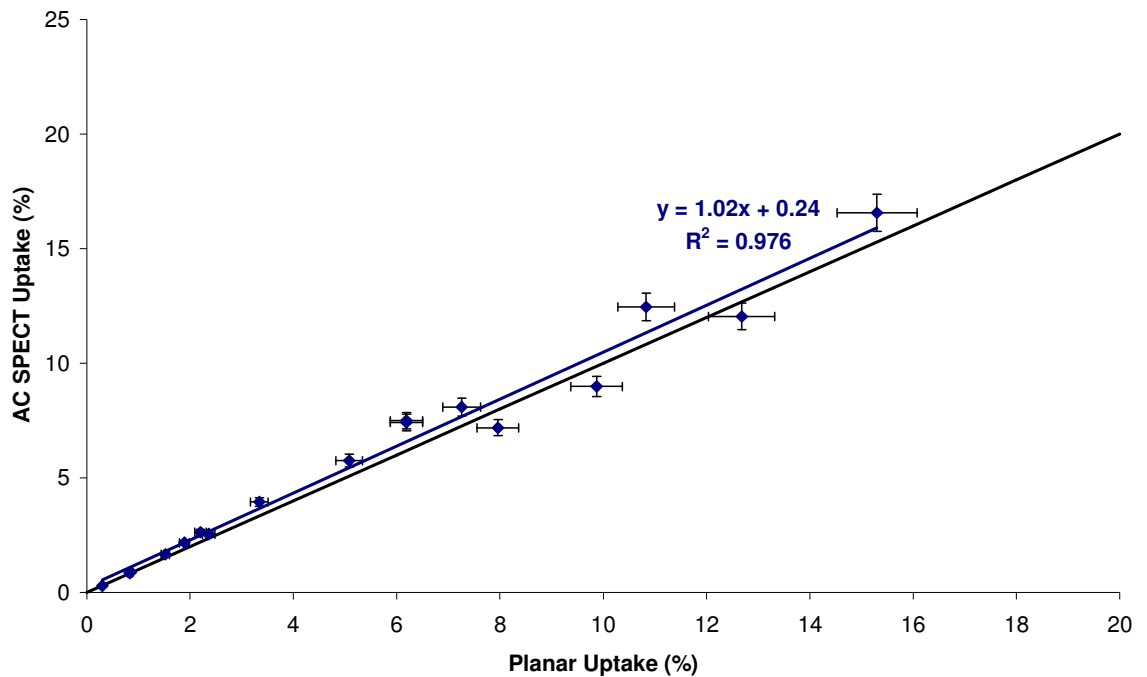


Figure 9.6 - Plot of uptake from attenuation corrected SPECT images versus uptake from planar image
The line of identity is shown in black and the best fit straight line to the data is shown in blue with its equation and the r^2 value from the method of least squares also displayed.

As was the case with the previous plots of the data from measurements of phantom “uptake”, the plot of AC SPECT uptake versus frame SPECT uptake in Figure 9.7 shows the data being much closer to the line of identity than was the case for the corresponding comparison of data from patient images shown in Figure 8.17. The phantom data are again a good fit to a straight line ($r^2 > 0.95$) with a gradient of close to 1. The patient data demonstrated a tendency for the AC SPECT uptake value to be considerably higher than that from the frame SPECT image.

For this comparison of phantom data, the Wilcoxon Signed Ranks test returned the following results: $p=0.029$, estimated median of -0.45% and 95% CI of $(-0.98\%, -0.09\%)$. The difference in calculated uptake is therefore statistically significant but, as before, the magnitude of the differences would not be of clinical significance.

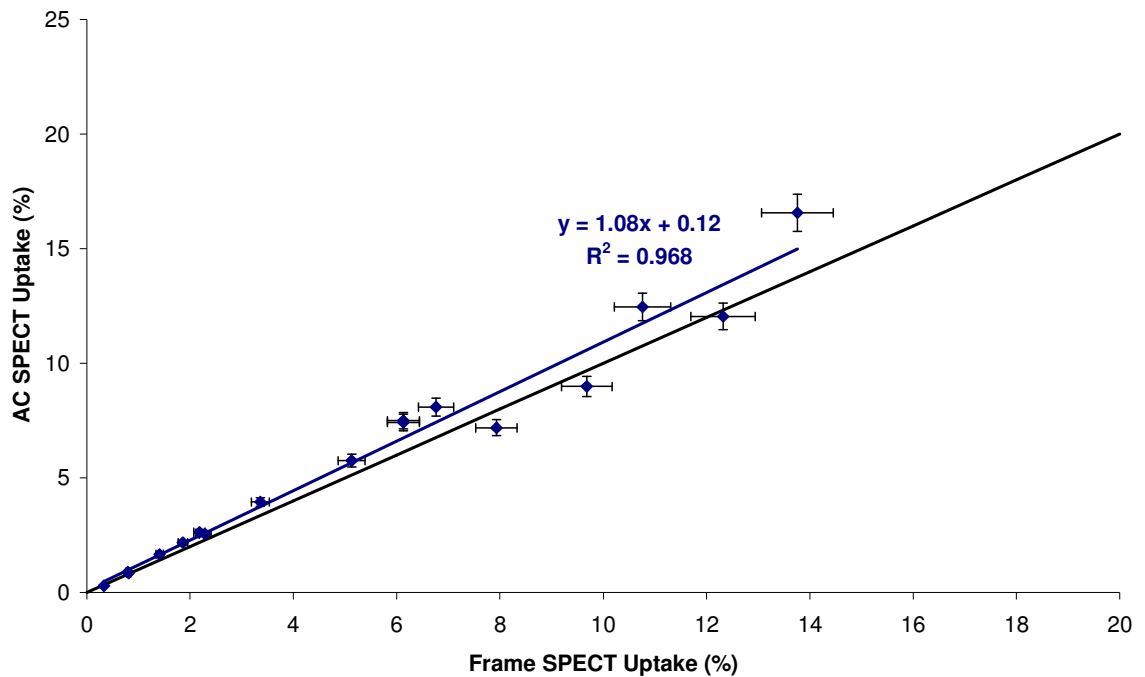


Figure 9.7 - Plot of uptake from attenuation corrected SPECT images versus uptake from frame SPECT image
 The line of identity is shown in black and the best fit straight line to the data is shown in blue with its equation and the r^2 value from the method of least squares also displayed.

The final comparison of the measured “uptake” of the phantom considered the SPECT and AC SPECT data and the resultant plot is shown in Figure 9.8. Of all the straight-line fit analyses carried out in these comparisons, this final result is the furthest from the line of identity, with a gradient of 1.11. This indicates that the uptake value calculated from the AC SPECT images tends to be higher than that calculated from the non-attenuation corrected SPECT data. This supports the findings of the plot in Figure 9.2, where the results from the SPECT images lay furthest from the line of identity, whilst those for the AC SPECT data were closest. It is also an expected result as the attenuation correction should account for the reduction in counts at the gamma camera caused by variations in the depth of origin of the gamma photons. A similar result was seen with the patient data (see Figure 8.16), although the gradient of the best fit straight line was larger at 1.30.

The Wilcoxon Signed Ranks test applied to the data gave $p=0.007$, estimated median of -0.61% and 95% CI of $(-1.26\%, -0.20\%)$, meaning that the difference was again statistically significant.

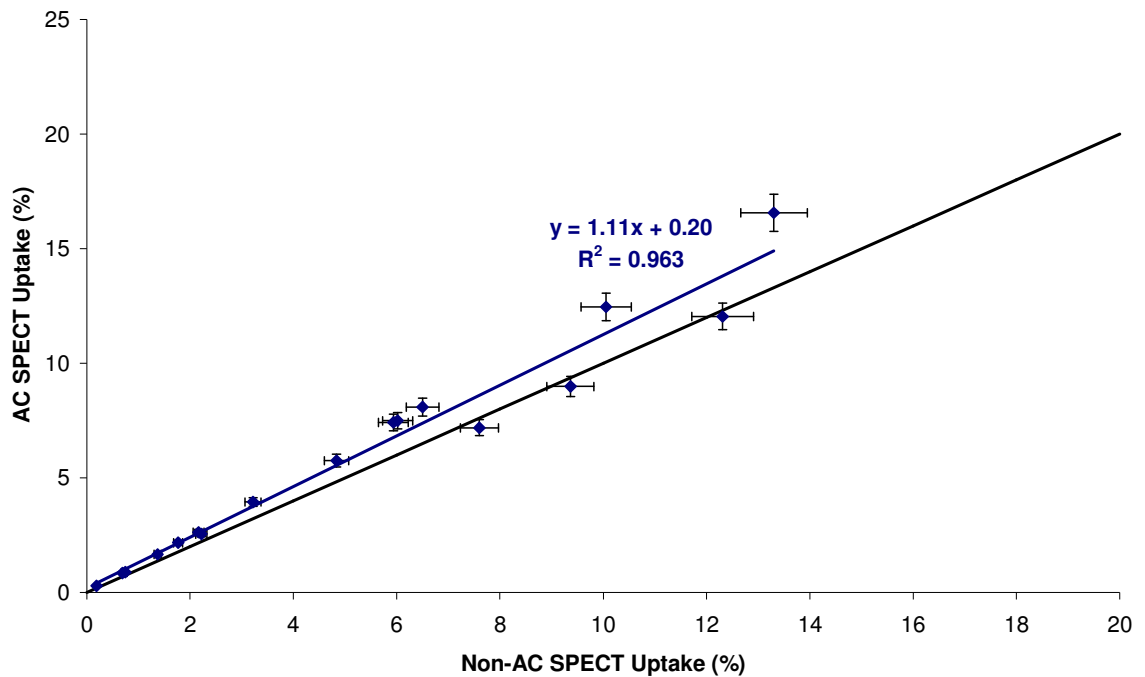


Figure 9.8 - Plot of uptake from attenuation corrected SPECT images versus uptake from SPECT images
 The line of identity is shown in black and the best fit straight line to the data is shown in blue with its equation and the r^2 value from the method of least squares also displayed.

The above comparisons all demonstrate that the uptake values calculated from the various different images acquired of a phantom are much closer than are those calculated from patient data. This is to be expected to an extent, as the phantom is an idealised situation and not truly physiological. However, the main reason for the differences is most likely to be the variation in uptake of a real thyroid gland over time, which is not the case in a phantom where the “uptake” remains fixed so long as radioactive decay of the ^{99m}Tc is taken into account.

9.3.3 CT Attenuation Corrected Uptake Values

A total of 3 SPECT/CT acquisitions of the thyroid phantom were carried out in order to assess the accuracy of the uptake measurement from images that were reconstructed using a CT mu-map for attenuation correction. All of the SPECT/CT acquisitions were carried out at the same time as one of the sets of planar and SPECT data acquisition discussed in Sections 9.3.1 & 9.3.2 above. This was to ensure that a direct comparison could be made with the uptake calculated from the planar image, the non-attenuation corrected SPECT images, the linear attenuation corrected images and the known “uptake” value.

Two different SPECT/CT uptake values were calculated, corresponding to the reconstruction of the data using the HERMES system and the reconstruction using the Siemens Syngo software. Both are iterative techniques using the CT mu-map as the basis for the attenuation correction of the reconstructed images but the Siemens method also includes a correction for scattered photons in the acquired images. The data were analysed on the HERMES system in the same way as has been described previously.

The results of the various uptake calculations on the 3 sets of phantom acquisitions are shown in Table 9.2. It is immediately clear that the uptakes calculated from the CT attenuation corrected data sets are considerably higher than those measured from the other images. They are also higher than the known values in all cases, with the images including both scatter correction and CT attenuation correction being the highest in general.

Known (%)	Planar (%)	Frame SPECT (%)	SPECT (%)	AC SPECT (%)	SPECT + CTAC (%)	SPECT + SC + CTAC (%)
2.89	2.36	2.29	2.22	2.55	3.45	5.63
11.09	9.87	9.68	9.36	8.70	15.89	15.60
13.28	7.96	7.93	7.60	7.19	19.36	21.43

Table 9.2 - Results of uptake measurements on 3 phantom acquisitions that included SPECT/CT

Known = actual “uptake” in phantom, Planar = uptake measured from planar image acquisition, Frame SPECT = uptake from anterior frame of SPECT acquisition, SPECT = uptake from reconstructed SPECT images not including attenuation correction, AC SPECT = uptake from reconstructed SPECT images with linear attenuation correction applied, SPECT + CTAC = uptake from HERMES reconstructed SPECT/CT data including attenuation correction from CT mu-map, SPECT + SC + CTAC = uptake from Siemens reconstructed SPECT/CT data including scatter correction and attenuation correction from CT mu-map.

Since attenuation correction carried out using the CT mu-map will give the most accurate correction for attenuation of counts prior to reaching the gamma camera detector, the fact that the uptake results from these data sets are highest of all is to be expected. However, they are considerably higher than the true “uptake” present in the phantom at the time of acquisition, meaning that this method may be over compensating for the effects of attenuation in the phantom image data sets. Unfortunately, the results data set was too small to successfully apply the Wilcoxon Signed Ranks test and so further acquisitions and analyses will be required to fully investigate the effect of CT attenuation correction on the uptake measurement.

9.4 Discussion

Since it is never possible to know an exact value for the “true” uptake of radiopharmaceutical in an organ, phantom studies must be used in order to assess the accuracy of different uptake measurement techniques. In this case, a total of 6 different image data sets involving both planar and SPECT images were used to perform an uptake calculation and the results were compared. The phantom used was constructed of tissue-like Perspex and filled with water in order to simulate the attenuation properties of the neck.

The main bulk of the analysis involved 17 data acquisitions and the use of 4 of these techniques: anterior planar image, anterior frame of a SPECT acquisition, reconstructed SPECT images with no attenuation correction applied and reconstructed SPECT images with the application of a uniform linear attenuation correction. Analysis was also carried out on a further 3 image data sets acquired on a SPECT/CT system and reconstructed incorporating the CT mu-map data in order to perform a more sophisticated, non-uniform, attenuation correction than the linear technique.

For each of the measurement techniques used in the main set of acquisitions, the calculated uptakes lay along a straight line with gradient <1 , indicating that the measured uptake tends to be lower than the true value for all techniques. This would not, however, have a significant clinical effect as the normal range is based upon measured uptakes without the true value being known. As expected, the uptake values calculated from the uniform attenuation corrected SPECT images were the closest to the known phantom “uptake”. This is due to the fact that there will always be some attenuation of photons between the point of origin in the phantom and the surface of the gamma camera detector, which the attenuation correction seeks to rectify. Since the materials in the phantom (Perspex and water) have similar attenuation properties at 140keV, (Hubbell & Seltzer, 1996), this linear correction will be reasonably accurate.

Also, when compared directly to one another, the results of the uptake calculations from each set of images are similar and, although the differences are statistically significant according to the Wilcoxon Signed Ranks test, the

magnitudes of the differences are small (<1%) and would not be significant in a clinical situation.

However, when the results of this phantom study are compared to those from the patient study described in Chapter 8, it is immediately clear that significant differences exist. The comparisons of the different calculated uptake values in the patient data lie much further from the line of identity than do those in the phantom study. In particular, the planar and frame SPECT data from the patient study are significantly more different than is the case for the same data sets from the phantom study.

Although the phantom is an idealised situation and so does not fully replicate the physiological uptake or imaging conditions of a true thyroid, the extent of the differences in results from the patient and phantom studies was not expected. The most likely explanation for the differences is the fact that the uptake of ^{99m}Tc -pertechnetate in a real thyroid gland does not stay constant over time (Andros *et al*, 1965, Shimmins *et al*, 1968, Esser *et al*, 1973, Atkins & Richards, 1968, Meller & Becker, 2002) whilst that in the phantom remains constant, so long as the effects of radioactive decay are taken into account.

Although work has been carried out by several groups to assess the changing ^{99m}Tc -pertechnetate uptake in the thyroid up to around 60 minutes post-injection (Andros *et al*, 1965, Shimmins *et al*, 1968, Esser *et al*, 1973, Atkins & Richards, 1968, Meller & Becker, 2002), there is little evidence in the literature of the pattern of uptake being studied beyond this time. As the maximum time of SPECT imaging post-injection was 106 minutes, with a mean of 72 minutes, it is not known how the uptake will have varied in the glands of the patients in the study between the planar and SPECT image acquisitions. Further work is therefore required to either assess the changing uptake over a longer period of time or to ensure that planar and SPECT imaging are carried out as close together as is possible to minimise any uptake change.

However, since the method used in this study for calculating thyroid percentage uptake from SPECT images was both time-consuming and labour-intensive, it is unlikely to be used in routine practice. The suggested further work is therefore unnecessary at this time. However, if automated methods of region of interest

(ROI) definition are improved over time, it may be possible to reduce the analysis time for SPECT uptakes and therefore make the method more practicable. Should this occur, work on determining the change in thyroid uptake of ^{99m}Tc -pertechnetate over an extended period of time would be worthwhile in order to validate the findings of this study.

The greater availability in recent years of SPECT/CT systems gives the opportunity to carry out non-uniform attenuation correction using a CT mu-map image to give a more accurate indication of the attenuation coefficient at each point in the acquired image data set. This should therefore produce images which are more physiologically accurate and therefore give a more accurate measurement of the uptake in an organ.

In this case, only a small number of acquisitions were performed using a SPECT/CT system as it did not become available until some time after the project had started. These preliminary results indicate that the uptake measured from CT attenuation corrected images is higher than that measured from planar, non-attenuation corrected SPECT images or SPECT images with a linear attenuation applied. The calculated uptakes are, however, also considerably higher than the known values, indicating that the CT attenuation correction tends to over-compensate for the effects of attenuation in the phantom. More phantom acquisitions and analysis are required in order to fully assess the affect of the CT attenuation correction on the calculated uptake.

9.5 Conclusions and Suggestions for Further Work

This phantom study has demonstrated that the measured uptake of ^{99m}Tc from planar and SPECT imaging tends to be lower than the true, known value. The results from performing uptake analysis on planar images, a single anterior frame from the SPECT acquisition, reconstructed SPECT images and reconstructed SPECT images with a uniform linear attenuation correction applied are similar, with no differences that would be of clinical significance demonstrated.

This is in contrast to a similar analysis performed on patient image data (see Chapter 8), where more marked differences between the calculated uptake

values were seen. This is most likely to be due to the time differences between planar and SPECT imaging of patients, during which time the uptake of ^{99m}Tc -pertechnetate may have varied significantly in the thyroid.

The preliminary results of the application of CT attenuation correction to the SPECT data from acquisitions on a SPECT/CT system indicate that there tends to be an over-compensation for the effects of attenuation and the resultant uptake calculated from the images is higher than the known value.

In order to further assess the differences between the results from the patient and phantom studies, either further acquisition of patient data with a minimal time difference between planar and SPECT acquisitions is required, or it is necessary to carry out a study to assess the change in ^{99m}Tc -pertechnetate in the thyroid gland over an extended period of time. However, since the method of calculating the uptake from SPECT images used in this study is time-consuming and labour-intensive, it is not expected that this work will be carried out unless a more rapid method of analysis involving automatic region of interest definition is found.

Further phantom acquisitions to consider the role of CT attenuation correction in uptake measurements would be interesting, however, and the preliminary results from this study suggest that this would be worthwhile.

Chapter 10 – Summary of Findings

This thesis describes the findings of two independent pieces of work carried out in the Department of Nuclear Medicine at Glasgow Royal Infirmary (GRI) - the first being a study into the use of dual-isotope subtraction SPECT in the imaging of the parathyroid glands and the second being a study into the use of SPECT imaging to calculate the uptake of the thyroid gland. The former intended to determine the clinical utility of dual-isotope subtraction SPECT for localising parathyroid adenomas prior to surgery and is described in Chapters 3 - 7 of this thesis. The latter made a comparison of the calculated uptake from planar and SPECT imaging to assess any differences and to determine if the SPECT technique could be used in routine clinical practice and is described in Chapters 8 & 9 of this thesis.

A custom designed and built thyroid/parathyroid phantom (see Chapter 2 of this thesis for further details) was used initially to determine if SPECT imaging of the thyroid and parathyroid glands was feasible and to establish suitable image acquisition parameters for each of the studies. The phantom demonstrated that the SPECT imaging was feasible and that a 180° anterior acquisition with 60 x 30s frames using a parallel hole low energy high resolution collimator would give acceptable images for both thyroid and parathyroid imaging.

An observer study with the findings compared to surgical reports was used to assess dual-isotope subtraction SPECT imaging for localisation of parathyroid adenomas. A total of 5 observers took part in the study, 3 being the department's consultant clinicians and 2 being experienced nuclear medicine clinical scientists. The results of the study demonstrated a clear increase in sensitivity for detection of true parathyroid lesions (surgery being the gold standard) when dual-isotope subtraction SPECT images were included for review.

These findings have led to a change in clinical practice at GRI, with all patients referred for parathyroid imaging now undergoing dual-isotope subtraction SPECT on a routine basis. Indeed, the SPECT image acquisition has replaced the first set of planar images which formed part of the previous routine imaging procedure (see Section 3.1.2 of this thesis for a description of the previous

procedure). The acquisition parameters have been modified slightly to improve the quality of the ^{99m}Tc -Sestamibi SPECT images by increasing the injected activity for each patient to the ARSAC limit of 900MBq and by increasing the acquisition time for each SPECT frame from 30s to 40s. These changes result in a higher total count acquisition for each SPECT frame and therefore reconstructed SPECT images with lower noise. The observers who took part in this study have commented on the improved image quality that resulted from these changes.

The recent availability of SPECT/CT in the department has led to further studies to assess the clinical utility of including a registered CT acquisition alongside the dual-isotope subtraction SPECT as standard for parathyroid imaging. This work was not far enough advanced to form part of this thesis, but a full assessment of the relative utility of SPECT/CT will be made in the future.

In contrast to the parathyroid work, the study into the use of SPECT imaging for calculating thyroid uptake has not led to any change in clinical practice at GRI. The findings were inconclusive, with differences being demonstrated between the calculated uptake values from planar and SPECT patient images that could not be easily explained. Further work carried out using the thyroid phantom designed for this study demonstrated no significant difference between the calculated planar and SPECT uptakes. This suggests that there is some physiological reason for the differences seen in the patient data that has not been taken into account. The most likely explanation is a change in the amount of ^{99m}Tc -pertechnetate present in the thyroid gland between the time that planar and SPECT imaging was carried out. However, no information on the uptake pattern of pertechnetate beyond 60 minutes is available in the literature and so no further explanation of the results is possible at present.

Although further work could be carried out to assess the physiological differences in uptake over time, the method used in this study for calculating thyroid uptake from SPECT images was too cumbersome and time-consuming to be used routinely. Therefore no change to clinical practice at GRI as a result of this study is expected and thyroid uptake will continue to be calculated from planar images.

This study has therefore resulted in a change of clinical practice for parathyroid imaging at GRI, with the introduction of dual-isotope subtraction SPECT routinely. Thyroid imaging remains unchanged, however, with the thyroid uptake being calculated from planar images.

Appendix A – Ethics Approval Documentation

North Glasgow University Hospitals
Division

Glasgow Royal Infirmary LREC (1)

4th floor, Walton Building
Glasgow Royal Infirmary
84 Castle Street
GLASGOW
G4 0SF



Telephone: 0141 211 4020
Facsimile: 0141 232 0752

16 November 2005

Mrs Jennifer L Dennis
Grade B Trainee Medical Physicist
NHS Greater Glasgow
Department of Nuclear Medicine
Queen Elizabeth Building, Glasgow Royal Infirmary
16 Alexandra Parade, Glasgow
G31 2ER

Dear Mrs Dennis

Full title of study: Investigation into high resolution data acquisition and quantitative data analysis in nuclear medicine functional imaging of the parathyroid and thyroid glands.
REC reference number: 05/S0704/85

The Research Ethics Committee reviewed the above application at the meeting held on 04 November 2005.

Ethical opinion

The members of the Committee present gave a favourable ethical opinion of the above research on the basis described in the application form, protocol and supporting documentation.

Ethical review of research sites

The favourable opinion applies to the research sites listed on the attached form.

Conditions of approval

The favourable opinion is given provided that you comply with the conditions set out in the attached document. You are advised to study the conditions carefully.

Approved documents

The documents reviewed and approved at the meeting were:

<i>Document</i>	<i>Version</i>	<i>Date</i>
Application	2	20 October 2005
Investigator CV		
Protocol	2 October 2005	
Covering Letter		20 October 2005
Summary/Synopsis	(Flowchart)	



05/S0704/85

Page 2

Participant Information Sheet	1 June 2005	
Participant Consent Form	1 June 2005	
CNORIS Confirmation of Cover Guidance note 2		
Supervisor's CV		19 October 2005

Research governance approval

The study should not commence at any NHS site until the local Principal Investigator has obtained final research governance approval from the R&D Department for the relevant NHS care organisation.

Membership of the Committee

The members of the Ethics Committee who were present at the meeting are listed on the attached sheet.

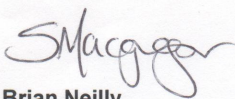
Statement of compliance

The Committee is constituted in accordance with the Governance Arrangements for Research Ethics Committees (July 2001) and complies fully with the Standard Operating Procedures for Research Ethics Committees in the UK.

05/S0704/85	Please quote this number on all correspondence
--------------------	---

With the Committee's best wishes for the success of this project

Yours sincerely

fr 
Dr Brian Neilly
Chair

Email: rose.gallacher@northglasgow.scot.nhs.uk

*Enclosures: List of names and professions of members who were present at the meeting and those who submitted written comments
 Standard approval conditions
 Site approval form (SF1)*

Copy to: *Dr. Caroline Watson
 University of Glasgow
 Research and Development Office
 Walton Building, Royal Infirmary
 Glasgow
 G4 0SF*

Glasgow Royal Infirmary LREC (1)					
LIST OF SITES WITH A FAVOURABLE ETHICAL OPINION					
<i>For all studies requiring site-specific assessment, this form is issued by the main REC to the Chief Investigator and sponsor with the favourable opinion letter and following subsequent notifications from site assessors. For issue 2 onwards, all sites with a favourable opinion are listed, adding the new sites approved.</i>					
REC reference number:	05/SO704/85	Issue number:	1	Date of issue:	16 November 2005
Chief Investigator:	Mrs Jennifer L Dennis				
Full title of study:	Investigation into high resolution data acquisition and quantitative data analysis in nuclear medicine functional imaging of the parathyroid and thyroid glands.				
<i>This study was given a favourable ethical opinion by Glasgow Royal Infirmary LREC (1) on 04 November 2005. The favourable opinion is extended to each of the sites listed below. The research may commence at each NHS site when management approval from the relevant NHS care organisation has been confirmed.</i>					
Principal Investigator	Post	Research site	Site assessor	Date of favourable opinion for this site	Notes ⁽¹⁾
Mrs Jennifer L Dennis	Grade B Trainee Medical Physicist	Glasgow Royal Infirmary	Glasgow Royal Infirmary LREC (1)	16/11/2005	
Approved by the Chair on behalf of the REC:					
..... (Signature of Chair/Administrator)					
(delete as applicable)					
..... (Name)					

(1) The notes column may be used by the main REC to record the early closure or withdrawal of a site (where notified by the Chief Investigator or sponsor), the suspension of termination of the favourable opinion for an individual site, or any other relevant development. The date should be recorded.

Appendix B – Patient Information Sheet & Consent Form



Glasgow Royal Infirmary Nuclear Medicine Department

Invitation to participate in a research study:

The use of three-dimensional nuclear medicine images for thyroid and parathyroid disorders.

You are being invited to take part in a research study. Before you decide whether or not you wish to take part, it is important for you to understand why the research is being done and what it will involve. Please take time to read the following information carefully and discuss it with others if you wish. Ask us if there is anything that is not clear or if you would like more information. Take time to decide whether or not you wish to take part.

Thank you for taking the time to read this information sheet.

What is the purpose of the study?

This study has been designed to test a new method of taking nuclear medicine images for patients with possible thyroid and parathyroid disorders. The study will involve an extra scan being taken when you come for your nuclear medicine appointment. This extra scan will take up to 30 minutes to complete. The information from this extra scan will allow a 3-dimensional (3D) picture of your thyroid/parathyroids to be created alongside the usual 2-dimensional (2D) images we collect. This 3D picture might give the doctors clearer information about your thyroid/parathyroids. This study has been set up to see how useful this extra information would be and if we should be collecting the 3D pictures for all patients coming to the department for thyroid and parathyroid scans.

Why have I been chosen?

You have been chosen to be a participant in this study because your doctor has asked that you have a scan of your thyroid gland or your parathyroid glands here at the Nuclear Medicine Department, Glasgow Royal Infirmary (GRI). All patients referred to this department for these scans are being invited to take part in the study and will receive this information leaflet.

Do I have to take part?

It is up to you to decide whether or not to take part. If you decide that you are happy to take part, you may be asked to sign a consent form. Not all patients receiving this leaflet will be asked to take part when they arrive in the department due to time constraints on our equipment. Unless you have signed the consent form, the extra scan will not be carried out. If you decide to take part you are still free to withdraw at any time and without giving a reason. A decision to withdraw at any time, or a decision not to take part, will not affect the standard of care you receive. If you do take part in the study, you will be given a copy of this information leaflet and a copy of the signed consent form to keep.

What will happen to me if I take part?

If you take part in the study you will have one extra scan taken when you come for your appointment. This will mean you have to lie still on your back on the scanning couch for a maximum of 30 minutes. After you have had all your scans, there is nothing else you need to do for this study. The investigators will then use the information from the extra scan to carry out the rest of the work for the study.

What do I have to do?

All you will need to do to take part in this study is to sign the consent form when you arrive at the department and then lie on the scanner bed for up to 30 minutes while an extra scan of your thyroid gland or parathyroid glands is taken. You will not be given any extra injections above those you will already be getting for your routine test. There will be no changes for you to make to any medication you are taking or your diet other than those that are recommended by your doctor for your routine treatment.

What are the side effects of taking part?

There will be no side effects to you from taking part in this study. The study only involves one extra scan being taken and you will not be given any other injections or medications as part of the study. You will not be asked to stop taking any medication or make any other changes to your lifestyle for the purposes of this study.

What are the possible disadvantages and risks of taking part?

There are no real disadvantages or risks to you from taking part in the study. You will not be required to have any other injections or take any other medication. You will receive a small radiation dose from the standard test that your doctor has referred you here for, but this study will not result in an increased radiation dose. The only requirement is for you to lie still on your back on a scanning couch for up to 30 minutes while the extra scan data is acquired.

What are the possible benefits of taking part?

The information from the extra scan will be available to the Nuclear Medicine consultant doctors, who will look at the results as well as those from the standard scans you will have. We are not certain at this stage if the information we obtain from the extra study scan will be beneficial for your treatment or not.

What if something goes wrong?

There will be very little excess risk to you from taking part in this study as you will not be receiving any extra radiation dose or medication, nor will any of your medication be withheld for the purposes of this study.

If you are unhappy with the level of service provided to you by the Nuclear Medicine Department, you make speak to any member of staff who will try to resolve the matter. If, however, you have any complaints about your treatment that you feel cannot be resolved by the staff within the department, there is a hospital complaints procedure that you can follow. If you wish to make a formal complaint, please contact the Patient Liaison Officer at Glasgow Royal Infirmary:

Anne Snape
Patient Liaison Department
Glasgow Royal Infirmary
84 Castle Street
Glasgow
G4 0SF
Tel: 0141 211 5112
E-mail: Anne.Snape@NorthGlasgow.Scot.NHS.UK

Will my part in this study be kept confidential?

All information which is collected about you during the course of the research will be kept strictly confidential. Any information about you which leaves the hospital will have your name, address and any other personal details removed so that you cannot be recognised from it.

What will happen to the results of the research study?

The results from this study will be published in peer-reviewed journals. All personal information about you will be removed before the results are published so that no-one can identify you from the publications.

Who is organising and funding the research?

The research is being organised by the staff in the Department of Nuclear Medicine, Glasgow Royal Infirmary. At present, no external funding has been secured for the study.

Who has reviewed the study?

The study has been reviewed by the Local Research Ethics Committee at Glasgow Royal Infirmary.

Contact for Further Information

If you have any questions about taking part in this study, please do not hesitate to contact us by post, telephone or e-mail using the details below:

Mrs. Jen Dennis
Department of Nuclear Medicine
Queen Elizabeth Building
Glasgow Royal Infirmary
16 Alexandra Parade
Glasgow
G31 2ER

Tel: 0141 211 4762 (Nuclear Medicine Reception)

E-mail: jen.dennis@northglasgow.scot.nhs.uk

Thank you very much for taking the time to read this leaflet.

**Glasgow Royal Infirmary
Nuclear Medicine Department**



Study Number:

Patient Identification Number for this trial:

CONSENT FORM

Title of Project: The use of three-dimensional nuclear medicine images for thyroid and parathyroid disorders.

Name of Researcher: Mrs Jennifer L Dennis

Please initial box

1. I confirm that I have read and understand the information sheet dated June 2005 (version 1) for the above study and have had the opportunity to ask questions.
2. I understand that my participation is voluntary and that I am free to withdraw at any time, without giving any reason, without my medical care or legal rights being affected.
3. I understand that sections of any of my medical notes may be looked at by healthcare professionals where it is relevant to my taking part in this research. I give permission for these individuals to have access to my records.
4. I agree to take part in the above study.

Name of Patient

Date

Signature

Name of Person taking consent
(if different from researcher)

Date

Signature

Researcher

Date

Signature

1 for patient; 1 for researcher; 1 to be kept with hospital notes

Appendix C – Scoring Sheets for Parathyroid Observer Study

Jen Dennis – PhD by Research

Observer: _____

Planar Parathyroid Image Study

Date: _____

PATIENT: _____

Number of abnormal foci seen: _____

Certainty of focus: definite suggestive equivocal negative

Location (thyroid): left anterior medial
right posterior lateral

ectopic (state): _____

Image quality:	<i>Sestamibi:</i> (poor) 1 <input type="checkbox"/> 2 <input type="checkbox"/> 3 <input type="checkbox"/> 4 <input type="checkbox"/> 5 <input type="checkbox"/> (excellent)
	<i>Iodine</i> (poor) 1 <input type="checkbox"/> 2 <input type="checkbox"/> 3 <input type="checkbox"/> 4 <input type="checkbox"/> 5 <input type="checkbox"/> (excellent)
	<i>Subtraction</i> (poor) 1 <input type="checkbox"/> 2 <input type="checkbox"/> 3 <input type="checkbox"/> 4 <input type="checkbox"/> 5 <input type="checkbox"/> (excellent)
Usefulness of subtraction: (not at all helpful) 1 <input type="checkbox"/> 2 <input type="checkbox"/> 3 <input type="checkbox"/> 4 <input type="checkbox"/> 5 <input type="checkbox"/> (very helpful)	

Additional comments: _____

Jen Dennis – PhD by Research
 Observer: _____

SPECT Parathyroid Image Study
 Date: _____

PATIENT: _____

Number of abnormal foci seen: _____

Certainty of focus: definite suggestive equivocal negative

Location (thyroid): left anterior upper medial
 right posterior lower lateral

ectopic (state): _____

Image quality:
Sestamibi: (poor) 1 2 3 4 5 (excellent)
Iodine: (poor) 1 2 3 4 5 (excellent)
Subtraction: (poor) 1 2 3 4 5 (excellent)

Usefulness of subtraction: (not at all helpful) 1 2 3 4 5 (very helpful)

Additional comments: _____

Jen Dennis – PhD by Research
 Observer: _____

Sestamibi Only (Planar & SPECT) Parathyroid Image Study
 Date: _____

PATIENT: _____

Number of abnormal foci seen: _____

Certainty of focus: definite suggestive equivocal negative

Seen on: early planar late planar SPECT

Location (thyroid): left anterior medial
 right posterior lower lateral

ectopic (state): _____

Image quality: Planar (poor) 1 2 3 4 5 (excellent)
 SPECT (poor) 1 2 3 4 5 (excellent)

Usefulness of SPECT: (not at all helpful) 1 2 3 4 5 (very helpful)

Additional comments: _____

Jen Dennis – PhD by Research *All Images (Planar & SPECT Dual-Isotope) Parathyroid Image Study*
 Observer: _____ Date: _____

PATIENT: _____

Number of abnormal foci seen: _____

Certainty of focus: definite suggestive equivocal negative

Seen on: early planar late planar SPECT SPECT sub

Location (thyroid): left anterior upper medial
 right posterior lower lateral

ectopic (state): _____

Image quality: *Planar* (poor) 1 2 3 4 5 (excellent)
SPECT (poor) 1 2 3 4 5 (excellent)

Usefulness of SPECT: (not at all helpful) 1 2 3 4 5 (very helpful)

Additional comments: _____

Bibliography

- Adami, S., Marocci, C. & Gatti, D. (2002) Epidemiology of primary hyperparathyroidism in Europe. Journal of Bone and Mineral Research 17 Suppl 2, N18-23.
- Adler, J.T., Sippel, R.S. & Chen, H. (2008) The influence of surgical approach on quality of life after parathyroid surgery. Annals of Surgical Oncology, 15(6), 1559-1565.
- Adler, J.T., Sippel, R.S., Schaefer, S. & Chen, H. (2009) Surgery improves quality of life in patients with “mild” hyperparathyroidism. American Journal of Surgery, 197(3), 284-290.
- Akram, K., Parker, J.A., Donohoe, K. & Kolodny, G. (2009) Role of single photon emission computed tomography/computed tomography in localization of ectopic parathyroid adenoma: a pictorial case series and review of the current literature. Clinical Nuclear Medicine, 34(8), 500-502.
- Anderson, S.R., Vaughn, A., Karakla, D. & Wadsworth, J.T. (2008) Effectiveness of surgeon interpretation of technetium Tc99m Sestamibi scans in localising parathyroid adenomas. Archives of Otolaryngology - Head and Neck Surgery, 134(9), 953-957.
- Andros, G., Harper, P.V., Lathrop, K.A. & McCardle, R.J. (1965) Per technetate-99m localization in man with applications to thyroid scanning and the study of thyroid physiology. Journal of Clinical Endocrinology and Metabolism, 25, 1067-1076.
- Ansquer, C., Mirallié, F., Carlier, T., Anney-Hunguenin, H., Aubron, F. & Kraeber-Bodéré, F. (2008) Preoperative localisation of parathyroid lesions. Value of ^{99m}Tc-MIBI tomography and factors influencing detection. Nuclear-Medizin, 47(4), 158-162.
- Arveschoug, A.K., Bertelsen, H., Vammen, B. & Brochner-Mortensen, J. (2007) Preoperative dual-phase parathyroid imaging with Tc-99m-Sestamibi: accuracy

and reproducibility of the pinhole collimator with and without oblique images. Clinical Nuclear Medicine, 32(1), 9-12.

Ashkar, F.S., Naya, J.L. & Smith, E.M. (1971) Parathyroid scanning with ⁷⁵Se-selenomethionine and glucagon stimulation. Journal of Nuclear Medicine, 12(11), 751-753.

Atkins, H.L. & Richards, P. (1968) Assessment of thyroid function and anatomy with technetium-99m as pertechnetate. Journal of Nuclear Medicine, 9, 7-15.

Beggs, A.D. & Hain, S.F. (2005) Localisation of parathyroid adenomas using ¹¹C-methionine positron emission tomography. Nuclear Medicine Communications, 26, 133-136.

Beierwaltes, W.H. (1991) Endocrine imaging: parathyroid, adrenal cortex and medulla, and other endocrine tumours. Part II. Journal of Nuclear Medicine, 32, 1627-1639.

Bekerman, C., Schulak, J.A., Kaplan, E.L. & Shen, K. (1977) Parathyroid adenoma imaged by Ga-67 citrate scintigraphy: case report. Journal of Nuclear Medicine, 18, 1096-1098.

Bénard, F., Lefebvre, B., Beuvon, F., Langlois, M-F. & Bisson, G. (1995) Rapid washout of technetium-99m-MIBI from a large parathyroid adenoma. Journal of Nuclear Medicine, 36, 241-243.

Berber, E., Parikh, R.T., Ballem, N., Garner, C.N., Milas, M. & Siperstein, A.E. (2008) Factors contributing to negative parathyroid localisation: an analysis of 1000 patients. Surgery, 144, 74-79.

Bergenfelz, A., Lindblom, P., Tibblin, S. & Westerdahl, J. (2002) Unilateral versus bilateral neck exploration for primary hyperparathyroidism: a prospective randomised controlled trial. Annals of Surgery, 236(5), 543-551.

Berne, R.M & Levy, M.N. (ed.) (1993) Physiology Third Edition Ch47, p885. St Louis, Missouri: Mosby-Year Book, Inc.

Besser, M.G., Cudworth, A.G. & Thorner, M.O. (1994) Clinical Endocrinology Second Edition, London: Mosby-Wolfe.

Billotey, C., Sarfati, E., Aurengo, A., Duet, M., Mündler, O., Toubert, M-E., Rain, J-D. & Najean, Y. (1996a) Advantages of SPECT in technetium-99m-Sestamibi parathyroid scintigraphy. Journal of Nuclear Medicine, 37, 1773-1778.

Billotey, C., Sarfati, E., Rain, J.D. & Najean, Y. (1996b) A new scintigraphic method in cases of persistence or recurrence of secondary or tertiary hyperparathyroidism [Abstract]. Kidney International, 50(5), 1773.

Bolster, A.A. & Waddington, W.A. (1996) Medical Devices Agency Gamma Camera Assessment Team: Gamma camera performance assessment protocol, London: MDA.

Bracewell, R.N. & Riddle, A.C. (1967) Inversion of fan-beam scans in radio astronomy. The Astrophysical Journal, 150, 427-434.

Brambilla, M., Cannillo, B., Dominietto, M., Leva, L., Secco, C. & Inglese, E. (2005) Characterisation of ordered-subsets expectation maximisation with 3D post-reconstruction Gauss filtering and comparison with filtered backprojection in ^{99m}Tc SPECT. Annals of Nuclear Medicine, 19(2), 75-82.

Bristol-Myers Squibb (2005) Cardiolite: summary of product characteristics Brussels, Belgium. Available at:
http://www.cardiolite.co.uk/bottom_links/product_characteristics.asp

Bruyant, P.P. (2002) Analytic and iterative reconstruction algorithms in SPECT. Journal of Nuclear Medicine, 43, 1343-1358.

Calendini-Viallet, C., Bussy, E., Lescout, J.M. & Rinaldi, J.P. (1997) Parathyroid adenomas with rapid washout: two case reports. Medecine Nucleaire, 21(7), 439-443.

Cann, C.E. & Prussin, S.G. (1980) Possible parathyroid imaging using Ga-67 and other aluminum analogues. Journal of Nuclear Medicine, 21, 471-474.

Carlier, T., Oudoux, A., Mirallié, E., Seret, A., Daumy, I., Leux, C., Bodet-Milin, C., Kraeber-Bodéré, F. & Ansquer, C. (2008) ^{99m}Tc -MIBI pinhole SPECT in primary hyperparathyroidism: comparison with conventional SPECT, planar scintigraphy and ultrasonography. European Journal of Nuclear Medicine and Molecular Imaging, 35(3), 637-643.

Casara, D., Rubello, D., Pelizzo, M.R. & Shapiro, B. (2001) Clinical role of $^{99m}\text{TcO}_4$ /MIBI scan, ultrasound and intra-operative gamma probe in the performance of unilateral and minimally invasive surgery in primary hyperparathyroidism. European Journal of Nuclear Medicine, 28, 1351-1359.

Cayo, A. & Chen, H. (2008) Radioguided reoperative parathyroidectomy for persistent primary hyperparathyroidism. Clinical Nuclear Medicine, 33, 668-670.

Chen, C.C., Holder, L.E., Scovill, W.A., Tehan, A.M. & Gann, D.S. (1997) Comparison of parathyroid imaging with technetium-99m-pertechnetate/Sestamibi subtraction, double-phase technetium-99m-Sestamibi and technetium-99m-Sestamibi SPECT. Journal of Nuclear Medicine, 38, 834-839.

Chen, J.J.S., LaFrance, N.D., Allo, M.D., Cooper, D.S. & Ladenson, P.W. (1988) Single photon emission computed tomography of the thyroid. Journal of Clinical Endocrinology and Metabolism, 66, 1240-1246.

Coakley, A.J. (2003) Nuclear medicine and parathyroid surgery; a change in practice [Editorial]. Nuclear Medicine Communications, 24, 111-113.

Delacroix, D., Guerre, J.P., Leblanc, P. & Hickman, C. (2002) Radionuclide and Radiation Protection Data Handbook 2002. France: Nuclear Technology Publishing.

DiGiulio, W. & Beierwaltes, W.H. (1964) Parathyroid scanning with selenium⁷⁵ labelled methionine. Journal of Nuclear Medicine, 5, 417-427.

Erbil, Y., Barbaros, U., Yanik, B.T., Salmaslioglu, A., Tunaci, M., Adalet, I., Bozbora, A. & Özarmağan, S. (2006) Impact of gland morphology and

concomitant thyroid nodules on preoperative localisation of parathyroid adenomas. Laryngoscope, 116, 580-585.

Esser, P.D., Atkins, H.L. & Robertson, J.S. (1973) Rate of accumulation of technetium 99m by the thyroid. American Journal of Roentgenology, 118, 827-830.

Even-Sapir, E., Keidar, Z., Sachs, J., Engel, A., Bettman, L., Gaitini, D., Guralnik, L., Werbin, N., Iosilevsky, G. & Israel, O. (2001) The new technology of combined transmission and emission tomography in the evaluation of endocrine neoplasms. Journal of Nuclear Medicine, 42(7), 998-1004.

Fjeld, J.G., Erichsen, K., Pfeffer, P.F., Clausen, O.P.F. & Rootwelt, K. (1997) Technetium-99m-Tetrofosmin for parathyroid scintigraphy: a comparison with Sestamibi. Journal of Nuclear Medicine, 38, 831-834.

Fröberg, A.C., Valkema, R., Bonjer, H.J., Krenning, E.P. (2003) ^{99m}Tc -tetrofosmin or ^{99m}Tc -sestamibi for double-phase parathyroid scintigraphy? European Journal of Nuclear Medicine, 30, 193-196.

Gallowitsch, H.J., Mikosch, P., Kresnik, E., Gomez, I. & Lind, P. (1997) Technetium 99m Tetrofosmin parathyroid imaging: results with double-phase study and SPECT in primary and secondary hyperparathyroidism. Investigative Radiology, 32(8), 459-465.

Gallowitsch, H.J., Mikosch, P., Kresnik, E., Unterweger, O. & Lind, P. (2000) Comparison between ^{99m}Tc -Tetrofosmin/pertechnetate subtraction scintigraphy and ^{99m}Tc -Tetrofosmin SPECT for preoperative localisation of parathyroid adenoma in an endemic goitre area. Investigative Radiology, 35(8), 453-459.

Gates, J.D., Benavides, L.C., Shriver, C.D., Peoples, G.E. & Stojadinovic, A. (2009) Preoperative thyroid ultrasound in all patients undergoing parathyroidectomy?. Journal of Surgical Research, 155, 254-260.

Gayed, I.W., Kim, E.E., Broussard, W.F., Evans, D., Lee, J., Broemeling, L.D., Ochoa, B.B., Moxley, D.M., Erwin, W.D. & Podoloff, D.A. (2005) The value of

^{99m}Tc -Sestamibi SPECT/CT over conventional SPECT in the evaluation of parathyroid adenomas or hyperplasia. Journal of Nuclear Medicine, 46(2), 248-252.

Gordon, L., Burkhalter, W. & Mah, E. (2002) Dual-phase ^{99m}Tc -Sestamibi imaging: its utility in parathyroid hyperplasia and use of immediate/delayed image ratios to improve diagnosis of hyperparathyroidism. Journal of Nuclear Medicine Technology, 30, 179-184.

Greene, A.B., Butler, R.S., McIntyre, S., Barbosa, G.F., Mitchell, J., Berber, E., Siperstein, A. & Milas, M. (2009) National trends in parathyroid surgery from 1998 to 2008: a decade of change. Journal of the American College of Surgeons, 209, 332-343.

Hall, R. & Evered, D.C. (1990) A Colour Atlas of Endocrinology Second Edition, London: Wolfe Medical Publications Ltd.

Hänninen, E.L., Vogl, T.J., Steinmüller, T., Ricke, J., Neuhaus, P. & Felix, R. (2000) Preoperative contrast-enhanced MRI of the parathyroid glands in hyperparathyroidism. Investigative Radiology, 35(7), 426-430.

Hara, N., Takayama, T., Onoguchi, M., Obane, N., Miyati, T., Yoshicka, T., Sakaguchi, K. & Honda, M. (2007) Subtraction SPECT for parathyroid scintigraphy based on maximisation of mutual information. Journal of Nuclear Medicine Technology, 35(2), 84-90.

Haynie, T.P., Otte, W.K. & Wright, J.C. (1964) Visualisation of a hyperfunctioning parathyroid adenoma using Se^{75} selenomethionine and the photoscanner. Journal of Nuclear Medicine, 5, 710-714.

Hays, M.T. & Berman, M. (1977) Pertechnetate distribution in man after intravenous infusion: a compartmental model. Journal of Nuclear Medicine, 18, 898-904.

Hays, M.T. (1978) Kinetics of the human thyroid trap: a compartmental model. Journal of Nuclear Medicine, 19, 789-795.

van Heerden, J.A. & Grant, C.S. (1991) Surgical treatment of primary hyperparathyroidism: an institutional perspective. World Journal of Surgery, 15, 688-692.

Heller, K.S., Attie, J.N. & Dubner, S. (1993) Parathyroid localization: inability to predict multiple gland involvement. The American Journal of Surgery, 166(4), 357-359.

Herrmann, K., Takei, T., Kanegae, K., Shiga, T., Buck, A.K., Altomonte, J., Schwaiger, M., Schuster, T., Nishijima, K., Kuge, Y. & Tamaki, N. (2009) Clinical value and limitations of [11C]-methionine PET for detection and localisation of suspected parathyroid adenomas. Molecular Imaging and Biology, 11(5), 356-363.

Hewin, D.F., Brammar, T.J., Kabala, J. & Farndon, J.R. (1997) Role of preoperative localisation in the management of primary hyperparathyroidism. The British Journal of Surgery, 84(10), 1377-1380.

Hilditch, T.E. & Alexander, W.D. (1980) Unexpected differences in early thyroidal trapping of iodide and pertechnetate. European Journal of Nuclear Medicine, 5, 115-117.

Hindié, E., Mellièrè, D., Jeanguillaume, C., Perlemuter, L., Chéhadé, F. & Galle, P. (1998) Parathyroid imaging using simultaneous double-window recording of technetium-99m-Sestamibi and iodine-123. Journal of Nuclear Medicine, 39(6), 1100-1105.

Hindié, E., Mellièrè, D., Jeanguillaume, C., Ureña, P., deLabriolle-Vaylet, C. & Perlemuter, L. (2000) Unilateral surgery for primary hyperparathyroidism on the basis of technetium Tc 99m Sestamibi and iodine 123 subtraction scanning. Archives of Surgery, 135(12), 1461-1468.

Hindié, E., Ugur, Ö., Fuster, D., O'Doherty, M., Grassetto, G., Ureña, P., Kettle, A., Gulec, S.A., Pons, F. & Rubello, D. (2009) 2009 EANM parathyroid guidelines. European Journal of Nuclear Medicine and Molecular Imaging, 36, 1201-1216.

Ho Shon, I.A., Yan, W., Roach, P.J., Bernard, E.J., Shields, M., Sywak, M., Sidhu, S. & Delbridge, L.W. (2008) Comparison of pinhole and SPECT ^{99m}Tc -MIBI imaging in primary hyperparathyroidism. Nuclear Medicine Communications, 29, 949-955.

Hubbell, J.H. & Seltzer, S.M. (1996) Tables of X-ray Mass Attenuation Coefficients and Mass Energy-Absorption Coefficients. Ionizing Radiation Division, Physics Laboratory, National Institute of Standards and Technology. Gaithersburg, MD: NIST. Available at:
<http://physics.nist.gov/PhysRefData/XrayMassCoef/cover.html>

Hung, G-U., Wang, S-J. & Lin, W-Y. (2003) Tc-99m MIBI parathyroid scintigraphy and intact parathyroid hormone levels in hyperparathyroidism. Clinical Nuclear Medicine, 28(3), 180-185.

ICRP (1975) ICRP Report 23: Report of the Task Group on Reference Man, pp.196-202. Oxford: Pergamon Press Ltd.

ICRP (1988) ICRP Report 53: Radiation Dose to Patients from Radiopharmaceuticals - A Report of a Task Group of Committee 2 of the International Commission on Radiological Protection, pp.197-200. Oxford: Pergamon Press Ltd.

ICRU (1989) ICRU Report 44: Tissue Substitutes in Radiation Dosimetry and Measurement, Bethesda, MD: ICRU.

Ishibashi, M., Nishida, H., Hiromatsu, Y., Kojima, K., Tabuchi, E. & Hayabuchi, N. (1998) Comparison of technetium-99m-MIBI, technetium-99m-Tetrofosmin, ultrasound and MRI for localisation of abnormal parathyroid glands. Journal of Nuclear Medicine, 39(2), 320-324.

van Isselt, J.W., de Klerk, J.M., van Rijk, P.P., van Gils, A.P.G., Polman, L.J., Kamphuis, C., Meijer, R. & Beekman, F.J. (2003) Comparison of methods for thyroid volume estimation in patients with Graves' disease. European Journal of Nuclear Medicine and Molecular Imaging, 30, 525-531.

- Jeanguillaume, C., Hindié, E., Meignan-Debray, S., Mellièrre, D. & Galle, P. (1997) Tc-99m Sestamibi and I-123 detection of a parathyroid adenoma in the presence of a cold thyroid nodule. Clinical Nuclear Medicine, 22(4), 258-260.
- Jensen, O.N. (1999) Prevalence of secondary hyperparathyroidism in patients aged 80 and over. Ugeskrift for Laeger, 161(16), 2362-2364.
- Judson, B.L. & Shaha, A.R. (2008) Nuclear imaging and minimally invasive surgery in the management of hyperparathyroidism. Journal of Nuclear Medicine, 49, 1813-1818.
- Kara Gedik, G., Bozkurt, F.M., Ugur, O., Grassetto, G. & Rubello, D. (2008) The additional diagnostic value of a single-session combined scintigraphic and ultrasonographic examination in patients with thyroid and parathyroid diseases. Panminerva Medica, 50(3), 199-205.
- Kettle, A.G. & O'Doherty, M.J. (2006) Parathyroid imaging: how good is it and how should it be done?. Seminars in Nuclear Medicine, 36(3), 206-211.
- Krausz, Y., Horne, T., Wynchank, S. & Halevy, A. (1995) Lateral neck imaging for spatial localisation of parathyroid tissue. Nuclear Medicine and Biology, 22, 391-394.
- Krausz, Y., Wilk, M., Saliman, F. & Chisin, R. (1997) Role of high-resolution pinhole tomography in the evaluation of thyroid abnormalities. Thyroid, 7(6), 847-852.
- Krausz, Y., Shiloni, E., Bocher, M., Agranovicz, S., Manos, B. & Chisin, R. (2001) Diagnostic dilemmas in parathyroid scintigraphy. Clinical Nuclear Medicine, 26(12), 997-1001.
- Krausz, Y., Bettman, L., Guralnik, L., Yosilevsky, G., Keidar, Z., Bar-Shalom, R., Even-Sapir, E., Chisin, R. & Israel, O. (2006) Technetium-99m-MIBI SPECT/CT in primary hyperparathyroidism. World Journal of Surgery, 30, 76-83.

Kresnik, E., Gallowitsch, H-J., Mikosch, P., Gomez, I. & Lind, P. (1997) Technetium-99m-MIBI scintigraphy of thyroid nodules in an endemic goitre area. Journal of Nuclear Medicine, 38(1), 62-65.

Lavelly, W.C., Goetze, S., Friedmann, K.P., Leal, J.P., Zhang, Z., Garret-Mayer, E., Dackiw, A.P., Tufano, R.P., Zeiger, M.A. & Ziessmann, H.A. (2007) Comparison of SPECT/CT, SPECT, and planar imaging with single- and dual-phase ^{99m}Tc-Sestamibi parathyroid scintigraphy. Journal of Nuclear Medicine, 48(7), 1084-1089.

Leslie, W.D., Dupont, J.O., Bybel, B. & Riese, K.T. (2002) Parathyroid ^{99m}Tc-sestamibi scintigraphy: dual-tracer subtraction is superior to double-phase washout. European Journal of Nuclear Medicine, 29, 1566-1570.

Longmore, M., Wilkinson, I., Turmezei, T. & Cheung, C.K. (2007) Oxford Handbook of Clinical Medicine Seventh Edition. New York: Oxford University Press.

Lorberboym, M., Minski, I., Macadziab, S., Nikolov, G. & Schachter, P. (2003) Incremental diagnostic value of preoperative ^{99m}Tc-MIBI SPECT in patients with a parathyroid adenoma. Journal of Nuclear Medicine, 44, 904-908.

Mariani, G., Gulec, S.A., Rubello, D., Boni, G., Puccini, M., Pelizzo, M.R., Manca, G., Casara, D., Sotti, G., Erba, P., Volterrani, D. & Giuliano, A.E. (2003) Preoperative localisation and radioguided parathyroid surgery. Journal of Nuclear Medicine, 44, 1443-1458.

Martini, F.H. (ed.) (2001) Fundamentals of Anatomy and Physiology Fifth Edition Ch18, pp.593-599. Upper Saddle River, NJ: Prentice Hall.

Mavai, R. & Caride, V.J. (1996) Pin-hole collimator, parallax, and the localisation of mediastinal parathyroid adenoma. Clinical Nuclear Medicine, 21(7), 527-529.

Meller, J. & Becker, W. (2002) The continuing importance of thyroid scintigraphy in the era of high-resolution ultrasound. European Journal of Nuclear Medicine, 29(S2), S425-S438.

Moinuddin, M. & Whynott, C. (1996) Ectopic parathyroid adenomas: multi-imaging modalities and its management. Clinical Nuclear Medicine, 21(1), 27-32.

Moka, D., Eschner, W., Voth, E., Dietlein, M., Larena-Avallaneda, A. & Schicha, H. (2000a) Iterative reconstruction: an improvement of technetium-99m MIBI SPET for the detection of parathyroid adenomas? European Journal of Nuclear Medicine, 27, 485-489.

Moka, D., Voth, E., Dietlein, M., Lorena-Avallaneda, A. & Schicha, H. (2000b) Preoperative localization of parathyroid adenomas using ^{99m}Tc -MIBI scintigraphy. American Journal of Medicine, 108(9), 733-736.

Moore, K.L. & Agur, A.M.R. (2007) Essential Clinical Anatomy Third Edition, Ch8, pp.608-610. Baltimore, MD: Lippincott Williams & Wilkins.

Neumann, D.R. (1992) Simultaneous dual-isotope SPECT imaging for the detection and characterisation of parathyroid pathology. Journal of Nuclear Medicine, 33, 131-134.

Neumann, D.R., Esselstyn, C.B.Jr., Kim, E.Y., Go, R.T., Obuchowski, N.A. & Rice, T.W. (1997a) Preliminary experience with double-phase SPECT using Tc-99m Sestamibi in patients with hyperparathyroidism. Clinical Nuclear Medicine, 22(4), 217-221.

Neumann, D.R., Esselstyn, C.B.Jr., Go, R.T., Wong, C.O., Rice, T.W. & Obuchowski, N.A. (1997b) Comparison of double-phase ^{99m}Tc -Sestamibi with ^{123}I - ^{99m}Tc -Sestamibi subtraction SPECT in hyperparathyroidism. American Journal of Roentgenology, 169, 1671-1674.

Neumann, D.R., Esselstyn, C.B.Jr., Madera, A., Wong, C.O. & Lieber, M. (1998) Parathyroid detection in secondary hyperparathyroidism with $^{123}\text{I}/^{99m}\text{Tc}$ -

Sestamibi subtraction single photon emission computed tomography. Journal of Clinical Endocrinology and Metabolism, 83(11), 3867-3871.

Neumann, D.R., Esselstyn, C.B.Jr. & Madera, A. (2000) Sestamibi/iodine subtraction single photon emission computed tomography in reoperative secondary hyperparathyroidism. Surgery, 128, 22-28.

Neumann, D.R., Obuchowski, N.A. & DiFilippo, F.P. (2008) Preoperative $^{123}\text{I}/^{99\text{m}}\text{Tc}$ -Sestamibi subtraction SPECT and SPECT/CT in primary hyperparathyroidism. Journal of Nuclear Medicine, 49(12), 2012-2017.

Nichols, K.J., Tomas, M.B., Tronco, G.G., Rini, J.N., Kunjumman, B.D., Heller, K.S., Szynter, L.A. & Palestro, C.J. (2008) Preoperative parathyroid scintigraphic lesion localization: accuracy of various types of readings. Radiology, 248(1), 221-232.

O'Doherty, M.J. & Kettle, A.G. (2003) Parathyroid imaging: preoperative localisation. Nuclear Medicine Communications, 24, 125-131.

Okada, J., Higashitsuji, Y., Tamada, H., Kawashiro, O., Fukuzaki, T., Suzuki, T. & Itou, H. (2003) Graphical analysis of $^{99\text{m}}\text{Tc}$ thyroid scintigraphy. Annals of Nuclear Medicine, 17, 235-238.

Otto, D., Boerner, A.R., Hofmann, M., Brunkhorst, R., Meyer, G.J., Petrich, T., Scheumann, G.F. & Knapp, W.H. (2004) Pre-operative localisation of hyperfunctional parathyroid tissue with ^{11}C -methionine PET. European Journal of Nuclear Medicine and Molecular Imaging, 31(10), 1405-1412.

Pant, G.S., Kumar, R., Gupta, A.K., Sharma, S.K. & Pandey, A.K. (2003) Estimation of thyroid mass in Graves' disease by a scintigraphic method. Nuclear Medicine Communications, 24, 743-748.

Papathanassiou, D., Flament, J-B., Pochart, J-M., Patey, M., Marty, H., Liehn, J-C. & Schwartz, C. (2008) SPECT/CT in localization of parathyroid adenoma or hyperplasia in patients with previous neck surgery. Clinical Nuclear Medicine, 33(6), 394-397.

- Pattou, F., Huglo, D. & Proye, C. (1998) Radionuclide scanning in parathyroid diseases. British Journal of Surgery, 85, 1605-1616.
- Peeler, B.B., Martin, W.H., Sandler, M.P. & Goldstein, R.E. (1997) Sestamibi parathyroid scanning and preoperative localisation studies for patients with recurrent/persistent hyperparathyroidism or significant comorbid conditions: development of an optimal localisation strategy. The American Surgeon, 63(1), 37-46.
- Pelizzo, M.R., Pagetta, C., Piotto, A., Sorgato, N., Merante Boschini, I., Toniato, A., Grassetto, G. & Rubello, D. (2008) Surgical treatment of primary hyperparathyroidism: from bilateral neck exploration to minimally invasive surgery. Minerva Endocrinologica, 33(2), 85-93.
- Profanter, C., Prommegger, R., Gabriel, M., Lucciarini, P., Moncayo, R. & Wetscher, G.J. (2003) Comparison of planar scintiscanning and pinhole subtraction SPECT in preoperative imaging of primary hyperparathyroidism in an endemic goitre area. The Endocrinologist, 13(2), 112-115.
- Quiros, R.M., Alioto, J., Wilhelm, S.M., Ali, A. & Prinz, R.A. (2004) An algorithm to maximise use of minimally invasive parathyroidectomy. Archives of Surgery, 139, 501-507.
- Rauth, J.D., Sessions, R.B., Shupe, S.C. & Ziessman, H.A. (1996) Comparison of Tc-99m MIBI and Tl-201/Tc-99m pertechnetate for diagnosis of primary hyperparathyroidism. Clinical Nuclear Medicine, 21(8), 602-608.
- Robin, N.I. (1996) The Clinical Handbook of Endocrinology and Metabolic Disease. Carnford, Lancs.: Parthenon Publishing.
- Rodgers, S.E., Lew, J.I. & Solórzano, C.C. (2008) Primary hyperparathyroidism. Current Opinion in Oncology, 20, 52-58.
- Rubello, D., Saladini, G., Casara, D., Borsato, N., Toniato, A., Piotto, A., Bernante, P. & Pelizzo, M.R. (2000) Parathyroid imaging with pertechnetate plus

perchlorate/MIBI subtraction scintigraphy: a fast and effective technique. Clinical Nuclear Medicine, 25(7), 527-531.

Rubello, D., Fanti, S., Nanni, C., Farsad, M., Castellucci, P., Boschi, S., Franchi, R., Mariani, G., Fig, L.M. & Gross, M.D. (2006) ^{11}C -methionine PET/CT in $^{99\text{m}}\text{Tc}$ -sestamibi-negative hyperparathyroidism in patients with renal failure on chronic haemodialysis. European Journal of Nuclear Medicine and Molecular Imaging, 33, 453-459.

Russell, C.F.J., Dolan, S.J. & Laird, J.D. (2006) Randomised clinical trial comparing scan-directed unilateral *versus* bilateral cervical exploration for primary hyperparathyroidism due to solitary adenoma. British Journal of Surgery, 93, 418-421.

Saeed, S., Yao, M., Philip, B. & Blend, M. (2006) Localising hyperfunctioning parathyroid tissue: MRI or nuclear study or both?. Clinical Imaging, 30, 257-265.

Sandler, M.P. & Patton, J.A. (1987) Multimodality imaging of the thyroid and parathyroid glands. Journal of Nuclear Medicine, 28, 122-129.

Sathe, P.A., Madiwale, C.V., Kandalkar, B.M., Bandgar, T.R., Shah, N.S. & Menon, P.S. (2009) Primary hyperparathyroidism: a clinicopathological experience. Indian Journal of Pathology and Microbiology, 52(3), 313-320.

Schachter, P.P., Issa, N., Shimonov, M., Czerniak, A. & Lorberboym, M. (2004) Early, postinjection MIBI-SPECT as the only preoperative study for minimally invasive parathyroidectomy. Archives of Surgery, 139, 433-437.

Serchuk, L.S., Tomas, M.B., Patel, M. & Palestro, C.J. (1997) SPECT and subtraction imaging of an ectopic parathyroid adenoma. Clinical Nuclear Medicine, 22(7), 459-462.

Sharp, P.F., Gemmell, H.G. & Smith, S.W. (ed.) (1998) Practical Nuclear Medicine Second Edition. Oxford: Oxford University Press.

- Shepp, L.A. & Vardi, Y. (1982) Maximum likelihood reconstruction for emission tomography. IEEE Transactions on Medical Imaging, MI-1(2), 113-122.
- Shimmins, J., Hilditch, T., Harden, R.McG. & Alexander, W.D. (1968) Thyroidal uptake and turnover of the pertechnetate ion in normal and hyperthyroid subjects. Journal of Clinical Endocrinology and Metabolism, 28, 575-581.
- Shimmins, J., Hilditch, T.E., Harden, R.McG. & Alexander, W.D. (1969) Neck extrathyroidal activity of ^{99m}Tc -pertechnetate. Journal of Nuclear Medicine, 10, 483-486.
- Sidhu, S., Neill, A.K., Russell, C.F.J. (2003) Long-term outcome of unilateral parathyroid exploration for primary hyperparathyroidism due to presumed solitary adenoma. World Journal of Surgery, 27, 339-342.
- Siperstein, A., Berber, E., Barbosa, G.F., Tsinberg, M., Greene, A.B., Mitchell, J. & Milas, M. (2008) Predicting the success of limited exploration for primary hyperparathyroidism using ultrasound, Sestamibi, and intraoperative parathyroid hormone: analysis of 1158 cases. Annals of Surgery, 248, 420-428.
- Slater, A. & Gleeson, F.V. (2005) Increased sensitivity and confidence of SPECT over planar imaging in dual-phase Sestamibi for parathyroid adenoma detection. Clinical Nuclear Medicine, 30, 1-3.
- Smith, J.R. & Oates, E. (2004) Radionuclide imaging of the thyroid gland: patterns, pearls and pitfalls. Clinical Nuclear Medicine, 29, 181-193.
- Sorva, A., Valvanne, J. & Tilvis, R.S. (1992) Serum ionized calcium and the prevalence of primary hyperparathyroidism in age cohorts of 75, 80 and 85 years. Journal of Internal Medicine, 231(3), 309-312.
- Spanu, A., Falchi, A., Manca, A., Marongiu, P., Cossu, A., Pisu, N., Chessa, F., Nuvoli, S. & Maddeddu, G. (2004) The usefulness of neck pinhole SPECT as a complementary tool to planar scintigraphy in primary and secondary hyperparathyroidism. Journal of Nuclear Medicine, 45, 40-48.

- Suehiro, M. & Fukuchi, M. (1992) Localization of hyperfunctioning parathyroid glands by means of thallium-201 and iodine-131 subtraction scintigraphy in patients with primary and secondary hyperparathyroidism. Annals of Nuclear Medicine, 6(3), 185-190.
- Sundin, A., Johansson, C., Hellman, P., Bergström, M., Ahlström, H., Jacobson, G.B., Långström, B. & Rastad, J. (1996) PET and parathyroid L-[Carbon-11] methionine accumulation in hyperparathyroidism. Journal of Nuclear Medicine, 37, 1766-1770.
- Taïeb, D., Hassad, R., Sebag, F., Colavolpe, C., Guedj, E., Hindié, E., Henry, J-F. & Mundler, O. (2007) Tomosintigraphy improves the determination of the embryologic origin of parathyroid adenomas, especially in apparently inferior glands: imaging features and surgical implications. Journal of Nuclear Medicine Technology, 35, 135-139.
- Taillefer, R., Baucher, Y., Potvin, C. & Lambert, R. (1992) Detection and localisation of parathyroid adenomas in patients with hyperparathyroidism using a single radionuclide imaging procedure with technetium-99m-Sestamibi (double-phase study). Journal of Nuclear Medicine, 33, 1801-1807.
- Takahashi, Y., Murase, K., Mochizuki, T., Higashino, H., Sugawara, Y. & Kinda, A. (2003) Evaluation of the number of SPECT projections in the ordered subsets-expectation maximisation image reconstruction method. Annals of Nuclear Medicine, 17(7), 525-530.
- Takamiya, Y., Farooqui, M., Rosner, N., Lin, E. & Blend, M.J. (2004) Comparison of pinhole vs low energy high resolution (LEHR) collimator sensitivity for detecting hyperfunctioning parathyroid (PTH) adenomas using dual-phase Tc-99m Sestamibi imaging [Abstract]. Journal of Nuclear Medicine Technology, 32(2), 112.
- Thomas, D.L., Bartel, T., Menda, Y., Howe, J., Graham, M.M. & Juweid, M.E. (2009) Single photon emission computed tomography (SPECT) should be routinely performed for the detection of parathyroid abnormalities utilising technetium-

99m Sestamibi parathyroid scintigraphy. Clinical Nuclear Medicine, 34(10), 651-655.

Thomas, S.K. & Wishart, G.C. (2003) Trends in surgical techniques. Nuclear Medicine Communications, 24, 115-119.

Tomas, M.B., Pugliese, P.V., Tronco, G.G., Love, C., Palestro, C.J. & Nichols, K.J. (2008) Pinhole versus parallel-hole collimators for parathyroid imaging: an intraindividual comparison. Journal of Nuclear Medicine Technology, 36(4), 189-194.

Torres, M.A., Tomas, M.B., Afriyie, M.O., Maguire, W.M. & Palestro, C.J. (1996) SPECT vs planar parathyroid scintigraphy: preliminary results [Abstract]. Clinical Nuclear Medicine, 21(4), 351.

Tourassi, G.D., Floyd, C.E.Jr. & Munley, M.T. (1991) Improved lesion detection in SPECT using MLEM reconstruction. IEEE Transactions on Nuclear Science, 38(2), 780-783.

Tublin, M.E., Pryma, D.A., Yim, J.H., Ogilvie, J.B., Mountz, J.M., Bencherif, B. & Carty, S.E. (2009) Localisation of parathyroid adenomas by sonography and technetium Tc-99m-Sestamibi single-photon emission computed tomography before minimally invasive parathyroidectomy: are both studies really needed?. Journal of Ultrasound in Medicine, 28(2), 183-190.

Udén, P., Chan, A., Duh, Q-Y., Siperstein, A. & Clark, O.H. (1992) Primary hyperparathyroidism in younger and older patients: symptoms and outcome of surgery. World Journal of Surgery, 16, 791-797.

Vahjen, G.A., Lange, R.C. & Merola, T.F. (1992) Thyroid uptake neck phantoms are not created equal. Journal of Nuclear Medicine, 33, 304-305.

Vanhove, C., Defrise, M., Franken, P.R., Everaert, H., Deconinck, F. & Bossuyt, A. (2000) Interest of the ordered subsets expectation maximisation (OS-EM) algorithm in pinhole single-photon emission tomography reconstruction: a phantom study. European Journal of Nuclear Medicine, 27, 140-146.

Wagner, R.H., Karesh, S.M. & Halama, J.R. (1999) Questions and Answers in Nuclear Medicine. St. Louis, MO: Mosby Inc.

Wakamatsu, H., Noguchi, S., Yamashita, H., Tamura, S., Jinnouchi, S., Nagamachi, S. & Futami, S. (2001) Technetium-99m tetrofosmin for parathyroid scintigraphy: a direct comparison with ^{99m}Tc -MIBI, ^{201}Tl , MRI and US. European Journal of Nuclear Medicine, 28, 1817-1827.

Wakamatsu, H., Noguchi, S., Yamashita, H., Yamashita, H., Tamura, S., Jinnouchi, S., Nagamachi, S. & Futami, S. (2003) Parathyroid scintigraphy with ^{99m}Tc -MIBI and ^{123}I subtraction: a comparison with magnetic resonance imaging and ultrasonography. Nuclear Medicine Communications, 24, 755-762.

Walters, T.E., Simon, S., Chesler, D.A. & Correia, J.A. (1981) Attenuation correction in gamma emission computed tomography. Journal of Computer Assisted Tomography, 5(1), 89-94.

Wanet, P.M., Sand, A. & Abramovici, J. (1996) Physical and clinical evaluation of high-resolution thyroid pinhole tomography. Journal of Nuclear Medicine, 37, 2017-2020.

Webb, S., Flower, M.A., Ott, R.J. & Leach, M.O. (1983) A comparison of attenuation correction methods for quantitative single photon emission tomography. Physics in Medicine and Biology, 28(9), 1045-1056.

Weber, A.L., Randolph, G. & Aksov, F.G. (2000) The thyroid and parathyroid glands. CT and MR imaging and correlation with pathology and clinical findings. Radiologic Clinics of North America, 38(5), 1105-1129.

Westerdahl, J. & Bergenfelz, A. (2007) Unilateral versus bilateral neck exploration for primary hyperparathyroidism: five-year follow-up of a randomised controlled trial. Annals of Surgery, 246, 976-981.

Wong, S.W., Chan, K.W., Paulose, N.M. & Leong, H.T. (2009) Scan-directed unilateral neck exploration for primary hyperparathyroidism: eight-year results from a regional hospital. Hong Kong Medical Journal, 15, 118-121.

Zaidi, H. (1996) Comparative methods for quantifying thyroid volume using planar imaging and SPECT. Journal of Nuclear Medicine, 37, 1421-1426.